IAEA-TECDOC-469

NEUTRON PHYSICS AND NUCLEAR DATA MEASUREMENTS WITH ACCELERATORS AND RESEARCH REACTORS

LECTURES PRESENTED AT THE
INTERRREGIONAL TRAINING COURSE
JOINTLY ORGANIZED BY THE
INTERNATIONAL ATOMIC ENERGY AGENCY
AND THE
USSR STATE COMMITTEE ON THE UTILIZATION OF ATOMIC ENERGY
AND HELD IN RIGA AND LENINGRAD,USSR, 18–30 MAY 1987

Please return this file to
ARCHIVES-AC ...../.....

A TECHNICAL DOCUMENT ISSUED BY THE
INTERNATIONAL ATOMIC ENERGY AGENCY, VIENNA, 1988

The IAEA does not normally maintain stocks of reports in this series. However, microfiche copies of these reports can be obtained from

INIS Clearinghouse
International Atomic Energy Agency
Wagramerstrasse 5
P.O. Box 100
A-1400 Vienna, Austria

Orders should be accompanied by prepayment of Austrian Schillings 100,– in the form of a cheque or in the form of IAEA microfiche service coupons which may be ordered separately from the INIS Clearinghouse.

NEUTRON PHYSICS AND NUCLEAR DATA MEASUREMENTS
WITH ACCELERATORS AND RESEARCH REACTORS
IAEA, VIENNA, 1988
IAEA-TECDOC-469

Printed by the IAEA in Austria
August 1988

FOREWORD

This report contains most of the lectures delivered at Riga and Leningrad, USSR from 18-30 May 1987 during the IAEA TC Interregional Training Course on Neutron Physics and Nuclear Data Measurements with Accelerators and Research Reactors. This Course was jointly organized by the IAEA and the USSR State Committee on the Utilization of Atomic Energy, following the recommendation of the Agency's International Nuclear Data Committee.

Similar to the previous Training Course which was held in 1983, the objectives of this Training Course were to enable the participants to become acquainted with recent developments in the field of fast neutron physics and to enhance their expertise in modern nuclear methods and techniques employed in the field of fast neutron physics and nuclear data measurements, and in technological applications of immediate benefit to their home countries. In addition to the nuclear data measurement techniques and calculational methods, a number of new topics, such as reaction cross sections for reactor dosimetry, thermoluminescent neutron dosimetry, treatment of measurement uncertainties, application of covariances in the evaluation of dosimetry reaction excitation functions, and application of solid state track detectors in nuclear physics were covered at this Course.

In order to avoid duplicate publication, several lectures have not been included in this report. These are:

- Zijp, W.L., "Treatment of measurement uncertainties", ECN-194, 1987.
- Avotinsh, Yu.A., Bugaenko, L.T., Dzelme, Yu.R., Tilix, Yu.E., "Lioluminescence", Riga, 1984.

as well as lectures presented at the previous Course and contained already in document IAEA-TECDOC-345, 1985.

EDITORIAL NOTE

In preparing this material for the press, staff of the International Atomic Energy Agency have mounted and paginated the original manuscripts as submitted by the authors and given some attention to the presentation.

The views expressed in the papers, the statements made and the general style adopted are the responsibility of the named authors. The views do not necessarily reflect those of the governments of the Member States or organizations under whose auspices the manuscripts were produced.

The use in this book of particular designations of countries or territories does not imply any judgement by the publisher, the IAEA, as to the legal status of such countries or territories, of their authorities and institutions or of the delimitation of their boundaries.

The mention of specific companies or of their products or brand names does not imply any endorsement or recommendation on the part of the IAEA.

Authors are themselves responsible for obtaining the necessary permission to reproduce copyright material from other sources.

CONTENTS

PLEASE BE AWARE THAT
ALL OF THE MISSING PAGES IN THIS DOCUMENT
WERE ORIGINALLY BLANK

NUCLEAR DATA REQUIREMENTS

V.N. MANOKHIN
Institute of Physics and Power Engineering,
Obninsk, Union of Soviet Socialist Republics

Abstract

A general review of nuclear data requirements for nuclear power engineering is given. The required nuclear data and the needed accuracy in nuclear data are described.

Introduction. Nuclear data activity is a multilateral scientific branch which is developed on the base of practical needs of power engeneering and technology.

The essential part of nuclear data activity is specifying and substantiating nuclear data accuracy requirements.

The needs in certain branches of science and technology determine the list of values, which characterize the interaction of radiation with nuclei, the incident particle energy range and the list of isotopes and materials, for which the data are required. There are nuclear needs in such regions of human activity as nuclear power engeneering, fusion problem, biomedicine, geophysics and geology, astrophysics and so on.

The problem of nuclear data requirements for nuclear reactors was examined by many authors and discussed at conferencies and meetings. This lecture is mainly devoted to nuclear data requirements for nuclear power engeneering. For those, who wants to acquaint with problem deeper, one should recommend the reviews [1,2], which were used for preparation of present lecture and contain a lot of referencies.

Nuclear data requirements for fission reactors. The most wide and hard requirements are for nuclear power engeneering. Its are needed for undestanding physical process, underlying the work of nuclear power stations, for calculation and optimization of parameters of reactors and nuclear power station as a whole, for the out-of-pile fuel cycle, for the choice of the alternative ways of nuclear power development.

It is necessary for reactor design to calculate the following parameters and effects:

- effective multiplication coefficient K_{eff}, which determines critical size of reactor;
- breeding ratio, which determines the doubling time of breeder reactors;
- variation of reactivity with burn-out of fuel and build-up of actinides and fission products in an irradiation period which determines the operational control requirements and also the fuel reactivity at the and of irradiation period;
- control rod reactivity;
- the factor of the peak to average power distribution, which influences directly the maximum power output;
- radiation damage effects, which effect directly economy, design and safety of nuclear reactors, as far as the maximum irradiation and therefore the company duration depends on radiation endurance of structural materials;
- coefficients of reactivity, which determine reactor kinetics and are related to reactor safety (these are Doppler and Sodium reactivity effects);
- decay heating of fuel elements, which is needed to design shut-down and emergency cooling system;

activity of irradiated materials (fuel, coolant and structural materials) for the determination of conditions of reactor equipment accessibility and reactor element handling, for the design of the shielding of fuel transportation and regeneration.

The nuclear data requirements are determined by reactor components and neutron energy reactor spectrum. In a whole the neutron data are needed for all the reactor materials and in the reactor energy spectrum range.

The range of neutron interactions in thermal reactors lies up to some eV; fast reactor neutrons comprises essentially more wide energy range - up to 10 MeV and more. Therefore, it necessary for thermal reactors to know the fission, radiative capture and elastic scattering cross sections in small energy range up to several eV, and also the low-lying resonance propeties of fertile

and fuel materials, which are important for reactor parameters calculations.

The nuclear data requirements for fast breeders are essentially more large. For fast breeders the inelastic scattering cross sections, (n,p)-,(n,α)-,(n,2n)- reaction cross sections and also angle and energy secondary particle disributions are needed in a whole neutron energy range.

The nuclear data are needed with required accuracy, because uncertainties in nuclear data lead to uncertainties in the prediction of reactor parameters. Large uncertainties in turn leed to the large and expensive margins in design.

The needed accuracy in nuclear data arrises from target accuracies - the demands to the accuracy predictions of certain facility parameters, determined on the base of technical-economic considerations. For example, the requirement to K_{ef} accuracy calculation is subtantiated by possiblity to cover relevant uncertainties without reactor reconstruction and change of reactor fuel composition. The contribution into the whole uncertainty at the expanse of nuclear data uncertainty must not exceed the uncertainty contribution because of uncertainty in fuel element production and other technoloqical uncertainties.

Below there is a review of requirements in nuclear data for fast neutron reactors, determined on the base of required accuracies (target accuracies) of above mentioned reactor parameters and first of all, K_{ef} and breeding ratio.

Main fission and fertile materials. There are high accuracy requirements for the fission (2%) and capture (3%) cross sections. Values ν (0,3%) of ^{235}U, ^{239}Pu, ^{238}U, for the inelastic scatte - ring cross sections (5-10%) of ^{238}U. This accuracy is determined first of all by calculation requirements for K_{ef} (1.0%) and BR (2%). As for the thorium fuel cycle reactors the same require - ments are needed for ^{233}U and ^{232}Th.

Structural materials. The nuclear data of the coolant and structural materials are required for the determination of reactivity effects,reactor neutron spectrum, the reactor neutron balance, material activity and heating. The data are needed for the capture and inelastic scattering cross sections of Na (coolant), Fe, Cr, Ni, Ti, Zr, Nb, Mo and so on. The required accuracies for capture cross sections are 5-10%, for inelastic scattering cross sections are 5%. Data are required on the resonance structure of the cross sections because resonance shielding effects and Doppler effects are significant. As far as the radiation damage problem is concerned the data are needed for (n,p)- and (n,α)- reactions, for activation reactions for the calculation of radiactive contamination (activation of coolant and mass transfer of steel) of the primary circuit, the pumps and heat exchangers, for the calculation of the reactor element activation which must be handled, transported, stored and reprocessed. The major activation reactions are given below:

$^{54}Fe(n,p)\,^{54}Mn$, $^{58}Ni(n,p)\,^{58}Co$, $^{58}Fe(n,\gamma)\,^{59}Fe$

$^{50}Cr(n,\gamma)\,^{51}Cr$, $^{54}Fe(n,\alpha)\,^{51}Cr$, $^{62}Ni(n,\gamma)\,^{63}Ni$

$^{58}Ni(n,\gamma)\,^{59}Ni$, $^{54}Fe(n,\gamma)\,^{55}Fe$, $^{22}Na(n,\gamma)\,^{23}Na$

Absorbers. Both natural and enriched boron are used as absorbers (tantalum is tested and Eu is being investigated). There are the following requirements in nuclear data for absorbers B, Eu, Gd,Er, Hf, Ta: capture cross sections -5%, scattering cross sections - 10%. The data on the individual isotopes are needed to predict the variation of reactivity with burnup and the activity and heating of the absorber.

TRANSACTINIDES. The nuclear data for transactinides are required for determination of build-up and burn-out of actinides and for the prediction of neutron activity of the fuel. We need to know the capture, fission and (n,2n)-reaction cross sections.

Some transactinides are built-up in power nuclear reactors in considerable amount. The neutrons cross sections of these isotopes are needed with high accuracy compared with that required for the main fissile and fertile isotopes. In reactors such isotopes are produced which because of hard γ-rays emission (^{232}U, ^{236}Pu, ^{238}Pu) or neutron emission (^{242}Cm, ^{244}Cm) leads to the main difficulties in fiel management at its transportation and reprocessing. The reactions which are essential for the production of ^{239}U: $^{233}U(n,2n)$ and $^{237}Np(n,2n)$, for the production of ^{238}Pu, ^{242}Cm, ^{244}Cm: $^{237}Np(n,\gamma)$, $^{241}Am(n,\gamma)$, $^{243}Am(n,\gamma)$, in the case of ^{236}Pu production: $^{238}U(n,2n)$, $^{237}Np(n,2n)$. The cumulated activity of

^{236}Pu and ^{238}Pu determines the fuel element production technology from Pu, produced by the chemical reprocessing of irradiated fuel. Its production cross sections should be known. It is important and for the calculation of ^{232}U build-up, which arises from the α -decay of ^{236}Pu and determines radiation conditions of fuel element production from uranium regenerated fuel. Important nuclear constant for the calculation of ^{232}U build-up in fast neutron reac - tors are also the data for $^{234}U(n,3n)$ and $^{235}U(n,\gamma)$.

Fission products. For determination of the reactivity effect of the bulk fission product (with accuracy of 10%) the capture and inelastic scattering cross sections should be known respectively with the accuracy 10% and 30%, The list of nuclides for which the improvement of capture cross section is important for the calculation of the bulk fission product capture cross section in fast reactors is given below.The contribution of each isotopes of the first qroup (^{133}Cs, ^{101}Ru, ^{99}Te, ^{147}Nd) to averaged cross sections is not less 5%, of the second qroup (^{103}Rh, ^{145}Nd, ^{97}Mo, ^{149}Sm, ^{102}Ru, ^{131}Xe, ^{98}Mo, ^{95}Mo, ^{151}Sm, ^{135}Cs, ^{93}Zr) - 5÷2%; of the third qroup (^{105}Pd, ^{141}Pr, ^{100}Mo, ^{153}Eu, ^{103}Ru, ^{104}Ru) - 2%, of the others is less 1%.

Components of fuel elements. For determination of neutron activity of fuel one should know (α,n)- reaction cross sections on light nuclides O (oxcide fuel) and C (carbon fuel).

Reactor dosimetry. Dosimetry reactions are used for the measurement of flux and neutron spectra in reactors.Knowlwdge of the irradiation conditions is required for interpreting the results of experimental irradiations for predicting material activation and for correlating the propeties of irradiated materials with irra - diation conditions. Two main factors affect the physics of structural materials: the displacement of atoms and the production of helium by (n,α)- reactions. The predictions of atomic displacement rates and helium production rates requires a knowledge of the total flux, the flux spectrum and the cross sections of the following reactions: $^{27}Al(n,\alpha)^{24}Na$, $^{56}Fe(n,p)^{56}Mn$, $^{63}Cu(n,2n)^{62}Cu$, $^{238}U(n,f)$ F.P., $^{237}Np(n,f)$ F.P., $^{58}Ni(n,2n)^{57}Ni$, $^{197}Au(n,\gamma)^{198}Au$, $^{239}Pu(n,f)$ F.P.

Conclusion. In addition nuclear power engeneering needs, based on fission reactors, many other regions of science and technology have very large needs in nuclear data. These are fusion reactor problem, biomedicine and medical radiology (neutron therapy, medical diagnostics and dosimetry), isotope production,radoactive waste manegement, astrophysics an so on. These are methods, used in different applyed regions: tracer technique (hydrology, medical diagnostics and so on),nOndestructive analysis (determination of fuel isotope composition), nuclear activation analysis(elemental determination of materials).

New regions of nuclear data applications are appeared for example such as nuclear safety, alternative reactors, spoce reactors,industrial applications,decommissioning of long-time operated fission reactors, high energy neutron dosimetry which widen the needs for nuclear data both in energy range and number of reactions. To meet these needs the experimental and theoretical investigations are made of radiation interactions with nuclei in many countries and during long period of time.

Nuclear data requirements, formulated by specialists from many countries, are published in WRENDA, issued by INDC[3].

The results of intensive activity of nuclear physicists allowed to meet many requirements, but nevetheless the present and future requirements put new tasks both in increasing nuclear data amount and improving reliability and accuracy of evaluated data.

REFERENCES

1. Rowlands J. Nuclear data for reactor design, operation and safety. - In: Proc.Conf. on Neutron Physics and Nuclear Data Harwell, 1978, p.7.
2. Manokhin V.N., Usachev L.N. Nuclear data requirements for fast reactors. - Atomnaja energia, 1984, v.57, N°4, p.234.
3. World Request List for Nuclear Data - WRENDA 83/84. Report INDC(SEC)-88. URSF. Vienna, 1983.

COUPLED CHANNEL METHOD FOR CALCULATION OF NEUTRON CROSS-SECTIONS

A.V. IGNATYUK, V.P. LUNEV, V.G. PRONYAEV
Institute of Physics and Power Engineering,
Obninsk, Union of Soviet Socialist Republics

Abstract

The basic concept of the couple-channel optical model used for the calculation of neutron cross sections is described. As typical examples, the results of the differential elastic and inelastic scattering for ^{52}Cr and the total neutron cross sections for ^{56}Fe, ^{208}Pb calculated by the channel method are given.

The development of nuclear power engineering demands the reliable determination of neutron cross-sections for a large number of stable and radioactive nuclei. Despite of a considerable number of experimental studies on the measurements of these cross - sections, the material, accumulated by the present time is still far from satisfactory both in the completeness of covered ener - gies and the consistency of the results from different measure - ments. The use of theoretical models for the analysis and the evaluation of neutron cross-sections is inevitable in this case. We may obtain the additional criteria of selection between the contradictory data and carry out an extrapolation of the existing data on the whole energy range.

The relations of the statistical theory of nuclear reactions based on the nuclear optical model are widely used in practical work on the neutron cross section analysis. The quality of the experimental data description in this approach is determined to a great extent by the choice of the concrete optical model parameters to be used.

The incident particle interaction with a nucleus is appro - ached in the simplest phenomenological formulation of the optical model, by the local complex spherical potential whose imaginary part simulates the nonelastic processes in the integral way [1]. The optical potential for neutrons is taken as usually

$$V(r) = -(V_v + iW_v) f_v(r) + 4ia_s W_s \frac{df_s(r)}{dr} + V_{so} \frac{\lambda_\pi^2}{r} \frac{df_{so}(r)}{dr} (\vec{l}\cdot\vec{s}) \quad (1)$$

where V_v is the depth of the real part of the potential; W_v and W_s - amplitudes of the volume and surface absorption, V_{so} - spin-orbit component of the potential, λ_π - pion Compton wave length;

$f_i(r) = \left\{1 + \exp\left[(r - r_i A^{1/3})/a_i\right]\right\}$ - form-factors of the corresponding parts of the optical potential.

The generalized optical model [2] now is used more often to take into account the strong channel coupling (SCC) between elastic and inelastic scattering channels with low-lying collective level excitations. In this model the optical potential is taken as a rule in form (1), but with the form-factors depending on the collective variables. Carring out the expansion of the form-factors on the spherical harmonics [2], it is not difficult to find an explicit form of coupling potentials between elastic and inelastic scattering channels.

One of two aims is usually pursued when the optical model is used for nuclear reaction cross section analysis: 1) to get the optimum description of the observed cross sections for a wide region of nuclei with one "universal" set of the optical potential parameters; 2) to obtain best description of the elastic scattering and total neutron cross sections for a specific nucleus and neutron energy. The physical content of the optical model is, of course, different in these cases being dependent on the problem under consideration. The derived optical model parameters reflect in the first case the common dependence of the mean single particle nuclear field changes and the nucleon absorption probability distribution in the nucleus. The optical model appears rather as a phenomenological way of parametrization of the energy averaged collision matrix properties in the second case. In this approach, the energy variations of the potential parameters, as well as fluctuations of the parameters for a neighbouring nuclei, may be caused not only by mean field variations, but include different structure effects involving individual features of the nuclei.

The universal sets of parameters of the spherical optical potentials have been discussed by many authors [3÷5] . It was shown [5] , that the sets of parameters obtained from the analysis of the neutron elastic scattering differential cross sections observed for high energies are, as a rule, unsatisfactory for neutrons with an energy below 10 MeV. The optimal set of parameters for low neutron energies seems to be the one obtained from the analysis of a large number of experimental data on elastic scattering of neutrons with energy below 8 MeV [3] :

$$V_v = 48.7 - 0.33E. \qquad r_v = r_s = r_{so} = 1.25,$$
$$W_s = 7.2 + 0.66E. \qquad a_v = a_{so} = 0.65, \qquad (2)$$
$$V_{so} = 7.5 \qquad a_s = 0.47$$

These parameters are obtained for a spherical optical model. At the same time most of the nuclei under analysis have low lying collective levels, which are very intensively excited through the direct mechanism of the inelastic scattering. But coupling of the elastic and inelastic scattering channels for high intensity direct transitions becomes essential, it demands a switch - over from one - channel to the generalized optical model. Apparently, it is better to use the parameters of the spherical potential found for magic nuclei [4,5] as a first approximation, when the parameters of the generalized potential are searched. It is possible also to use parameters (2) with a reduced amplitude of the optical potential imaginary part. The reduction factor for the imaginary part is defined by the number of coupled channels taken into account, and usually it is taken from condi - tion of the consistent description of the total neutron cross-sections.

In recent years the SCC method has been more widely used in the practice of the neutron cross section analysis and numerous examples of description of the neutron elastic scattering differential cross-sections obtained by this method are presented in papers [4 - 8] . Despite the definite spread of the optical po - tential parameters derived in this analysis, as a whole the conclusion can be drawn, that the nucleus-to-nucleus fluctuation of the parameters derived in the framework of the SCC method is considerably less, than that of the individual sets of the spherical optical model parameters. Furthemore, the parameters of the real part of the optical potentials for low energy neutrons agree with the traditional parameters of the single particle shell model potential much better than with the similar parameters of the one-channel optical analysis. This consistiency of the results is one of the important achievements of the generalized optical model.

As typical example, the description of the differential elastic and inelastic scattering of 5,6 and 7 MeV neutrons at 2^+ level of ^{52}Cr achieved in SCC method [9] is shown in Fig.1.

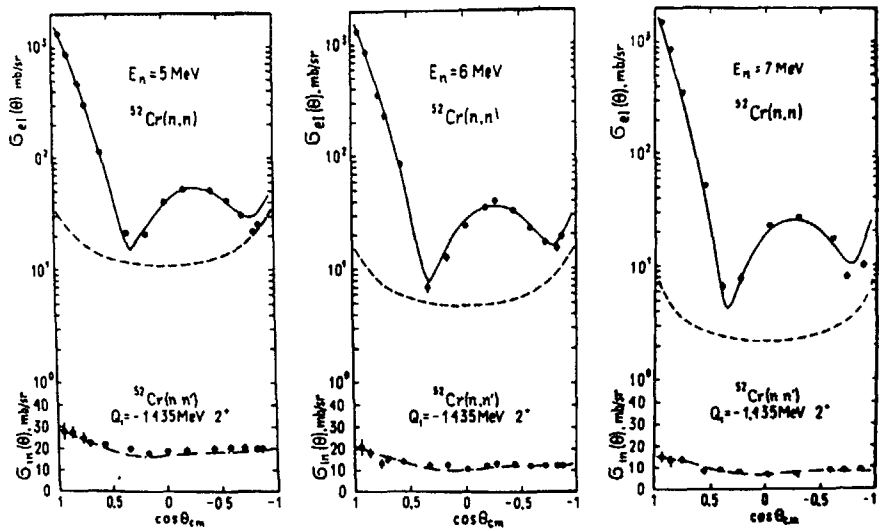

Fig. 1. Differential cross-sections for elastic and inelastic neutron scattering at 2^+ level of ^{52}Cr nuclei (solid and dot-dashed lines). The contribution of the compound elastic scattering is shown by a dashed line, and direct processes - by a dot line. Points stand for the experimental data.

A good description of the observed asymmetry of the neutron inelastic scattering angular distributions enables us to give a fairly reliable determination of the contribution of the direct reaction mechanism which, appears dominating over the compound mechanism for the neutrons with energies higher than 6 MeV. Re - sults of the analysis of the inelastic scattering integral cross-

sections at the first 2^+ level are presented in Fig. 2. The cross-sections of the direct transitions are changed insignificantly, when the neutron energy is reduced, while the scattering cross-section through the compound nucleus is increased comparatively fast.

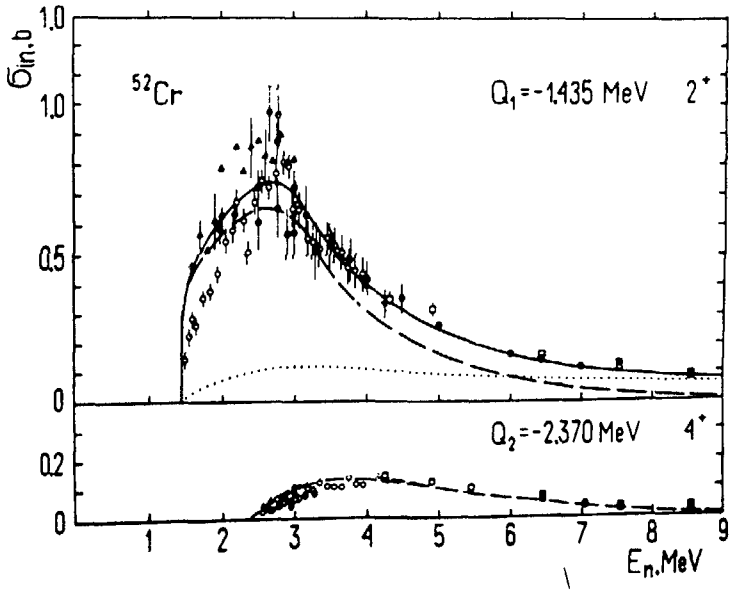

Fig. 2. Inelastic scattering excitation functions at 2^+ and 4^+ level of ^{52}Cr nuclei. The same designation as in Fig. 1.

Substantial scatter of experimental points for neutrons with an energy below 3 MeV is caused first of all by systematical errors in measurements made by different authors. This scatter is partly eliminated when the methods are improved and the results of the last measurements are as a rule much more consistent than the experimental data obtained earlier. Experimental data on the excitation function of the 4^+ level in ^{52}Cr nucleus are also shown in Fig. 2. The statistical theory present a fairly good description of the observed integral cross-sections for neutrons with an energy from the threshold to 7 MeV and the necessity of taking into account the direct processes arises only in the region of higher energies. At the present time the similar results of the analysis of differential and integral neutron scattering cross sections within the frames of the SCC method exist for a wide range of light, middle and heavy nuclei [4, 6, 8].

Note, that the spherical and generalized optical models may give noticeably different cross sections of the compound nucleus formation with a similar good description of the total neutron cross-sections. These differences are caused by the interference redistribution of the flow between strong coupled elastic and inelastic scattering channels and this redistribution as a rule is not reduced to a simple reduction of the absorption cross-section at the integral contribution of the direct inelastic processes. As an example, the calculations results of a neutron absorbtion cross section by ^{238}U nucleus are presented in Fig. 3.

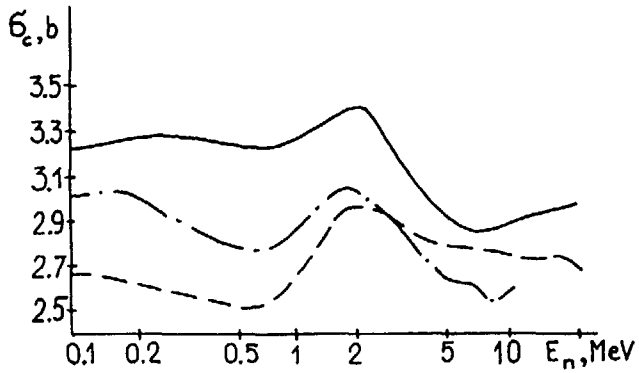

Fig. 3. Compound nucleus formation cross-section for reaction ^{238}U + n in SOM (dashed and dot-dashed lines) and for deformed optical potential (solid line).

The variation of the compound nucleus formation cross-section predicted by the generalized optical model is, as shown in [10], very important for the consistent theoretical description of fission and neutron inelastic scattering by the highly deformed actinide nuclei.

Consistincy of the optical model predictions with the experimentally observed values of the neutron strength functions becomes essential for the analysis of low-energy parts of the total

neutron cross-section and isolated levels excitation functions [4-6] . The optical models with the universal set of potential parameters reproduce only the general dependence of the neutron strength function from the mass number [1,2] . Though the change from the spherical to generalized optical model as a whole improves the experimental data description, the descrepancy between the theory and the experiment remains cousiderable for specific nuclei [4-6] .

The neutron strength functions are closely connected with the transmission coefficients,directly determining the absorption and elastic and inelastic scattering cross-sections for neutrons with a compound nucleus formation. Analysing the excitation functions near the threshold of the isolated 2^+ levels, we may check the correctness of the d-wave strength functions description by the optical model,the direct experimental information for which is practically absent. As it was shown earlier [4] analyzing the experimental data on the inelastic scattering cross sections with an excitation of the first 2^+ levels, one in fact always get the improved description of the near-threshold region of the low-lying levels excitation functions for the optical potentials that improve the description of the low energy part of the total neutron cross section.

The deviations from the optical model predictions observed in the neutron strength functions and nearthreshold parts of the excitation functions indicate an important role of the intermediate structures, which are not appeared in a few channel versions of the SCC method. It is necessary to expand considerably the number of the coupled reaction channels and accordingly to reduce the imaginary part of the optical potential responsible for the remaining ignored open and closed decay channelsof nucleus. Various versions of the solution of this problem actually differ only in methods of modelling the nuclear states structure corresponding to different reaction channels.

A high number of coupled channels creates substantial technical difficulties for traditional direct methods of the solution of the differential equation system of the generalized optical model [2] . These difficulties and associated large expenditures of the computer time to some extent may be overcome by utilizing the iterative method of the coupled equations solution, realized in the ECIS-code [11] . We have utilized this code for analysis of the low energy neutron cross-sections for the group of iron and lead nuclei. The coupling of the elastic scattering channel with 20 - 25 most collective one-phonon excitations and two-phonon multiplets corresponding to $2^+ \otimes 2^+$ and $2^+ \otimes 3^-$ target nucleus excitations was taken into account. Spectroscopic characteristics of the considered excitations were taken from the experimental data analysis on the Coulomb excitation of the levels and direct transition cross-sections for charged particles.

The total neutron and reaction cross-sections obtained in such approach for ^{56}Fe nucleus are shown in Fig. 4 in comparison with the known experimental data and spherical optical model (SOM) results obtained with the optical set of parameters [12] .

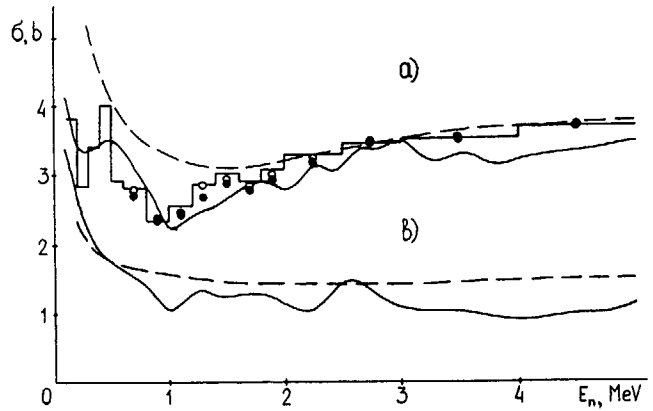

Fig. 4. Comparison of the total (a) and reaction (b) cross-sections in MCCM (solid line) with evaluated data (histogram) and averaged experimental data (open and closed circles). Dashed line presents the SOM results with parameters [12] .

Consideration is given to a rather good description of the cross-sections for neutrons with an energy below 3 MeV, which is not achievable in the SOM without anomalous local variations of the optical potential parameters.

The results of the similar calculations for ^{208}Pb nucleus are presented in Fig. 5. As far the spectroscopic characteristics of the coherent phonon excitations for this double magic nucleus are known up to 7 MeV excitation energy and the level density is

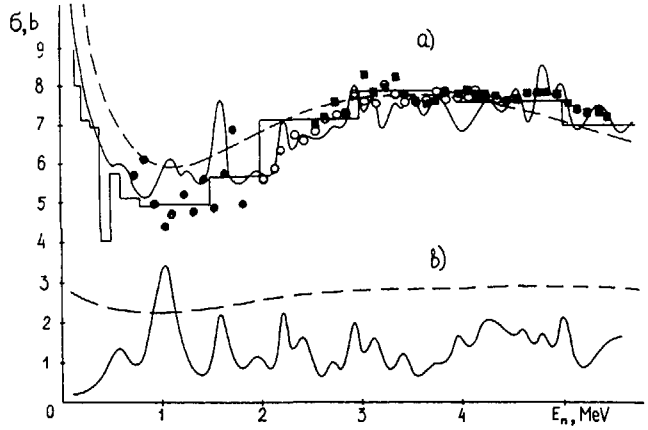

Fig. 5. The same as in Fig. 4 but for ^{208}Pb nucleus.

rather low, it was passible to take into account all "strong" phonon excitations. Due to this a very low value of the imaginary optical potential (W_s = 0.1 MeV) was taken in the multi-channel coupling model (MCCM). For comparison, the calculation results in the SOM with the same parameters of the real part of potential as in MCCM but with traditional value (W_s = 5.0 MeV) [13] of the imaginary potential are shown. One can see that the global description of the total neutron cross-section is about the same, but there are the intermediate structure in the cross sections and the optical reaction cross section obtained in MCCM is lower than those predicted in the SOM.

Determination of the effective spherical potential for the entrance channel, which is locally equivalent (at any energy point) to the generalized MCCM potential, presents a big interest for the valid interpretation of the individual sets of optical potential parameters. We assumed that the geometrical parameters of the form-factors for both potentials coincide and the amplitudes of the imaginary part (W_s) and surface addition to the real part (ΔV_s) of the effective potential were determined from equality of the real and imaginary parts of the elastic scattering channels S-matrix in MCCM and SOM. W_s and ΔV_s values thus obtained are shown in Fig. 6.

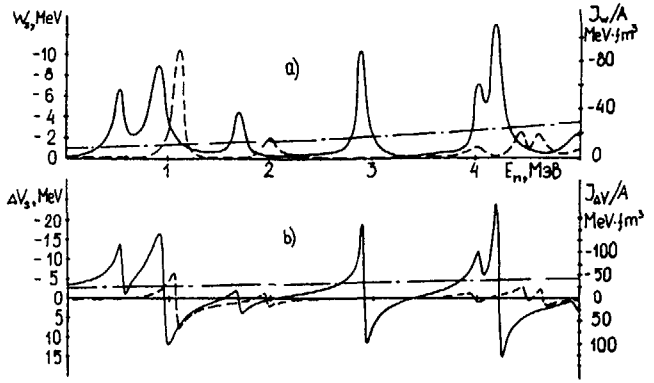

Fig. 6. Imaginary (a) and real (b) components of the effective MCCM optical potential for $S_{1/2}$ - (solid) and $P_{1/2}$ - wave (dashed line). Dot-dashed line-results of the phenomenological model [14].

Resonance structures in $W_s(E)$ are concerned with the corresponding door-way states of the system and the energy dependence in $\Delta V_s(E)$ reflects the relation existing between the real and imaginary parts based on dispersion relation [14]

$$\Delta V_s(E) = \frac{1}{\pi} \int_{-\infty}^{+\infty} \frac{W_s(E')}{E' - E} dE' \qquad (3)$$

The amplitude of the SOM imaginary potential obtained from the experimental data analysis and corresponding surface addition to the real potential (3) are shown in Fig. 6. The direct comparison of the empirical SOM parameters and MCCM effective potential parameters is doubtful because the conditions of the neutron cross-section averaging are different for the considered models. However, the substantial difference of the effective optical potentials for s- and p- waves attracts attention . Similar

differences were marked repeatedly in the microscopic calculations of the optical potentials [15,16] , and these differences may be of principle value for interpretation of the observed neutron strength functions. Most of the microscopic calculations show the need of the selecting different optical potentials for even and odd orbital waves.

The conclusion can be drawn on the basis of numerous examples of the experimental data analysis carried out by the present time that the coupled channel method makes it possible to carry out the most strict and successive consideration of the direct, intermediate door-way and compound nucleus reaction mechanisms from the standpoint of their interference. Transition from the one-channel optical model to the generalized coupled channel model removes the main part of the groundless fluctuations of the optical potential parametrs. Consistent account of the individual features of the excited level spectrum allows a consistent description of the neutron strength functions and intermediate neutron cross section structure to be obtained. Thus the increase of the number of channels under consideration is, evidently, one of the most perspective directions for the further development of the neutron cross-section description within the optical-statistical approach.

REFERENCES

1. Hodgson P.E. - The optical model of elastic scattering,Oxford, Clarendon Press, 1963.
2. Tamura T. - Rev.,Mod.Phys., 1965, v.37, p.679.
3. Pasechnik M.V., Korzh I.A., Kashuba I.E. -In: Neutron physics, Kiev, Naukova Dumka, 1972, part 1, p.253.
4. Bychkov V.M., Ignatyk A.V., Lunev V.P. et al. - Phys. of Elem. Part. and Atomic Nucl., 1983, v.14, p.373.
5. Young P.G. - In: Meeting on Use of Optical Model for Calculations of Neutron Cross Sections below 20 MeV. Paris: OECD. 1986, p.127.
6. Haouat G. - In: Neutron Induced Reactions. Bratislava, VEDA, 1980, p.333.
7. Sartori E. Report in International Nuclear Model Code Intercomparision. NEANDC-182A(1984).
8. KlepatskijA.B.,Konshin V.A., Sukhovitskij E.Sh. Report INDC (CCP) - 161/L, Vienna: IAEA, 1981.
9. Korzh I.A., Mishchenko V.A., Pasechnik M.V., Pravdivij N.M., Atomnaya Energiya 1984, v.57, p.262.
10. Ignatyuk A.V., Klepatskij A.B., Maslow V.M., Suhovitskij E.Sh. Yadernaya fizika, 1985, v.42, p.569.
11. Raynal J. In: Materials of Workshop on Nuclear Model Compu - ter Codes. Trieste: IAEA, 1984.
12. Moldauer P. Nucl.Phys., 1963, v.47, p.65.
13. Haouat G. et al. Report NEANDC(E)-180/L (1978).
14. Mahaux C., Ngo H. Nucl.Phys., 1982,v.A378,p.205.
15. Lev A., Beres W.P., Divadeenam M. Phys. Rev.,1974,v.C9, 2416.
16. Osterfeld F. In: Use of Optical Model for Calculations of Neutron Cross Sections below 20 MeV. Paris: OECD, 1986, p.29.

THEORETICAL ANALYSIS AND SYSTEMATICS OF THRESHOLD REACTION CROSS-SECTIONS

V.M. BYCHKOV
Institute of Physics and Power Engineering,
Obninsk, Union of Soviet Socialist Republics

Abstract

Theoretical analysis of nuclear reaction cross sections is often used in nuclear data. In this survey, the theoretical description (including direct, pre-equilibrium and equilibrium contributions) of neutron threshold reactions in the energy region up to 20 MeV, the dependence of the results on the parameters used in calculations and the systematical trends of the cross-section dependence from the neutron and proton number in the target nucleus were discussed.

Theoretical analysis of the nuclear reaction cross-sections and the particle emission spectra is offen used in nuclear data evaluation. It is therefore important to investigate the applicability of the theoretical models for different reaction types and energy regions and to estimate the accuracy of calculations.

In this survey we shall consider the theoretical descrip - tion of neutron threshold reactions in the energy region up to 20 MeV, the dependence of the results on the parameters used in calculations and the systematical trends of the cross-section dependence from the neutron and proton number in the target nucleus.

1. Classification of threshold reaction cross-sections.

1.1. Total cross-section of the reaction $A(V_0,V_1)B$. Here V_0 is the incident particle, A is the target nucleus, V_1 is the emitted particle and B is the residual nucleus. The states of the residual nucleus are not specified, e.g. a transition could occur to any level, wich decays further through gamma-transitions. The corresponding cross-section shall be denoted as $\sigma_{v_0v_1\gamma}$ to distinguish it from the cross-section $\sigma_{v_0v_1}$, wich at the energy above two particle emission threshold is equal to the sum :

$$\sigma_{v_0v_1\gamma} + \sigma_{v_0v_1v_2} + \sigma_{v_0v_1v_3} + \dots$$

The (n,p) reaction cross-section for example is equal to:

$$\sigma_{np} = \sigma_{np\gamma} + \sigma_{npn} + \sigma_{np\alpha} + \sigma_{n2p}$$

The total cross section $\sigma_{v_0v_1\gamma}$ is usually measured by the activation method or (below two-particle emission threshold) by the direct registration of the particle V_1.

1.2. Differential and partial cross-sections. Differential $\sigma_{v_0v_1}(E',\theta')$ and partial $\sigma_{v_0v_1}(U,I,\pi)$ cross-sections are determined by the spectrometry of the emitted particles. In case of the partial cross-section a given state of the residual nucleus is specified by the excitation energy U, momentum I and parity π. They are related to the total cross-section as :

$$\sigma_{v_0v_1\gamma} = \sum_{I\pi} \int_U \sigma_{v_0v_1\gamma}(U,I,\pi)\, dU ;$$

and

$$\sigma_{v_0v_1\gamma} = \int_E \int_\theta \sigma_{v_0v_1\gamma}(E,\theta)\, dE\, d\theta ;$$

1.3. The activation cross-section, e.g. a yield of the residual nucleus in a given, long - lived state (isomer or ground).

This type of cross-section differs from the previous by the cumulative population of the long-lived state through the gamma - cascades. This is illustrated by the following scheme:

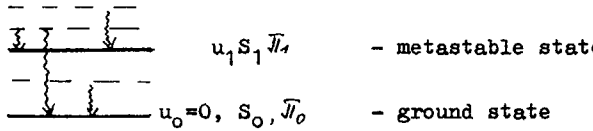

The relation between the total cross-section of the reaction $A(v_0v_1)B$ and the activation cross-sections is as follows:

$$\sigma_{v_0v_1\gamma} = \sigma^{g}_{v_0v_1\gamma} + \sigma^{m_1}_{v_0v_1\gamma} + \sigma^{m_2}_{v_0v_1\gamma} + \dots$$

These cross-sections are measured by the activation method.

The ground state activation cross-section $\sigma^{g}_{v_0v_1\gamma}$ is equal to the total cross-section if there is no metastable states, or if their time of life relative to the decay to the ground state are considerably less than the ground state time of life. In some cases the activation cross-section is equal to the sum of diffe - rent processes leading to the same residual nucleus, for example:

$$\sigma^{act}_{npn\gamma} = \sigma_{npn\gamma} + \sigma_{nd\gamma}.$$

I.4. Particle production cross-section. This is a yield of a given particle in the nuclear reaction. For example, the helium production cross-section would be:

$$\sigma_\alpha = \sigma_{n\alpha\gamma} + \sigma_{nan\gamma} + \sigma_{nn\alpha\gamma} + \sigma_{n\alpha p\gamma} + 2\sigma_{n2\alpha\gamma} + \dots$$

2. Theoretical description of the threshold reaction cross-sections.

The approach applied here is based on subdivision of the reaction mechanism into direct, preequilibrium and equilibrium contributions. The equilibrium part of the paticle emission spectrum can be written in Hauser-Feshbach [1] formalism as:

$$\sigma^{eq}_{\nu_0\nu_1}(E_1, I_1, \pi_1)\Delta E_1 = \frac{\pi}{k^2}\frac{1}{(2I_0+1)(2S_0+1)}\sum_{J\pi}(2J+1)\cdot$$

$$\cdot\sum_{\ell j} T^{J\pi}_{\ell j}(E_0)\sum_{\ell_1 j_1}\frac{T^{J\pi}_{\ell_1 j_1}(E_1)\,\rho(u_1, I_1, \pi_1)\,\Delta E_1}{N(E_c, J\pi)} \qquad (2.1)$$

where: $N(E_c J\pi) = \sum_\nu \sum_{I'\pi'}\sum_{\ell' j'}\int_0^{E_c-B_\nu} dE_\nu\, T^{J\pi}_{\nu\ell' j'}(E_\nu)\,\rho_\nu(E_c-B_\nu-E_\nu, I'\pi') +$

$$+\sum_{I'\pi'}\sum_{\chi L}\int_0^{E_c} dE_\gamma\, T^{J\pi}_{\gamma\chi L}(E_\gamma)\,\rho_\gamma(E_c-E_\gamma, I'\pi').$$

here : U_1, I_1, π_1 are the excitation energy, spin and parity of the residual nucleus after emission of particle with energy E_1;

$E_\nu(\gamma)$, ℓ, j are the energy of the emitted particle or gamma-quantum, its orbital and total momentum;

B_ν is the separation energy of particle ν in the compound nucleus;

E_c, J, π are the excitation energy, spin and parity of the compound nucleus;

$E_c = E_{\nu_0}\frac{A}{A+m_{\nu_0}} + B_{\nu_0}$, where A is the target nucleus mass, E_{ν_0} and m_{ν_0} are the energy and mass of the incident particle ν_0;

K_{ν_0} is particle ν_0 wave number;

$T_{\nu\ell j}(E_\nu)$ are the optical model transmission coefficients for particles;

$T_{\gamma\chi L}(E_\gamma)$ are the transmission coeficients for gamma-quantum, characterized by multipolarity L and transition type X;

$\rho(U, I, \pi)$ is nuclear level density at excitation energy U: For discrete levels:

$$\rho(U, I, \pi) = \sum_i \delta(U-U_i)\,\delta_{II_i}\,\delta_{\pi\pi_i}$$

The following conditions must be fulfilled in formula (2.1):

$U_1 = E_c - B_{\nu_1} - E_1$; $|\ell - S| \le j \le \ell + S$; $|I_0 - j| \le J \le I_0 + j$.

$|I_1 - j_1| \le J \le I_1 + j_1$; $\pi_0(-1)^\ell = \pi = \pi_1(-1)^{\ell_1}$.

where π_0 is the parity of the target nucleus ground state.

The total emission spectrum of particle ν in the first cascade of reaction is written as :

$$\frac{\partial\sigma_{\nu_0\nu_1}}{\partial E_1}(E_1, I_1, \pi_1)\Delta E_1 = q_\nu\frac{\partial\sigma^{eq}_{\nu_0\nu_1}}{\partial E_1}(E_1, I_1, \pi_1)\Delta E_1 + \frac{\partial\sigma^{pre}_{\nu_0\nu_1}}{\partial E_1}(E_1)\Delta E_1 +$$

$$+\sigma^{dir}_{\nu_0\nu_1}(E_1, I_1, \pi_1); \qquad (2.2)$$

where :

$$q_\nu = 1 - \frac{1}{\sigma_a}\left[\sum_{E_1 I_1\pi_1}\sigma^{dir}_{\nu_0\nu_1}(E_1, I_1, \pi_1) + \int_{E_1}\frac{\partial\sigma^{pre}_{\nu_0\nu_1}}{\partial E_1}(E_1)\,dE_1\right]$$

In order to compare the spectrum with the experimental data it is further summed over I, π :

$$\frac{\partial\sigma_{\nu_0\nu_1}}{\partial E_1}(E_1)\Delta E_1 = \sum_{I\pi}\frac{\partial\sigma_{\nu_0\nu_1}}{\partial E_1}(E_1, I_1, \pi_1)\Delta E_1 \qquad (2.3)$$

The emission spectrum of particle ν_2 in the second cascade of reaction is as follows:

$$\frac{\partial\sigma_{\nu_0\nu_1\nu_2}}{\partial E_2}(E_2, I_2, \pi_2)\Delta E_2 = \sum_{I_1\pi_1}\int_0^{E^{max}}\frac{\partial\sigma_{\nu_0\nu_1}}{\partial E_1}(E_1, I_1, \pi_1)\,dE_1\cdot$$

$$\cdot\frac{\sum_{\ell_2 j_2} T^{I_1\pi_1}_{\ell_2 j_2}(E_2)\,\rho(U_2, I_2, \pi_2)}{N(U_1, I_1, \pi_1)}; \qquad (2.4)$$

where: $E^{max} = E_c - B_{\nu_1} - B_{\nu_2} - E_2$;

$|I_2 - j_2| \le I_1 \le I_2 + j_2$; $\quad |\ell_2 - s_2| \le j_2 \le \ell_2 + s_2$.

The particle spectrum in the first cascade of the reaction, wich is followed by gamma emission (for example $(n,n'\gamma)$ may be written as :

$$\frac{\partial \sigma_{\nu_0 \nu_1}}{\partial E_1}(E_1)\Delta E_1 = \sum_{I_1 \pi_1} \frac{\partial \sigma_{\nu_0 \nu_1}}{\partial E_1}(E_1, I_1, \pi_1) \sum_{I' \pi'} \int_0^{E_1^{max}} \frac{\sum_{\kappa_c} T_{\gamma \kappa_c}^{I_1 \pi_1}(E_2)\, \rho(E_c - B_{\nu_1} - E_1 - E_2, I' \pi')}{N(E_1, I_1, \pi_1)}$$

where $E_\gamma^{max} = E_c - B_{\nu_1} - E_1$. (2.5)

The corresponding reaction cross-sections can be obtained by integration of the spectrum over the energy of the emitted particle.

All the cross-section types, described in paragraph 1, except the activation cross-section, can be calculated using this approach. In order to calculate the activation cross-section one has to compute the cumulative population of the residual nucleus levels due to the gamma-cascades :

$$\rho_f^{I\pi}(E_f, I_1, \pi_1) = \frac{T_{\gamma \kappa_c}^{I\pi}\, \rho(E - E_\gamma, I_1, \pi_1)}{N(E, I, \pi)}; \qquad (2.6)$$

The contribution of the nonequilibrium mechanisms in the total emission spectrum can be calculated in the frameworks of the preequilibrium and direct reaction models.

The preequilibrium spectrum of the nucleons may be written in a simple closed form approach [2] :

$$\frac{\partial \sigma_{\nu_0 \nu_1}}{\partial E_1}(E_1)\Delta E_1 = \sigma_a \sum_{\substack{n=n_0 \\ (\Delta n = 2)}}^{\bar{n}} p_n^x \frac{\omega_{n-1}(u)}{\omega_n(E_c)} \frac{\lambda_{em}(E_1, n)}{\int_0^{E_c - B_\nu} \lambda_{em}(E', n)\, dE' + \lambda_+(E_c, n)} \qquad (2.7)$$

where σ_a is the incident particle absorption cross-section;

p_n^x is the relative probability of the occurence of particle x in the n-exciton state;

$\lambda_{em}(E_1, n)$ is the rate of emission of particle ν_1 with energy E_1 in n-exciton state :

$$\lambda_{em}(E_1, n) = \frac{(2S_\nu + 1)\, \sigma_{inv}(E_1)\, m_\nu\, E_1\, dE_1}{\pi^2 \hbar^3} \qquad (2.8)$$

$\sigma_{inv}(E_1)$ is the inverse reaction cross-section;

$\lambda_+(E_c, n)$ is the average rate of trasition from n to n+2 exciton state.

$$\lambda_+(E_c, n) = \frac{2\pi}{\hbar} |\bar{M}|^2 \frac{g^3 E_c^2}{p+h+1} \qquad (2.9)$$

where $|\bar{M}|^2$ is the mean matrix element of a two-particle interaction;

p,h are the numbers of particles and holes in a state n.

The density of the exciton states is given by formula:

$$\omega_n(u) = \frac{g^n u^{n-1}}{p!\, h!\, (p+h+1)} \qquad (2.10)$$

where g is the mean density of single particle states.
Taking into account (2.8)-(2.10) and the fact that λ_+ in the denominator (2.7) dominates on the initial stage of reaction, the final formula may be written as:

$$\frac{\partial \sigma_{\nu_0 \nu_1}}{\partial E_1}(E_1)dE_1 = \sigma_a \frac{(2S_{\nu_1} + 1) m_{\nu_1} \sigma_{inv}(E_1) E_1\, dE_1\, g_r}{4\pi^3 \hbar^2 |\bar{M}|^2 g_c E_c^3} \sum_{n=5} \left(\frac{g_c u}{g_c E_c}\right)^{n-2} p_n^x (n-1) \qquad (2.11)$$

The only unknown parameter in this formula is $|\bar{M}|^2$. One of the two following parametrizations of $|\bar{M}|^2$ is used in practice :

a) $|\bar{M}|^2 = FM \cdot A^{-3} E^{-1}$

b) $|\bar{M}|^2 = \alpha A / g^4$

In the latter case it is assumed that $g_r = g_c = g$ and $|\bar{M}|^2$ does not depend upon the excitation energy and individual properties of the nucleus. A satisfactory description of the high energy part of the emission spectrum has been achieved using parametrization (b) for reactions (n,p) and (n,n') at the neutron incident energies 10-20 MeV [3,5] .

At the energies considered here the most important contribution to the direct interaction gives the inelastic scattering with excitation of the collective states. This contribution can be calculated in the frameworks of the coupled channed method or the DWBA. Another direct mechanism the contribution of wich increases with the energy is the multistep scattering of the incident particle on the nucleons of the nucleus. According to the existing terminology we shall name this process the multy-step direct mechanism, and the process described by (2.11) we shall name the multy-step compound mechanism [6] .

Comparision of the calculated emission spectra and the re - action excitation functions with the experimental data are shown in Fig. 1.

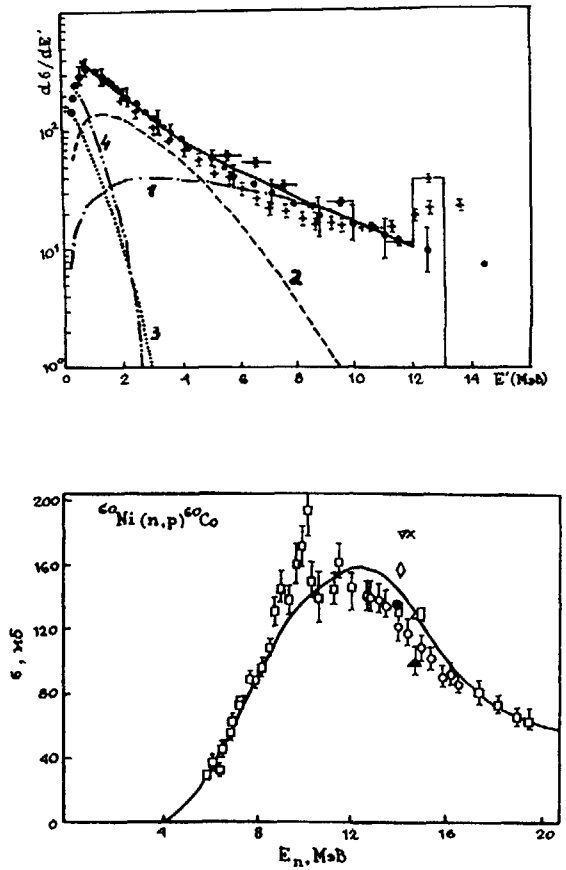

Fig. 1. Neutron emission spectrum and (n,p) reaction excitation function on Ni.
(1,2 - preequilibrium and equilibrium spectrum of the first emitted neutron,
3, 4 - the second neutron in reactions (npn) and (n2n)).

3. Parameters of the nuclear models and the accuracy of the theoretical predictions.

The results of calculations are the most sensitive to the parameters of the level density model. The most widely used in practice is Fermi-gas formula with "back shift" [10] :

$$\rho(U,I,\pi) = \frac{1}{2}\rho(U,I)$$

$$\rho(U,I) = \frac{1}{24\sqrt{2}}\,\frac{2I+1}{\sigma^3 a^{1/4}}\,\frac{\exp\{2\sqrt{a(U-\delta)}\}}{(U-\delta+t)^{5/4}}\,\exp\left\{-\frac{I(I+1)}{2\sigma^2}\right\} \qquad (3.1)$$

$$\sigma^2 = \frac{6}{\pi^2}\langle m^2\rangle\sqrt{a(U-\delta)}\;;\quad \langle m^2\rangle = 0.24\,A^{2/3}$$

t is derived from the equation: $U-\delta = at^2 - t$.

The particle transmission coefficients are obtained in the frameworks of the optical model. A modern survey of the global optical model parameters has been published in [9] .

The results of calculations are less sensitive to the optical model parameters than to the level density parametrs; the dependence from the transmission coefficients is more pronounced inthe weak reaction channels.

The gamma-ray transmission coefficients are connected to the radiative strength function $f_{\chi L}(\varepsilon_\gamma)$ as:

$$T_{\chi L}(\varepsilon_\gamma) = 2\pi\, f_{\chi L}(\varepsilon_\gamma)\,\varepsilon_\gamma^{2L+1}\;; \qquad (3.2)$$

In the nuclear excitation energy range considered here the most significant contribution to the radiative width gives E1 transition. When using a selfconsistent parameters of the lewel density formula and the average lewel distance at the neutron binding energy $\langle D_0\rangle$, the average radiative widths for $A > 80$ are satisfactorily described with the strength function:

$$f_{E1}(\varepsilon_\gamma) = C_0\,\frac{A\,\varepsilon_\gamma\,\Gamma_R}{(\varepsilon_\gamma^2 - E_R^2)^2 + \varepsilon_\gamma^2\Gamma_R^2} \qquad (3.3)$$

where Γ_R = 5 MeV, E_R = 80 $A^{-1/3}$MeV, Co = $100/A^{3/2}$MeV^{-2} . On the basis of the comparision of the thoretical calculations with the experimental data we can conclude, that the most reliable are the theoretical predictions for the strong channels of the reaction

(first of all the neutron channels: (n,n'), (n,2n)). In this case the accuracy of the predicted total cross-sections can be as good as 10%. For the weak channels (for example (n,p), (n,α), (n,np)) it is probably impossible at present stage to obtain reliable results without some additional fitting to the experiment.

The theoretical approach discribed above was used together w with the systematics of neutron cross-sections at E_n = 14.5 MeV in creation of the threshold reaction cross-section library "BOSPOR" [7].

4. Systematics of the threshold reaction cross-sections at E_n = 14 MeV.

The majority of the threshold reaction cross-sections measurements has been done at the neutron energy 14-15 MeV. Systema - tizing the available experimental data we can observe some defi - nite dependencies of cross-sections from Z and A of the target nucleus.

In 1964 V.Levkovski [11] proposed the following simple (N-Z) dependence of the (n,p) and (n,α) reaction cross-sections:

$$\sigma_{np} = 0.73\,\sigma_a \cdot \exp\left(-33\,\frac{N-Z}{A}\right) \quad (mb)$$
$$\sigma_{n\alpha} = 0.29\,\sigma_a \exp\left(-33\,\frac{N-Z}{A}\right) \quad (mb) \qquad (4.1)$$

where: σ_a is the neutron absorption cross-section,

$$\sigma_a = \pi r_0^2 \left(A^{1/3}+1\right)^2 ; \quad r_0 = 1.4\cdot 10^{-13}$$

The empirical (N-Z) dependence was also found for (n,2n) reaction cross-section:

$$\sigma_{n2n} = \sigma_a \left(1 - k \exp\left\{-m\,\frac{N-Z}{A}\right\}\right) \qquad (4.2)$$

where k = 1.812 and m = 12.09.

The theoretical interpretation of isotopical dependence of (n,p) and (n,2n) cross-sections has been done in [7,8].

For (n,2n) reaction it is asumed that:

$$\sigma_{n2n} = \sigma_{n2n}^{eq} + \sigma_{n2n}^{neq} \qquad (4.3)$$

Having used the Weisskopf-Ewing model to express σ_{n2n}^{eq} and the exciton model to estimate σ_{n2n}^{neq}, we obtain:

$$\sigma_{n2n}^{eq} = \sigma_{nM}^{eq}\left[1-\left(1+\frac{E_n-S_n}{T}\right)e^{-\frac{E_n-S_n}{T}}\right] \qquad (4.4)$$

where: Sn is the neutron binding energy,

$T \simeq \sqrt{\frac{E_n-\delta}{a}}$ is the nuclear temperature;

$$\sigma_{nM}^{eq} = \sigma_a - \sigma_{np} - \sigma_{n\alpha} ; \quad \sigma_{n2n}^{neq} = \sigma_{nn'}^{pre}\,\frac{E_n-S_n}{E_n} \qquad (4.5)$$

Having used Weizsachker's formula to determine Sn, we obtain:

$$W_{A,Z} = \alpha A - \beta A^{2/3} - \gamma\frac{Z^2}{A^{1/3}} - \varepsilon\frac{(A/2-Z)^2}{A} + \delta ;$$
$$S_n = W_{A,Z} - W_{A-1,Z} = -\frac{\varepsilon}{2}\frac{N-Z}{A} + \Delta_n ; \qquad (4.6)$$

where $\frac{\varepsilon}{2}$ = 47.4 MeV, $\Delta_n = (\alpha + \delta_{A,Z} - \delta_{A-1,Z})$.

Taking into account, that E_n = 14.5 MeV, $T = 10/\sqrt{a} \simeq 1$ MeV, $\Delta_n \simeq 16.5$ MeV, we obtain:

$$\sigma_{n2n} = \sigma_{nM}\left\{0.68 + \frac{N-Z}{A} - 5.2\left[\frac{\varepsilon}{2}\frac{N-Z}{A} - 1\right]e^{-\frac{\varepsilon}{2}\frac{N-Z}{A}}\right. \qquad (4.7)$$

where $\sigma_{nM} = \sigma_a\left[1-e^{-33\frac{N-Z}{A}}\right]$.

(N-Z) dependence of σ_{np} cross-section is deduced by applying the detailed balance method:

$$\sigma_{np} = \sigma_a \int_0^{E_p^{max}} W_{cp}(E)\,dE \qquad (4.8)$$

where $E_p^{max} = E_n + S_n - S_p$; $W_{cp} = \frac{N_p}{N_c} W_{pc}^{*}$

W_{ep} (E) is the proton emission rate from the compound nucleus;
W_{pc}^{*} (E) is the probability of the inverse process (e.g. proton absorption by the residual nucleus);
Nc, Np are the densities of states before and after the proton emission.

Expressing Nc and Np through the level density in the Fermi-gas model and $W^{*}_{pc}(E)$ through the cross-section for inverse process $\sigma_p(E)$, and assuming, that:

$$\sigma_p(E) = \begin{cases} 0. & E < B_k \\ \pi R^2 \left(1 - \frac{B_k}{E}\right) & E \geq B_k \end{cases} \qquad (4.9)$$

where R is the nucleus radius and Bk is the coulomb barrier, we obtain :

$$\sigma_{np} = C_1 \sigma_a \exp\left\{\sqrt{\frac{a}{E_n}}\left(-S_p - B_k + \delta\right)\right\} \qquad (4.10)$$

S_p is determined using Weizsäcker's formula:

$$S_p = W_{A+1,Z} - W_{A,Z-1} = \alpha - \beta\frac{2Z-1}{A^{1/3}} + \frac{\varepsilon}{2}\frac{N-Z+1}{A} + \Delta_p \qquad (4.11)$$

Substituting S_p and $B_k \simeq 0{,}2\beta\frac{2Z-1}{A^{1/3}}$ in-to (4.10) we obtain the final expression:

$$\sigma_{np} = C_1 \sigma_a \exp\left\{\sqrt{\frac{a}{E_n}}\left(-\frac{\varepsilon}{2}\frac{N-Z+1}{A} + 0{,}8\beta\frac{Z-1}{A^{1/3}} - \Delta\right)\right\} \qquad (4.12)$$

It is clear from the equation (4.12) that the isotopical depen - dence of the (n,p) cross-section is due to (N-Z) dependence of the proton binding energy in the target nucleus.

The values of the parameters of formula (4.12) are as follows:

$C_1 = 0{,}706$; $\varepsilon/2 = 50$; $\beta = 0{,}73$($0{,}8\beta = 0.58$), $\Delta = 3.26$. The neutron energy is taken to be 14.5 MeV and level density parameter a is approximated as $A/10$ MeV^{-1}. Formula 4.12 gives results agreeng to wi-thin 20% with the experimental data for 80% of the nuclei considered. Figure 2 compares the isotopic dependence of σ_{np} at energies of 14-15 MeV predicted by Levkovski formula (dashed line) and by formula (4.12) (solid line).

It is important to note that formula (4.12) was deduced assuming the nonequilibrium mechanism of the reaction and taking into account only the first cascade of particle emission. This approach is valid mainly for medium and heavy nuclei ($A > 80$). For nuclei with $a \approx 80$ we must bear in mind that the compound nucleus mechanism (or equilibrium mechanism) dominates in the reaction,

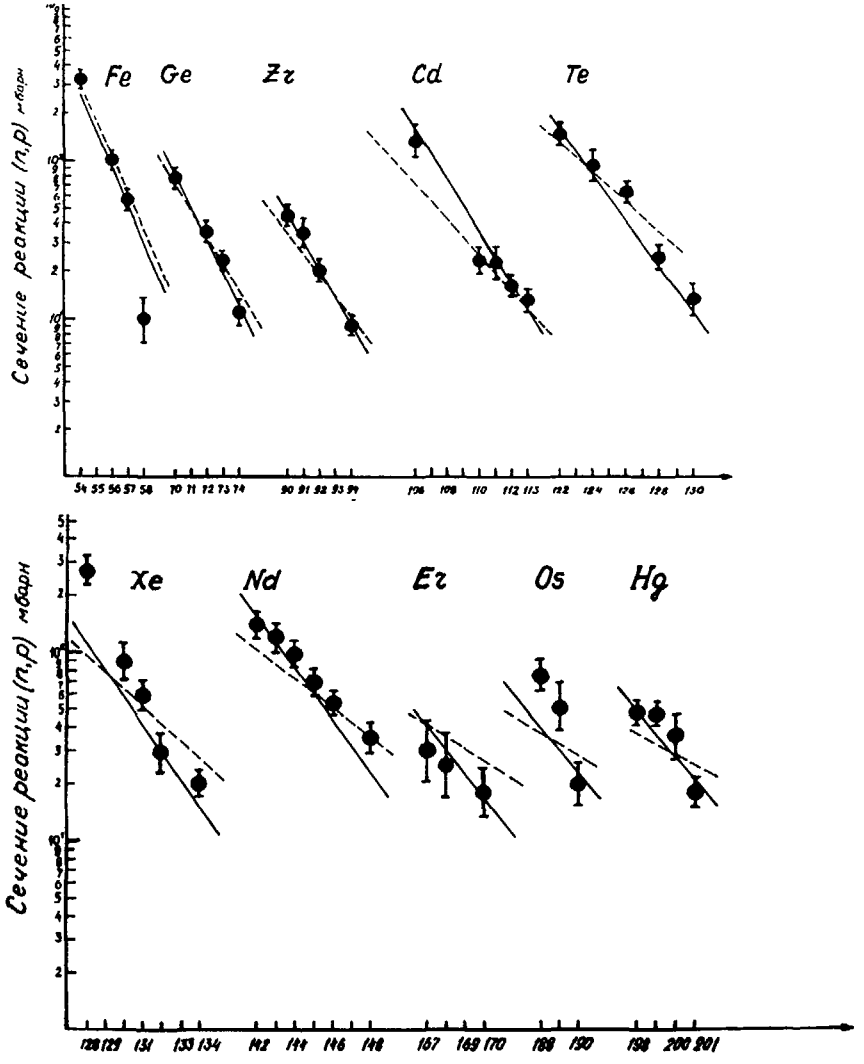

Fig. 2. Isotopic dependence of σ_{np} cros-section at E_n = 14.5 MeV.
- . - - Levkovski's formula
——— - present work

and at the energy E_n = 14-15 Mev the second cascade of the reaction can be open (e.g. $\sigma_{np} = \sigma_{np\gamma} + \sigma_{npn}$). In this case we must rewrite equation (4.8) as:

$$\sigma_{np} = \sigma_a \frac{\Gamma_p}{\Gamma_n + \Gamma_p} \simeq \sigma_a \frac{\Gamma_p}{\Gamma_n} \quad \text{(assuming } \Gamma_p < \Gamma_n\text{)}. \qquad (4.13)$$

where Γ_p, Γ_n are the proton and neutron emission widths in Weisskopf -Ewing model.

Using againg Fermi-gas model of level density and formula (4.9) to estimate $\sigma_p(E)$ we obtain:

$$\sigma_{np} = C_1 \sigma_a \exp\left\{ \sqrt{\frac{a}{E_n}} \left(- Q_{np} - B_k + \delta' \right) \right\} \qquad (4.14)$$

In this formula σ_{np} depends on reaction energy Qnp, but not on the proton binding energy as in (4.10). Having used Weizsatcker's formula to determine Qnp, we obtain:

$$\sigma_{np} = C_1 \sigma_a \exp\left\{ \sqrt{\frac{a}{E_n}} \left(- \varepsilon \frac{N-Z+1}{A} + 0.8 \frac{Z-1}{A^{1/3}} + \Delta' \right) \right\} \qquad (4.15)$$

As it is seen from formula (4.15) we shall expect twice a stronger isotopic dependence of σ_{np} for light mass nuclei than it is given by formula (4.12). This is demonstrated on Fig.3 where experimental data on $\sigma_{np} = \sigma_{np\gamma} + \sigma_{npn}$ are plotted.

Similar (N-Z) systematics exist for other neutron threshold reaction at energy E_n = 14-15 MeV. A modern survey of these data is given in [12] .

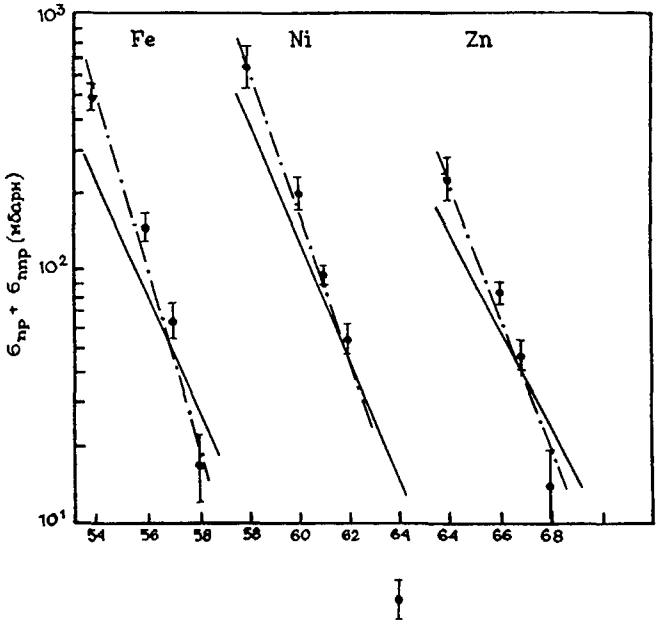

Fig. 3. Isotopic dependence of $\sigma_{np} + \sigma_{npn}$ at E_n = 14.5 MeV on light nuclei - formula.

REFERENCES

1. W.Hauser, H.Feshbach. Phys.Rev. 87,366, 1952.
2. C.K.Cline, M.Blann. Nucl.Phys. A172, 225, 1971.
3. G.M.Braga-Mareazzan et al. Phys.Rev. C6,(4), 1398, 1972.
4. L.Milazzo-Colli, G.M.Braga-Marcazzan. Nucl.Phys. A210,297,1973.
5. V.Plyaskin, V.Trykova. Voprosy atomnoj nauki i tekniki. Ser. Yadernye konstanty. 21, 62 (1976).
6. C.Kalbach. Phys.Rev. C23, 124, 1981.
7. V.Bychkov et al. INDC(CCP)-146/LJ, IAEA, 1980.
8. V.Bychkov et al. Preprint FEI - 809, Obninsk, 1978.
9. P.Young. NEANDC-222 "U", p. 127, Paris 1985.
10. W.Dilg, W.Schantl, H.Vonach. Nucl.Phys. A217, 269, 1973.
11. V.Levkovski, Zh. Eksp. Teor. Fiz. 18, 213, 1964.
12. R.A.Forrest. Report AERE R 12419, 1986.

LEVEL DENSITY OF EXCITED NUCLEI

A.V. IGNATYUK
Institute of Physics and Power Engineering,
Obninsk, Union of Soviet Socialist Republics

Abstract

The paper describes the development of level density theory for excited nuclei, taking into account the shell, superfluid and collective characteristics of nuclei.

Many contempory ideas concerning the properties of atomic nuclei have been based on research into the ground and low-lying states of nuclei. With the gradual refinement of nuclear theory, increasingly successful descriptions of the structure of low-lying levels have been obtained. However, at higher excitation energies there is such a rapid increase in the number of nuclear levels that spectroscopic analysis of each one becomes impracticable. Under these conditions it is both natural and legitimate to change to a statistical description of the number of excited levels in which the main statistical characteristic of the nucleus is the excited level density.

Simple analytical relationships for the state density $\rho(U)$ of a nucleus with a given excitation energy U and for the level density $\rho(U,J)$ of a nucleus with a given angular momentum J are obtained using the Fermi-gas model [1]:

$$\rho(U) = \frac{\sqrt{\pi}}{12\, a^{1/4} U^{5/4}} \exp\left(2\sqrt{aU}\right)$$

$$\rho(U,J) = \frac{2J+1}{2\sqrt{2\pi}\,\sigma^3} \rho(U) \exp\left\{-\frac{J(J+1)}{2\sigma^2}\right\} \qquad (1)$$

Here σ is the spin dependence parameter and $a = \pi^2 g/6$ is the level density parameter, which is proportional to the single-particle state density g near to the Fermi energy.

In the Fermi-gas model the state equations determining the dependence of the excitation energy U, the entropy S and the other thermodynamic functions of the nucleus on its temperature t also have a simple form:

$$U = at^2 \quad , \quad S = 2at \quad , \quad \sigma^2 = m_f^2 g t \qquad (2)$$

Here, m_f^2 is the mean square value of the projection of the angular momentum of single-particle states close to the Fermi energy, which can also be related to the moment of energy of the heated nucleus $\mathcal{J}_0 = g m_f^2$. The interrelationship between the thermodynamic functions (2) and the state density of the excited nucleus (1) is clear. In a quasic-classical approximation it is a simple matter to evaluate the main parameters of the Fermi-gas model:

$$a = 2\left(\frac{J}{3}\right)^{1/3} \frac{\mu r_0^2}{\hbar^2} A \quad , \quad \mathcal{J}_0 = \frac{2}{5} \frac{\mu r_0^2}{\hbar^2} A^{5/3} \qquad (3)$$

where μ is the nucleon mass, r_0 is the radial parameter and A is the mass number.

The most direct information on the level density of highly-excited nuclei is obtained from experimental neutron resonance density data. Many laboratories have collected such information, and compilations of data on the mean observed distance between resonances D_ℓ can be found in Refs [2, 3].

For the majority of nuclei, the observed resonances correspond to neutrons with zero orbital moment (so-called s-neutrons), therefore the value of D_s is related to the excited-level density of the compound nucleus by the relationship:

$$D_s^{-1} = \begin{cases} \frac{1}{2}\left\{\rho(B_n+\Delta E/2, I_0+1/2)+\rho(B_n+\Delta E/2, I_0-1/2)\right\} & \text{for } I_0 = \neq 0, \\ \frac{1}{2}\rho(B_n+\Delta E/2, 1/2) & \text{for } I_0 = 0 \end{cases} \qquad (4)$$

where B_n is the neutron binding energy, ΔE is the magnitude of the energy interval for which the resonances are being examined, I_0 is the target nucleus spin, and the coefficient 1/2 before the sum takes into account the fact that s-neutrons form resonances only of a particular parity. If necessary, resonances for p-neutrons too can be taken into consideration analogously.

The experimental values of D_s are normally used as source data, from which the magnitude of the level density parameter can be derived by means of relationships (1) and (4).

Many authors have carried out such an analysis [4-8]. Early papers on the systematization of experimental data had already noted regular differences in the level density of even-even, odd and even-odd nuclei analogous to the differences in the binding energies of these nuclei. In order to take this effect into account in the Fermi-gas model relationships, it is usual to introduce the so-called effective excitation energy, defined as:

$$U^* = U - \begin{cases} \delta_Z + \delta_N & \text{for even-even nuclei,} \\ \delta_Z & \text{for nuclei with even Z,} \\ \delta_N & \text{for nuclei with even N,} \\ 0 & \text{for odd-odd nuclei,} \end{cases} \qquad (5)$$

where δ_τ is the corresponding phenomenological correction for even-odd differences in nuclear binding energies [4]. The values obtained in this analysis for the level density parameter are shown in the upper part of Fig. 1 in the form of the ratio a/A. The values obtained differ greatly from the quasi-classical evaluation (3). In the lower part of Fig. 1 the shell corrections to the nuclear mass formula are given, determined by the

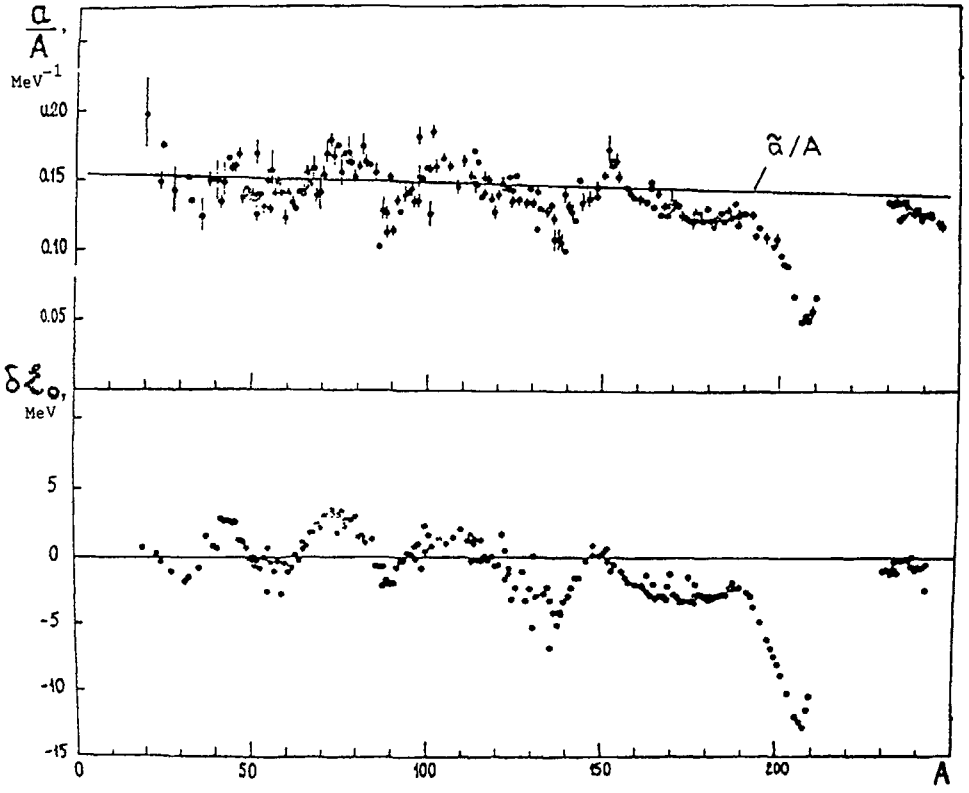

Fig. 1. Relation of the Fermi-gas level density parameter a to the mass number (above) and shell correction to the mass formula (below).

relationship:

$$\delta\xi_0 = M_{exp}(Z,A) - M_{KM}(Z,A,\beta) \qquad (6)$$

where M_{exp} is the experimental value of the mass defect, and M_{KM} is its liquid drop component calculated for the equilibrium deformation of nuclei β (9). The clear correlation of the ratio a/A and the shell corrections is a direct indication of the important role of shell effects in the description of the level density and other statistical characteristics of excited nuclei.

With the gradual accumulation of measurement results for low-lying level spectra over a wide range of nuclei, it has become possible to use data on the observed rate of increase in the total number of levels to analyse level density behaviour in the low-energy region [4, 8]. An extrapolation into this region of the Fermi-gas dependence with parameters found from neutron resonance density analysis does not, as a rule, describe the experimental data. It has been noted that the observed energy dependence of the cumulative number of levels N(U) is described much better by the law:

$$N(U) = \exp\{(U-U_0)/T\} \qquad (7)$$

where U_0 and T are free parameters determined by fitting to the corresponding data. The quantity N(U) is related to the level density by the relationship:

$$\rho_{lev}(U) = \frac{dN}{dU} = \frac{1}{T}\exp\{(U-U_0)/T\} \qquad (8)$$

and it is easy to see that in the physical sense the parameter T simply corresponds to the nuclear temperature. Since the value of this parameter is assumed to be constant in the energy range considered, relationship (8) has been called the constant temperature model.

In order to obtain a description of the level density for the whole range of excitation energies from zero to the neutron binding energy, the low-energy dependence (8) has been "joined" to the Fermi-gas dependence of the level density (1) in some papers [4, 8]. The link between both models' parameters can be found in this case from the condition of continuity of the function itself and of its first derivatives at the joining point.

$$U_0 = U_x - T\ln\rho_{FG}(U_x), \quad T^{-1} = \sqrt{\frac{a}{U_x^*}} - \frac{3}{2U_x^*} \qquad (9)$$

Here U_x^* is the effective energy of the joining point taking account of corrections (5) for the even-odd effects. An analysis of experimental data within the framework of this phenomenological approach has been carried out in Refs. [4, 8], and Fig. 2 shows the systematization of the values obtained for

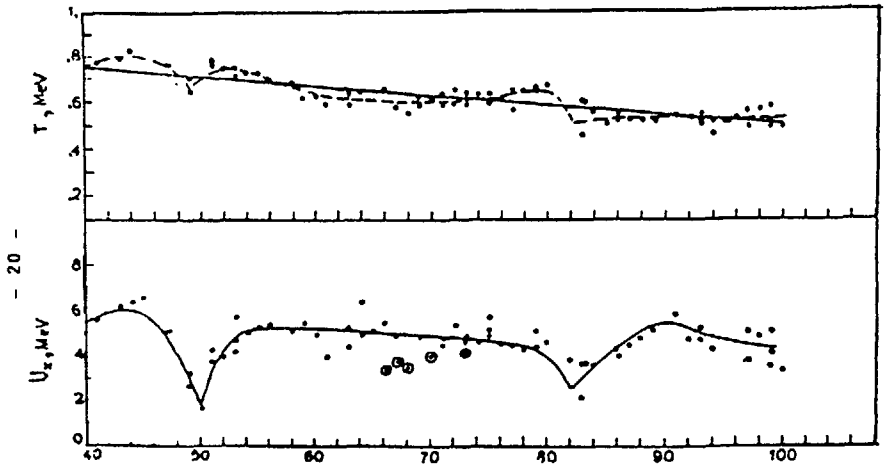

Fig. 2. Dependence of the nuclear temperature T and the excitation energy below which the level density behaviour approximates to the constant temperature model on the number of neutrons [8].

the nuclear temperature and energy U_x. The value in fact determines the energy below which the description of the level density in the Fermi-gas model with determination of the effective excitation energy in the neutron resonance region becomes unsatisfactory, and it can be seen that for the majority of nuclei this energy is rather high.

In Refs [7, 10], a rather different approach is developed to the problem of simultaneous parametrization of neutron resonance density and low-lying nuclear level density. It has been shown that both sets of experimental data can be described on the basis of Fermi-gas model relationships if, for each nucleus, both the level density parameter a and also the displacement δ_{ef} are used as free parameters in determining the effective excitation energy (5). Since for odd-odd nuclei the displacement thus found is negative, the above approach has been described as the Fermi-gas model with backward displacement [10]. In Ref. [7] all experimental data on low-lying nuclear levels and neutron resonance density were analysed using this model, and the empirical values of the parameter a and the quantity δ_{ef} were found for the entire range of mass numbers. In view of the redetermination of the effective excitation energy, the values obtained for the parameter are naturally somewhat lower then those shown in Fig. 1. However, the general picture of dependence of the level density parameter on the mass number is not significantly altered by this.

For a number of nuclei the existing experimental data on the spin of low-lying levels can be used to analyse the excited-level distribution in terms of angular momentum [7]. The level density dependence on angular momentum (1) obtained on statistical considerations agrees rather well on the whole with the experimental data. However, the number of levels with identified spins is still comparatively low, and the errors in the values found for the spin dependence parameter are quite significant.

On the whole, this discussion leads to the conclusion that the Fermi-gas model relationships are a comparatively simple and convenient method for parametrizing the experimental data on nuclear level density. The model itself, however, does not give any explanation for the shift in excitation energy and the even-odd differences in level density, or for the differences between the experimental values of the level density parameter and quasi-classical evaluations. An interpretation of all these properties can be provided on the basis of more rigorous methods of calculating the nuclear level density, taking into account the shell inhomogeneities in the single-particle level spectrum, on the one hand, and including consideration of superfluid and collective effects due to effective interaction of nucleons, on the other [11-13]. A detailed discussion of these methods can be found in the monograph [13]. Rigorous microscopic methods for calculating level density are extremely laborious, however, and this severely limits their possibilities for practical application to experimental data analysis. For this reason there is an urgent need for a level density description to be developed which would take basic ideas concerning the structure of highly-excited nuclear states into account to the extent required while at the same time being sufficiently simple and convenient for practical application.

The influence of superconducting-type pair correlations on nuclear properties can be characterized by the value of the correlation function Δ_o, which directly determines the even-odd differences in nuclear mass and the magnitude of the $2\Delta_o$ gap in the spectrum of quasi-particle excitations of even-even nuclei. The critical temperature t_{cr} of the phase transition from the superconducting (superfluid) state to normal is also related to the correlation function:

$$t_{cr} = 0.567\ \Delta_o \tag{10}$$

The excitation energy corresponding to the critical temperature is:

$$U_{cr} = 0.472\ a_{cr}\Delta_o^2 - n\Delta_o \tag{11}$$

where n = 0, 1 and 2 for even-even, odd and odd-odd nuclei, respectively. Above the critical energy the excited state density and other thermodynamic nuclear functions can be described by Fermi-gas relationships in which it is essential to use the excitation energy:

$$U^* = U - E_{cond} \tag{12}$$

Here, E_{cond} is the condensation energy, determining the lowering of the system's ground state as a result of correlation effects. In the continuous spectrum approximation it is described by the relationship:

$$E_{cond} = 0.152\ a_{cr}\Delta_o^2 - n\Delta_o \tag{13}$$

Below the phase transition point (10), the expressions for the thermodynamic functions of the nucleus are complex in form, and they will not be considered here. Suitable expressions for practical calculations can be found in Refs [13, 14]. The differences between the characteristics determining the level density energy dependence in the superfluid model of the nucleus and in the Fermi-gas model are clear from the results of calculations using the continuous spectrum approximation, shown in Fig. 3. This diagram also shows the energy dependences of the temperature and the parallel moment of inertia $\mathcal{J}_{\parallel}$.

The shell inhomogeneities of the single-particle spectrum lead to a particular energy dependence of the level density parameter a(U). The shell effects on the level density become weaker with an increase in excitation energy, and for sufficiently high energies the dependence of parameter a on the mass number tends to the quasi-classical value (3). These important features of the behaviour of the level density parameter can be explained in general terms by the shell correction method [11, 13]. The clear correlation of shell corrections (6) with the values of a/A in the experimental data (Fig. 1) can be used to construct a phenomenological systematization of variations in the level density parameter of the Fermi-gas model [14]. The basis of this systematization is the relationship:

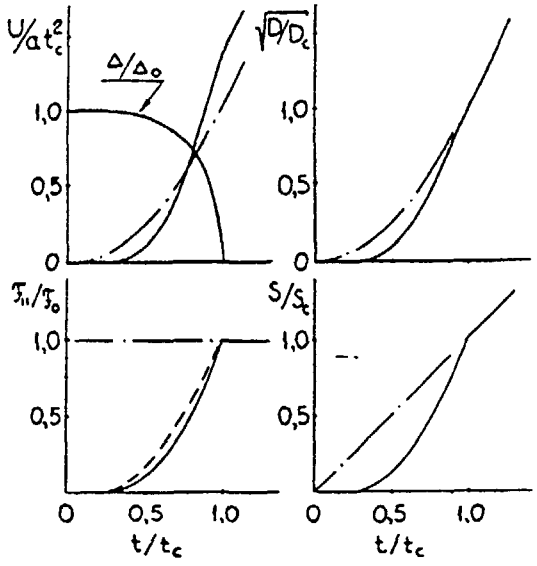

Fig. 3. Temperature dependence of the thermodynamic characteristics of the superfluid model of the nucleus (continuous curves) and the Fermi-gas model (dot-dashed curve).

$$a(U,Z,A) = \begin{cases} \tilde{a}(A)\{1 + \delta\Sigma_0(Z,A)\, f(U^*)/U^*\} & \text{for } U \geq U_{cr} \\ a_{cr}(U_{cr},Z,A) & \text{for } U < U_{kp} \end{cases} \quad (14)$$

in which â corresponds to the asymptotic value of the level density parameter at high excitation energy, and the dimensionless function $f(U) = 1 - \exp(-\gamma U)$ determines the parameter's energy behaviour at lower excitations.

When considering coherent effects of a collective nature the expression for the level density can be presented in the form

$$\rho(U,J) = \rho_{qp}(U,J)K_{vibr}(U)K_{rot}(U) \quad (15)$$

where ρ_{qp} is the density of quasi-particle (non-collectivized) excitations of the nucleus; and K_{vibr} and K_{rot} are coefficients for level density enhancement due to vibrational and rotational excitations, respectively.

In the adiabatic approximation [15], the coefficient K_{rot} is determined by the form of the nucleus:

$$K_{rot} = \begin{cases} 1 & \text{for spherical nuclei,} \\ \mathcal{I}_\perp t & \text{for deformed nuclei.} \end{cases} \quad (16)$$

This evaluation was made on the assumption of mirror and axial symmetry of the deformed nuclei. The known stable nuclei in the mass regions of the rare earth elements $150 \leq A \leq 190$ and the actinides $A \geq 230$ have this form. For non-axial forms, such as fissile actinide nuclei may have at the top of the barrrier, the rotational enhancement of the level density becomes even greater [15];

The level density vibrational enhancement coefficient for the microscopic approach [13] is defined by the relationship

$$K_{vibr} = \prod_i \left\{ \frac{1 - \exp(-\omega_i^\circ/t)}{1 - \exp(-\omega_i/t)} \right\}^{g_i} \quad (17)$$

where ω_i is the energy of vibrational modes in the excited (heated) atom, ω_i° is the quasi-particle excitation energy corresponding to these modes, and g_i is the degeneracy of the collective modes. The presence of quasi-particle excitation energies in expression (17) tend to unity, and so only coherent collective excitations with a significant difference $\omega_i^\circ - \omega_i$ make a major contribution to K_{vibr}. Note that in the microscopic approach, the symmetry conditions of the nuclear Hamiltonian impose particular relations on the vibrational and rotational excitations, and as a result the adjusted microscopic calculations of K_{rot} may differ from the adiabatic evaluation.

In the case of sufficiently heated nuclei, evaluation of K_{vibr} is quite simple using the formula obtained for the liquid drop model

$$\tilde{K}_{vibr} = \exp\left\{ 1{,}694 \left(\frac{\rho_0}{t^2 a} \right)^{2/3} R_0^2 t^{4/3} \right\} \quad (18)$$

where α is the surface tension coefficient, and ρ_0 is the density of nuclear matter. If in (18) we put $\alpha = 1.2$ MeV/fm^2, corresponding to the phenomenological surface energy parameters of the mass formula [9], then for the level density in the region of neutron resonances we obtain $\tilde{K}_{vibr} \simeq 2\text{-}4$.

Using the model described above, the number of parameters characterizing the excited nucleus remains practically the same as for the Fermi-gas model. In Ref. [15] this approach was used to analyse experimental data on neutron resonance density. The experimental values of the shell corrections from Ref. [9] shown in Fig. 1 were used for $\delta\zeta_o$, and the correlation function of the nuclei was taken as $\Delta_o = 12/\sqrt{A}$ MeV. The optimum value of the parameter $\gamma = 0.064$ MeV^{-1} was determined by minimizing the deviations of the calculated level density values from the experimental values. The level density parameters $a(B_n)/A$ thus obtained, and also the corresponding asymptotic values of the parameters $\tilde{a}/A$, are shown in Fig. 4.

For the nuclear mass regions $150 \leq A \leq 190$ and $A \geq 230$, in which the rotational sequences of low-lying levels are clearly expressed, and also for spherical nuclei with $A \simeq 204$–210 near to the doubly magic isotope of lead, the values obtained for the parameter a cluster around the value $\tilde{a}/A = 0.094$ MeV^{-1}. However, in the region of transition nuclei $190 < A \lesssim 200$ there are systematic deviations from the expected asymptotic values of a. To illustrate these deviations more clearly, the lower part of Fig. 4 gives a comparison of the adiabatic evaluation of K_{rot} with those values of this parameter which would be required to obtain the observed neutron resonance density on the assumption that $\tilde{a}/A = 0.094$ MeV^{-1}. In the region of transition nuclei the required values of the coefficient K_{rot} are 2–3 times lower than the adiabatic evaluation, but significantly higher than the liquid-drop evaluation of the coefficients K_{vibr}. Thus, for transition nuclei the level density parameter description obtained should be applied with some care.

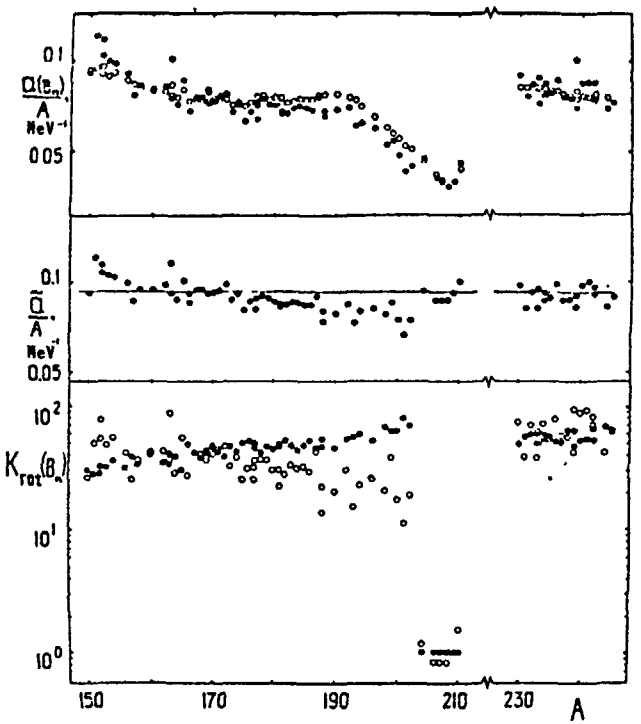

Fig. 4. Systematization of the relation of the level density parameter $a(B_n)$ to the mass number (above) and of the asymptotic values of this relation (middle), obtained from analysis of neutron resonance density (•) and on the basis of relationships (14) with a single set of parameters (°). The lower part of the diagram shows the values of $K_{rot}(B_n)$ corresponding to the experimental values for a/A (•) and the values for $a/A = 0.094$ MeV^{-1}(°).

At first glance, it may seem that the systematization of level density parameters established here is not very different from the neutron resonance density systematization based on the Fermi-gas model relationships (Fig. 1). But this is not the case: the lower values of the level density parameters obtained when collective effects are taken into account represent a major difference between these systems. These values agree well both with the results of theoretical calculations of the parameters using the Woods-Saxon potential levels scheme, and with experimental data derived from the spectra of inelastically scattered neutrons with energies of up to 7 MeV [15]. This agreement in the data is very important, as the evaporation spectra are sensitive precisely to the magnitude of the level density parameter, and not to the absolute value of the level density. Using the traditional Fermi-gas model without taking into account collective effects, it is impossible to explain the divergence between the values of the parameter a obtained from resonance data and from evaporation spectra. Proper consideration of collective effects is also very important if there is to be a consistent description of the probability of fission of higly-excited nuclei [16].

To extend the above approach to the nuclear mass region A < 150, it is necessary to obtain a more correct systematization than the liquid drop evaluation (18) for the vibrational increase in the level density of highly-excited nuclei. In Ref. [17] it was shown that, in analysing coherent effects in heated nuclei, the collective excitations must be characterized not only by their average energy, but also by a specific damping width. This width is determined by the dispersion of the collective mode intensity over nearly lying excitations of quasi-particle pairs, on the one hand, and by the fragmentation of the intensity over multi-quasi-particle excitations on the other hand. It is to be expected that collective excitation damping in nuclei would, to some extent, be similar to zero mode sound damping in the Fermi-liquid theory [18], i.e., that it can be described by the relationship:

$$\gamma(\omega) = \mathrm{const}\,(\omega^2 + 4\pi^2 t^2) \tag{19}$$

Taking damping into account, the level density vibrational enhancement coefficient can be written in the form:

$$K_{vibr} = \prod_{\lambda} \left\{ \frac{(1+e^{-\bar{\omega}_\lambda^\circ/t})^2 - 4e^{-\bar{\omega}_\lambda^\circ/t}\cos(\bar{\gamma}^\circ/2t)}{(1+e^{-\bar{\omega}_\lambda/t})^2 - 4e^{-\bar{\omega}_\lambda/t}\cos(\bar{\gamma}/2t)} \right\}^{\lambda+1/2} \tag{20}$$

where $\bar{\omega}_\lambda$ and $\bar{\omega}_\lambda^\circ$ are the average energies of multipole collective and incoherent two-quasi-particle excitations of the nucleus, respectively.

For a phenomenological description of the temperature dependence of the collective excitation energies we have used expressions from the simplest schematic model (the two degenerate levels model [19])

$$\bar{\omega}_\lambda = \left[\bar{\omega}_\lambda^\circ - \zeta(t)\,(\bar{\omega}_\lambda^\circ - \omega_\lambda^{exp})\right]^{1/2} \tag{21}$$

where ω_λ^{exp} represents the experimental values of the energy of the lowest collective levels of the nuclei, $\bar{\omega}_\lambda^\circ$ represents the mean energies of two-quasi-particle excitations in the shell model, and the function $\zeta(t) = \exp(-ct^2/\omega_\lambda^{exp})$ is determined on the basis of parametrization of theoretical calculations of the collective excitation energies of heated nuclei [20]. The temperature variations in the average

energies of collective 2^+ and 3^- excitations obtained in this approximation, as well as the corresponding level density vibrational enhancement coefficients for the nuclei ^{56}Fe and ^{60}Ni, are shown in Fig. 5. The values obtained for the coefficients K_{vibr} are close both to the results of microscopic calculations of the collective level density enhancement in the ^{56}Fe nucleus [12, 13], and to the results of empirical analysis of all experimental data available for this nucleus on the level density at different excitation energies [20].

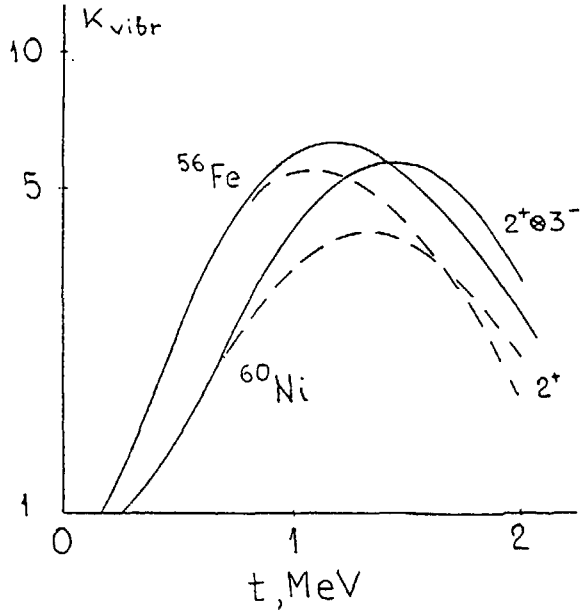

Fig. 5. Temperature dependence of the averaged energies of quadrupole (dashed curves) and actual excitations (dot-dashed curves) of ^{56}Fe and ^{60}Ni nuclei (above) and the level density vibrational enhancement coefficients corresponding to these excitations (below).

Figure 6 shows a level density description for iron-group nuclei over a broad range of excitation energies, and for comparison also the results of a

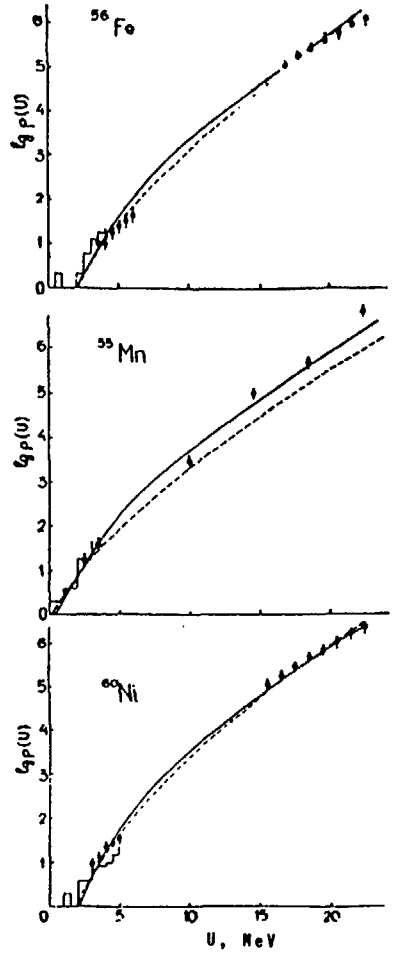

Fig. 6. Description of the level density energy dependence of nuclei in the iron group in the superfluid nucleus model taking into account collective effects (continuous curves) and for the backward displacement Fermi-gas model (dashed curves).

level density description using the Fermi-gas model [7]. In making this comparison, however, it is essential to bear in mind the fundamental difference between the descriptions used with regard to their approaches to the choice of parameters. In the Fermi-gas model the parameters a and δ for each nucleus examined are chosen independently on the basis of the available experimental data for $\rho(U)$. Consequently, these parameters serve purely for adjustment and their physical meaning may be substantially distorted by effects not considered in the Fermi-gas model. In the method we suggest, the parameters are determined on the basis of a consistent analysis of shell, superfluid and collective characteristics of nuclei and this gives a physical basis to the parameters obtained and renders them to a considerable extent distortion-free.

On the whole, it now seems almost obvious that, in systematical analysis of the level density of nuclei, it is essential to use models which are more consistent than the Fermi-gas model, yet inevitably also more complex. The complexities of the analysis can be justified by the mutual consistency of the parameters obtained to characterize the various types of experimental information on the statistical properties of nuclei, and also by the close interrelationship between the theoretical concepts used and the models derived to describe the structure of low-lying nuclear states.

REFERENCES

[1] BETE, G., "Fizika yadra" (Nuclear Physics), Vol. 3, Gostekhizdat, Moscow (1948).

[2] MUGHABGHAB, S.F., DIVADUNAM, M., HOLDEN, N.E., Neutron Cross-Section, Vol. 1, N.Y.-London, Academic Press, 1981 and 1984.

[3] BELANOVA, T.S., IGNATYUK, A.V., PASHCHENKO, A.B., PLYASKIN, V.I., "Radiatsionnyj zakhvat nejtronov" (Radioactive capture of neutrons), Ehnergoatomizdat, Moscow, (1986)

[4] GILBERT, A., CAMERON, A., Can. J. Phys., 43 (1965) 1446.

[5] MALYSHEV, A.V., "Plotnost' urovnej i struktura atomnykh yader" (Level density and structure of atomic nuclei), 5, Atomizdat, Moscow (1969).

[6] BABA, H., Nucl. Phys. A159 (1970), 625.

[7] DILG, W. et al., Nucl. Phys. A217 (1973), 269.

[8] REFFO, G., Nuclear Theory for Applications, Trieste, IAEA (1980) 205.

[9] MYERS, W.D., SWIATECKI, W.J., Ark. Fys. 36 (1967), 593.

[10] VONACH, H.K., HUIZENGA, J.R., Phys. Rev. B138 (1965) 1372.

[11] HUIZENGA, J.R., MORETTO, L.G., Ann. Rev. Nucl. Sci. 22 (1972) 427.

[12] VDOVIN, A.I., VORONOV, V.V., MALOV, L.A. et al., EhChAYa 7 (1976) 952.

[13] IGNATYUK, A.V., "Statisticheskie svojstva vozbuzhdennykh atomnykh yader" (Statistical properties of excited atomic nuclei), Ehnergoatomizdat, Moscow (1983).

[14] BOR, O., MOTTEL'SON, B., "Struktura atomnogo yadra" (Structure of the atomic nucleus), Vol. 2, Mir, Moscow (1977).

[15] IGNATYUK, A.V., ISTEKOV, K.K., SMIRENKIN, G.N., Yad. Fiz. 29 (1979) 875.

[16] IGNATYUK, A.V., SMIRENKIN, G.N., ITKIS, M.G. et al., EhChAYa 16 (1985) 709.

[17] BLOKHIN, A.I., IGNATYUK, A.V., Yad. Fiz. 23 (1976) 293.

[18] LANDAU, L.D., ZhEhksp.Teor. Fiz 32 (1957) 59.

[19] VAUTHERIN, D., VINH MAU, N., Phys. Lett. B120 (1983) 261.

[20] BLOKHIN, A.I., IGNATYUK, A.V., SOKOLOV, Yu.V., et al., Izv. Akad. Nauk SSSR, Ser. Fiz., [-] (1985) [-].

FISSION CROSS-SECTION CALCULATION

S.A. EGOROV, V.A. RUBCHENYA
Khlopin Radium Institute,
Leningrad, Union of Soviet Socialist Republics

Abstract

A method based on the statistical Hauser-Feshbach theory for the calculation of fission cross sections was described. The main values, the level densities and the transmission coefficients in the different reaction channels are discussed in detail. As an example, the results of Cm(n,f) reaction calculations are presented.

---

1. Introduction.

Fission is a collective process, which results in the formation of two fragments. The statistical character of their kinetic and exitation energy distributions points at the equilibrium of the initial fission state. This idea is supported by the analysis of the angular distribution of the fission fragments as well as by the systematics of fission half-lives and the experimental information about the induced low energy fission.

It makes it possible to use the statistical Hauser-Feshbach theory for the calculation of fission characteristics. The fission probability P_f, one of the main values of fission is connected with the fission cross section

$$\sigma_f(E) = \sigma_c(E) \cdot P_f(E) \qquad (1)$$

where $\sigma_c(E)$ is the compound nucleus formation cross section. The existence of the direct reactions may be accounted by the introduction of the multiplier q_{pre} expressing the part of nuclei surviving preequilibrium decay. It may be calculated in the different approaches such as exiton model /1,2/, intranuclei cascade /3/, coupled channel models /4/.

For the compound nucleus formation cross section σ_c the coupled channel model is appropriate, because it accounts the deformation of the nuclei, essential for the fissile nuclei. The transmission coefficients T_{lj}, given by the model, express the probability of the particle absorbtion with the orbital moment l, resulting in the formation of the spin j nuclear state. Thus, fission cross section may be written

$$\sigma_{af}(\varepsilon_0) = q_{pre} \cdot \frac{\pi}{k^2} \sum_{I\pi} g_I \sum_{cc'} \frac{T_c(\varepsilon_0) \cdot T_{c'}^f(E)}{N(E,I,\pi)} S_{cc'}^{I\pi}(E) \qquad (2)$$

where k is the wave number of the bombarding particle, g the statistical factor, T_{lj} the entrance channel c transmission coefficients, S the fluctuation width correction factor, N the Hauser-Feshbach denominator, T_f the transmission coefficient in the fission c' channel. The Hauser-Feshbach denominator includes the sum of the transmission coefficients of all the open channels, satisfying the angular momentum and the parity selection rules.

$$N(E,I,\pi) = \sum_a \sum_{I'\pi'} \sum_{sl} \int_0^{E-B_a} d\varepsilon_a T_{al}(\varepsilon_a)\, \rho_a(E-B_a-\varepsilon_a, I', \pi') + \qquad (3)$$
$$+ \sum_{I'\pi'} \sum_{\kappa L} \int_0^{E} d\varepsilon_\gamma T_{\gamma\kappa L}(\varepsilon_\gamma) \cdot \rho_\gamma(E-\varepsilon_\gamma, I', \pi') + \sum_{c'} T_{c'}^f(E)$$

where $\rho_a(E)$ is the level density of the residual nucleus, T_γ the γ-ray transmission coefficient. It follows from (3), that the main values, necessary for σ_f calculation are the level densities and the transmission coefficiens in the different reaction channels.

2. Level density.

For the level density calculation phenomenological Fermi-gas /5,6/ as well as semimicroscopical models are used. Well known problems exist for the Fermi-gas models. They are connected with the impossibility of superconductivity and shell effects correct account. That is why even the evaluation of the model parametres for every nuclei doesn't garantee the quality of the level density discription for the wide energy range/7/. Moreover, such evaluation is possible only when the neutron resonance data exists.

The Fermi-gas models are difficult to use in the fission calculation, because of the lack of connection with the microscopical quantities. It leads to some arbitrary suppositions for the calculation of the transitional states density. The model parametres are fixed for the ground states deformations and can't be applied for barrier ones.

The microscopical approach is free of all these disadvantages. In the various modifications it may be succesfully applied for the whole energy region. The low energy region is specified

by the strong level density fluctuations caused by shell effects. Here the combinatorial method of $\rho(E)$ calculation is appropriate /8/. In this region the superconductivity model in the form of BCS +blocking formalism may be used. In the frame of this model the quasiparticle energy is connected with the pairing gap as follows:

$$\mathcal{E}_\kappa^\nu = \sum_\nu \mathcal{E}_i + 2\sum^\nu \mathcal{E}_i v_i^2 - \frac{\Delta^2}{G} \qquad N - N_s - \upsilon = 2\cdot\sum^\nu v_i^2 \qquad \frac{\Delta\upsilon}{G} = \sum^\nu u_i v_i \qquad (4)$$

$$u_i^2 = \frac{1}{2}\left(1 + \frac{\mathcal{E}_i - \lambda\upsilon}{E_i}\right) \qquad v_i^2 = \frac{1}{2}\left(1 - \frac{\mathcal{E}_i - \lambda\upsilon}{E_i}\right) \qquad E_\kappa^\nu = \mathcal{E}_\kappa^\nu - E_0$$

where $\mathcal{E}_i$ is the single-particle (s-p) energy, $\lambda\upsilon$ the chemical potential for the given set of quasiparticles, E° the ground state energy, N_s the number particles not included in the superconductivity model equations. The presence of the upper sign means the striking off υ definite states.

For the s-p spectra calculations the deformed Woods-Sackson potential was used. The shapesof the nucleus was described as proposed by Pashkevich /10/ in the form of Cassini ovaloids, realised in DIANA program. Parametres of the potential were the same as in /9/. The equilibrium deformations were calculated within Strutinski /11/ method. The resulting quadrupole ε and hexadecapole α_4 deformations for for nuclei with Z=90-98 are presented in the table 1. The constants of the pairing correlations used were G_n= 24.5/A, G_z=27.5/A. The rotational bands were built on the quasiparticle states.

$$E(I,K,\Pi) = E_\kappa + A\left(I(I+1) - K^2\right) + B(-1)^{I+\frac{1}{2}}\delta_{K,\frac{1}{2}}\,(I+\tfrac{1}{2}) \qquad (5)$$

where the values of A and B were taken corresponding the deformation of states under consideration. When regarding the transitional states on the first axially-asymmetric barrier, one must increase the number of states with given I in (2*I+1) times for even nuclei and in (2*I+1)/2 for odd ones. For the external barrier the number of the transitional states must be doubled because of the reflection symmetry violation:

Level density energy dependence is smooth for higher energies, where statistical description is appropriate. For axially-symmetric nuclei it is written

$$\rho(E,K) = \frac{\omega(E)}{\sqrt{2\pi}\,\sigma_\perp}\exp\left(-\frac{K^2}{2\sigma_\perp^2}\right) \qquad (6)$$

where $\omega(E)$ is the intrinsic(quasiparticle) level density

Table 1. The observed $\langle D\rangle$ and calculated $D_{I\pm\frac{1}{2}}$ neutron resonance spacing. For details see the text.

Nucleus	ε	α_4	B_n MeV	I_0^π target	$\langle D\rangle$ eV	$D^{calc}_{I-\frac{1}{2}}$ eV	$D^{calc}_{I+\frac{1}{2}}$ eV	$\frac{D^{calc}}{\langle D\rangle}$	X
^{230}Th	0.226	0.076	6.79	$5/2^+$	0.40	3.0	2.2	3.2	2.12
^{231}Th	0.233	0.076	5.13	0^+	9.8 ± 1.6	43		4.37	2.95
^{233}Th	0.237	0.067	4.79	0^+	16.6 ± 0.9	52.		3.15	2.46
^{233}U	0.240	0.078	5.74	0^+	4.1	30.		7.33	3.71
^{234}U	0.239	0.073	6.84	$5/2^+$	0.61 ± 0.07	4.2	3.1	2.96	1.93
^{235}U	0.242	0.070	5.31	0^+	10.6 ± 0.5	34		3.23	2.35
^{236}U	0.241	0.066	6.55	$7/2^-$	0.438 ± 0.038	3.4	2.8	3.41	2.32
^{237}U	0.244	0.062	5.13	0^+	16.2 ± 0.8	37		2.26	1.65
^{238}U	0.243	0.057	6.14	$1/2^+$	3.5 ± 0.3	28.	9.5	2.04	1.51
^{239}U	0.244	0.053	4.80	0^+	24.8 ± 2.3	51.		2.04	1.50
^{238}Np	0.247	0.065	5.48	$5/2^+$	0.74 ± 0.06	6.5	4.9	3.19	2.50
^{239}Pu	0.246	0.058	5.65	0^+	9.2 ± 0.7	18.		1.92	1.24
^{240}Pu	0.245	0.054	6.53	$1/2^+$	2.38 ± 0.06	19.	6.5	2.04	1.33
^{241}Pu	0.245	0.050	5.24	0^+	13.5 ± 0.5	28.		2.07	1.47
^{242}Pu	0.243	0.045	6.30	$5/2^+$	1.34 ± 0.1	4.7	3.6	1.52	0.81
^{243}Pu	0.242	0.040	5.04	0^+	14.23 ± 0.54	31		2.18	1.64
^{245}Pu	0.237	0.028	4.72	0^+	11.4 ± 4	45		3.92	3.10
^{242}Am	0.247	0.050	5.53	$5/2^-$	0.58 ± 0.04	5.0	3.7	3.67	2.52
^{243}Am	0.245	0.046	6.58	1^-	0.45	1.6	1.5	1.71	1.00
^{244}Am	0.244	0.043	5.36	$5/2^-$	0.68 ± 0.06	5.3	4.0	3.34	2.36
^{243}Cm	0.243	0.041	5.70	0^+	17.6 ± 3.3	13		0.73	-0.60
^{244}Cm	0.241	0.036	6.80	$5/2^+$	0.50 ± 0.2	2.3	1.7	2.00	1.23
^{245}Cm	0.240	0.031	5.52	0^+	11.8 ± 1.2	17		1.40	0.57
^{246}Cm	0.238	0.028	6.45	$7/2^+$	1.14 ± 0.14	2.9	2.4	1.17	0.30
^{247}Cm	0.237	0.025	5.16	0^+	21.3 ± 5.3	31		1.47	0.78
^{248}Cm	0.234	0.021	6.21	$9/2^-$	1.2	3.6	3.2	1.43	0.69
^{250}Bk	0.232	0.019	4.97	$7/2^+$	1.1	4.8	4.0	2.00	1.43
^{250}Cf	0.232	0.011	6.62	$9/2^-$	1.07 ± 0.14	1.7	1.5	0.75	-0.57
^{253}Cf	0.220	0.001	4.79	0^+	16	31.		1.93	1.44

$$\rho(E,I) = \tfrac{1}{2}\sum_{K=-I}^{I} \rho(E-E_{rot},K) = \frac{\omega(E)}{\sqrt{8\pi}\,\sigma_{\parallel}} \sum_{K} \exp\left(-\frac{I(I+1)}{2\sigma_{\perp}^2} - \frac{K^2}{2\sigma_{eff}^2}\right) \quad (7)$$

Here I is the nuclear spin, K its projection on the symmetry axis, $\sigma_{\perp}$, $\sigma_{\parallel}$ the spin cutoff parametres $\frac{1}{\sigma_{eff}^2} = \frac{1}{\sigma_{\parallel}^2} - \frac{1}{\sigma_{\perp}^2}$. For non-axial symmetric states

$$\rho(E,I) = G_{sym}(2I+1)\,\omega(E)\exp\left(-\frac{(I+\tfrac{1}{2})^2}{2\bar{\sigma}^2(E)}\right) \quad (8)$$

Contribution of the rotation may be accounted by the total and intrinsic level densities comparison

$$K_{rot}(E) = \frac{\rho_{tot}(E)}{\omega(E)} = \sum_{I} \frac{\rho(E,I)}{\omega(E)} = \quad (9)$$

$\sigma_{\perp}^2/(\sqrt{2\pi}\,\sigma_{\parallel})$ with axial symmetry

$\sigma^2/\sqrt{2\pi}$ without axial symmetry

Intrinsic level density $\omega(E)$ was calculated within semimicroscopical superconductive quantum-statistical model /13-15/

$$\omega(E) = (2\pi)^{-3/2}\left(\det S''\right)^{-1/2} e^{S(E)} \quad (10)$$

where S(E) is the system entropy, $\det S''$ the matrix second derivatives determinant on $\beta=\frac{1}{T}$, $\alpha_n=\frac{\mu_n}{T}$, $\alpha_z=\frac{\mu_z}{T}$, $\mu_{n,z}$ neutron and proton chemical potentials. For the nuclear temperature, less than T_{cr} (critical temperature of superconductive-normal state transition) entropy is

$$S = 2\sum_{\tau=n,z}\left[\ln\left(1+\exp(-\beta E_{\tau i})\right) + \frac{\beta E_{\tau i}}{1+\exp(\beta E_{\tau i})}\right] \quad (11)$$

the pairing gap together with μ_τ are found from the system of equations

$$E + E_0 = \sum_{\tau}\left[\sum_{i} \varepsilon_{\tau i}\left(1 - \frac{\varepsilon_{\tau i}-\mu_\tau}{E_{\tau i}}\,th\,\frac{E_{\tau i}}{2T}\right) - \frac{\Delta_\tau^2}{G_\tau}\right] \quad (12)$$

$$N_\tau = \sum_{i}\left(1 - \frac{\varepsilon_{\tau i}-\mu_\tau}{E_{\tau i}}\,th\,\frac{E_{\tau i}}{2T}\right) \qquad \frac{2}{G_\tau} = \sum_{i}\frac{1}{E_{\tau i}}\,th\,\frac{E_{\tau i}}{2T} \quad (13)$$

The critical energy is determined from (12) when $\Delta_\tau=0$, $T=T_{cr}$, which is found from (13) when $\Delta_\tau=0$, $E_{\tau i}=(\varepsilon_{\tau i}-\mu_\tau)$. System of equations is the same for the temperatures $T>T_{cr}$, assuming $E_{\tau i}=|\varepsilon_{\tau i}-\mu_\tau|$. In the level density calculation the same s-p spectrum was used.

For the quantum numbers I and K distributions superconductivity model expressions /6/ were used. The moments of inertia, suitable for ellipsoidal deformation ε were the following

$$F_{\perp} = \frac{2}{5} m_0 r_0^2 A^{5/3}(1-\varepsilon^2)^{-2/3} \qquad F_{\parallel} = \frac{6}{\pi^2}\overline{\Omega^2}\,a\,(1-\varepsilon^2)^{1/3} \qquad \overline{\Omega^2} = M\,A^{2/3} \quad (14)$$

where the mean square of the s-p spin was determined from combinatorial K-distributions. M was equal 0.19 ± 0.2 for all the nuclei investigated. Statistical expressions were used too for the evaluation of spin cutoff parametres

$$\sigma_{\parallel}^2 = \overline{\Omega^2}\; g \cdot T \quad (15)$$

where g is the s-p level density near the Fermi-surface. The values g and were determined from the averaging of corresponding characteristics of s-p spectra within 3-4T energy interval.

Combined combinatorial-statistical approach describes the main features of level densities in the wide energy range. For the low energy region energy and spin distributions are non-statistical. This is shown in fig.1,2 for the nuclei of different parity. In fig.3 energy dependence of spin cutoff parameter is presented. Analysis of fig.1-3 shows that ρ_{tot} becomes smoooh quickly enough. That is not the case for the spin distributions, in which shell effects can be seen up to the high energies.

The exact account of the superconductivity and shell effects in the combined approach guarantees the quality of level density description in the wide energy range. Fig.1 illustrates the agreement with exsperimental data for low energies. However, superconductive model doesn't include residual interaction of multipole-multipole type. This difficulty may be overcome by the introducing the vibration enhancement coefficient K_{vibr} /6/.

$$K_{vibr} = \exp\left(17\left(\frac{3mA}{4\pi G_{ld}}\right)^{2/3} T^{4/3}\right) = \exp\left(X\,T^{4/3}\right) \quad (16)$$

recieved from the study of small vibrations of liquid drop, where G_{ld} is the coefficient of surface tension. The values X, determined from the comparison with neutron resonance data /7/ are presented in the table 1. It is evident, they are maximum for odd-odd nuclei, because it accounts residual neutron-proton interaction.

It is seen from the comparison, the collectivization of states leads to 2-3 times increase of the level density for neutron binding energy B_n. This result coinsides with the conclusion of /18/, recieved within exact account of residual interaction. Thus,

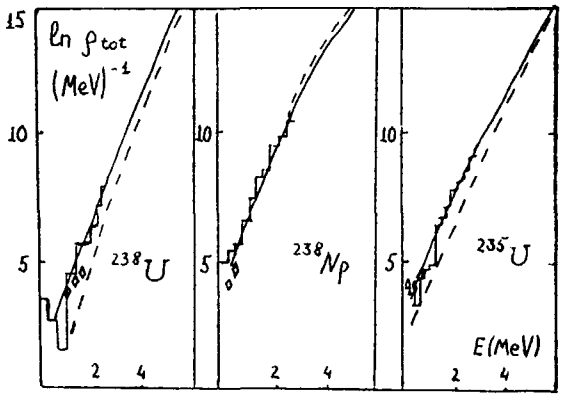

Fig.1 The experimental and calculated level densities. The histogram is the combinatorial, the full line is the quantum-statistical model and the dotted curve is the phenimenological superconductivity model /6/ calculation.

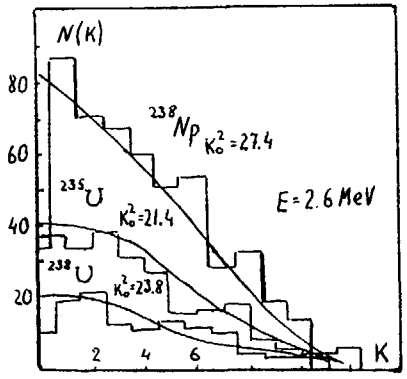

Fig.2 K-distributions of the descrete spectra (histogram) and their approximation by the statistical formulae (6)

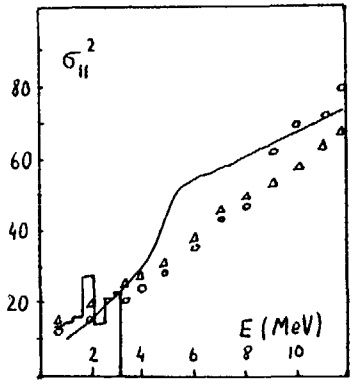

Fig.3 The histogram and the full line are the combinatorial and the superconductivity model calculations. The circles and the triangles show the results of the statistical approximation with averaging in 3 and 4T intervals.

the values of vibration and rotation (fig.4) enhancement are equal at the neutron binding energy for equilibrium deformation.

The transitional states level density has several pecularities. First, s-p level density is known to be greater for barrier deformations, than for ground state ones /16/. With the same pairing it leads to the increase of pairing gap Δ. For instance, in the case of ^{238}U such increase reaches 20 and 40% for the first and second barriers correspondingly. For the energies less U_{cr} it leads to the change of the level density energy dependence. It is equivalent to 10-15% increase of Fermi-gas parameter a in the phenomenological models. Intrinsic level densities of ^{236}U at the deformations $\varepsilon = 0.55, \alpha_4 = 0.08$; $\varepsilon = 0.85, \alpha_4 = 0.12$ corresponding approximately to the barrier ones are presented in fig.4 together with (E) at the equilibrium deformation. Second, perpendicular moment of inertia exeeds parallel one greatly, especially for the second barrier. It leads to the increasing role of the rotation in the level density formation (fig.4), that is enhanced by the axial-symmetry violation too.

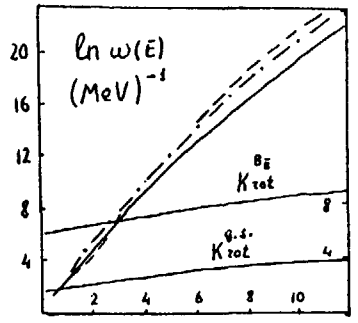

Fig.4 Comparison of the internal level densities at the equilibrium deformation ⁄, at the first ⁄ and at the second ⁄ barriers. Krot are shown at the equilibrium and second barrier deformations.

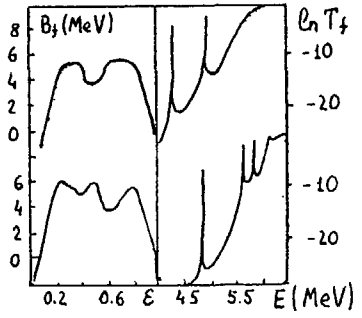

Fig.5 Deformation dependence of the fission barrier under consideration a) and b) corresponding penetrability Tf.

3. Fission transmission coefficients.

Transmission coefficients were calculated within the frames of many-humped one dimentional barrier penetration. This model made it possible to describe main effects regarded in the actinide nuclei σ_f: the existence of subbarrier resonances /16/ and the plateau in the fission cross sections /17/.

Fission barrier may be approximated by several connected parabolas /16/ characterised by the heights B_f and the curvatures $\hbar\omega$. The penetration of such barrier is calculated within two main assumptions: the complete damping of the fission motion in the first well and WKB approximation for the barrier penetration calculation.

Fig.6 demonstrates the shape barrier dependence within these assumtions. The fission barrier penetration, which can be calculated for the connected parabolas and for the barrier, given in the form of a table approximated by splains was calculated by code PENBAR using numerical Schredinger equation solution. It permits to solve the equation by Numerov, Cowell and Runge-Kutt methods /18/.

The experimental resonances compared with the penetration ones are more smooth and wide. For the description of damping it was proposed to take into account the interaction between fission and internal degrees of freedom. It may be done by the introduction of the imaginary part iW to the potential in the second well region /19/. But the proposed linear energy dependence $W(E)$ is unrealistic, that is evident from the following.

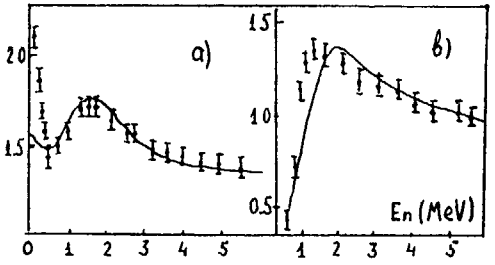

Fig.6 The results of the statistical calculation of the neutron-induced ^{241}Pu (a) and ^{244}Pu (b) fission cross sections /20/.

The absorbtion of the fission motion in the second well is possible only by means of internal states exitation and correspondingly must be proportional the number of such states.

$$W(E,I,K,\Pi) = \varkappa\, \rho(E,I,K,\Pi) \qquad (17)$$

where $\varkappa$ characterizes the interaction of the internal and fission degrees of freedom. The introduction of the imaginary part leads to the widening of the even-even nuclei resonances and nearly to the complete dissapiaring of them in the odd and doubly odd nuclei. The level density $\rho(E)$ of the latter is much greater, that causes earlier complete damping. In this case barriers must be regarded independently with penetration coefficient equal

$$T = \frac{T_a\, T_b}{T_a + T_b} \qquad (18)$$

where T_a and T_b are the penetrabilities of separate barriers which may be calculated using the expression for the parabolic barrier

$$T_{a(b)} = \int_0^E \frac{\rho_{a(b)}(U)}{1+\exp\left(2\pi\left(B^{I}_{a(b)} - E - U\right)/\hbar\omega_{a(b)}\right)}\, dU \qquad (19)$$

where $\rho_{a(b)}$ is the transitiohal states level density.

4. Calculated fission cross sections.

The knowledge of the level densities and transmission coefficients in all the channels allows one to calculate fission cross sections. Reference /20/ may be regarded as the example of the succesful σ_f calculation. The exploitation of the phenomenological superconductivity model permitted authors to describe "plateaus" in the fission cross section. This required, however, to fit the main model parameter pairing gap for every nuclei. The use of the smooth level density formalism made it impossible to describe the subbarrier dependence of σ_f.

The semimicroscopical quanto-statistical model leaves no freedom to the arbitrary choice of Δ, which is calculated exactly. It makes it possible to describe σ_f energy dependence practically without parametres. Moreover, the combined approach allows us to explain the existence of the subbarrier irregularities in σ_f of some nuclei, and their difference for various nuclei.

The results of Cm(n,f) reaction calculations are presented in fig.7,8. The existence of the irregularities is connected in our approach with the structure of the transitional states on the one-humped internal fission barrier. The influence of such spectrum on subbarrier energy dependence is demonstrated in fig.7. It allows to conclude,that not only subbarrier behaviour,but also the fission barrier parametres are dependant on the spectrum used in the calculation. Parametres of the first barrier,determined from the statistical analysis together with the values from /16/ are placed in the table 2. Our barrier heights are systematically lower,than those of /16/,that is caused by using there Fermi-gas level density /5/ underestimating low energy level density.

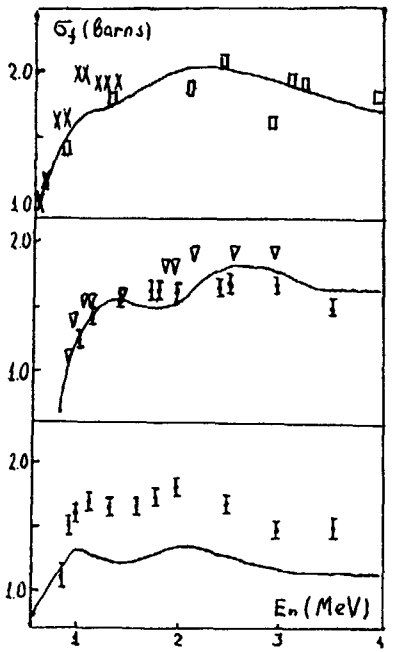

Fig.7 Cm isotopes calculated fission cross sections. Experimental data are taken from references X-/21/, □-/22/, ∇-/23/, I-/24/, Δ-/25/.

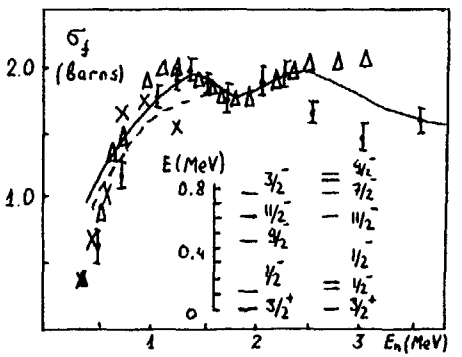

Fig.8 $^{245}Cm(n,f)$ cross section. calculation was fulfilled with two sets of transitional states The full curve corresponds to the set b).

Nucleus	B_f MeV	$\hbar\omega$ a)	B_f MeV	$\hbar\omega$ b)
^{243}Cm	6.7	0.8	6.1	0.8
^{245}Cm	6.3	0.8	6.0	0.8
^{247}Cm	6.2	0.8	5.7	0.6
^{249}Cm	5.7	0.8	5.3	0.9

Table 2. The parametres of the first fission barrier from /16/ a) and this work.

It leads to the decrease of T_c^f (2) that means overestimating of the barriers. Our results allow to make an affirmation about the lack of strong odd-even differences in Cm barrier heights,recieved in /16/.

REFERENCES

1.Griffin J.J.,Phys.Lett.17(1966)478
2.Cline C.K.,Blann M.,Nucl.Phys.A172(1971)225
3.Bunakov V.E.,Sov.J.Phys. of Elementary Particles and Atomic Nuclei 11(1980)1285
4.Tamura T.,Rev.Mod.Phys.37(1965)679
5.Gilbert A.,Cameron A.,Canad.J.Phys.43(1965)1446
6.Ignatyuk A.V. et al.,Sov.J.Nucl.Phys.29(1979)875
7.Antsipov G.Y. et al.,Report INDC(CCP)-182,Vienna,IAEA(1982)
8.Vdovin A.I. et al.,Sov.J.Phys.of Elementary Particles and Atomic Nuclei,7(1976)952
9.Egorov S.A. et al.,Proceedings of the conference "Neutron Physics",Kiev,1(1983)290
10.Pashkevich V.V.,Rubchenya V.A.,Bulletin of Data Centrum of Leningrad Instituite of Nuclear Physics,Leningrad(1976)
11.Strutinski V.M.,Sov.J.Nucl.Phys.3(1966)614
12.Bohr A.,Mottelson B.R.,"Nuclear Structure",v.2,ch.4

13.Decowski P. et al.,Nucl.Phys.A110(1968)129
14.Ignatyuk A.V.,Shubin Ju.M.,Sov.J.Nucl.Phys.8(1968)1135
15.Rubchenya V.A.,Sov.J.Nucl.Phys.11(1970)1028
16.Bjornholm S.,Lynn J.E.,Rev.Mod.Phys.52(1980)725
17.Cuprianov V.M. et al.,Sov.J.Nucl.Phys.39(1984)281
18.Melcanoff M.A. et al.,Methods of Computational Physics6(1966)
19.Back B.B. et al.,Nucl.Phys.A165(1971)449
20.Ignatyuk A.V. et al.,Sov.J.Nucl.Phys,42(1985)569
21.Vorotnikov P.E. et al.,Sov.J.Nucl.Phys.40(1984)1141
22.Britt H.C.,Wilhelmy J.B.,NSE72(1979)222
23.Moore M.S.,Keyworth G.A.,Phys.Rev.C3(1971)1656
24.Fomushkin E.F. et al.,Sov.J.Nucl.Phys.40(1984)1141,36(1982)582
25.Koontz P.,Barton D. In:Neutron Cross-Sections and Technology, 1(1968)597

NUCLEAR DATA FOR CALCULATION OF TRITIUM PRODUCTION IN NUCLEAR POWER REACTORS

L.V. DRAPCHINSKIJ, S.V. KHLEBNIKOV, S.S. KOVALENKO
Khlopin Radium Institute,
Leningrad, Union of Soviet Socialist Republics

Abstract

The mechanisms of tritium production and the current status of nuclear data for calculation of tritium production in nuclear power reactors are described. It is concluded that the extended theoretical and experimental investigations on the ternary fission and (n,^{3}H) reactions are needed.

INTRODUCTION

At present attention to the problems connected with tritium production in nuclear power reactors is growing. The significance of these problems is caused by tritium emission into environment which accompanies the operation of nuclear power plants and reprocessing plants. Tritium is of particular interest because of its direct incorporation into water and organic tissue. Tritium has a relatively small radiotoxicity,but due to high exchange rate with hydrogen of organic compounds, its behaviour in ecosystems is insufficiently examined. Because of increase in tritium content in all environments the problems dealing with the account of tritium production sources in nuclear fuel and structural materials become of great importance.

TRITIUM AND ITS SOURCES

Tritium is an unstable isotope with a half-life of 12.35 yr:

$$^3H \rightarrow {}^3He + \beta^- + \tilde{\nu}.$$

In this case soft β-rays with a continuous β-spectrum are emitted. The maximum electron energy is of 18.594 keV with the mean one 5.57 keV.

Despite a negligible tritium half-life compared to the geological time, it is contained in the atmosphere and natural

water. Main natural sources of continuous ^3H production in the atmosphere are nuclear reactions caused by cosmic protons and neutrons with oxygen and nitrogen: ^{14}N (n, ^3H)^{12}C, ^{14}N (n, ^3H)3 ^4He e.a. A mean rate of ^3H natural production is of 0.14 - 0.9 at $^3H/(cm^2.S)$. Cosmic bombardment generates 0.5 - 1 kg ^3H annually and its total amount in the environment is about 7-14 kg /1/*. Main chemical forms of tritium are tritiated water (HTO) and tritiated hydrogen (HT).

The civilian and military use of nuclear energy resulted in the appearance of additional intensive source of tritium. Until recently artificial ^3H production was related mainly to nuclear weapon tests in the atmosphere (6 - 30 MCi per 1 Mt thermonuclear explosion) /2/. At present the operation of nuclear power plants and reprocessing plants has become one of the most important sources of tritium production. The ^3H production in nuclear reactors is caused by the fuel-cycle nuclei ternary fission, the neutron reactions with Li and B contained in structural materials and absorber rods, the neutron interactions with ^2H, Li, B in the coolant. Main tritium-producing reactions of that type are schematically shown in Fig. 1. The ^3H production rate in reactors of various types in the first three years of operation is

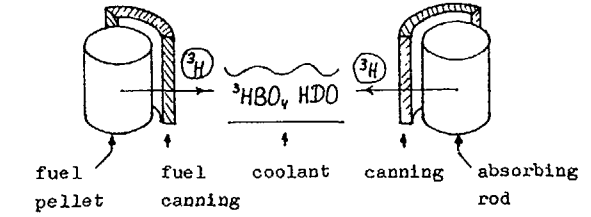

$^{235}U(n,f)^3H$ HDO(n,γ)HTO $^{10}B(n,2\alpha)^3H$

$^{239}Pu(n,f)^3H$ $^{10}B(n,2\alpha)^3H$ $^{10}B(n,\alpha)^7Li(n,n'\alpha)^3H$

$^{238}U(n,f)^3H$ $^{10}B(n,\alpha)^7Li(n,n'\alpha)^3H$ $^{11}B(n,n2\alpha)^3H$

$^6Li(n,\alpha)^3H$

$^{11}B(n,n2\alpha)^3H$

Fig. 1. Tritium production in nuclear reactor and the ways of its acess into the coolant.

* ^3H specific activity is about $9.64.10^3$ Ci/g $\approx 10^4$Ci/g = $= 3.7.10^2$ TBq/g.

shown in Fig. 2 /2/. It appears that most of tritium is produced in heavy-water reactors and fast breeders. Tritium production is

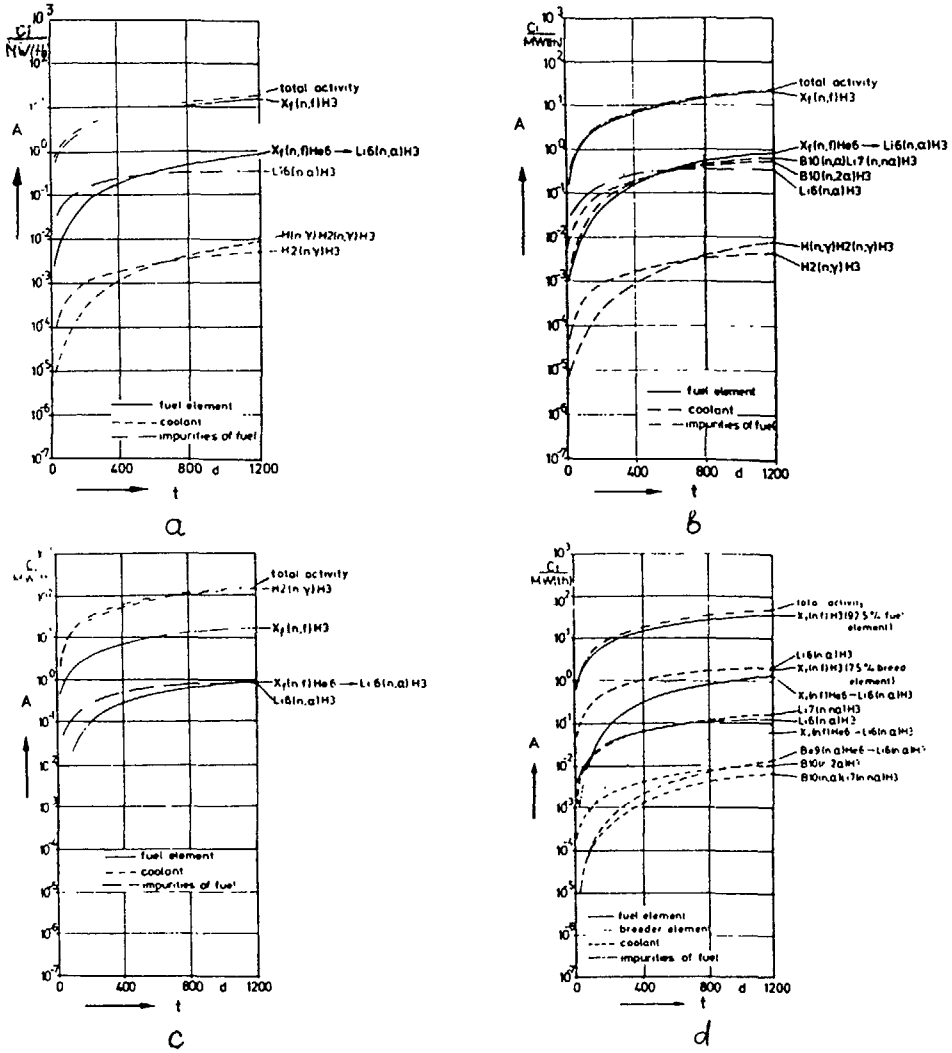

Fig. 2. Tritium production per 1 MW (th) in various types of reactors in the first three years of operation /2/.
a) - boiling-water reactor (BWR)
b) - pressurized-water reactor (PWR)
c) - heavy-water reactor (HWR)
d) - sodium-cooled fast breeder reactor (FBR)

mainly caused by ternary fission except that in heavy-water reactors. Greater ^{3}H emission rate in pressurized-water reactors compared to boiling-water reactors results from the formation of tritium due to boron added to the water which was assumed to be 500 ppm. It should be noted that only small part of ^{3}H formed in fuel elements and absorber rods is released into the environment. To get into the coolant ^{3}H has to diffuse through zirconium or steel canning, as shown in Fig. 1. Main part of ^{3}H is retained in a fixed state and is released in reprocessing plants. In the Soviet power reactors due to ternary fission 0.37 - 0.74 TBq/ /(MW (e).yr) (in VVER and RBMK-types) and 0.74 - 1.5 TBq/ /MW (e).yr) (in BN-type) of tritium is produced /3/.

TRITIUM PRODUCTION CAUSED BY TERNARY FISSION

In the middle 40-ies N.A. Perfilov (USSR) and L.V. Alvarez (USA) discovered that in some cases long-range α-particle emission takes place in fission. This phenomenon called "ternary fission" draws constant attention because of its importance for nuclear physics*. ^{235}U ternary fission is best studied. The long-range α-particles proved to be not the only light charged particles (LCP), emitted in the fission process. Emission of ^{3}H, ^{6}He, ^{1}H, ^{2}H, ^{8}He nuclei (according to probability decrease) and Li, Be, B, C, N, O, F and other elements was also found. LCP yields for thermal neutron induced ^{235}U fission are given in Table 1. Considerable discrepancy of data, often above the error limits, is due to a small probability of phenomenon.

LCP energy distributions are usually by the gaussians represented. Main parameters of LCP energy distributions (most probable energy and FWHM) for the thermal neutron induced ternary ^{235}U fission are given in Table 2 /5, 6/. LCP angular distribution is close to normal with small FWHM. The most probable emission angle is about 90° relative to the direction of flight of fragments. This indicates that LCP are emitted from the region between the nascent fragments and then accelerated by the Coulomb field of fragments. Data analysis shows that LCP yield,

* So-called "true" ternary fission with three gragments of comparable masses (probability 10^{-7} I/binary fission) is not considered here.

Table 1

LCP yields for thermal neutron induced ^{235}U fission /4/

LCP	Yield, LCP/fission	Number of publications
^{1}H	4.10^{-5}	1
^{2}H	$1.2.10^{-5}$	1
^{3}H	$(0.8\pm0.10)10^{-4}$ to $(2.4\pm0.7)10^{-5}$	7
^{5}H	7.10^{-6}	1
^{3}He	6.10^{-5}	1
^{4}He	$(1.30\pm0.01)10^{-3}$ to $(4.35\pm0.50)10^{-3}$	26
^{6}He	$1.5.10^{-5}$	2
^{8}He	$1.8.10^{-7}$	1
Li (sum of isotopes)	3.10^{-7} to $1.9.10^{-6}$	2
Be (sum of isotopes)	9.10^{-8} to $6.8.10^{-6}$	2
^{7}Be	3.10^{-9}	1
^{8}Be	$(5\pm2)10^{-8}$ to $1.7\ 10^{-6}$	2
^{10}Be	4.10^{-6}	
B (sum of isotopes)	$(5.1\pm0.7)10^{-8}$ to 2.10^{-7}	2
C	$(1.9\pm0.1)10^{-6}$	1
N	$(8.9\pm2.0)10^{-8}$	1
O	$(6.1\pm1.2)10^{-7}$	1
F	$(2.1\pm0.7)10^{-8}$	1

Table 2

Parameters of LCP energy distributions for the thermal neutron induced ternary ^{235}U fission /6/

LCP	Most probable energy, MeV	FWHM, MeV
^{1}H	8.6 ± 0.3*	6.9±0.5*
^{2}H	8.6 ± 0.15	7.1±0.2
^{3}H	8.2 ± 0.15	6.5±0.2
^{4}He	15.9 ± 0.1	9.8±0.1
^{6}He	11.3 ± 0.15	10.8±0.4
^{8}He	9.3 ± 0.25	8.9±0.6
^{7}Li	15.1 ± 0.3	13.3±0.6
^{8}Li	13.8 ± 0.4	11.0±1.3
^{9}Be	17.5 ± 0.4	12.9±0.9
^{10}Be	17.7 ± 0.4	16.1±0.6
^{11}Be	15.9 ± 0.8	15.3±2.3
^{12}Be	12.0 ± 1.5	15.8±2.7

* - according to /5/.

energy and angular distributions are independent on the type of nuclei and on the excitation energy up to 20 MeV at least.

Ternary fission is the main source of ^{3}H production in nuclear power reactors of most types. Though a main part of works dealing with the ternary fission are devoted to ^{4}He emission, there are a number of works on ^{3}H emission in $^{233,235}U$, ^{239}Pu thermal neutron fission and in ^{252}Cf spontaneous fission. There are only few works concerning a fast neutron induced fission. Experimental ^{3}H yield data are presented in Table 3.

Table 3

^{3}H yield in ^{233}U, ^{235}U, ^{239}Pu thermal neutron induced ternary fission and in ^{252}Cf spontaneous fission

Nuclei	Neutron energy	^{3}H yield	
		Number of ^{3}H per total number of fissions	Number of ^{3}H per 100 α-particles
^{252}Cf	-	$1.9\pm0.06.10^{-4}$ /4/	6.42 ± 0.20 /7/
		$(2.21\pm0.05).10^{-4}$ /5/	6.7 ± 1.1 /7/
		$(2.13\pm0.18).10^{-4}$ /6/	8.46 ± 0.28 /7/
^{233}U	thermal	$(2.42\pm0.15).10^{-3}$ /9/	3.60 ± 0.16 /10/
	reactor	$(2.25\pm0.07).10^{-3}$ /9/	4.60 ± 0.20 /10/
		$(2.46\pm0.18).10^{-3}$ /9/	
	slow		8 ± 1 /11/
	14 MeV		11 ± 2 /11/
^{235}U	thermal	$(0.95\pm0.08).10^{-4}$ /12/	6.2 ± 0.5 /14/
	reactor	$(0.80\pm0.10).10^{-4}$ /13/	6.3 ± 0.2 /15/
		$(2.4\pm0.8).10^{-5}$ /6/	
	slow		8 ± 1 /11/
	14 MeV		11 ± 2 /11/
^{239}Pu	thermal	$(1.35\pm0.13).10^{-4}$ /16/	7.2 ± 0.3 /17/
	reactor	$(1.07\pm0.08).10^{-4}$ /14/	6.8 ± 0.3 /14/

To determine ^{3}H yields in fission two methods are used /18-20/: radiochemical methods and method of LCP identification. Radiochemical method consists in ^{3}H separation from a target and measuring its activity. The number of fission events is determined via γ-spectrometry of fission products (^{140}Ba, ^{137}Cs,

^{144}Ce e.a.). A main contribution into the total error gives errors of ^{3}H activity determination and those arising because of consideration of other channels of ^{3}H production. The method of LCP identification consists in registration and identification of all the particles emitted and their kinetic energy determination. The LCP identification method is used at the Radium Institute (Leningrad, USSR) where a number of ternary fission process investigations have been performed since the phenomenon discovery. Recently the experimental set-up was made and preliminary experiments on the ^{3}H yields determination in fission were performed. Measurements of ^{3}H yield in fission induced by 14.5 MeV neutrons with heavy nuclei were carried out.

A scintillation CsI(Tl) detector, 1.4 mm thick, 40 mm in diameter, was used for LCP registration. Fission fragments and α-particles were rejected by a tin foil. LCP identification was carried out by a pulse shape discrimination method. LCP yield measurements are bound up with great difficulties because of a high background caused by (n, p) and (n,α) reactions on CsI(Tl) and structural materials. The use of LCP registration in coincidence with fragments made it possible to decrease the background considerably. An ionization current pulse chamber was used for fragment detection to ensure the minimal resolution time of coincidence circuit. Experimental arrangement is shown in Fig. 3. The results of first ^{3}H-yield measurements for 11 nuclei from ^{232}Th to ^{242}Pu are given in Table 4. The accuracy achieved is better than 10 %. The measurements in other energy ranges are planned.

At present different theoretical explanations of ternary fission process are known. The dynamic ternary fission model which includes dynamic characteristics of fissioning nucleus /21/ can be used as a base for further development of theoretical approaches. This model makes it possible to achieve satisfactory description of LCP yields by the use of only two fitted parameters.

TRITIUM PRODUCTION IN NEUTRON-INDUCED REACTIONS

To get data concerning ^{3}H production under neutron bombardment it is necessary to measure the amount of reaction products. For this purpose the post-irradiation high-sensitive mass spec-

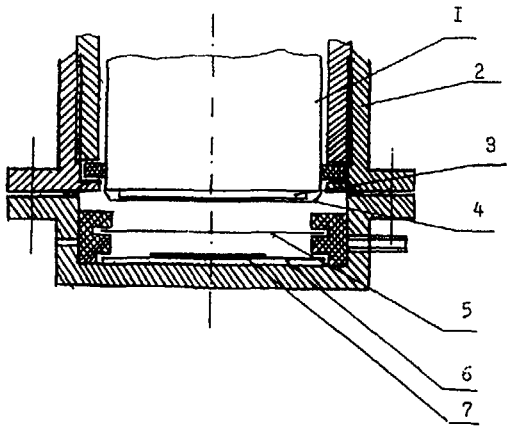

Fig. 3a. Detector unit

1. Photomultiplier; 2. Body;
3. CsJ (Tl); 4. Sn-foil 13.2 mg/cm^2 thick;
5. Collecting electrode of fission chamber, Al-foil 2.2 mg/cm^2 thick; 6. Target backing;
7. Fissionable material layer.

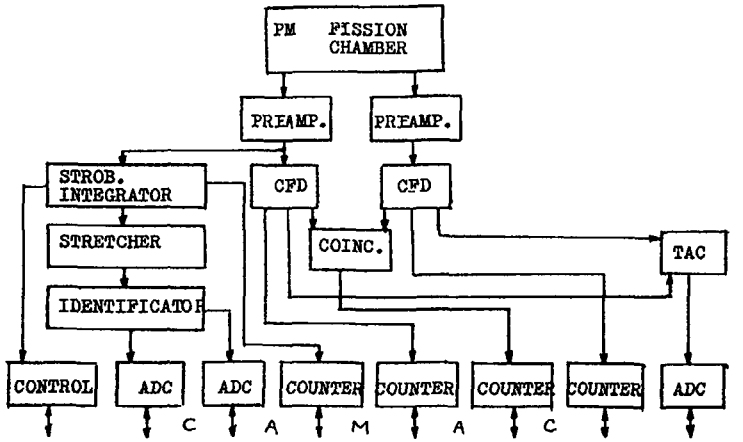

Fig. 3b. Experimental set-up.

trometry is used sometimes. Using this method helium production when boron is irradiated in a fast breeder reactor was investigated./22/. In general one may say that the sensitivity of the method is not sufficient to obtain the gas production cross sec-

Table 4

^{3}H yields for 14.6 MeV neutron induced fission

Nucleus	^{3}H yields	
	per 100 α -particles	number of ^{3}H per total number of fissions*
^{232}Th	8.5 ± 0.9	$(0.51 \pm 0.34).10^{-4}$
^{233}U	6.3 ± 0.6	$(1.47 \pm 0.19).10^{-4}$
^{234}U	10 ± 1	-
^{235}U	6.9 ± 0.7	$(1.33 \pm 0.15).10^{-4}$
^{236}U	6.6 ± 0.7	-
^{238}U	12.3 ± 1.2	$(1.54 \pm 0.21).10^{-4}$
^{237}Np	5.3 ± 0.5	$(1.35 \pm 0.17).10^{-4}$
^{239}Pu	10 ± 1	-
^{240}Pu	9.0 ± 0.9	-
^{241}Pu	12.8 ± 1.3	-
^{242}Pu	8.5 ± 0.9	-

* Ratios of α -particle yields in 14 MeV neutron fission to those in ^{235}U thermal neutron fission were used for determination of α -particle yields.

tions in the whole neutron energy range of interest with the neutron sources available.

Much higher sensitivity can be obtained if reaction products are radioactive with suitable half-lifes. In this case mass spectrometric measurements are replaced by radioactivity determinations. The (n, ^{3}H) reaction cross sections are determined by using low-level counting either of extracted tritium or produced residual nuclei. In many cases the application of radiochemical separation methods increases the sensitivity of the activation method considerably /23/. This technique has been applied e.g. in the determination of ^{7}Li (n, n'α)^{3}H cross section /36/. In this case Li_2CO_3 enriched to 99.97 % in ^{7}Li was used as a target. Tritium produced in the reaction has been converted to HTO and measured by β -counting after mixing with a liquid scintillator.

A direct registration of the charged particles is used in (n, ^{3}H) cross section measurements. Difficulties in performing such experiments are as follows: low count rates (1) and the problems of background caused by other charged particles which may be produced by neutrons in the target (2). Most of the measurements were performed with 14 MeV-neutrons, where an intense neutron sources are available.

The vast majority of experimental data refer to thermal neutron region. Experimental thermal cross section data can be divided into three groups:

i) fission cross sections measured with 0.0253 ev-neutrons;
ii) Maxwellian spectrum averaged fission cross sections;
iii) reactor spectrum averaged fission cross sections.

If the energy dependence of the reaction cross sections obeys the 1/v law in the thermal region, the cross section value averaged over the Maxwellian spectrum:

$$N(E)dE = \frac{2\sqrt{E}}{\sqrt{\pi}\,E_T^{3/2}} \cdot \exp\left(-\frac{E}{E_T}\right) \cdot dE$$

is equal to the cross section σ_0 for 0.0253 eV neutrons. In other case:

$$\bar{\sigma} = g_w \cdot \sigma_0$$

where g_w - parameter representing the deviation of the cross section from the 1/v law in the thermal region. It can be calculated from the expression:

$$g_w = \frac{2}{\sqrt{\pi}\,\sigma_0\,E_T^2} \cdot \int_0^\infty \sigma(E) \cdot E \cdot \exp\left(-\frac{E}{E_T}\right) dE$$

A vast information on (n, ^{3}H) cross sections in thermal region is available now. Tha data in the fast neutron region are rather poor:

1. Experimental data obtained up to 1970 demonstrate a great spread. The maximum discrepancy reached 3 orders of magnitude (^{32}S, ^{40}Ca). This may be caused by contaminations in a tar-

get material. In many cases - if activation method is used - high cross section (n, 2n) or other reactions leading to the same product nuclei can distort the experimental data.

2. Most of the experiments were performed with the light nuclei (Li, Be, B). For other elements the experimental data are very scarce. More than half the elements are not investigated at all.

3. Most data refer to the region $14.2 \lesssim En \lesssim 14.9$ MeV. The excitation functions of (n, ^{3}H) reactions are inadequately investigated.

The theoretical methods are of great importance in the evaluation of (n, ^{3}H) reactions cross sections especially in the case of lack of experimental information and in intercomparison of data. Except light ($Z \lesssim 20$) nuclei, the statistical model is used for ^{3}H emission calculations /25/. There are some indications on an increase in the direct reaction contribution as the mass number grows /26/. The neutron interactions with light nuclei are usually described using the distorted waves method /27/. The particle emission during the equilibration process is described using various models or preequilibrium decay /28/.

Together with the successive theoretical approaches, the values of (n, ^{3}H) reaction cross sections may be estimated using the semiempirical expressions of different types. The empirical formula for $E_n \simeq 14$ MeV is known /29/ :

$$\sigma_{(n,^3H)} = 4.52(A^{1/3}+1)^2 \exp -10\frac{N-Z}{A}, \text{ mb.}$$

The agreement with the experimental data is believed to be less than 70 % for $20 \lesssim Z \lesssim 44$. For the odd nuclei this formula may underestimate the cross section values down to one order. For $Z > 44$ modified formula of this type is given in /30/:

$$\sigma(n,^3H) = 7.684(A^{1/3}+1)\exp -13\frac{N-Z}{A}, \text{ mb.}$$

An analytical method of (n, ^{3}H) reaction cross sections calculations for the nuclei with $Z \gtrsim 20$ at $En \simeq 13$-20 Mev is proposed in /31/:

$$\sigma(n,^3H) = e^{ax^2 + bx + c},$$

where $x = (\frac{A}{A+1} \cdot En + Q)$; En - neutron energy; Q - reaction energy; a, b, c - parameters fitted for every nucleus. The use of this expression permits both to describe the excitation functions and to take into account the even-odd cross-section differences. The procedure of analytical approximation for the excitation functions of (n, charged particle) reactions is proposed /32/ for nuclei with $23 \lesssim A \lesssim 197$ at $En < 20$ MeV. The set of semiempirical parameters based on the evaporation model enabled to achieve a satisfactory agreement in the excitation function values of (n, p), (n, α) and (n, ^{3}H) reactions more than for 50 nuclei.

Data recommended for the most important ^{3}H-producing reactions in thermal power reactors are given in Table 5.

The ^{2}H (n, γ) ^{3}H reaction

Experimental data are available only for the thermal neutrons and at $En \simeq 14$ MeV. The cross section values between the areas were obtained from the inverse reaction ^{3}H(γ, n)^{2}H by taking into account the detailed balancing principle /33/:

$$\sigma_{(n,\gamma)}(E_n) = E_\gamma^2 [2Mc^2(E_\gamma - Q)]^{-1} \sigma_{^3H(\gamma,n)^2H}(E_\gamma).$$

The recommended data from the JENDL-2 are shown in Fig. 4. It should be noted that at 14 MeV the recommended value is one third from the experimental one measured using a counter telescope.

The ^{6}Li (n, α) ^{3}H reaction

High cross sections and Q values, as well as simplicity of the fast ^{3}H and α-particles registration resulted in utilizing ^{6}Li (n, α) ^{3}H reaction for neutron monitoring. It is used as a standard for neutron energies from the thermal region up to 100 keV where the cross section follows the 1/v law. The non-1/v behaviour at greater energies is caused by the existence of the resonance when E_n is about 240 keV. A lot of data on this reaction are available. The data spread is 0.5 % in the thermal region, and it is equal to 1 %, 2 %, 4 % and 5 % when E_n is about 10 keV, 30 keV, 450 keV, and 750 keV, respectively.

Table 5

Data recommended for the most important reactions leading to ^3H production in nuclear reactors

Q - nuclear reaction energy; σ_0 - 0.0253 eV neutron cross-section; σ_{14} - 14 MeV neutron cross-section

Nucleus (abundance ratio, %)	Nuclear reaction	Residual nucleus	Q, MeV	σ_0 b	σ_{14} b
^1H (99.985)	$^1H(n,\gamma)$	^2H	2.224	0.3326(7)	$3.08.10^{-5}$
^2H (0.015)	$^2H(n,\gamma)$	^3H	6.257	0.519(7)	$9.5.10^{-6}$
^6Li (7.5)	$^6Li(n,\alpha)$	^3H	4.782	935.9[a] 941.3[b]	$25(3).10^{-3}$
^7Li (92.5)	$^7Li(n,n'\alpha)$	^3H	-2.47		0.340[c] 0.335[d] 0.319[e] 0.286[f]
^{10}B	$^{10}B(n,\alpha)$	^7Li	2.790	3838(6)[b] 3836.6[a]	
	$^{10}B(n,\alpha_0)$	^7Li	2.790	244.25	
	$^{10}B(n,\alpha_1)$	^7Li	2.312	3592.3	
^{10}B (20)	$^{10}B(n,2\alpha)$	^3H	0.2305		$94(20).10^{-3}$

a) - ENDF/B-V b) - /34/ c) - /35/

d) - ENDF/B-IV e) - JENDL-2 f) - JENDL-3

The ^7Li (n, n'α) ^3H reaction

The contribution of this reaction in ^3H production in power reactors is negligible because of high threshold. But this reaction would play a prominent role in energetics based on ^3H-^3H fusion. The first excited level of ^7Li(E* = 0.478 MeV) decays by γ-emission, the second one (E* = 4.63 MeV) by the channel $^7Li \rightarrow {}^4He + {}^3H$. The available data accuracy varies from 15 % to 25 % being insufficient for practical purposes. The recommended cross-section data from various data libraries are shown in Fig. 4. The disagreement of data shows that the new cross-section measurements are needed.

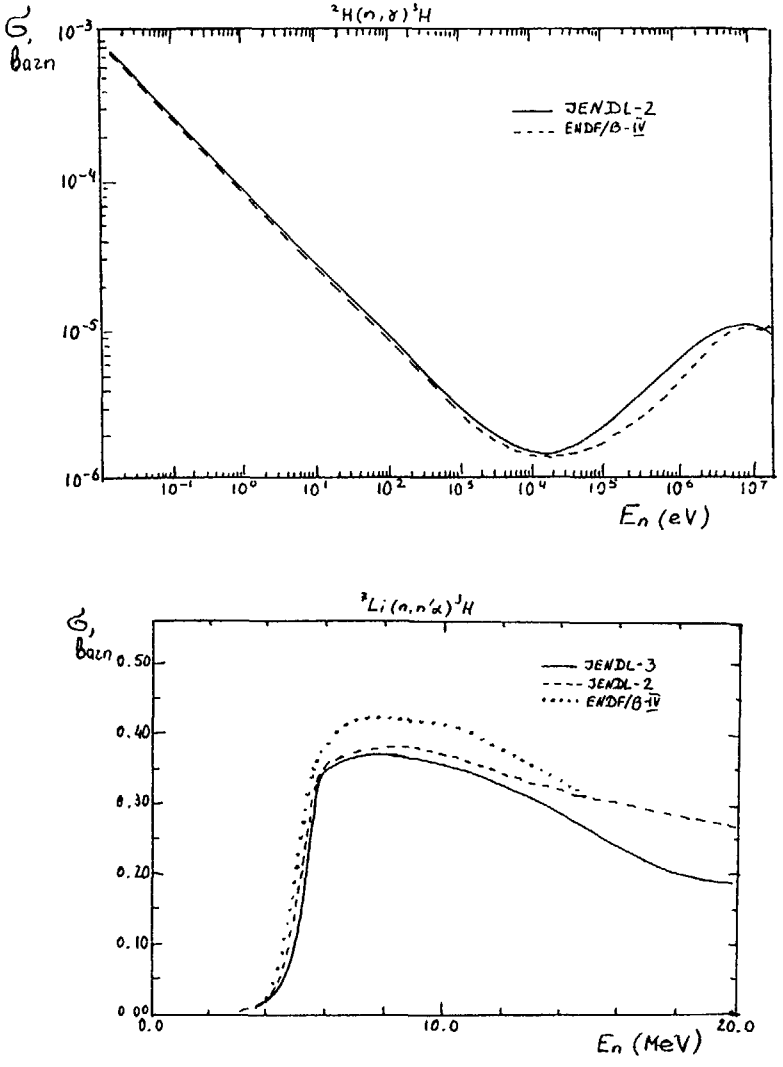

Fig. 4. Recommended cross-section data for some ^3H-producing reactions in nuclear reactor

The $^{10}B(n,\alpha)^{7}Li$ reaction

The cross-sections of two main channels - $^{10}B(n,\alpha_0)^{7}Li$ and $^{10}B(n,\alpha_1)^{7}Li^*$ - are well known. They are often used as standard in neutron flux monitoring at $E_n \lesssim 200$ keV by means of α- or γ-counting. The first channel corresponds to the formation of ^{7}Li in the ground state. The second one corresponds to the first excited state ($E^* = 0.478$ MeV). The available $\sigma_{n\alpha_0}$ and $\sigma_{n\alpha_1}$ data accuracy is better than 2 % at $E_n \lesssim 10$ keV; 3 % in the region up to 100 keV and about 7 % at $E_n \gtrsim 1$ MeV.

CONCLUSION

The ecological safety of the nuclear power plants greatly depends on the results of the investigations of ^{3}H production in nuclear power plants. For further increase of the ^{3}H production cross-section data accuracy the extended theoretical and experimental investigations on the ternary fission and (n, ^{3}H)-reactions are needed.

REFERENCES

1. Magdi M., Ragheb M.H. - Atomkernenergie. - Kerntechnik, 1981, vol. 38, N 2, S. 85.
2. Proc. of the Intern. Symp. on the Behaviour of Tritium in the Environment, San Francisco, 16-20 Oct. 1978, IAEA, Vienna, 1979.
3. Chechetkin Yu.V., Yakshin E.K., Yesherkin V.M. Cleaning of radioactive gaseous vastes. M., 1986 (in Russian)
4. Gorbachev V.M., Zamyatnin Yu.S., Lbov A.A. Interactions of radiations with nuclei. M., 1976 (in Russian).
5. Dacowski M., Chwaszczewska J. et al. - Phys. Lett., 1967, vol. 25B, p. 213.
6. Vorobyov A.A., Seliverstov D.M., Grachev V.T. et al. - Phys. Lett., 1972, vol. 40B, p. 102.
7. Whetstone S.L., Thomas T.D. - Phys. Rev., 1967, vol. 154, N 4, p. 1174.
8. Horrocks D.L. - Phys. Rev., 1964, vol. 134, N 6B, p. 1219
9. Horrocks D.L. - Trans. Amer. Nucl. Soc., 1965, vol. 8, p.12
10. Cosper S.W., Cerny J., Gatty - Phys. Rev., 1967, vol.154, N 4, p. 1193.
11. Cumpstey D.E., Vass D.G. - Physics and Chemistry of Fission, IAEA, Vienna, 1980, p. 128 (Proc. Intern. Symp. on Physics and Chemistry of Fission, Julich, BRD, 14-18 May 1979).
12. Thu Phong Doan et al. - Nucl. Phys., 1967, vol. A96, N 3, p. 588.
13. Vorobyov A.A., Seliverstov D.M., Grachev V.T. et al. - Phys. Lett., 1969, vol. 30B, p. 332.
14. Adamov V.M., Drapchinsky L.V., Kovalenko S.S. et al. - Yad. Fiz., 1969, vol. 9, N 4, p. 732 (in Russian).
15. Albensius E.L., Ondrejcin R.S. - Nucleonics, 1960, vol. 18, N 9, p. 100.
16. Sloth E.N., Horrocks D.L., Boyce E.Y., Studier M.N. - J.Inorg. and Nucl. Chem., 1962, vol. 24, p. 337.
17. Krogulski T., Chwaszczewska J., Dakowski M. - Nucl. Phys., 1969, vol. A128, p. 219.
18. Vorobyov A.A., Grachev V.T., Komar A.P. et al. - At. Ener., 1969, vol. 27, N 1, p. 31 (in Russian)
19. Nobles R.A. - Phys. Rev., 1962, vol. 126, p. 1508.
20. Vorobyov A.A., Grachev V.T., Kondurov I.A. et al. - Yad. Fiz., 1974, v. 20, N 3, p. 461 (in Russian).
21. Kovalenko S.S., Rubchenya V.A. - Ternary fission. M., 1986 (in Russian).
22. Farra H., McElroy W.N., Lippincott E.P. - Nucl. Techn., 1975, vol. 25, p. 305.
23. Quaim S.M., Wölfe R. - Nucl. Phys., 1978, A295, p. 150.
24. Heinrich F., Tanner F. - Helv. Phys. Acta, 1963, vol. 36, p. 298.
25. Ignatyuk A.V. Statistical properties of excited nuclei. M., 1983 (in Russian).
26. Quaim S.M., Wölfe R. - NEANDC(E)-232U, 1982, vol. Y, p.26.
27. Nuclear Spectroscopy. Acad. Press, NY, 1960.
28. Hodgson P.E. - Nuclear reactions and nuclear structure. -. Clarend. Press, 1971, Oxford.
29. Quaim S.M., Stöcklin G. - Nucl. Phys., 1976, vol. A257, p. 233.

30. Woo T.W., Salaita G.N. - Intern. Conf. on Nucl. Cross Sections for Techn., Oct. 22-26, 1979, Knoxwille, USA. - NBS Special Publication 594, 1980, p. 853.
31. Bödy Z.T., Mihaly K. - INDC(HUN)-22L, IAEA, 1986.
32. Zhao Zhixiang, Zhou Delin - INDC(CPR)-8/L, IAEA, 1986.
33. Shibata K., Narita T., Igarasi S. - JAERI-M 83-006, 1983.
34. Holden N.E. BNL - NCS - 52388, 1981.
35. Threshold neutron reactions cross-sections. Ed. by Bychkov V.M. et al. M., 1982 (in Russian).
36. Nuclear Data for fusion reactor technology. IAEA-TECDOC-223, IAEA, Vienna, 1979.

NUCLEAR DATA MEASUREMENT

N.V. KORNILOV, V.M. PIKSAJKIN
Institute of Physics and Power Engineering,
Obninsk, Union of Soviet Socialist Republics

Abstract

Precision neutron flux measurement is one of the most important requirements in nuclear data measurements. The paper concentrates on questions to do with measuring neutron flux and determining the various corrections, using the H(n,n), $^{235}U(n,f)$, $^{238}U(n,f)$, $^{27}Al(n,\alpha)$ and $^{197}Au(n,\gamma)$ standard nuclear reactions as examples.

The business of nuclear data includes working out requirements, making precision measurements, carrying out theoretical calculations using various models, evaluating the data and building up libraries. Of these activities, nuclear data measurement is the most costly and time-consuming; the need to achieve a given degree of accuracy makes its own demands on the way the experiment has to be set up and run.

Nuclear data evaluation is an indispensable part of the experiment. Nowadays, when there are experimental data available for many reactions, the evaluation has to precede the experiment; at this compilation stage, analysing the data enables us to establish what degree of accuracy has been attained and whether it meets our requirements. Carrying out the evaluation beforehand allows us to pinpoint the systematic errors and select a type of experiment which is unrelated to ones which have already been done, and to determine the degree of accuracy needed to ensure that the information content from the new experiment will be sufficient. Once the experiment is over, recommendations are formulated and new sets of evaluated data are compiled.

Because of the fact that a nuclear datum is not just a measured value, but also the error in that value, it becomes particularly urgent for that error to be defined and the correlations between the various values established [1]. In carrying out the experiment, we give serious attention to

studing the characteristics of neutron sources. For "monoenergetic" sources we determine, by calculation and by experiment, the neutron distribution functions, mean energy and energy dispersion [2, 3]; the background components are studied and various methods are used to determine the neutron flux [4]. The various correction factors are studied in detail; as a rule, we use not only the calculated values, we also do special research in order to define the corrections experimentally. Standard reactions play an important role in nuclear data measurement (IAEA Technical Report Series No. 227, IAEA, Vienna, 1983); these include reactions with well-known characteristics which make it possible to develop reliable detection systems. Using standard reactions makes it easier to compare results from different laboratories and makes data analysis simpler.

The features of nuclear data measurement listed above take in such a wide circle of problems that even a brief overview of what progress has been made in the last few years would take much more than one lecture. Bearing in mind the practical orientation of this course, we will concentrate from now on on questions to do with measuring neutron flux and determining the various corrections, using the H(n,n), ^{235}U(n,f), ^{238}U(n,f), ^{27}Al(N,α) and ^{197}Au(n,γ) standard nuclear reactions as examples. This enables us, firstly, to familiarize ourselves with the methods for using the standard reactions, and, secondly, enables us to use that experience to measure other nuclear reactions. In Ref. [25], a $4\pi(\beta-\gamma)$ coincidence system was used to measure the activity of samples of gold. A 4π proportional counter was used as a detector to measure β-particles; a high (70-80%) counting efficiency was obtained, and a double extrapolation method can be used [26]. N_β in expression (4) is equal to:

$$N_\beta = A(E_\beta + (1 - E_\beta)f),$$

where E_β is the β-counting efficiency, and f is a factor dependent on the γ-counting efficiency of the β-channel.

We can see from this that $N_\beta \to A$ when $E_\beta \to 1$ in accordance with the linear law. The experiment measures the value $x = N_c/N_\gamma \simeq E_\beta$, which tends towards E_β when $x \to 1$, although the correspondence is much more complex than a linear function. $N_\beta(1)$ and $A'(1)$ give the absolute activity, and their divergence $\Delta = N_\beta(1) - A'(1)$ can be used as a measure of how accurately they have been determined. In Ref. [25], it is established that when the functions $A'(x)$ and $N_\beta(x)$ are used, Δ is a function of the thickness of the sample (which indicates that the method is incorrect) and can reach 4% (for samples $\simeq$ 30 mg/cm^2). As Ref. [25] shows, function A' becomes linear in variable x^{-1}, and Δ then decreases by a factor of about ten.

In Ref. [27], a $2\pi(\beta-\gamma)$ system was used to measure the activity of samples of aluminium. The β-particle detector was made of a plastic scintillator 0.5-2 mm thick. The advantages of this kind of detector are faster response, ease of manufacture and reliability, and its disadvantages are low E_β values of $\leq$30%, which means that the method described above cannot be used. The model developed to calculate K was checked using a ^{60}Co source, which has a similar decay scheme to ^{24}Na; the lower energy of the β-particles leads to an increase in how far K differs from unity: $1.02 < A'/A < 1.09$. Experiments using detectors of various thicknesses showed that A'/A was a linear function of the calculated value of K; A'(K = 1) coincides with the "passport" activity, although the slope of the function, at 0.92, differs from unity. For samples of aluminium up to 130 mg/cm^2, the method used gives a value for K of $1 < K \leq 1.011$. In experiments to accuracies of within $\simeq$ 0.5% with aluminium samples of various thicknesses, no variation in activity as a function of thickness could be detected, which shows how little K differs from unity and indirectly confirms the evaluation given above.

We conclude with a list of references which examine the various questions of nuclear data measurement in detail. The features of various neutron sources and how they were used are gone into thoroughly in the collection edited by Tsereyaks [28], and the latest developments in the field were presented at the IAEA meeting on neutron source properties in Leningrad, [9-13 June] 1986. A review of methods of using "standard" nuclear reactions is given if Ref. [29]. There is much useful information to be found in

Ref. [4] on the characteristics of the "standard" reactions, the degrees of accuracy achieved to date and the various detectors used.

1. The H(n,n) reaction

The hydrogen nucleus neutron scattering reaction is traditionally regarded as the best standard, first and foremost because of the great accuracy with which the cross-section is known. However, achieving that high accuracy entails a number of difficulties with the methods used:

(1) Recoil protons with energies from 0 to E_{max} must be detected;

(2) Multiple interaction processes are important, and the smaller the detector the greater the loss of events due to edge effects.

When using this reaction, the process of interaction between neutrons and the detector material is typically modelled as invariant. At neutron energies of < 1 MeV, proportional counters containing hydrogen are effective. Ref. [5] (see also the bibliographies given in these references) give detailed analyses of various questions concerning the use of proportional counters to determine neutron flux at energies from 0.3 to 1 MeV. The fact is demonstrated that a suitable choice of model for the counter successfully eliminates systematic error, and good agreement is achieved between the calculated and experimental recoil proton distributions; the total error in the flux measurement is from 1.8 to 2.1%. At higher neutron energies of > 1 MeV, organic scintillators containing hydrogen are used. The 1 Mev limit is a relative one and has to do with the noise limit of the photomultiplier. Typical values for the discrimination thresholds of organic detectors are about 200 keV. The efficiency of a medium-sized (< 10 cm) detector can be measured to within about 2 to 3%, and within these limits a Monte Carlo calculation can be carried out [4, 6]. The main difficulties with nuclear flux measurements using these types of detector arises in defining the significant proportion of the events which are lost below the discrimination threshold and in allowing for the (n,n) and (n,α) processes in the hydrogen nuclei at high energies.

These difficulties are eliminated in "black" detectors, so-called [7]. The detector design (diameter and height > 10 cm) emphasizes multiple neutron interactions, which leads to a redistribution of recoil proton energies (Fig. 1). The efficiency of these detectors at neutron energies between 0.5 and 3 MeV is about 90%, and their main advantages are the low proportion of events lost beneath the discrimination threshold and a significantly reduced effect on the results of the calculation due to partial cross-section errors. Amongst the disadvantages are a high γ-quanta background because events cannot be identified from the form of the pulse, and relatively poor temporal resolution. The efficiency of "black" detectors can be determined with an accuracy of about 1.4%. In these "black" detectors, the H(n,n) reaction plays a decisive role in forming the spectra of the reaction products, although the accuracy requirement for the cross-section is significantly less; the principal condition is that all the neutrons entering the detector should interact completely and be counted.

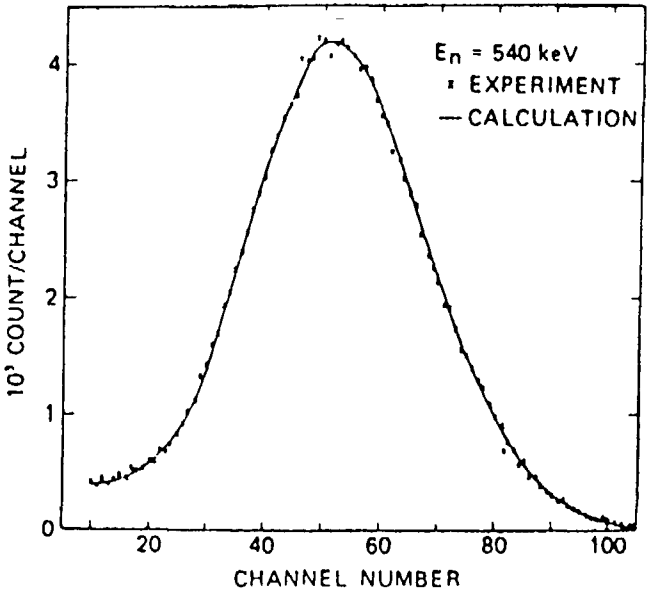

Fig. 1. Proton spectrum in NBS "black" neutron detector at E_n = 540 keV.

The role of (n,p) scattering is more important as a standard in "thin" detectors, so-called. A proton recoil telescope is described in Ref. [8] (other variants are described in the works given as references in Refs [4] and [8]), which consists of two proportional counters and a surface barrier detector; these were used in experiments using neutrons with energies from 6 to 14 Mev. The calculation programme included all the parts of the experiment from the neutron source to the detector. Fig. 2 shows the measured and the calculated recoil proton spectra for E_n = 6 MeV. The reason for the divergence at low energies is unclear. A detailed analysis of the partial errors shows that an accuracy of about 2% can be attained using this detector, and the authors stress that the error in using this method is comparable with the accuracy of the (n,p) scattering process and its angular distribution. The use of "thin" detectors reduces the uncertainty due to multiple interactions, but increases recoil proton escape from the sensitive material.

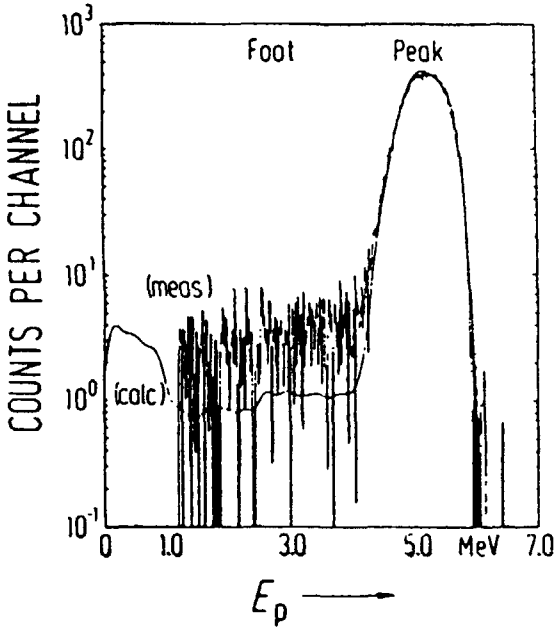

Fig. 2
Proton recoil spectrum of telescope from [8].
Solid line-results of calculation.

An original solution to this problem is suggested in Ref. [9]. Two thin, optically isolated plastic scintillators (Δ = 0.2565 [missing text]) are optically coupled to two pairs of photomultipliers. The second scintillator (along the beam path) registers recoil protons escaping from the first scintillator (Fig. 3). The calculated efficiency (30% of E_n) was determined using the Monte Carlo method in experiments with accompanying particles at 2.45 MeV and 14 Mev. Despite the small size of the detector, the multiple scattering components were 11% (2.45 Mev) and ≈ 4% (14 MeV). In order to take multiple scattering into account, the counting efficiency of the detector is described using the expression:

$$\varepsilon = \sigma_H (a_1 + a_2\sigma_C + a_3\sigma_H),$$

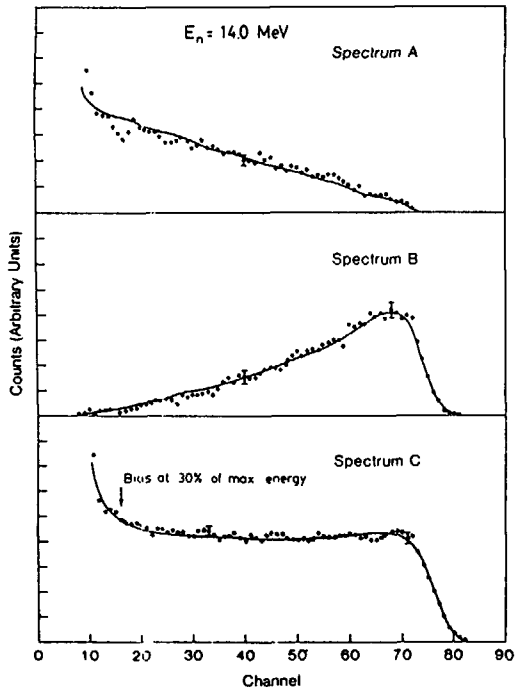

Fig. 3
Proton recoil spectra of double thin detector [9].
A - spectrum of the first scintilator
B - total spectrum of the I and II in coincidence
C - A+B response function of ideally thin detector

where σ_H and σ_C are the interaction cross-sections with hydrogen and carbon respectively, and a_i are the fitting parameters.

The detector efficiency is determined to an accuracy of 0.7% at E = 14 MeV and increases to ≃ 1.5% at ≃ 2 MeV.

The idea of using a grid ionization chamber with a radiator containing hydrogen was put into practice in Ref. [10]. The chamber and grid provide information on the total proton energy and angle of escape. Comparison of the measured and the calculated values showed a systematic absence of recoil protons in the low-energy part of the spectrum, which the authors link to the non-homogeneity of the radiator and a deviation from the cosine law for the determination of proton free path in the the radiator.

Another important area in which the H(n,n) reaction is used is in determining neutron flux in experiments for studying elastic and inelastic scattering [11, 12]. The sample of the material being studied is replaced by a sample containing hydrogen. Neutrons scattered at a certain angle have a given energy $E_o\cos^2\theta$; because of the connection between neutron energy and angle of scattering, the multiple scattering correction is small and the most important thing is the reduction in the input and output neutron fluxes, which can be calculated analytically using the formulas shown in Refs [12] and [13]. In Ref. [12], neutron scattering in the scintillator containing hydrogen (detector-scatterer) is used to determine the efficiency of neutron detectors. With only a monoenergetic neutron source of about 14 MeV, detector efficiencies at energies from 1 to 10 Mev were successfully measured. In Ref. [12], corrections for the edge effect, flux reduction and energy resolution of the detector-scatterer are analytically calculated.

2. Fission reactions

The $^{238}U(n,f)$ and $^{235}U(n,f)$ fission cross-sections are known to within 2 to 3% for a wide range of neutron energies, and to all appearances within about 1% for ^{235}U at about 14 MeV [14]. This wide range was obtained with ionization chambers for fission in 2π geometry [4, 15, 16].

For this kind of experiment, the most important correction is for the loss of fragments below the discrimination threshold. There is enough of this kind of information for us to determine the total number of interactions if we can compare the discrimination level with the residual fragment free path; in practice, two independent corrections are made: for self-absorption in the layer and loss below the discrimination threshold down to zero amplitude.

Self-absorption in the layer is analysed in detail in Ref. [17]. Without showing the complete calculation, we shall show just the final correlations.

The probability $I(t_o)$ that a fragment will not be recorded is equivalent to:

$$I(t_o) = (^{to}/R - \eta)^2 \frac{R}{2to} (1 - {}^{a_2}/2), \qquad (1)$$

when the angle β between the direction of the beam and the normal to the layer is 0; and

$$I(t_o) = (^{to}/2R + \eta)\ (1 - {}^{a_2}/2) \qquad (1)$$

when $\beta = \pi$;

t_o, R are the thickness of the layer and the mean fragment free path;

a_2 is the coefficient of the second Legendre polynomial describing the angular distributions of the fragments relative to the neutron flux; and

η is the ratio of the velocity of the centre of inertia of the neutron-fissioning nucleus system and the mean velocity of the fission fragments;

$$\eta = (E_o\ A_f/T_f)^{1/2}/(A + 1) \simeq 0.005(E_o)^{1/2},$$

where A_f is the mean mass number of the fragments and their kinetic energy $T_f \simeq 85$ MeV. In working out the formulae, the following simplifying assumptions were made:

(1) The neutron flux is perpendicular to the layer;

(2) The fissile material is taken to be an ideal plane parallel layer;

(3) The angular distribution of the fragments is described by a second Legendre polynomial alone;

(4) The effect of movement in the centre of gravity can be allowed for by altering the limits of the integration

$$\pm S = \pm t/R \text{ to } \pm (S - \eta) \text{ for } \beta = 0, \text{ and } \pm (S + \eta) \text{ for } \beta = \pi;$$

(5) The values of t_o/R and η are small and can be defined using first-order terms;

(6) Where $\beta = 0$, all fragments formed at a depth $t < \eta R$ will be detected.

Self-absorption of fragments is determined experimentally in Ref. [18] (Fig. 4). The primary influence on the measured value is the quality of the layer, i.e., its homogeneity. For UF_4 layers deposited by vacuum evaporation, the measured value is

$$\Delta = 1/2R = (0.105 \pm 0.07)\text{cm}^2/\text{mg} \qquad (2)$$

From this we can derive the mean free path of the fragments $R = (4.76 \pm 0.32)$ mg/cm^2. The value obtained is less than the experimental mean free path data. Ref. [19] gives the free paths in uranium for various neutron energies from thermal to $\simeq$ 14 MeV as R_l of between 10 and 11 mg/cm^2 and R_h between 8 and 9 mg/cm^2 for light and heavy fragments respectively. The lower value of R obtained from expression (2) is evidently due to the fact that the method used to find the formula takes into account the inhomogeneity of the layer (see Fig. 4, for a more friable layer of U_3O_8). This value should therefore be the one used in defining

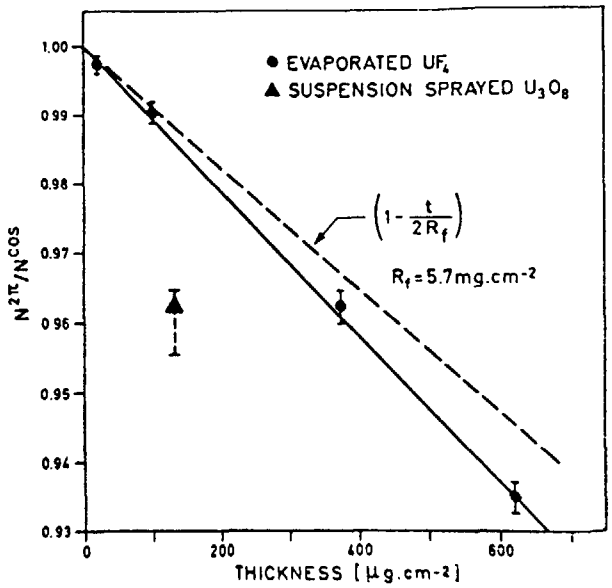

Fig. 4
Part of fission fragments lost under the threshold of discrimination in 2π - ionization chamber versus upon thickness of the layer.

fragment loss in accordance with formulae (1). As Fig. 4 shows, the accuracy of the self-absorption determination depends on the quality of the layer. In the best case, with $t_o < 0.2$ mg/cm^2, an accuracy of 0.5% can be attained.

To determine the proportion of the fragments lost through the discrimination amplitude, the form of the energy distribution must be known. A simple evaluation can be obtained as follows:

$$f(E,t)\, dE\, dt = W(S)\, dS\, dt$$

$$f(E)\, dE = \frac{dE}{t_o} \int_0^{t_o} W(S) \frac{\partial(S,t)}{\partial(E,t)}\, dt,$$

Where $f(E)$ is the energy distribution of the fragments;
$W(S)$ is their angular distribution;
$S = t/R(E_x)$ is the cosine of the angle of escape of the fragment relative the normal; and
$E_x = E_{max} - E$ is the energy of the fragments left in the layer.

Taking into account that

$$\partial(S,t)/\partial(E,t) = t\cdot(dR/dE_x)\cdot R^{-2}(E_x),$$

we can write:

$$f(E) = \frac{(dR/dE_x)}{t_0 R^2(E_x)} \int_0^{t_0} W(t/R(E_x))\, t\, dt$$

We can evaluate the possible alteration in $f(E)$ where $E \to 0$ for $W(S) = \text{const}$. The minimum error or detection threshold is determined by the maximum energy of the α-particles and protons from the (n,p) and (n,α) reactions in the substrate material. For $E \simeq 14$ MeV, $E_{thr.} \simeq 10$ MeV. With the help of data about the ionization losses and free paths of heavy ions [20], we can obtain the following result:

$$f(0)/f(10\ \text{MeV}) \simeq 0.8$$

The extrapolation in the form of constants from the area of the depression in the fragment spectrum (Fig. 5) is thus a competent one. If the number of fragments lost below the discrimination threshold is between 1 and 3%, this extrapolation may lead to a systematic increase in the number of events by from 0.2 to 0.6%.

The calculations above are more qualitative in nature than otherwise, and indicate possible errors in determining detection efficiency. In the absence of additional research, the accuracy is in reality $\simeq$ 1%.

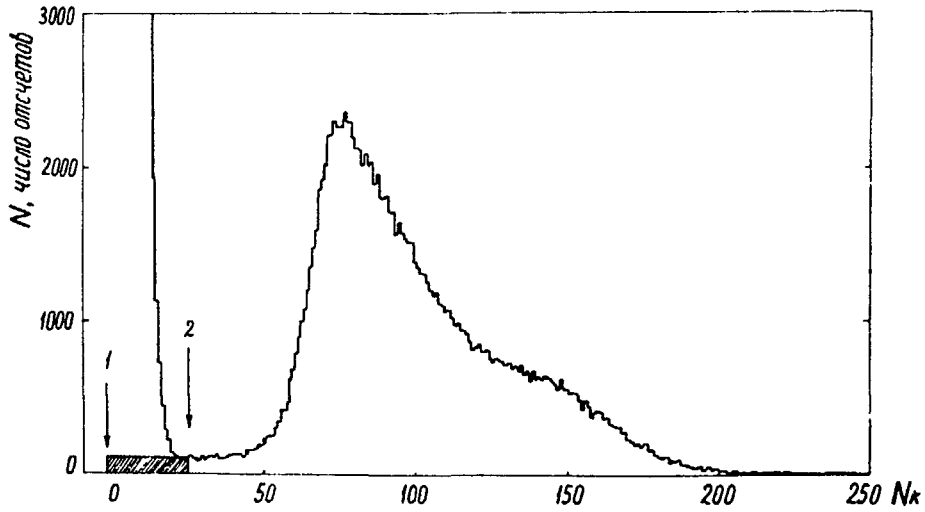

Fig. 5
Spectrum of fission fragments in 2π - fission ionization chamber. Thickness of the $^{238}UF_4$ layer - 0.27 mg/cm^2, $E_n \sim$ 14 MeV
Numerically indicated: 1 - zero ADC, 2 - threshold of the discriminator

The degree of accuracy obtained in "weighing" layers was studied during international checking of ^{235}U samples prepared in various laboratories. No deviation greater than 0.35% was found in the given values. This value evidently gives an idea of how accurately the number of nuclei can be determined.

3. The $^{27}Al(n,\alpha)$ and $^{197}Au(n,\gamma)$ reactions

The radiation capture cross-section is used as a standard at energies between 0.2 and 1 MeV, accuracy $\simeq$ 4%, and as a rule at $E \simeq 14$ MeV (accuracy $\simeq$ 1%). The use of this reaction at energies between 6 and 10 MeV is made problematical because of the resonance structure of the cross-section [22]. The reaction is used in an activation method, and the determining accuracy is thus that of the measurement of sample activity (for (n,γ), how accurately the slowed neutron background is allowed for is of

primary importance). We shall go more deeply into two methods of measuring activity: γ-quanta counting using a calibrated detector and the (β–γ) coincidence method. The measuring accuracy of Ge(Li) detectors is determined by the accuracy of the standard γ-quanta sources (1 to 1.5%) and by the accuracy with which the various corrections are made: for dead time, pile-up effect and γ-quanta cascade coincidence. All these effects can be determined with an accuracy of from 0.5 to1% [23]. As Fig. 6 shows, at γ-quanta energies of between 800 and 1500 keV, accuracies of ≈ 1% can be achieved, at transitional energies of 300 to 80 keV it is from 2 to 3% and at energies of < 300 keV it is ≈ 2%. The following expression is used for the interpolation:

$$\ln \varepsilon(E_\gamma) = \sum a_i (\ln(E_\gamma))^i, \quad i = 0, 1, 2 \qquad (3)$$

where a_i are coefficients determined using the method of least squares.

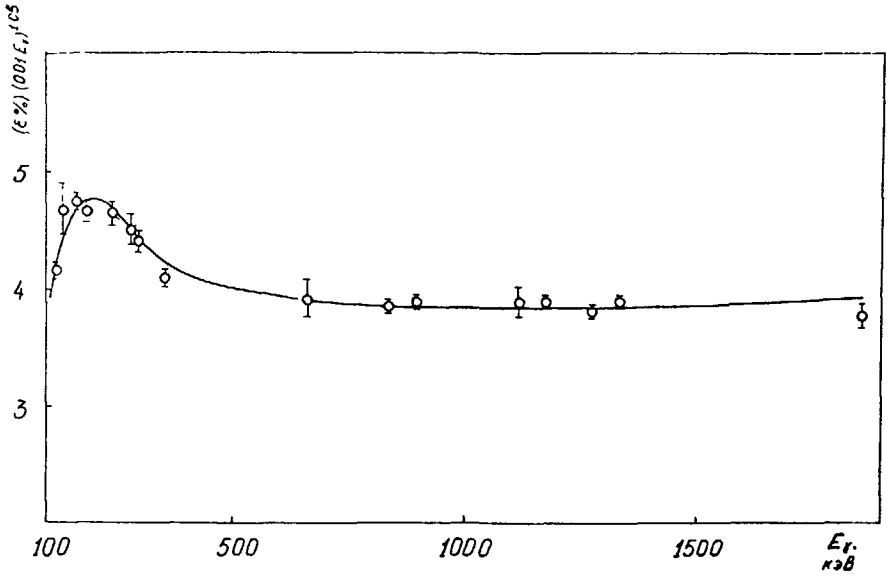

Fig. 6
Efficiency of Ge(Li) detector and its description with expression 3.

Thus, E_γ = 1.39 and 2.75 MeV for the (n,α) reaction. The absolute efficiency of the detector can be determined with an accuracy of ≈ 1%.

For the capture reaction, the situation is not so good. In Ref. [24], the efficiency of a Ge(Li) detector at E = 412 keV and with a correction for self-absorption was determined with an accuracy of ≈ 0.5% for samples measured using the (β–γ) coincidence method.

When measuring the activity of samples of aluminium, the primary uncertainty is the correction for cascade γ-quanta coincidence. For E (1.39) = 0.24%, this correction is from 5 to 6%, and can be correctly determined only by measuring total efficiency/photoabsorption, vapour formation and Compton scattering/detection of 2.75 MeV γ-quanta. When samples with compact geometries are activated, the specific activity varies with sample thickness; in this case, there may be a noticeable correlation between specific activity and attenuation of γ-quanta in the sample, and the efficiency of the detector may depend on the distance between it and the sample.

The decay scheme of the reaction products in this case and others makes (β–γ) detection possible. An idea that is simple in principle is complicated by the fact that there are no β-detectors that are insensitive to γ-particles. The measured activity A' is correspondingly related to the true activity A by the equation

$$A' = \frac{N_\beta \cdot N_\gamma}{N_c} = A \cdot K, \qquad (4)$$

where N_β, N_γ and N_c are the counting rates in the β- and γ-detectors and the coincidence channel and K is a coefficient which is a is a complex function of the efficiency of γ-quanta detection in the β-channel, the thickness of the foil, the decay scheme and the design of the unit. A calculation of K allowing for all these results in an unwieldy expression, in which it is difficult to establish how well the model of the experimental set-up corresponds to the real situation. For that reason, the value for K must be

found by experiment and based on experiment. An important criterion for the correctness of the method used to define A is the lack of any correlation between it and sample thickness.

REFERENCES

[1] SMITH, D.L., Non-evaluation applications of covariance matrices, ANL/NPH-67 (1982).

[2] KORNILOV, N.V., Possibilities of experimental determ. and theor. prediction of properties of acc. based neutron sources, IAEA Advisory Group meeting on Neutron Source Properties, Leningrad [9-13 June] 1986.

[3] CSIKAI, J., LANTOS, Zs., BUEZKO, G.M., Investigation on the properties of D+D and D+T neutron sources, ibid.

[4] GAYTHER, D.B., Nuclear standard reference data, IAEA-TECDOC-335, Vienna (1985) 345.

[5] DAVLETSHIN, A.N., TOLSTIKOV, V.A., Yadernye konstanty (Nuclear Constants) 7 (1971) 277.
DAVLETSHIN, A.N., PLATONOV, V.P.' TOLSTIKOV, V.A., Yadernye konstanty (Nuclear Constants) 9 (1972) 107.

[6] SIMAKOV, C.P., The measurement of inelastic neutron scattering, lecture given as part of course.

[7] POENITZ, W.P., Nucl. Instrum. Methods 109 (1973) 413
LAMAZE, G.P., MEIER, M.M., WASON, O.A., Proc. Conf. on Nuclear Cross-sec. and Techn., Washington (1975) 73.
RENNER, C., HILL, N.W. et al., Nucl. Instrum. Methods 154 (1978) 525.

[8] BREDE, H.J., COSACK, M. et al., IAEA-TECDOC-335, Vienna (1985) 341.

[9] DIAS, M.S., JOHNSON, R.G., WASSON, O.A., Nucl. Instrum. Methods 224 (1984) 532; see also IAEA-TECDOC-335, Vienna, 1985, 467.

[10] KNITTER, H.-H., BUDTZ-JØRGENSON, C., BAX, H., see [6] p.471.

[11] CRANBERG

[12] KORNILOV, N.V., PLYASKIN, V.I., Institute of Physics and Power Engineering Preprint 496, Obninsk; Proc. All-Union Conference on Neutron Physics, Kiev (1975) Part 6, 261.

[13] BARYBA, V.Ya., ZHURAVLEV, B.V., KORNILOV, N.V. et al., Institute of Physics and Power Engineering Preprint 671, Obninsk (1976).

[14] See [4].

[15] SMITH, D.L., MEADOWS, J.W., ANL/NDM-10 (1975).

[16] KORNILOV, N.V., ZHURAVLEV, B.V. et al., At. Ehnerg. 49 fascicle 5 (1980) 283.

[17] CARLSON, G.W., Nucl. Instrum. Methods 119 (1974) 97.

[18] BUDTZ-JØRGENSON, C., KNITTER, H.-H., IAEA-TECDOC-335, Vienna (1985) 476.

[19] GORBACHEV, V.M., ZAMYATIN, Yu.S., LBOV, A.A., The interaction of radiations with the nuclei of heavy elements and the fission of the nuclei, a handbook, Atomizdat (1976) [in Russian].

[20] NEMETS, O.F., GORMAN, Yu.V., Guide to Nuclear Physics, Naumova dumka, Kiev (1975) [in Russian].

[21] POENITZ, W.P., MEADOWS, J.W., see [6] p.405.

[22] KORNILOV, N.V., RABOTNOV, N.S. et al., IAEA-TECDOC-335, Vienna (1985) 135.

[23] KNOLL, G.F., Radiation Detection and Measurement (1979).

[24] DAVLETSHIN, A.N., TIPUNKOV, O.A. et al., At. Ehnerg. 46 fascicle 2 (1980) 87.

[25] GARAPOV, Eh.F., GRYAZKOV, A.N. et al., in The Metrology of Neutron Radiation Vol.1 (Proc. 2nd All-Union Meeting) (1974) 121.

[26] MENKE, H., FAHLAND, J., in Standardization of Radionuclides (Proc. Symp. Vienna, October 1966) IAEA, Vienna (1967) 183.

[27] KORNILOV, N.V., KAGALENKO, A.B. et al., paper at conference on neutron physics, 1987.

[28] [TSEREYAKS (ed.),] Neutron Sources for Basic and Applications, Pergamon Press (1982).

[29] CARLSON, A.D., Prog. Nucl. Energy 13 (1984) 213.

SYSTEMATICS OF TRANSURANIUM NUCLEI FISSION CROSS-SECTIONS

B.I. FURSOV
Institute of Physics and Power Engineering,
Obninsk, Union of Soviet Socialist Republics

Abstract

The paper presents the principles of constructing the systematics of transuranium nuclei fission probability characteristics based on the current model of fission barrier and statistical approach. Fission probability energy dependence was investigated. The results of systematics were shown in comparison with the experimental data.

INTRODUCTION

The Lecture suggested to your consideration aims at demonstrating an importance and practical use of systematics of experimental data on heavy nuclei fission probability. The material will be presented schematically so as to save time. This problem is given in more detail in Refs. /1-5/.

Characteristics of heavy nuclei fission probability are of great interest from the standpoint of valuable practical and scientific aspects of the information contained in them. In a wide range of excitation energy values the nuclear fission and neutron emission processes are dominating modes of compound nucleus decay. Probability of these concurent reactions is determined by the corresponding mean widths: the fission Γ_f and neutron Γ_n ones.

The feature of heavy nuclei fission in the (n,f)-reaction is availability of the "plateau" region in the fission cross-section σ_f as a function of neutron energy. This property of fission cross-sections $\sigma_f \simeq \sigma_c \Gamma_f/(\Gamma_f+\Gamma_n)$ is explained by a weak dependence on E_n for the values figured in this expression: a compound nucleus formation cross-section σ_c and a ratio Γ_n/Γ_f. A concept of "plateau" in the dependence $\sigma_f(E_n)$ is approximated as well as the assumption σ_c = const and Γ_n/Γ_f = const. However these approximations are often made use of not only for the sake of simplicity, but due to insufficient knowledge of the energy of these

values, particularly Γ_n/Γ_f . This situation exist in reality regardless of high practical requirements to the accuracy of experimental measurements and theoretical description nuclear physics constants, the dependence $\sigma_f(E_n)$ being among the most important.

In spite of the volume of experimental information on fission cross-sections and nuclei fissility of recent years being essentially increased, the scientific and practical needs are often beyond its scope. In this context we may observe such problems as e.g. neutron-excessive fusion in multiple neutron-capture reactions in high fuel burn-up reactors, in nuclear explosions, in astrophysical media, or alternatively, the formation of neutron-deficient nuclei as a result of multiple neutron emission by excited nuclei, particularly in heavy ion reactions.

The urgency of creating systematics, that allow the fission cross-sections to be evaluated fairly accurately in the region Z-(nuclear charges) and N-(neutron numbers) inaccessible nowadays for experimental study is identified by the following reasons:

1. Nuclides, whose fission probability was studied in (n,f)-reactions or in direct with charged particles are concentrated in the vicinity of stability valley and experimental possibilities to extand this area is essentially exhausted.

2. For the time being the theory does not allow the fairly accurate prediction of fission process characteristics of interest, that is why the phenomenological approach predominates in the description of these characteristics.

3. Systematics of fission cross-sections and Γ_n/Γ_f values, which have been well-spread and used up to now, are purely empirical, they do not take into account the basic physical regularities, that imposes severe restrictions on their applicability.

In the present lecture I am going to deal with three problems. First, I shall present the principles of constructing the systematics of transuranium nuclei fission probability characteristics based on the current model of fission barrier and statistical approach in the description of excited nuclei decay widths. The results of systematics will be shown in comparison with the experimental data, some of empirical systematics.

Second, I shall demonstrate the effectiveness of practical employment of the developed systematics with the realistic evaluations of understudied curium isotopes fission cross-sections taken as an example.

Third, I shall show, how certain regularities in the description of fission probability energy dependence can be established on the basis of experimental data analysis. The forthcoming detailed study of this dependence is the next step in the investigation region under study and is essential for the concordant description of partial cross-sections in the wide range of neutron energy.

I. Systematics of Nuclear Fission Probability Characteristics.

(Fission Barriers, Γ_n/Γ_f values, Nuclear Fissilities, Fission Cross-sections).

Systematics is based on the analysis of the strength of all the experimental evidence. The principal sources of data were neutron fission cross-sections in the first "plateau" region (E_n = 2-4 MeV) and excitation function (i.e. fissility $P_f = \sigma_f/\sigma_c$) for the fission process following the direct reactions (^{3}He,df), (^{3}He,tf), (t,pf) etc. at the identical excitation energies ($E = E_n + B_n$). In our analysis we have classified and descriminated the data by the excitation energy. The data on value $\Gamma_n/\Gamma_f = P_f^{-1} - 1$ obtained from the multiple neutron emission reactions correspond to higher energies $\overline{E}$ and are omitted in the analysis.

The term "plateau" actually expresses the basic property of the fissibility or fission cross-section, that is a weak energy dependence. This "rule" in addition to being approximated is suitable only in the restricted energy range depending on the ratio of fission threshold E_f and neutron emission B_n. However, with high variation of Γ_n/Γ_f in a wider energy range being taken into account, the constancy of the Γ_n/Γ_f value in the "plateau" region should be admitted nontrivial. It is this favorable circumstance that allowed the fission cross-section systematics to be constructed in the "plateau" region depending on the nucleon composition of fissile nucleus A and Z.

To proceed with our discussion let us give a btief consideration of separate aspects of Γ_n/Γ_f value theoretical description. In the excitation energy region of interest the statistical approach is applicable to the description of compound-nucleus decay widths. We attempted to obtain simple analytical ratioes, that is why we adopted level density model with a constant temperature widely and effictively used for experimental data description in the

low-excitation region $\rho(U) = c \cdot \exp(U'/T)$, which enabled us to obtain a simple ratio for Γ_n/Γ_f

$$\Gamma_n/\Gamma_f = G \cdot \exp\left(\frac{E_f' - B_n'}{T}\right),$$

where G = const, mentioned below, T = const = 0,5 MeV, E_f' and B_n' - are *effective values of fission and neutron emission thresholds* respectively. A close consideration of corrections for even-odd variations to the thresholds and level density shows, that they are mutually compensating and the last ratio is transformed to the form:

$$\Gamma_n/\Gamma_f = G \cdot \exp\left(\frac{E_f - \langle B_n \rangle}{T}\right)$$

where E_f-is the real fission barrier, and the value $\langle B_n \rangle$ -is the compound-nucleus binding energy averaged by the adjacent isotopes. The resulting expression is easily generalised for the case of double-humped fission barrier, where two transient systems associated with inner and outer humps A and B must be taken into account:

$$\Gamma_n/\Gamma_f = G_A \cdot \exp\left(\frac{E_f^A - \langle B_n \rangle}{T}\right) + G_B \cdot \exp\left(\frac{E_f^B - \langle B_n \rangle}{T}\right) \quad (*)$$

The top section of fig.1 illustrates experimental values of $\lg(\Gamma_n/\Gamma_f)$, which were taken as a basis when constructing the systematics, the bottom one - a totality of $\langle B_n \rangle$ values calculated by *the nuclear mass tables*. *Fig.1* shows that whereas the lines Z = const, N = const for $\langle B_n \rangle$ form a regular structure, i.e. a grid in all the nuclear range under consideration, $\lg(\Gamma_n/\Gamma_f)$ has this property only on a relatively narrow segment. Hence, the only conclusion can be drawn: the dependence of the fission barrier value E_f^A and E_f^B on the Z and N essentially affects the $\lg(\Gamma_n/\Gamma_f)$ value dependence on the nucleon nuclear composition.

That is why it is required to develop a fairly simple, but at the same time correct description of fission barrier heights E_f^A and E_f^B in a wide range of values Z and N so as to construct the Γ_n/Γ_f value systematics and, therefore, the σ_f fission cross-section systematics. The potential energy $V(\alpha)$ can be represented as a sum of two components: liquid-drop model energy $\tilde{V}(\alpha)$- and that of a shell correction $\delta W(\alpha)$, according to which the barrier heights E_f^A and E_f^B can be expressed as

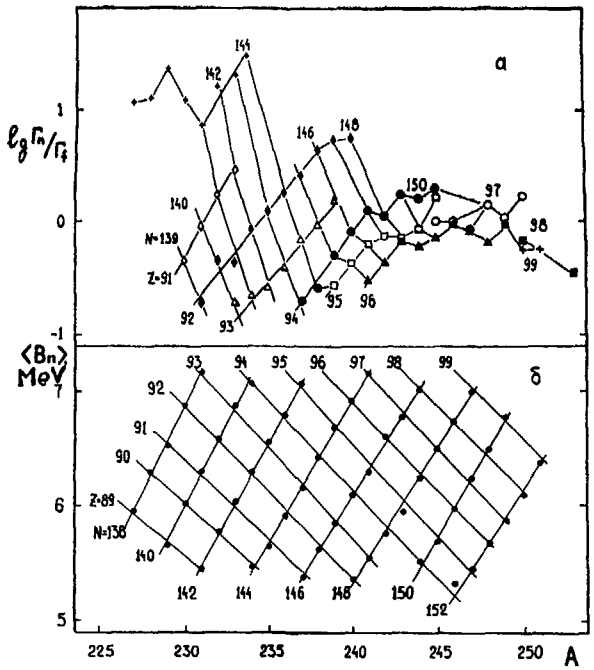

Fig.1. The correlation of the dependences of $\lg(\Gamma_n/\Gamma_f)$ and $\langle B_n \rangle$ on the mass number of A. The lines connect points with fixed values of Z and N.

$$E_f^i = \tilde{V}(\alpha) - \delta W_g + \delta W_f^i,$$

where i - A or B, δW_g - is the shell correction for the ground state of nuclear equilibrium deformation counted from the $\tilde{V}(0)$= 0 ground liquid-drop model state, δW_f^i - is the shell correction for the i-th maximum $V(\alpha)$ counted from the potential liquid-drop model energy at the appropriate deformation $\tilde{V}(\alpha_i)$.

Here we have no opportunity to dwell upon the details of the barrier calculation /3/. Note, that the liquid-drop component of barrier was calculated within the Cohen-Swiatecki parametrization /6/ using the Myers-Swiatecki parameters /7/. The shell correction of the ground state $\delta W_g(Z,N)$ was calculated as a difference

between the experimental nuclear masses and the masses calculated by the liquid-drop model. The variation low of shell corrections δW_f^A and δW_f^B with nucleon number was established empirically in the form a universal weak dependence.

The barrier values E_f^A and E_f^B obtained as a result of calculations within the unified description for a wide complex of nuclei from uranium to fermium in the best way corresponded to the values known from the experiment. The root-mean-square deviation of calculated barrier values from the experimental ones was $\Delta E_f^A = \Delta E_f^B = 0{,}26$ MeV that is comparable with the spread of values by different authors and the barrier determination error presented by them.

From ratio (*) it follows, that there are only constant G_A and G_B left to be determined for the universal description of the value Γ_n/Γ_f over the whole transuranium nuclear range. We determined them by the adjustment for the experimental values Γ_n/Γ_f known from fission cross-section measurements with the best accuracy. They turned out to be equal to: $G_A=0{,}37$; $G_B=1{,}00$. In the course of adjustment for Γ_n/Γ_f value extraction from σ_f according to the ratio $\Gamma_n/\Gamma_f = \sigma_c/\sigma_f - 1$ the mean value $\sigma_c = 3{,}1$ barn was adopted for ^{238}U in the "plateau" region (E_n= 2-4 MeV) evaluated from the calculation by the coupled-channel model.

The values Γ_n/Γ_f calculated with the resulting constants enabled us to obtain the fission cross-section value σ_f for the whole complex of nuclei shown by a line in Fig.2 and are compared with the experimental values of fission cross-sections for all the nuclei studied by the present time as well as with the empirical systematics /8/ (dashed line). The dark sings show neutron data, the light ones - the fission cross-sections "derived" from nuclear fissility measurements in direct reactions. The relative root-mean-square error of the present systematics for experimental points n = 63 in the uranium-einsteinium nuclear range was 15%, that met the requirements for "exotic" isotope fission cross-section accuracy.

Comparison of experimental data with the empirical Behrens systematics ignoring any physical regularities is shown to give a good description of the data in the uranium-neptunium-plutonium nuclear range. The agreement is violated when removing from it to

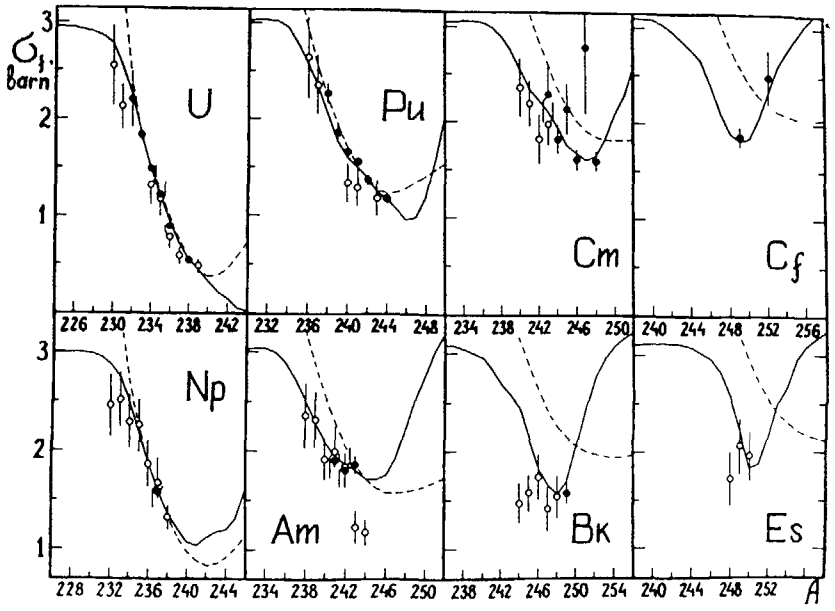

Fig.2. The comparison of the neutron fission cross-sections values calculated according to the present systematics with the experimental ones. The black points are the data measured in the (n,f)-reaction: the light points are the results "similated" from the fission probability measurements in direct reactions. The solid line is the present systematics (calculation), the dashed line is the systematics by Behrens /8/ (calculation).

the region of small N as well as large Z. At sufficient shortage of neutrons the Behrens systematics gives a physically sensless result: the fission cross-section is more, than the compound-nucleus formation cross-section. A disagreement of the Behrens systematics with the experimental data in the region $Z \geqslant 96$, where it can be rejected as that being out of keeping with the test is still more essential.

II. Curium Isotopes Fission Cross-Section Evaluation by Fast Neutrons

We shall show, in which way the developed systematics of fission cross-sections in the first "plateau" range can be employed for curium isotopes fission cross-section evaluation. An unsatisfactory state of experimental data results in great disagreements in evaluated values of fission cross-sections. Our opinion is, that none of the existing curium isotope fission cross-section evaluations can be recommended for application in the whole range E_n = 0.1-20 MeV.

Nowadays satisfactory data are available only for the isotope ^{245}Cm /9/. In order to obtain a realistic evaluations of other isotopes the following steps were undertaken:

- consideration was given not only to the neutron data, but the fission probability results studied in the direct reactions by Britt et al /10/;
- an unified approach to the selection and intercorrelation of the experimental data was realized;
- the fission cross-section systematics described above was adopted as a basis.

The basic experimental data for curium isotopes are concentrated in the low energy range $E_n \lesssim$ 1-2 MeV. Alternatively, a statistical approach is applicable above this energy, that is why we applied the systematics as reference values for the range $E_n \gtrsim$ 2MeV for fission cross-section description, that enabled us to avoid gross error when analysing the few and inconsistent data.

Information of the compound-nucleus formation cross-section σ_c permiting the data P_f and σ_f to be intercompared is required for the joint consideration and description of the data on fission cross-section $\sigma_f(E_n)$ and fission probability in the direct reactions $P_f(E)$:

$$\sigma_f(E_n) = \sigma_c(E_n) \cdot P_f(E_n+B_n).$$

In our work we used the results of $\sigma_c(E_n)$ calculations by the coupled-channel model with the parameters for ^{246}Cm according to /11/. For other nuclei-targets with a mass number A it was assumed, that

$$\sigma_c^A(E_n) = \sigma_c^{246}(E_n) \cdot (A/246)^{2/3}.$$

The analysis of fission probability energy dependence for curium isotopes shows, that in a wider neutron energy range E_n = 2-20 MeV it can be considered constant with a reasonable accuracy. This value was taken from the systematics:

$$P_f^A(E_n) = P_f^\circ = \text{const} \qquad E_n \geqslant 2 \text{ MeV}$$

The fission probability energy dependence $P_f(E)$ below this energy ($E_n < 2$ MeV) based on the available complex of experimental data normalized to the value P_f° in the interval E_n = 2-4 MeV. The experimental data displacement in the course of normalization as a rule did not exceed the experimental errors.

The complex of normalized experimental data was approximated by the rational function (code PADE 2). A set of functions $P_f(E)$ was obtained as a result of approximation for all curium compound-nuclei with A = 241-249 from the fission threshold up to the "plateau" region (E_n = 2-4 MeV). The value $P_f(E)$ below this energy is based on the smoothed experimental dependence and for higher energies (E_n = 2-20 MeV) the value $P_f(E)$ was assumed equal to P_f° = const.

The reaction (n,nf) is imitiated at the compound-nucleus A fission in the energy range above $E_n \simeq$ 6 MeV, and above $E_n \simeq$ 12 MeV the reaction (n,2nf) is started where the nuclei A-1 and A-2 respectively are fissioned. If the data on the fission probability $P_f(E)$ are known in the excitation energy range from the fission threshold up to the "plateau" for chain isotopes A, A-1, A-2, the total fission cross-section can be calculated over the whole neutron energy range above the thresholds of reactions (n,nf) and (n,2nf):

$$\sigma_f(E_n) = \sigma_f^A(E_n) + \Delta\sigma_f^{A-1}(E_n) + \Delta\sigma_f^{A-2}(E_n)$$

where

$$\sigma_f^A(E_n) = \sigma_c(E_n) \cdot P_f^\circ(A),$$

$$\Delta\sigma_f^{A-1}(E_n) = \sigma_c(E_n)\left[1-P_f^\circ(A)\right] \int_0^{E_n} P_f^{A-1}(E_n-\epsilon)N(\epsilon)d\epsilon,$$

$$\Delta\sigma_f^{A-2}(E_n) = \sigma_c(E_n)\left[1-P_f^\circ(A)\right]\left[1-P_f^\circ(A-1)\right] \cdot$$

$$\int_0^{E_n-B_n^{A-1}} N(\epsilon_2)d\epsilon_2 \int_0^{E-B_n^A-\epsilon_2} P_f^{A-2}(E_n-B_n^{A-1}-\epsilon_2-\epsilon_1)d\epsilon_1 .$$

For the spectrum of emitted neutrons

$$N(\epsilon) = \frac{\epsilon}{T^2} \exp(-\frac{\epsilon}{T})$$

the value $T_1=T_2=T=0,5$ MeV close to data /12/ was accepted.

The curium isotopes fission cross-section evaluation was performed using this approach, the result of this evaluation are shown in Fig.3-9 together with other evaluations and experimental data /13-23/. Figure captions: x-axis-neutron energy E_n (MeV), y-axis-fission cross-section σ_f (barn), ——— present evaluation, - - - evaluation INDL/A (Italy. Bologna), - · - evaluation JENDL 2 (Japan), -··- evaluation KEDAK (FRG, Israel), -···- evaluation ENDF/B-5 (USA), ◓ - present systematics, signs - experimental data.

An algorithm of experimental data description and their prediction in the energy range where the data are missing is realized in the present evaluation, that is common for all curium isotopes considered and physically consistent. Regardless of the essential forced renormalization of inconsistent data and simplification of the model for high-energy fission cross-section description this step enables us to go ahead in the evaluation of curium isotope fission cross-section by fast neutrons.

The recommended curves uncertainty in the range $E_n < 6$ MeV was estimated as 10-15% (for ^{242}Cm, ^{247}Cm - 20%). In the region $E_n > 6$ MeV the uncertainty increases $\sim$ 1,5 times.

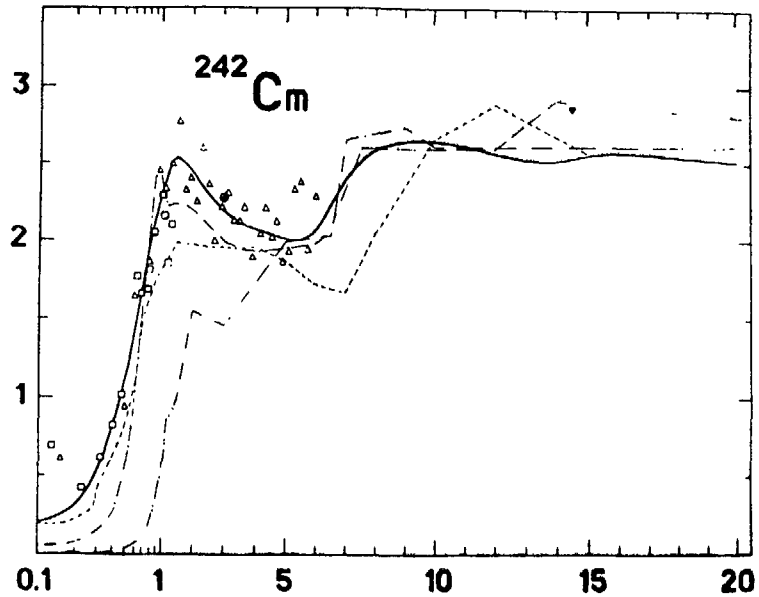

Fig.3. ^{242}Cm. △ - /10/, □ - /15/, ▼ - /16/.

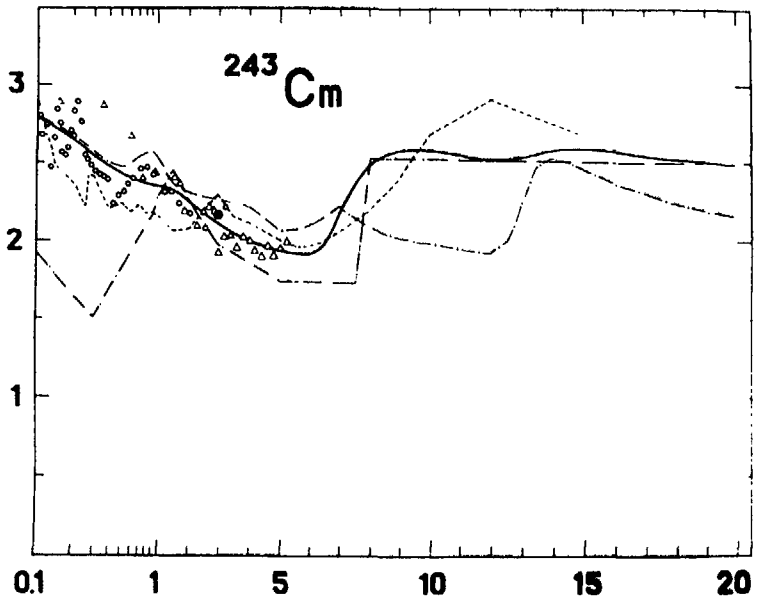

Fig.4 ^{243}Cm. △ -/10/, ○ -/17/.

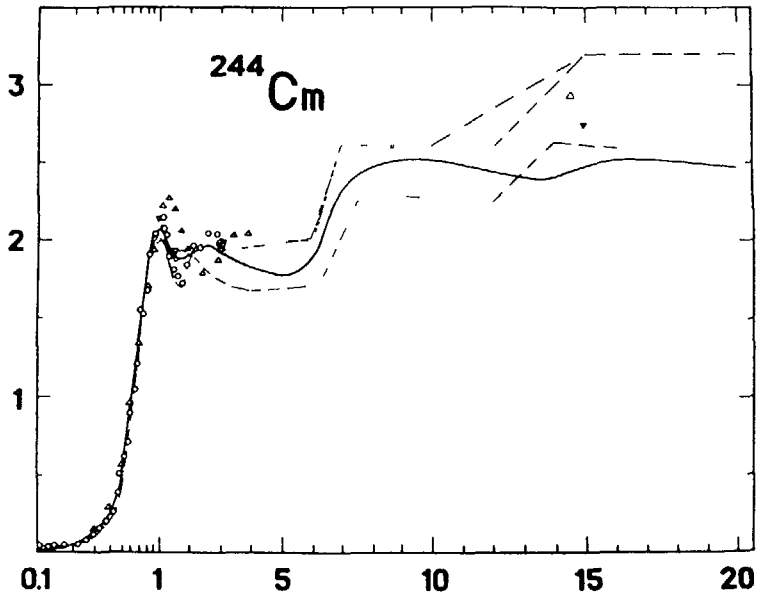

Fig.5 ^{244}Cm. ○-/14/, △-/16, 19/, ▽-/20/.

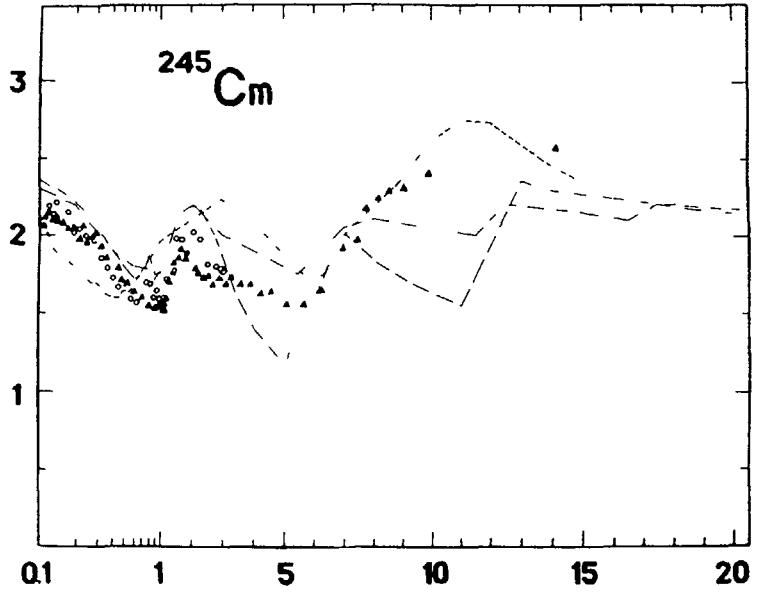

Fig.6 ^{245}Cm. ▲-/9/, ○-/14/.

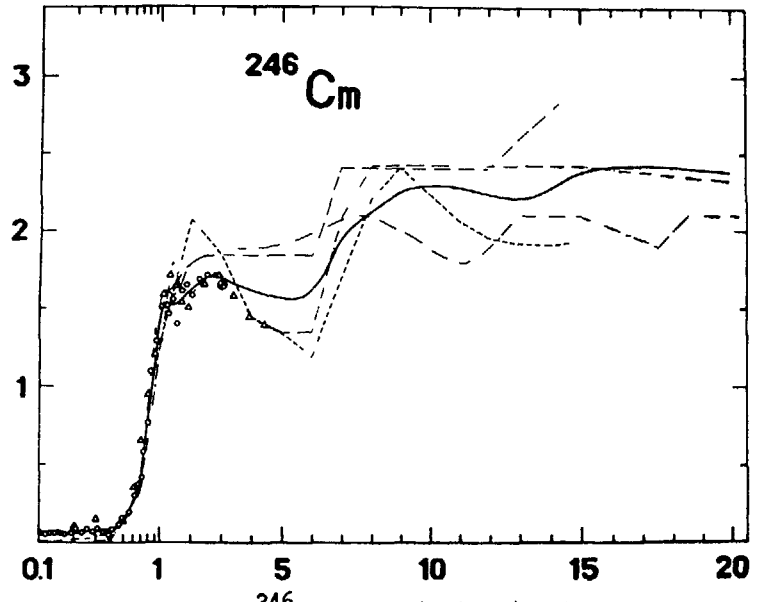

Fig.7 ^{246}Cm. ○-/14/, △-/19/.

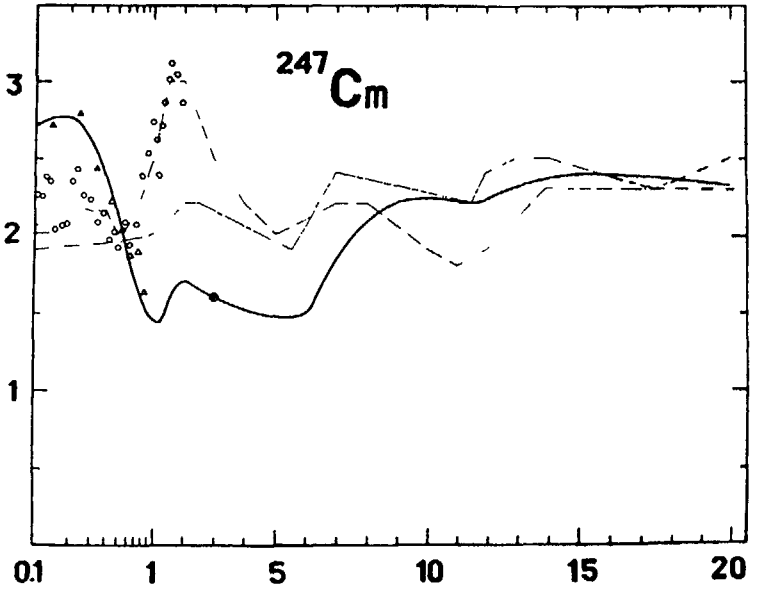

Fig.8 ^{247}Cm. ○-/14/, △-/13,21/.

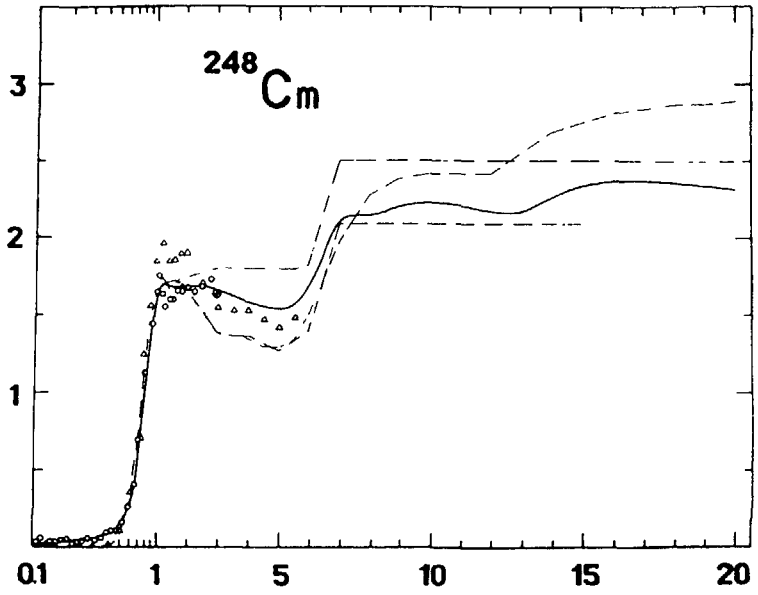

Fig.9 ^{248}Cm. ○-/14/, △-/22/.

III. On Fission Probability Energy Dependence of Transuranium Nuclei.

The previous two sections of the lecture have shown, that application of fission probability constancy approximation in the first "plateau" region allowed the useful conclusions on mean fission cross-section dependence on a nucleon composition to be drawn in a wide range of Z and N.

The next step of data systematization should consist in taking into account a fission probability energy dependence $P(E_n)$ over the whole energy range $E_n \leq 20$ MeV. Unfortunately, the state of experimental data today does not allow the final conclusions on the nature of this dependence to be drawn. That is why we shall confine ourselves to individual considerations based on the analysis of the experimental data available.

Fig.10 (top section) shows fission cross-sections in the first "plateau" range measured by us /23/. The bottom section of

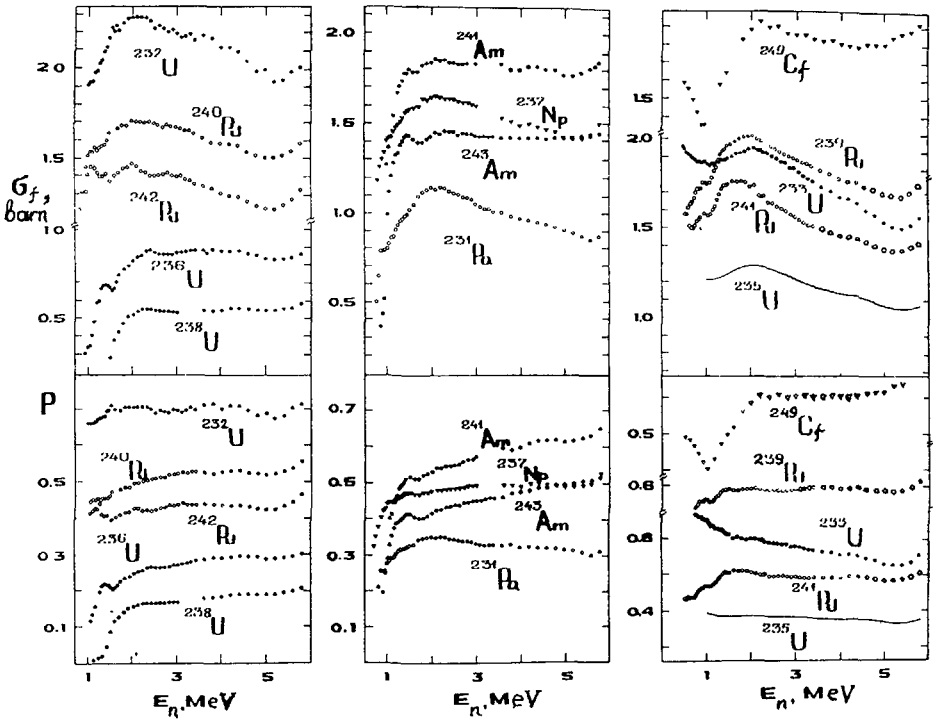

Fig.10. Neutron fission cross-section (top section) and fission probability (bottom section) in the first "plateau" region.

the figure presents fission probability P of these nuclei. As E_n grows a monotonous approximately linear variation of $P(E_n)$ is established for all nuclei. The various fission probabilities differing a few times, the energy dependence $P(E_n)$ can be conveniently featured by a relative value

$$\beta = P^{-1} \frac{dP}{dE_n} = \frac{d \ln P}{dE_n}$$

Fig.11 presents the values β evaluated at the interval E_n = 3-5 MeV from the experimental data in Fig.10 as depending on the mass number A-1 of the nucleus-target. The values β obtained in the similar way from a series of other Refs. /9,24/ are presented ibid. The following conclusions can be drawn on the basis of the above data:

1. Even-odd differences are inherent to fission probability energy dependences at the "plateau" region: N-even nuclei-targets are specified as having larger values β in comparison with N-odd nuclei-targets.

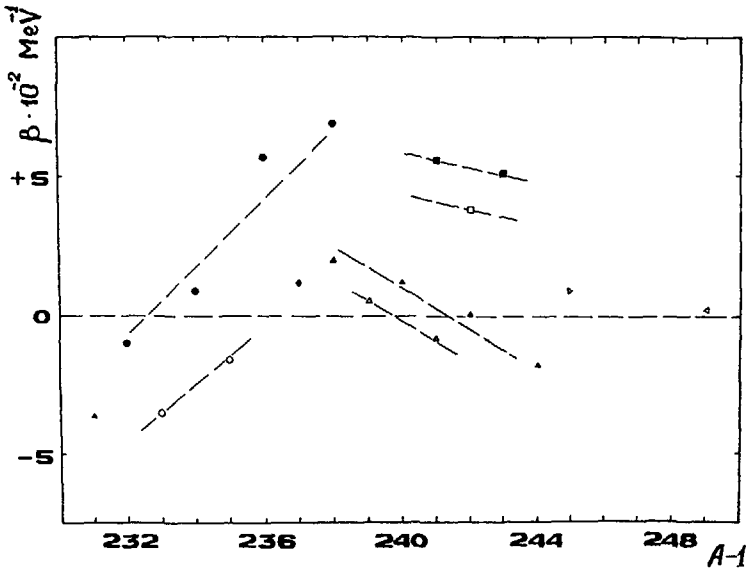

Fig.11. Value β as a function of nucleus-target mass number (A-1). Dark points - N-even targets, light one - N-odd targets: ▽ Pa; ●, ○ U; ◆ Np; ▲, △ Pu; ■, □ Am; ▷ Cm; ◁ Cf.

2. The value β grows as N increases for the same parity of uranium isotopes, but it drops for plutonium and americium.

3. The value $\beta \lesssim 5 \cdot 10^{-2} MeV^{-1}$ specifies the scale of the real pattern deviation of the systematics based on the constancy of fission probability in the first "plateau" range.

In the region of higher energies E_n the fission becomes emissive resulting in energy dependences of fission cross-section $\sigma_f(E_n)$ and fission probability $P(E_n)$ assuming the shape of stepped curves. Each elevation followed by the second, third,... "plateau" are associated with the new possibility of fission after 1, 2,... neutron emission of residual nuclei A-1, A-2,... . A neutron extracts (on an average) the energy ~ 7 MeV, that is why the incident neutron energy value for the centres of the first, second and third "plateau" is E_n = 3, 10 and 17 MeV.

In Fig.12 the total fission probabilities P_t (taking into ac-

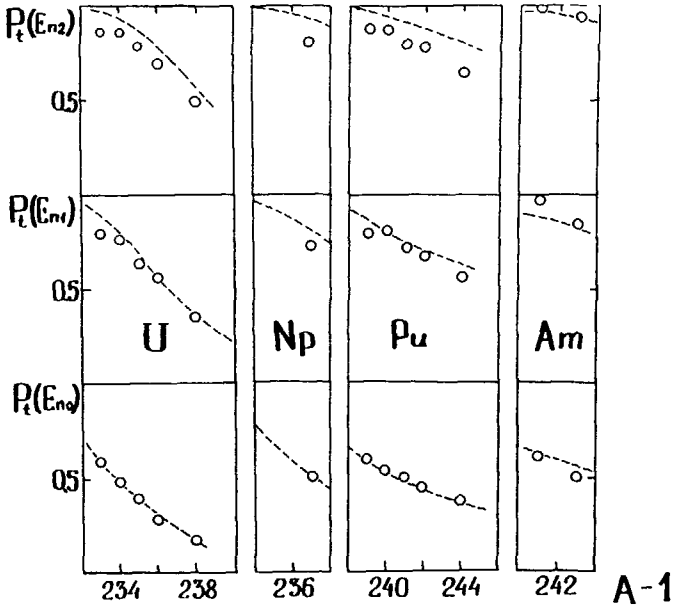

Fig.12. The total fission probability in the center of 1,2,3 "plateau". E_{no} = 3 MeV (bottom section), E_{n1} = 10 MeV, E_{n2} = 17 MeV (top section). Dashed line - calculations according present systematics, ○ - experimental data /24/.

count all possibilities of the fission process) are compared in the 1st, 2nd and 3rd "plateau", which are obtained from experimental fission cross-section /24/ and calculated by the systematics suggesting fission probability in dependence on energy. An agreement of the experimental data (points) with the calculated curves (dashed line) on the bottom section is trivial - it specifies the degree of experimental fissility adjustment in the present systematics. In the top section of Fig.12 (the third "plateau") the to-

tal fissility demonstrates deviations correlated with the behaviour of the value β for the first "plateau" in Fig.10:

a) The lower is the value of β in Fig.10, the higher is the deviation for light U isotopes and heavy Pu isotopes;

b) The deviation is missing within the error limit for Am isotopes.

From these considerations a conclu ion can be drawn, that the energy dependence of fission probability $P_A(E_n)$ in the energy range above the first "plateau" ($E_n > 6$ MeV) acquires the new features: for all nuclei except Am the parameter β with the growth of the energy E_n decreases so, that in the case being positive in the first "plateau", it changes its sign at a higher energy. Thus, the dependence $P_A(E_n)$ for the nuclei U-Pu acquires a decreasing manner as E_n grows.

An isotopes as opposed to a group of nuclei U-Pu demonstrate a non-decreasing energy dependence of fission probability $P_A(E_n)$. In this case a more specific conclusion is hindered, the total fission probability actually reching the limit ($P_t \simeq 1$), thus losing a sensitivity to the energy dependency of initial nucleus fission probability $P_A(E_n)$. Should the information of transuranium nuclei (Cm-Cf) fission probability by neutrons with energy $E_n \simeq$ 14 MeV be adopted in the analysis, we can see the fission probabilities of these nuclei will be $P_t \simeq 1$ as for Am. Thus, the second group of the transplutonium nuclei is united by an indication of non-decreasing dependence $P_A(E_n)$.

The result of this consideration can be supported by the analysis being beyond the possibilities of our brief talk in the fact, that transuranium nuclei are devided into two groups. The first ($Z \leqslant 94$) is with the decreasing fission probability dependences on the neutron energy $P_A(E_n)$ and the second with the increasing one.

The detail investigation of given dependence should yet been made. It is needed more comprehensive and systematic experimental data and it also requires application of more sophisticated theoretical approach.

REFERENCES

1. Istekov K.K., Kupriyanov V.M., Fursov B.I., Smirenkin G.N. Yadernaya Fizika, 1979, v.29, p.1156.
2. Kupriyanov V.M., Istekov K.K., Fursov B.I., Smirenkin G.N. Yadernaya Fizika, 1980, v.32, p.355.
3. Kupriyanov V.M., Smirenkin G.N., Fursov B.I. Yadernaya Fizika 1984, v.39, p.281.
4. Smirenkin G.N., Fursov B.I. Voprosy Atomnoj Nauki i Techniki, ser. "Yadernyje Konstanty", 1985, N°2, p.31.
5. Smirenkin G.N., Fursov B.I. Yadernaya Fizika, 1987, v.45,p.319.
6. Cohen S., Swiatecki W.J. Annals of Physics 1963, v.22, p.406.
7. Myers W.D., Swiatecki W.J. Arkiv föf Fysi , 1967, v.36, p.343.
8. Behrens J.V., Howerton R.J. Nucl.Sci.Eng., 1978, v.65, p.464.
9. White R.M., Browne J.C. Proc. Conf. Nuclear Data for Science and Technology (1983, Antwerp), 1983, p.218.
10. Britt H.C., Wilhelmy J.B. Nucl.Sci.Eng., 1979, v.72,p.222.
11. Ch.Lagrange. Report NEANDC (E) 228 "L", 1982.
12. Knitter H.H., Budtz-Jørgensen C. ibid /9/, p.744.
13. Britt H.C., Gavron A. et.al. Phys.Rev.Lett.,1977, v.38,p.1457.
14. Moore M.S., Keiworth G.A. Phys.Rev.C., 1971, v.3, p.1656.
15. Vorotnikov P.E., Dmitriev S.V. et.al. Yadernaya Fizika, 1984, v.40, p.1141.
16. Fomushkin E.F.,Gutnikova E.K. et.al. Yadernaya Fizika, 1967, v.5, p.966.
17. Silbert M.C. Report LA-6239-MS, 1976.
18. Fulwood, Dixon D.K.,et.al. Report LA-4420, 1970, p.157.
19. Fomushkin E.F., Novoselov G.F. et.al. Yadernaya Fizika, 1980, v.31, p.39.
20. Koontz P.G., Barton D,K. Proc.Conf.Neutron Cross-Sections and Technology (Washington, D.C.,1968), v.1, p.597.
21. Back B.B., Ole Hansen, et.al. Proc.Symp.of Physics and Chemistry of Fission (Rochester,1973), IAEA,Vienna,1974, v.1, p.25.
22. Fomushkin E.F., Novoselov G.F.,et.al. Yadernaya Fizika, 1982, v.36, p.582.
23. Fursov B.I., Kupriyanov V.M., Smirenkin G.N. et.al. Atomnaya Energiya, 1977, v.43, p.181,p.261; 1978, v.44, p.236; v.45, p.440; 1979, v.46, p.35; 1983, v.55,p.31; 1985, v.59,p.283, p.339; 1986, v.61, p.383.
24. Behrens J.V., Carlson G.W.,et.al. Nuclear Sci. Eng., 1977, v.63, p.250; 1978, v.66, p.205, p.433; v.68, p.128; 1981, v.77, p.444; 1982, v.80. p.393.

INELASTIC NEUTRON SCATTERING (NEUTRON SPECTROMETRY)

S.P. SIMAKOV
Institute of Physics and Power Engineering,
Obninsk, Union of Soviet Socialist Republics

Abstract

Consideration is given to experimental methods of inelastic neutron interaction differential cross-section measurement, with a neutron or γ-quantum detected in the exit channel. In this case the principal emphasis is placed on the method of time-of-flight neutron spectrometry. The paper deals with the physical and methodological aspects of the method associated with neutron generation, detector shielding and determination of its performance, final scatterer dimensions correction control, separation of elastic end inelastic neutron scattering. Presentation is given to a correlation experiment technique, which allow a neutron spectrum from the (n,n') reaction to be detected when the cnannel is open for the (n, 2 n) reaction aswell.

Possibilities of the methods are illustrated by the experimental data on cross-sections of the processes.

For the interaction of 1-20 MeV energy neutrons with nuclei the nonelastic processes, i.e. inelastic scattering, (n, 2n), (n, 3n) reactions, (n,f), (n,n'f) etc. in the case of fissile nuclei, account for approximately 50% of the total cross-section. The spectra of secondary neutrons from these reactions, having discrete or continuous energy distribution and a certain dependence on the angle of emission (differential cross-sections), contain information on the interaction mechanism and the excitation state structure in the residual nuclei. From this point of view the experimental and theoretical investigation of inelastic scattering differential cross-sections is an essential task, an interest to which is supported for a few decades. For the time being the technique of neutron experiments has been essentially developed, a great amount of experimental data has been obtained, our insight into physics of these processes has been intersified on the basis of their analysis. Recently a new advancement has been observed-correlation experiments have appeared, which permit detection of neutron spectra only from the reaction (n,n') or (n,2n) with both channels open.

Inelastic interaction differential cross-sections can be measured in various methods characterized by individual scopes of application, the type and accuracy of the resulting data and requires a specific set of experimental devices. Either prompt γ-radiation as a result of the final nucleus excited state de-excitation, or directly secondary neutrons, or mutual correlation of γ-quanta and neutrons can be detected in these experiments as a reaction product.

Though we do not aim at comprehensive analysis, we shall consider only the principal features of widely-used methods, in this case the methodical problems associated with a time-of-flight fast-neutron spectrometry method will be discussed in more detail.

Methods of measuring differential cross-section of inelastic neutron interactions. The method based on prompt γ-quanta spectra detection originated as a result of final nucleus excited state de-excitation provides information on partial cross-sections of (n,n'), (n,2n) reactions etc.Utilization of Ge(Li) detectors in advanced spectrometers enables us to obtain energy resolution 3-5 keV and to measure excitation functions for individual levels in heavy and odd nuclei. However, when the energy of incident neutrons exceeded above the reaction threshold by 1-3 MeV, the number of simultaneous excited levels grows, the scheme of γ-transitions becomes more complicated and as a consequence the partial reaction cross-sections are extracted with great errors. This method is inapplicable

for γ-transitions detection between close-lying levels ($\lesssim$ 100 keV), since the process of γ-quanta inner conversion on the atomic electron shell progresses at these energies with higher probability.

Partial cross-sections of (n,n') and (n,2n) reactions with excitation of levels in the excitation energy range 0.1-2.0 MeV for a great number of nuclei were measured at γ-quanta spectrometers functioning in various laboratories of the world /1-6/. The accuracy of the resulting cross-sections (~ 10%) allows the conclusions to be drawn on the probability of population, spin and parity of the excited level, on the contribution of different reaction mechanisms. However, with this method employed, valuable information on angular neutron distributions leaving the nucleus in the present excited state. These data can be obtained only in the techniques permitting the direct detection of secondary neutrons.

To detect energy and angular distributions of secondary neutrons the recoil-proton spectrometrs and most widely the time-of-flight spectrometers are used.

The method of recoil-nuclei neutron spectrometry is based on the following property of elastic neutron scattering on protons: recoil protons in the laboratory coordinate system are uniformly energy distributed from zero to the energy equal to the incident neutron energy. The detector response function appears to be more complicated in a real detector (hydrogenous scintillator with a photomultiplier or proportional counter filled with hydrogen or methane) due to final energy resolution, recoil proton escape out the sensitive volume, multiple scattering and others. The spectrometer response function measurement or calculation with the required accuracy is a prominent task of this method, for its being employed for neutron spectrum regeneration from the instrumentation spectrum of recoil protons. The unfolding procedure consists in solving an integral equation, that is, generally speaking an incorrect task. In the case of continuous energy distributions an accuracy of the data being regenerated is rather low (25-100%, e.g. as in Ref./7/). The scope of application for spectrometers on the basis of hydrogen proportional counters is approximately from 0.01 to 1 MeV, their energy resolution in this region 10-5%. Recoil proton scintillation spectrometers are adopted for neutron detection in the range 0.1-20 MeV, with a resolution 40-4%.

To all appearances the portion of inelastic neutron scattering differential cross-sections measured by the recoil proton method is comparatively insignificant due to mathematical problems and great errors concerned with the need of investigating and introducing a correction for response function.

The time-of-flight method most commonly used in spectrometry is based on neutron E energy determination by time-of-flight t of the registered distance (flight path) L : $E(\text{MeV}) = (72.3 \cdot L[\text{m}]/t[\text{nsec}])^2$. Relative energy resolution of the spectrometer $\Delta E/E$ is determined by the overall time resolution Δt and the path length uncertainty ΔL: $\Delta E/E = 2 \cdot \sqrt{(\Delta t/t)^2 + (\Delta L/L)^2}$.

Table I shows flight times and energy resolutions in the energy range from 0.1 up to 10 MeV for a spectrometer with typical parameters Δt= 3 nsec, ΔL= 3 cm for two path lengths 2 and 10 m. An energy resolution comparable with the recoil proton method can be obtained as can be seen in measuring fast neutron spectra by time-of-flight method with the pathlength 2 m, and we can approach the resolution obtained in the γ-spectrometry method with the path length 10 m. Note, that the increase of path length from 2 up to 10 m results in the decrease of spectrometer aperture by a factor of 25.

TABLE 1

E, MeV	L = 2 m		L = 10 m	
	t, nsec	$\frac{\Delta E}{E}$, %	t, nsec	$\frac{\Delta E}{E}$, %
0.1	457	3	2287	0.7
1.0	72	9	729	1.0
10.0	46	13	229	2.7

The main technical components of the time-of-flight neutron spectrometer are: a pulsed neutron source (target), a sample under investigation (scatterer), a background-radiation-protected neutron detector, a system of monitors for control of the neutron yield from the target as well as electronic devices for processing and accumulating signals from the detector. Fig.1 shows a digram of this spectrometer taken as an example /8,9/. We shall consider some of its components in more detail.

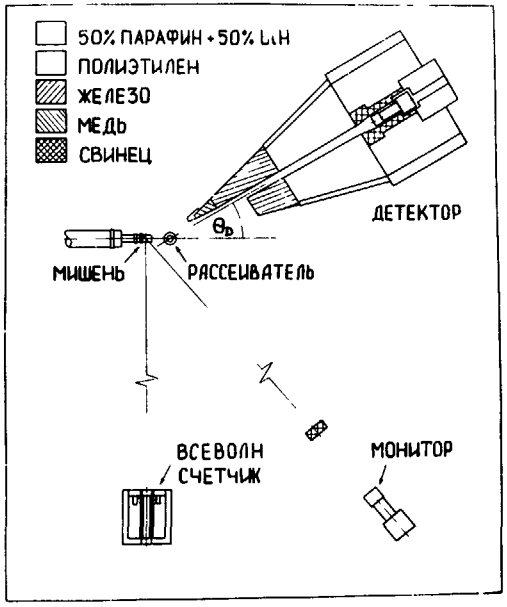

Fig I. Experimental diagram for measuring secondary neutron spectra by the time-of-flight method.

Neutron source. Pulsed neutron sources with the specific requirements on the yield rate, monoenergy, contribution of background neutrons /10/ are employed in time-of-flight neutron spectrometry. Reactions between hydrogen isotopes and lightest nuclei are most suitable for this purpose. Charged particles are accelerated in electrostatic (recharged) accelerators, cascade generators and cyclotrons operating in the pulsed conditions and giving the pulses of the width 1-5 nsec , pulse-repetition interval T= 200-1000 nsec and average current on the target 1-10 μkA. Numerous factors of physical and engineering nature effect the choice of a neutron source in the prescribed energy range. Fig.2 illustrates a comparison of neutron yields from various reactions at an angle 0° to the incident beam, in this case the target thickness provides neutron energy spead 10 keV at all energies /11/. Thick lines in Fig.2 correspond to

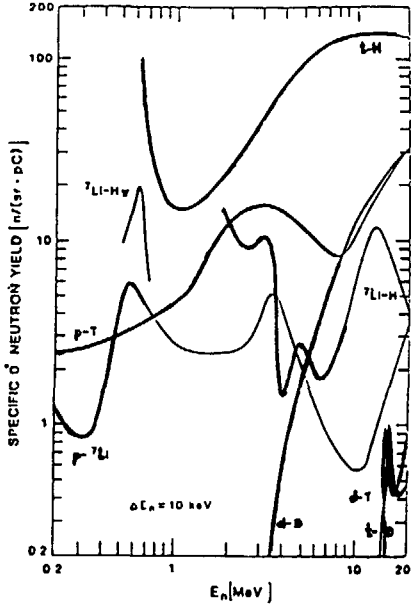

Fig.2. Dependence of neutron yield at an angle 0° as a function of neutron energy (energy resolution 10 KeV); thick lines denote monoenergetic regions (the figure is taken from Ref. /11/).

the energy region, where the present reaction is a monoenergetic source of neutrons. Emphasis is placed on the fact that the so called "inverse" reactions $H(t,n)^3He$ and $H(^7Li,n)^7Be$ provide significantly greater yield at an angle 0° than the corresponding "direct" reaction $^3H(p,n)$ and $^7Li(p,n)$. However, in addition to the value of neutron yied the factors like a type, energy and current of ionsaccelerated at a given accelerators, energy release, straggling and background neutron yield in structural materials of the target greatly effect the choice of a neutron source. This results in the fact, that nowadays the reaction T(p,n) and D(d,n) are most frequently used to obtain 1-10 MeV neutrons, and T(d,n)- neutrons with energies 14 MeV and grater 20 MeV. The difficulties related to radioactive tritium or litium acceleration restrict a wide application of promising sources on the basis of "reverse" reactions /12,13/.

A gas target is the most optimal engineering design of the target to yield neutrons with the energies above 5 MeV from the standpoint of yield rate and background neutron contribution. Fig.3 shows a diagram of this target as an example /14,15/. A

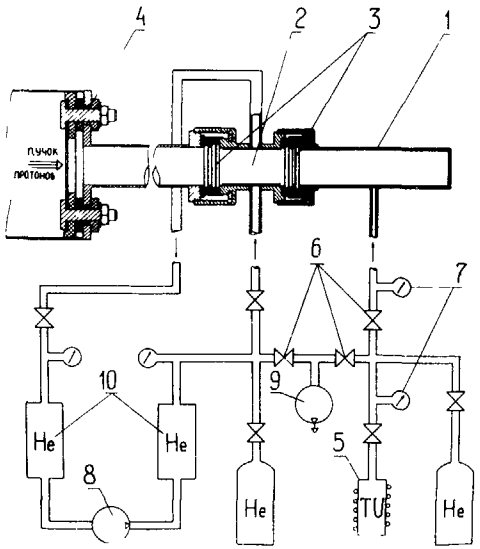

Fig.3. Diagram of gaseous tritium target layout: 1,2- tritium and helium volumes; 3-foils; 4-laminas; 5--uranium tritide bottle; 6--valves; 7-pressure sensors; 8-microcompressor; 9-pump; 10- inert material volumes.

thin-walled cylinder is filled with tritium at uranium trithide decomposition at a temperature 400-500°C. A beam of protons or deutrons penetrates the target space through thin foils of ^{58}Ni or Mo, where the (p,n) or (d,n) reaction threshold is relatively large. A cooling helium flow circulates over the closed loop between two foils. Pulsed neutron-fluxes with the parameters useful for time-of-flight neutron investigations can be obtained at the electrostatic recharging accelerator EGP-10M with a use of this target (see table 2).

TABLE 2.

Reaction	T(p,n)	T(d,n)
Neutron energy, MeV	5-8	21
Yield at 0°, 10^8 n/sr.sec	2-1	0.8
Energy resolution, MeV	0.07-0.05	0.2
Contribution of background neutrons, %	0.03-1.0	85

Shielding. Neutron emission into the total solid angle 4π (strong forward anisotropy is observed only in "reverse" reactions) is characteristic of the above mentioned neutron sources. That is why the flux of neutrons scattered by the sample located at a certain distance from the target is essentially less, than the neutron flux going into the detector directly from the target. This results in the need of creating massive shielding around the source or detector with a collimating aperture yielding sample-incident or scattered neutrons flux.

Geometry of the experiment with a shielded neutron source ("behind the wall") with the collimating aperture available, which creates a narrow neutron beam in the direction towards the scatterer (the so-called closed geometry) was widely used in the

experiments with 14-MeV neutrons /6,16/. Here, the decrease of neutron flux in the sample due to the increase of a source-sample distance can be balanced out by the growth of deutron flux from the accelerator. None the less, we fail to obtain a path length more than 3 m /16/ in these experiments, and consequently, a high energy resolution of the spectrometer.

From this point of view the open experimental geometry is more adequate, when the scatterer is located at a distance 10-15 cm from the unprotected neutron source and the detector is in the massive shielding (Fig.1). The shielding should provide the required attenuation coefficients for the direct neutron flux from the target ($\sim 10^{-6}$) and the test-room induced neutron background ($\sim 10^{-4}$) so as to obtain the required relation between the effect and the background. When investigating interaction of neutrons with the initial energy of several MeV the most appropriate materials - iron, copper . The spectrum of neutrons scattered by the room is shifted to the region of smaller energies with hydrogeneous materials (polyethelene, water, paraffin) as most promising for protection. For γ-shielding in the course of neutron moderation and capture the neutron detector is installed in a lead housing. An effective means of γ-background reduction is inclusion of lithium-6 (in the form of LiH-compound) with its large cross-section of none-radiative neutron absorption with the energies below 1 MeV.

Detector shielding represents a massive structure weighting a few tons. It rotates around the scatterer by the special quides for measuring the spectra of scattered neutrons. In some laboratories multidetector systems were engineered with the number of detectors from 4 to 16 /17-20/. No doubt, that these systems allow the experimental data set rate to be increased.

Scatterer. In the experimental geometry shown in Fig.1, when the detector rotates around the sample, a cylinder or a hallow cylinder with a vertically-oriented axis is the most reasonable form of scatterer. The dimensions and weight of the scatterer are selected from the condition of compromise between the reasonable scattered-neutron count rate in the detector and the value of correction for multiple interactions and neutron flux attenuation in the sample. The neutron flux density and energy variation taking place within the limit of a solid angle at which the sample is visible from the target, should also be taken into account. From this point of view the hallow scatterer is the most optimum one because with the same correction value a greater mass of the material under study can be obtained.

All these effect related to the final dimensions of the scatterer must be taken into account when extracting neutron cross-sections from the experimental data. E.g. if $\frac{d\sigma'}{dEd\Omega}$ is an experimental cross-section of neutron scattering on the sample normalized to the flux in its centre, then the double-differential cross-section of neutron interaction with the present nucleus to be found is determined from the ratio $\frac{d\sigma}{dEd\Omega} = \frac{d\sigma'}{dEd\Omega} \cdot f^{-1}(E,\theta)$, where $f(E,\theta)$ is the correction function for the effects related to the final dimensions of the scatterer.

Analytic and numeral methods have been developed for $f(E,\theta)$-function calculation. Analytic methods /21,22/ based on a series of approximations are comparatively simple, convenient for calculation and demonstrate the sample-processes physics in a form easy to grasp. Thus according to the recommendation of the author of Ref./22/

$$f(E,\theta) = f(E) = Si(E_o) \cdot T^{-1} \cdot Sf(E)$$

where $Si(E_o)$ and $Sf(E)$ are functions of incident and dispersed neutron flux attenuation and $T(E_oE)$ - is a function taking into account multiple scattering contribution.

For comparison Fig.4 shows the correction value calculated according to this recommendation, as well as in the Monte-Carlo method /23/. The calculations were performed for a niobium hallow scatterer (4.5 cm in height, o/i diameters 4.5 and 2.0 cm, weight 432 g) for neutrons with the initial energy 8 MeV. The results of the both calculations can be seen to be close, though in the energy range below 1 MeV where they disagree the Monte-Carlo method should be favoured due to its ability to take into account the experiment geometry and cross-section of neutron

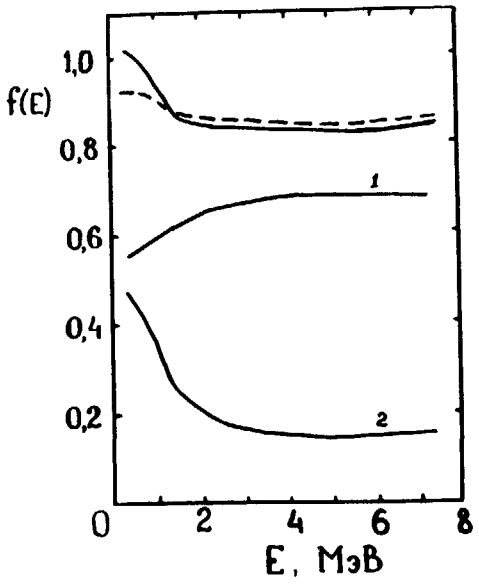

Fig.4. Dependence of correction for final dimensions of niobium sample on secondary neutron energy:
- - - - - analitical calculation /22/;
------- Monte-Carlo calculation (1 and 2 -contribution of single- and multiple interactions).

interaction with niobium with greater accuracy. This figure also demonstrates the relation between single- and multiple interactions in the sample of the indicated sizes. The total correction value is 15% at the secondary neutron energy above 2 MeV, an accuracy of this value is about 3%. The calculations performed in the Monte-Cerlo method also show f(E) to vary for this sample by +5% with the transition from scattering angle 30° to the angle 150°.

Detector. To measure a neutron spectrum in the time-of-flight method we need a detector with good energy resolution and high neutron detection efficiency. Scintillation detector on the basis of a crystalline (stilbene), plastic (NE110) or liquid scintillator (NE 213, 218) and a fast photomultiplier meet these requirements. Special-purpose electronic circuits with a constant-fraction discrimination enable us to compensate the effect of output signals amplitude spread for this detector and to obtain time marking of the detector moment. In addition to this the electronic circuits identifying neutrons from γ-quanta by the pulse shape, that allows the tens-thousands-fold suppression of the events related to γ-quanta /24/ were widely spread. The detector of the described design with the scintillator thickness 4-5 cm provides resolution 1-3 nsec, its detection efficiency is 30-50%, and it permits the threshold to be reached for the neutron energy 50 keV.

One of the most essential features of the detector in neutron spectrometry responsible for the accuracy of the data being measured is the dependence of detector efficiency on neutron energy. Measurement of ^{252}Cf spontaneous fission neutron spectrum by the time-of-flight method is a convenient means of its determination. For this purpose a light ionization chamber with a layer of californium is used, the signal indicative of the fission event and neutron emission moment is picked off thischamber. The fission neutron spectrum shape is currently known with the accuracy 2-4% /26/. Fig.5 shows an efficiency curve of the detector made of stilbene crystal 6.3 cm in diameter and 3,9 cm in height and FEU-30 determined in this method /9/. An efficiency curve determined in the alternative method - by the neutron yield from the

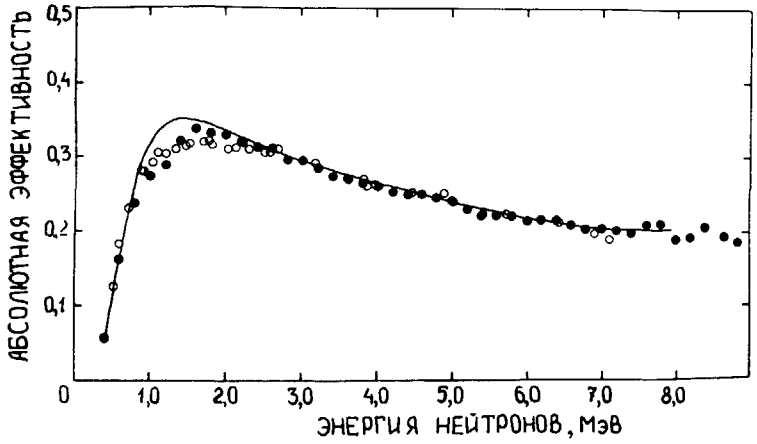

Fig.5. Neutron detector efficiency determined by ^{252}Cf neutron fission spectrum (•), by T(p,n) reaction neutron yield (°) and calculated by the Monte-Carlo method (-).

reaction T(p,n) is shown ibid. If the energy of neutrons from the reaction used for neutron generation essentially varies from an angle and this reaction cross-section is well-known (in the case of T(p,n) with an accuracy 2-10% /11/), then the neutron source itself can be adopted for detector efficiency calibration.

The physics of the processes occurring at neutron interaction with the detector scintillator are fairly well known, that is why efficiency of this detector can be calculated. A solid curve in Fig.5 shows the efficiency calculation performed by the Monte-Carlo method using code /27/. You can see that various experimental and calculated methods of efficiency determination are in adequate agreement. Deviation of the calculated curve from the experimental one in the range 1-1.5 can be explained by the n-γ discrimination circuit effect which is hard to be taken into account in the calculation.

Separation of elastic and inelastic scattering. In the time-of-flight neutron spectrometry there is a unique and rather complicated methodological problem that is separation of inelastically-scattered neutrons from elastically-scattered ones. In most cases the neutrons scattered elastically and with the excitation of the first nuclei levels have similar energies, so the spectrometer resolution appears insufficient for their time-of-flight separation. The result is a complex overall spectrum particularly at small angles of scattering, where the elastic scattering contribution is great. A fraction of neutron time spectrum with the initial energy 6.5 MeV scattered on the nucleus ^{113}In at an angle 30° is shown in Fig.6 as an example.

The task consists in finding elastically-scattered neutrons line form (i.e. spectrometer response function) in the region where the neutron spectra of the two processes overlap. As a rule, the following factors made the leading contribution to its shaping: spectrometer time resolution (including pulse duration and detector resolution) in general defining the top section of the elastically -scattered neutrons peak; and neutron interaction with a detector shielding collimator shaping a peak tail drawn in the range of small energies.

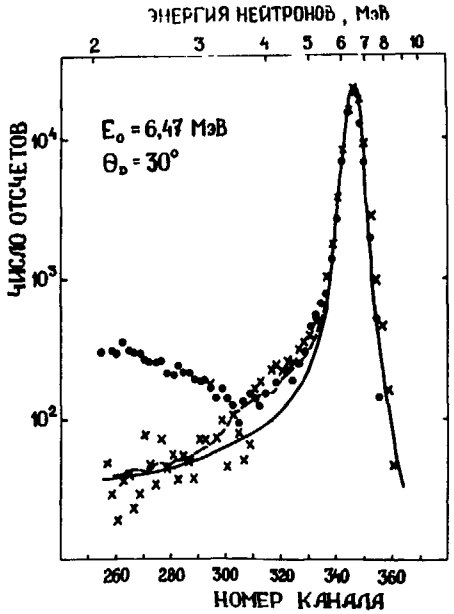

Fig.6. Instrument spectra of neutrons scattered on ^{113}In sample (•) and ^{12}C (x) and spectrum of direct neutron flux from the target(—); - - - - calculated spectrum of neutrons scattered on ^{12}C sample.

The method of measuring the direct neutron flux from the target is convenient for spectrometer response function determination. In this case the above-mentioned factors are experimentally taken into account. The response function measured in this manner is shown in Fig.6 by a solid line /28/. If a sample of ^{12}C, ^{40}Ca or ^{208}Pb is located on the place of the scatterer, then the spectrometer response function can be determined by the elastically-scattered neutrons peak by these nuclei at fairly good spectrometer resolution, because the first excited level is comparatively high. ^{12}C, where U_1 = 4.4 MeV, seems to be the most suitable one. However, in Fig.6 you can see, the spectrum of neutrons inelastically scattered on carbon appreciably differ from the direct flux spectrum from the target. Analysis of this disagreement have shown, that it is associated with the contribution of multiple interactions in the carbon sample /28/. This is confirmed by the calculations performed by the Monte-Carlo method and giving a good description of the spectrum of neutrons scattered on the C-sample.

We dwelt upon certain though, of course, far from all aspects of the method of time-of-flight neutron spectrometry. The method was extremely widespread in the task of secondary neutron energy - and angular distributions investigation in a wide range of initial neutron energies (1-25 MeV). Investigation is carried out for the excitation functions of individial levels from the reactions (n,n'), (n,2n), (n,3n) /32-36/ etc. As an example, Fig.7 shows energy and angular distributions of neutrons from the reaction ^{115}In (n,n') at the energies from 5 up to 8 MeV, as well as the results of theoretical calculations performed with take into account equilibrium and direct processes demonstrating the degree of our insight into this reaction mechanism.

Correlational experiments. When the incident neutron energy exceedes the (n,2n) reaction threshold, the spectrum of secondary neutrons detected in the above-mentioned methods represents an overall (inclusive) spectrum of neutrons from the reactions (n,n') and (n,2n). The study of mechanisms of each of these reactions and their mutual competition with the both channels open is indeed of great interest. The corresponding experimental methods have been developed to measure differential neutron spectra of only one reaction (exclusive spectra). Their specific feature is neutron detection (by the time-of-flight method) in coincidence with the detection either of the second neutron (measurement of neutron spectra from (n,2n) reaction /38-49/), or γ-quantum with the prescribed energy (corresponding to excited states discharge after (n,n') reaction /41-44/). These experiments are still unique, the rate of data acquisition being a few orders of magnetude less; there is also a requirement of the correct consideration of accidental (spurious) coincidences.

The procedure and results of this experiment will be illustrated on the example of ^{56}Fe (n,n'γ) reaction neutron spectra measurement at the energy 14 MeV /44/. The measurement techinique is based on the following property of this reaction. All ^{56}Fe nucleus states excited in the reaction (n,n') are discharged through the lowest state 2^+ with the energy 847 keV. As far as

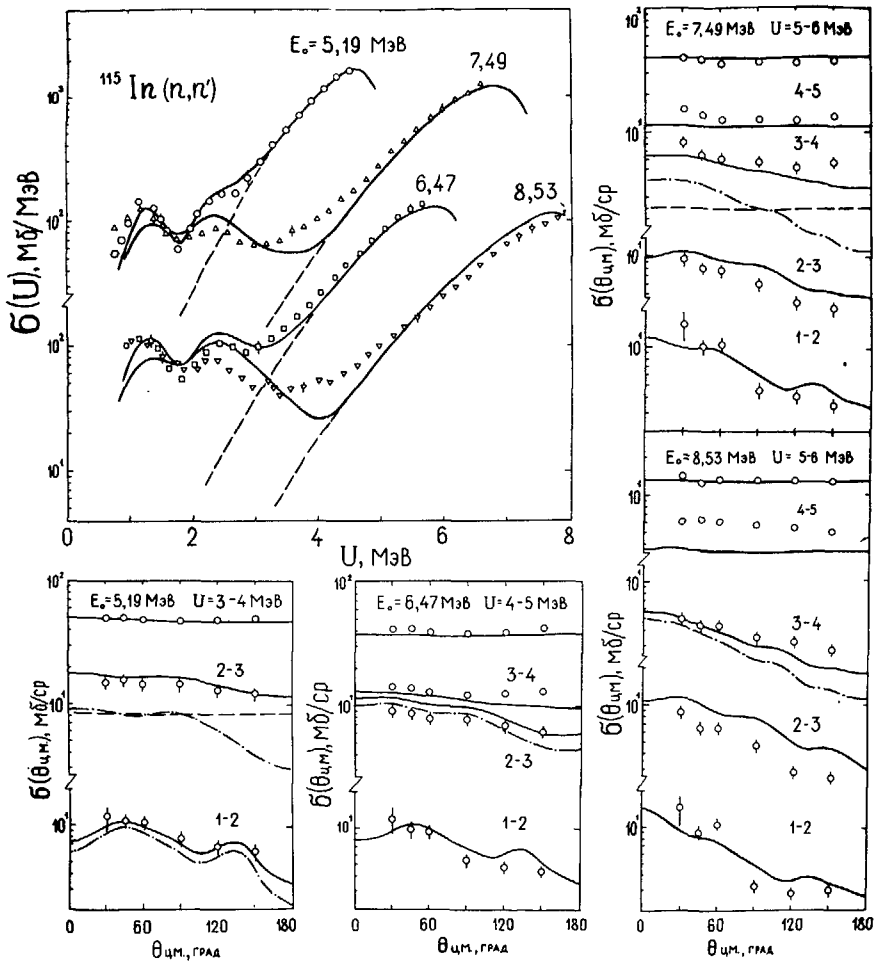

Fig.7. Energy and angular distributions of neutron from ^{115}In (n,n') reaction.
Curves - theoretical calculations of cross-sections within the framework of equilibrium (---), direct (-·-) mechanisms and their total (——).

the nucleus ^{55}Fe formed in the (n,2n) rection is free of γ-transitions with this energy, it is the reaction ^{56}Fe (n,n'), that the secondary neutron spectrum measured in the coincidence with γ-quanta with the energy 847 keV corresponds to.

The experimental diagram is shown in Fig.8. The T(d,n) reaction neutron with the energy 14.1 MeV interact with the sample located directly on the target. The scattered neutrons are detected by the scintillation detector by the time-of-flight method, and γ-quanta - by the Ge(Li) detector. Electronic circuit of fast-slow coincidences executes the γ-quanta selection by two parameters: by time-of-flight (a window 16 nsec in width is cut-off) for the purpose of isolation of γ-quanta produced in the sample and the target, and by energy (a window 20 keV in width) aimed at isolation of γ-quanta with the energy 847 keV. In the case of event recording in this window the neutron detection by the scintillation detector is resolved.

The specific corrections related to accidental coincidences, that can essentially distort the (n,n') reaction neutron spectrum are typical of this type of experiment. One type of accidental coincidences is due to the probability of occurrence of two or more interaction events of 14 MeV neutrons with the sample for the period of time under analysis (coincidence time). These events can be taken into account in the experimental way-through subtraction of the inclusive neutron spectrum from the neutron spectrum measured for coincidence with γ-quanta; through normalizing them in the elastic scattering range. Accidental coincidences can also appear as a result of multiple interaction of one neutron with the sample. Contribution of these spurious events is calculated by the Monte-Carlo method /45/.

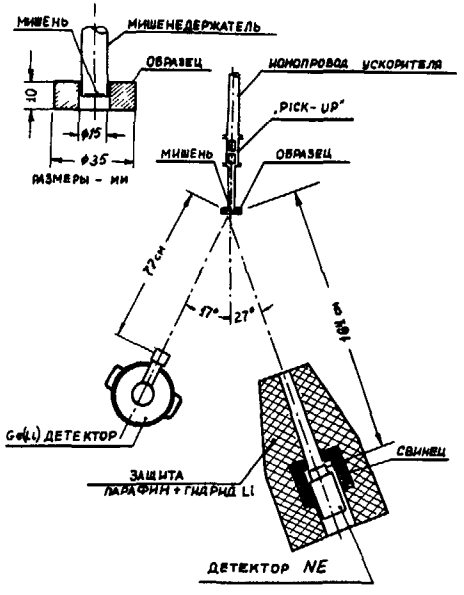

Fig.8. Diagram of correlation experiment for measuring neutron spectra from $^{56}Fe(n,n'\gamma)$ reaction at energy 14MeV

Fig.9 shows the expiremental results of the overall ^{56}Fe (n,n'+2n) reaction neutron spectrum at the energy 14 MeV, measured by the time-of-flight method /46/, and the $^{56}Fe(n,n')$ reaction neutron spectrum (with and without the correction for multiple interactions), measured by the correlation method.

Comparison of these spectra with the theoretical calculations results allows our ideas about these reaction mechanisms to be refined and the parameters of exited nuclei states to be determined. In particular, the evaluation of mean radiative width of unbound nucleus states ^{56}Fe : $\langle\Gamma_\gamma\rangle = 1.5 \pm 1$ eV /45/ was found from the $^{56}Fe(n,n')$ reaction neutron spectrum.

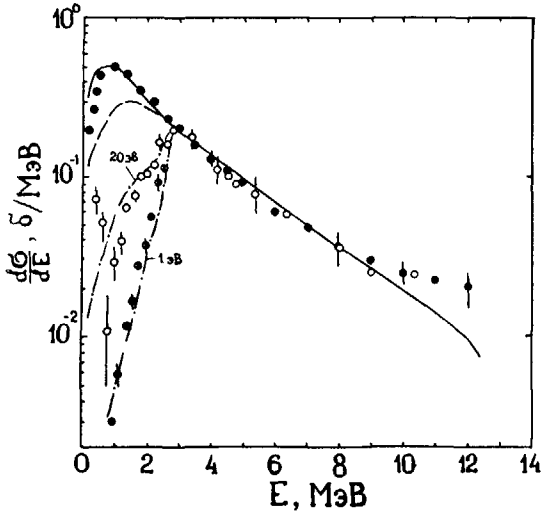

Fig.9. Experimental neutron spectra from $^{56}Fe(n,n'+2n)$ reaction (●) and $^{56}Fe(n,n')$ (○ - without correction for multiple interaction, ⊗ - with correction). Curves-theoretical calculations of these processes cross-section with the indicated $\langle\Gamma_\gamma\rangle$

REFERENCES

1. Haouat G., Lachkar J., Lagrange C.R. e.a. Nucl. Sci and Engin, 1982, v.81, p.491.
2. Beghian L.E., Keqel G.H.R., Marcella T.V. IBid, 1978, v.69, p. 191.
3. Olsen D.K., Morgan G.L., McConnell NBS Specialpublication, 1980, v.594, p.677.
4. Kazulya B.G., Kozulin E.M. et al. Problems of Atomic Science and Engineering, Ser. Nuclear Constants, 1980, v.4(39),p.14.
5. Konobeevsky E.S., Musaelyan R.M. et al, In: Elementary Particles and Atomic Nucleus Physics, 1982, v.13, p.300.
6. Hlavac S., Oblozinsky P. Nucl.Instr. and Meth, 1983,v.206, p. 127.
7. Shin V., Hasegawa T.,Hyodo T., Nucl. Sci and Tech., 1980, v.17, p.531.
8. Trufanov A.M., Nesterenko V.S. et al, Experiment Devices and Technique, 1979, N2, p.50.
9. Simakov S.P., Lovchikova G.N., et al. "Neutron Physics", M., 1980, v.1, p.320.
10. Uttley C.A. In "Neutron Sources for Basic Physic and Applications", Pergamon Press, Oxford, 1983, v.2, p.19.
11. Drosg M., Proc. IAEA Consultants Meeting on Neutron Source Properties. Leningrad, 9-13 June 1986.
12. Drake D.M., AUchampaug G.F. et al, Nucl.sci. Eng.,1977, v. 63, p.401.
13. Dave J.H., Gold S.R. e.a. Nucl.Instr. Meth., 1982, v.200, p.285.
14. Lovchikova G.N., Salnikov O.A. e.a. Proc.IAEA Cons.Meeting on Neutron Source Properties, Leningrad, 9-13 June 1986.
15. Fetisov N.I., Simakov S.P. et al, Experimental Devices and Technique, 1980, N6, p.22.
16. Kozyr Yu.E., Prokopets G.A.,Strizhak V.I. Ukrajian Physical Journal, 1975, N20, p.2061.
17. Lachkar J., McEllisten M.T., e.a. Phys.Rev., 1976, v.C14, p.933.
18. Eckstein P., Helfer H., e.a., Nucl.Inst.Meth., 1980, v.169, p.533.
19. Smith A.B. Nucl.Inst.Meth.,1969,v.50, p.277.
20. Hausen L.F. Report BNL-NCS-5102,1982,p.51.
21. Kinney W.E. Nucl.Instr.Meth.,1970, v.83, p.15.
22. Engelbrecht C.A. Nucl.Instr.Meth.,1971, v.93, p.103.
23. Popov V.I., Kotelnikova G.V., Problems of Atomic Science and Engineering, Ser. Nuclear Constants, 1974,v.16,p.113.
24. Kurashev A.A., Identification of Pulses from Radiation Detectors. Atomazdat, 1979.
25. Baryba V.Ya, Kornilov N.V. et al., Problems of Atomic Science and Engineering, Ser. Reactor Engineering, 1977, v.5(19), p.45.
26. Grundl J., Eisenhauer C. Report IAEA-208, Vienna,1978, v.1, p.53.
27. Chulkov L.V. Report IAE-2594, Moscow, 1975.
28. Simakov S.P., Lovchikova G.N. et al. Problems of Atomic Science and Engineering, 1981, v.5(44), p.23.
29. Smith A.B., Guenther P.T. Report ANL/NDM-69, Agronne, 1982.
30. Kinney W.E., Perey F.C. Proc. Washington 1975, p.883.
31. Hanseh L.F., Pohl B.A. e.a. Phys.Rev.,1986, v.C34,p.2075.
32. Salnikov O.A., Lovchokova G.M. e.a. Nuclear Constants, 1971, v.7, p.134.
33. Hermsdorf D., Meister A. e.a. ZFK-277, Dresden, 1977.
34. Takahashi A. e.a. Report A-83-01, Osaka, 1983.
35. Marcinkowski A., Finlay R.W. e.a. Nucl.Sci.Eng., 1983, v. 83, p.13.
36. Mellema S., Finlay R.W. e.a. Phys.Rev.,1983,v.C33, p.481.
37. Simakov S.P., Lovchikova G.N. e.a. "Neutron Physics", M., 1984, v.1, p.185.
38. Boucher R., Gondrang J.C. e.a. Conf.Sur les Const.Nucl., Paris, 17-21 oct., 1966.
39. Voignior J.,Proc. 3 rd Conf. Neutr Cross Sect. and Techn., Knoxville, 1971, p.306.
40. Schroder V., Scobel W. e.a. Zeit. fur Phys., 1978, v.A287, p.353.

41. Stengl G., Uhl M., Vonach H. Nucl. Phys., 1977, v. A290, p. 109.
42. Kozyr Yu.E., Prokopets K.A., Sov.Jour. of Nuclear Physics, 1978, v. 27, p.816.
43. Betak E., Breznik I et al. Proceedings of AS USSR, Ser.phys. 1985, v.49, p. 1023.
44. Lychagin A.A., Devkin B.V. et al. Preprint FEI-1722,Obninsk, 1985.
45. Lychagin A.A., Simakov S.P. e.a. Fast Neutron Physics, Zagreb, 1986, p.272.
46. Lychagin A.A., Devkin B.V. et al. Preprint FEI-923,Obninsk, 1973.

REACTION CROSS-SECTIONS FOR REACTOR DOSIMETRY AND ACTIVATION CALCULATION

A.B. PASHCHENKO
Institute of Physics and Power Engineering,
Obninsk, Union of Soviet Socialist Republics

Abstract

The current status of threshold reaction cross-section data for reactor dosimetry and activation calculation was reviewed. Systematic (n,p) and (n,2n) reaction cross sections at ~ 14 MeV were presented. The analytical representation of energy dependence of cross sections was discussed. Comparison of evaluated cross sections with integral experimental data has shown that in the whole, a good agreement of recommended cross-section averaged over the neutron spectrum of ^{235}U thermal neutron fission with the integral experiment results is observed.

I. Introduction.

Activation cross-sections affected by neutrons should be known to calculate afterheat in cores, to assess radiological situation when dealing with irradiated fuel, coolant, equipment. They are required for the development of nuclear fuel accumulation safe-guard means, for the assessment of valuable radioisotope yield, for the analysis of environment contamination and neutron detector efficiency calculation [1] . The requirements for the accuracy of reactor dosimetry and activation calculation differential cross-sections are defined by the specific features of the problems to be solved. The required accuracy for differential cross-sections in the most cases is 10-15% [2], however, e.g. for the reactions used as references [3] , it should be much better, about several percents.

The state - of - the - art nuclear data for activation calculation is yet incapable of meeting the growing requirements for the accuracy and amount of cross-sections to the full extent [4, 5] ; the consumers as a rule wanting information on wide neutron energy range cross-sections. The situation when the user can obtained what is known as recommended data in most cases suits him; under the recommended data we understand not purely experimental results of cross-sections measurements, but the data subjected to a certain intermediate procedure of their analysis and processing, when the measurement data by various authors are compared, the cross-sections are renormalized if required to bring them in agreement with the available standards, the data are analysed within the framework of theoretical models, the microscopic cross-sections are corrected within the errors assigned to them by the integral measurement data. In the last years this proces - sing has been commonly called nuclear data evaluation.

An International Programme of coordinated evaluation of microscopic cross-sections has been developed and is under way [6, 7] for reactor dosimetry and integral experiments in "bench-mark" neutron fields taking into account a significance of neutron da - ta for reactor dosimetry. As a result of this long and goal - directed work under the aegis of the Nuclear Data Section of IAEA initiation was given to the International Radiation Dosimetry File-IRDF, consisting of two data libraries prepared in the ENDF/B-V format: the library of evaluated reaction cross-sections most commonly used in reactor dosimetry and "bench-mark" neutron spectra library.

The cross-section library include the whole dosimetry file ENDF/B-V, as well as the cross-sections evaluated in some other laboratories of the world. The main result of generating this file consists in the scientific world's being provided with a uni - fied set of recommended cross-sections for reactor dosimetry and this enables us to predict the measurement results on the basis of the unified dosimetry file. In their turn the intercomparison results of the measurement data and their predictions make it possible to update the recommended cross-section so as to obtain the required accuracies not yet reached in a number of cases.

2. Some Notes Concerning Neutron Spectrum Determination Activation Method.

Since long ago the activation methods were employed for measuring neutron fluxes. Recently more advanced methods of neutron flux and spectrum measurement have been developed, e.g. those using helium and hydrogen proportional counters, scintillation and semiconductor detectors, but it is the activation methods that make it possible to work in the complex radiation intensive fields.

The task of differential neutron spectrum unfolding $\varphi(E)$ by the results of activation measurements is reduced to solving a set of Fredholm's equations of the I $\underline{st}$ type:

$$\int \sigma_i(E)\varphi(E)dE = q_i \qquad i = 1, 2, \ldots n \qquad (1)$$

where $\sigma_i(E)$ is an energy dependence of the i's threshold reaction cross-section,

q_i - is a reaction rate (activity under saturation referred to a single isotope - detector nucleus).

Rigorously mathematical solution to this equation is incorrect, i.e. there are numerous solutions satisfying equation (1). Certain additional assumptions are required to obtain physically validated

results. There are applicable computer programmes for the solution of these equations.

The success of the neutron spectrometry activation method application is dependent on the accuracy of the cross-sections employed. The cross-section knowledge level can be unequal in the energy range under consideration. The most accurate knowledge of the reaction cross-section is required for the energy range, where the sub-integral function, called a detector response function, has its maximum. It is usually observed at the energies 3 - 4 Mev more, than the detection threshold.

The neutron spectrum determination accuracy is also depen - dent on other nuclear data, such as half - lives and decay-schemes of activation nuclei reaction products. The methods of spectra unfolding can be discussed as well as detector fabrication engineering, measurement error correlation and reliability evalua - tion of results. Here we won't dwell upon these specific problems. They are mentioned so as to emphasize the fast of the cross section uncertainties not being a single source of errors as the spectra were unfolded in the activation method, and taking this into account some reasonable requirements should be imposed on the cross-section accuracy.

3. About CJD Threshold Reaction Evaluated Cross-Section Library.

The threshold reaction cross-sections were evaluated on the basis of experimental data compilation 9 . The measurement result analysis for a wide range of nuclei confirms some conclusions given in 4 , which are concerned with the general situation on the availability and quality of experimental information on the threshold reaction cross-sections:

1/ The measurements were basically performed in the activation method, which suggests a formation of a residual radioactive nucleus with a half-life suitable for the analysis. Not so often, usually in the case of reactions with charged particle emission the method of the direct outgoing particle monitoring is employed. But these measurements as a rule are performed with less accuracy. That is why the experimental information in the most cases exists for the reactions with "comfortable" half-life.

2/ A lot of measurements, basically earlier ones were performed with monoenergetic neutrons at cascade and electrostatic generators with the maximum energy of accelerated protons or deuterons up to 3Mev, using reaction $D(d,n)^3He$, $T(d,n)^4He$ and $T(p,n)^3He$. Note the following as a result of applying neutron sources of the above type:

a) Absense of experimental data in the neutron energy range 6 ÷ 12 Mev for the most of isotopes important in applied tasks;

b) insignificant amount and generally bad quality of the data in the vicinity of reaction thresholds, where high monoenergetic neutrons intensity is required due to low values of the cross-sections;

c) there are relatively many measurements of alternate quality between 13 and 15 Mev.

3/ Recently a number of laboratories have acquired accelera - tor permitting 6 ÷ 12 Mev neutron generation for neutron measure - ments. Measurements covering the total energy range of interest have been performed e.g. at Chalk River (D.C.Santry, J.B.Butler),

CBNM Geel (H.Liskien, A.Paulsen), Los Alamos (R.S.Prestwood, B.P. Bayhurst et al.) and more recently at ANL (D.L.Smith, J.N.Meadows), and Bruyenes - Le - Chatel (J. Frehaut G. Mosinski).

As a result of the critical analysis of the experimental data the most reliable from our point of view values of the measured cross-sections were selected. This implies, that the studies performed with enriched isotopes, semiconductor detectors and yielding the results, which agree within an experiment errors are given preference to. The data essentially differing from the same results by the other authors were not taken into account.

The calculations of excitation functions of all the competitive reactions and those analysed were made within the optical - statistic approach taking into account the integral contribution of non-equilibrium mechanisms of the reaction by an exiton model to obtain the recommended cross-sections.

The basis pre-condition of the development and employment of this method of threshold reaction excitation function evaluation was the fact that the experimental data for the reliable cross-section evaluation in the energy range up to 20 Mev was merely insufficient. In addition to this the data by different authors are often in more essential disagreement, that the above measurement errors.

A characteristic situation with experimental data is shown in fig. 1.

Due to incompleteness and inconsistency of experimental information in these cases the reliable evaluation of cross-sections is difficult to be performed as well as it is hard to obtain the recommended excitation functions of threshold reactions over the whole incident neutron energy of interest.

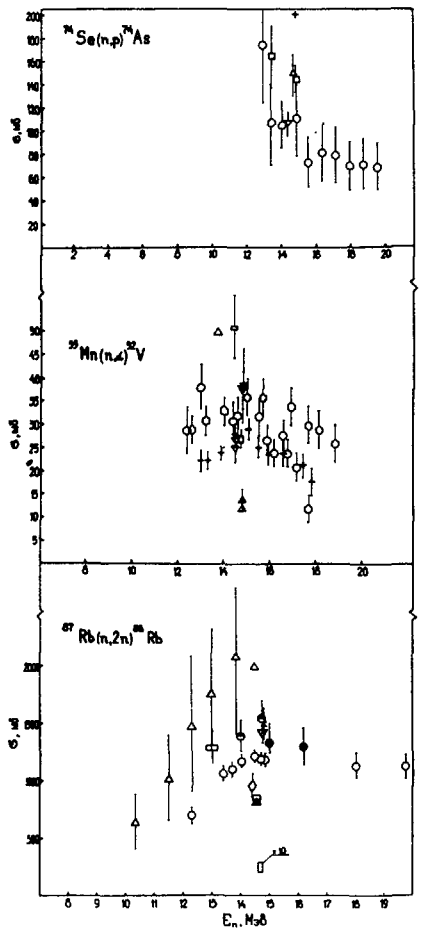

Fig.1. $^{74}Se(np)^{74}As$, $^{55}Mn(n\alpha)^{52}V$ and $^{87}Rb(n2n)^{86}Rb$ reaction cross-sections measured by various authors. The experimental data are designated according to [9]

The microscopic cross-sections analysis employing calculations by the theoretical models of nuclear reactions enables us to compare the results of the experiments performed at alternative energies and with varying resolution allows the total supplementary information recovered from a wider range of nuclear data to be applied in the analysis of the particular cross-section using the known theoretical relations.

This makes it possible first, to exclude obviously erroneous data from the totality of nuclear data and, second, to evaluate the reaction cross-sections for the energy ranges of incident particles and mass numbers of nuclear targets lacking the experimental data.

A great importance at threshold reaction excitation function evaluation was attached to the cross-sections at the energy of incident neutrons 14-15 MeV. As it was already noted the (n,p), (n,α) and (n,2n) reaction cross-section measurements were performed either at this energy only or the experimental data for this energy essentially exceeded those for all other energy ranges. When classifying extensive experimental data one can observe the trends and find a dependence in the behaviour of 14 MeV neutron reaction cross-sections.

Various authors make note of the fact of systematic (n,p) reaction cross-section reduction at neutron energies ~ 14 Mev as the isotope atomic weight of each element grows. Fig.2 illustrates the dependence

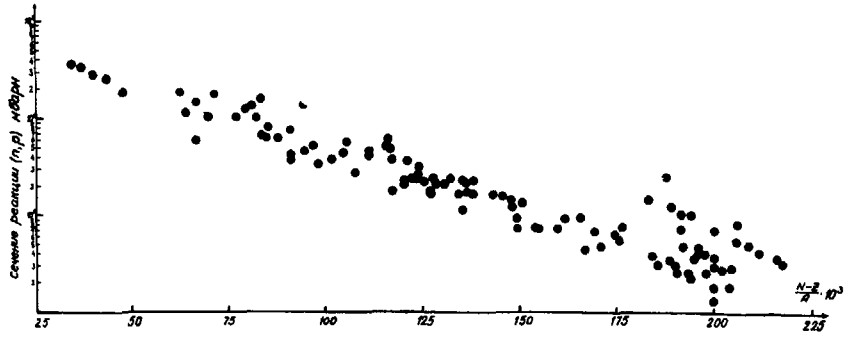

Fig.2. Dependence of experimental (n,p) reaction cross-sections at bombarding neutron energies ~ 14-15 Mev on the parameter (N - Z) / A.

σ_{np} at E_n ~ 14 - 15 Mev on the parameter (N - Z)/A in the logarithmic scale. In a wide interval of mass numbers this dependence can be seen to be fairly accurate described by a straight line. It was first indicated by V.N.Levkovsky [11] who had suggested the empirical relation application for (n,p) reaction cross-section calculation at E_n ~ 14-15 Mev.

$$\sigma_{np} = 7.3 \cdot \sigma_{abs} \cdot \exp\left(-33\frac{N-Z}{A}\right) \qquad (2)$$

The similar dependence of (n,p) reaction cross-section on the number of neutrons and protons in a nucleus at the incident neutron energy ~ 14,5 Mev was obtained in Ref.[10] on the basis of normal statistical relations for the nuclear reaction cross-section and Weitzsäcker's formula for nuclear binding energy:

$$\sigma_{np} = 0.706 \cdot \sigma_{abs} \cdot \exp\left[\sqrt{\frac{A}{145}}\left(-49,97\frac{N-Z+1}{A} + 0,584\frac{Z-1}{A^{1/3}} - 3,258\right)\right] \qquad (3)$$

where $\sigma_{abs} = \pi r_0^2 (A^{1/3}+1)^2$, $r_0 = 1,4 \cdot 10^{-13}$ cm

The observed dependence of (n,p) reaction cross-section on parameter (N-Z)/A is shown to be caused by the exponential reaction cross-section dependence on the proton binding energy in the nucleus.

The fig.3 show, that relation (3) gives a more accurate reflection of the isotopic cross-section dependence (a solid line), that (2), that is particularly noticeable on heavy nuclei.

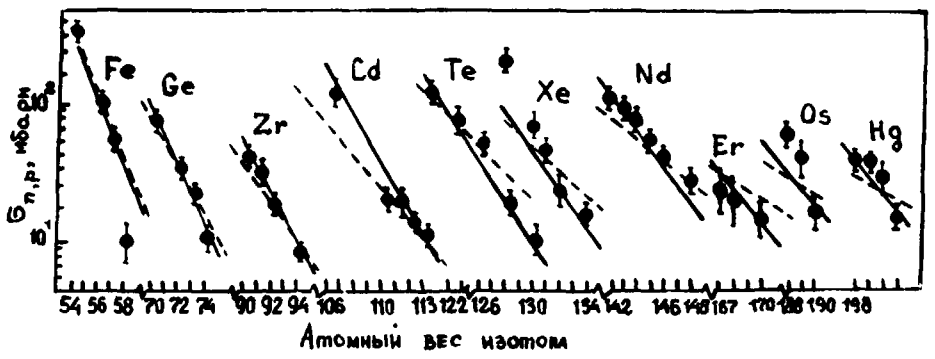

Fig.3. Isotopic dependence of (np) reaction cross-sections at bombarding neutron energy $E_n \sim 14{,}5$ Mev.

Refs. [12, 13] indicate an existence of the empirical (n,2n) reaction cross-section dependence at incident neutron energy ~ 14-15 Mev:

$$\sigma_{n2n} = \sigma_{abs}\left[1 - k\exp\left\{-m\,\frac{(N-Z)}{A}\right\}\right] \qquad (4)$$

A simple dependence of the (n2n) reaction cross-section on the number of protons and neutrons in the nucleus at the incident neutron energy ~ 14,5 Mev was obtained in Ref. [10] on the basis of the sequential particles emission taking into account non-equilibrium neutron emission in the first reaction stage and Weitzsäcker's formula for the nucleus binding energy. The isotopic cross-section dependence is shown to be associated with the neutron binding energy dependence in the nucleus on the parameter (N-Z)/A. In fig. 4 the experimental data are compared with the predictions by the resulting formula (a solid line).

The statistic analysis of the cross-section prediction reliability as well as σ_{np} and σ_{n2n} calculations accuracy evaluation showed the derived formulas are suitable for predicting

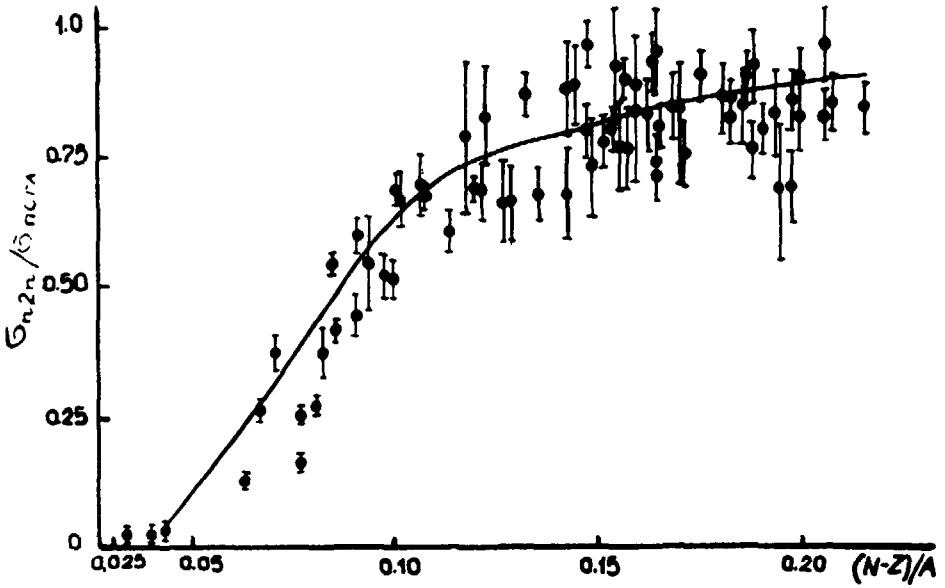

Fig.4. Comparison of experimental data with predictions on (n,2n) reaction cross-section systematic at $E_n \sim 14{,}5$ Mev.

the (n,p) and (n,2n) reaction cross-sections at $E_n \sim 14$-15 Mev for the nuclei lacking the experimental data. Simplifications and approximations employed at derivation of the formulas for calculating σ_{np} and σ_{n2n} at $E_n \sim 14 \div 15$ Mev enable us to see the boundaries of their applicability and to explain the cases of disagreement for the results of comparing the experimental cross-sections with the predictions by empirical systematics.

From the standpoint of the present - day user the information on nuclear data for certain elements is considered existing only in the case when it is represented on a certain data unit in the particular format as a library of evaluated cross-sections with the computer connection and permits computer treatment. The recom-

mended excitation functions of threshold reaction obtained as a results of the evaluation are arranged in the computer Library of Evaluated Threshold Reaction Cross-Section-BOSPOR-80 and are included into the INDL/V - file of the Nuclear Data Section of IAEA in the format ENDF/B. The Library incorporates 142 recommended exitation functions of (n,p), (n,α) and (n,2n) reactions for 99 stable isotopes of 59 elements.

Energy dependences of cross-sections from BOSPOR are presented also in the unified analytical form [14] . In this case two principal aims were pursued:

a) to employ the appropriate formulae for $\sigma(E)$ in analytical calculations thus providing the possibility of fast calculation of the required cross-section at any value of the energy $E \leqslant 20$ Mev;

b) to reduce the volume of numerical infor mation to be sto - red without an essential decrease of evaluated data accuracy.

The analytical representation was performed on the basis of PADE second - type approximation. This approximation is the rational function $f^{[L]}_{(E)} = P_N(E)/Q_M(E)$, where $P_N(E)$ and $Q_M(E)$ - are polynomials of powers N and M, respectively, and L = N+M+1 is the total number of parameters. It can be parametrized in various ways. One of the most convenient ones is polar expansion (at $N \leqslant M$):

$$f^{[L]}(E) = \sum_{i=1}^{\ell_1} \frac{a_i}{E - P_i} + \sum_{k=1}^{\ell_2} \frac{\alpha_k (E - \varepsilon_k) + \beta_k}{(E - \varepsilon_k)^2 + \gamma_k^2} + C \qquad (5)$$

Under the first total sign there are the terms corresponding to actual poles of the approximant, under the second sign - the terms corresponding to complex poles.

In the search of the best approximation the functional representing an average relative accuracy of approximation was minimized:

$$S = \sqrt{\frac{1}{N_{ex}} \sum_{i=1}^{N_{ex}} \frac{(f_i - f_{ai})^2}{f_i^2}} \qquad (6)$$

where N_{ex} - is the total number of points;

f_i, f_{ai} - are the values of approximated function and approximation in the $i^{\underline{th}}$ point.

The average relative accuracy of approximation was: for 81 curves - less than 1%, for 43 curves - from 1 % to 2%, for the rest - from 2% to 5%.

The code HELP can be utilized so as to reproduce the cross - section energy dependence using the expansion parameters, arranged in the computer in the form of a library.

4. Approximation of Reaction Cross-Sections with Charged Particle Emission near threshold.

The recommended excitation functions of threshold reactions with a charged particle emission in BOSPOR have one common disadvantage. All of them begin with a certain threshold value of incident neutron energy called an efficient reaction threshold, and its value is always slightly more, than the corresponding energy threshold, whereas it follows from the correct understanding of the nuclear reaction mechanism, that the threshold reaction excitation function should have very small (though non-zero) values in the interval from the energy reaction threshold up to the efficient one as well. The cross-section evaluation method employing theoretical models that is applied at the BOSPOR arrangement did not make it

possible to determine correctly a cross-section below the effi - cient reaction threshold. In most cases this phenomenon is of insignificant concern, because according to our evaluations the contribution of the earlier ignored " tail " the averaged over reactor neutron spectrum cross - section is of a per - cent (see Table 5.2). However, in a number of neutron metrology tasks (e.g. at neutron spectra unfolding by the reaction rate measured) the proper way of taking into account the near-threshold energy range cross-sections is up to the energy reaction threshold. This also enables us to obtain physically correct representation of recommended reaction cross-section energy dependence with an emis - sion of charged particles over the whole interval of incident neu - tron energies.

That is why for the (n,p) and (n,α) reaction cross-sections BOSPOR, corrected with allowance for the recent data for differential and integral experiments, their energy - dependence was ana - lytically approximated to the reaction cross-section threshold [15]. The approximation method employed allows the reaction cross-secti - ons with charged particle emission deep below the barrier to be calculated. In this case the general features typical of tne threshold reaction cross-section energy dependence were applied and certain physical assumptions were made.

A section $[Q, Q + B]$ (for exothermal reactions - $[0, B]$) was chosen as a section of approximation, where Q - is the reac - tion threshold, B - is the Coulomb barrier height. When determi - ning the form of approximation and the section of approximation the following factors were taken into account:

a) Availability of reliable evaluated data on the cross-section energy dependence over the most part of the section $[Q,Q+B]$, in the interval $[Q_1,Q_1+B]$, $Q < Q_1 < B$.

b) Nuclear reaction excitation function progression due to the Coulomb barrier effect at the section $[Q, Q_1]$ where it was required to calculate the cross-section.

c)Asymptotic cross-section behaviour in the vicinity of the threshold (endothermal reactions) or at neutron energies close to zero (exothermal reactions). The endothermal reaction cross-sec - tion is known [16] to vary in the mentioned region by the law:

$$\sigma(E) \sim \sqrt{E-Q} \cdot \exp\left\{-\sqrt{2}\,\pi Z_B z_b e^2 \sqrt{\mu}/\hbar\sqrt{E-Q}\right\} \qquad (7)$$

whereas the exothermal reaction cross-section varies by the law:

$$\sigma(E) \sim \exp\left\{-\sqrt{2}\,\pi Z_B z_b e^2 \sqrt{\mu}/\hbar\sqrt{E+Q}\right\} \qquad (8)$$

Taking into account the above - mentioned the reaction cross-section in the interval under investigation is represented in the form:

$$\sigma(E) = \sqrt{E-Q} \cdot T_0(E-Q) \cdot g(E) \qquad (9)$$

$$\sigma(E) = T_0(E+Q) \cdot g(E) \qquad (10)$$

taking into account an effect of the basis physical factors, that is the availability of the reaction threshold and Coulomb barrier. The function g(E) describes an effect of the ignored factors,and $T_0(E)$ - the Coulomb barrier factor for protons and α-particles with an angular momentum l = 0.

Then in the interval $[Q_1, Q + B]$ the function g(E) is repro - duced taking into account the recommended energy dependence of the cross-section and is approximated by a rational function $g_a(E)$ using the code PADE2 [17] . Hereupon the $g_a(E)$ approximation function is extrapolated in the region $[Q, Q_1]$ and the near - threshold reaction cross-section is calculated via formulae (9) and (10).

5. Comparison of Evaluated Cross-Sections with Integral Experimental Data and Discussion of Results.

The integral experiment results are usually utilized for verification of evaluated microscopic nuclear data. This is due to the accuracy of the latter being higher as a rule. The integral measurements in the neutron spectra of various forms differing in "the degree of hardness" must be for analysis of a wide range of microscopic cross-section dependence on the interactive neutron energy.

The decisive requirement for the integral test result to be applied for differential cross-section verification consists in the fact, that the neutron field, where the measurement is being made should be qualified fairly well.

The most studied neutron spectra are U-235 thermal fission and Cf-252 spontaneous fission ones.

5.1. Fission Neutron Spectrum Representations.

Spectrum average cross-section will be considered those calculated via the formula

$$\langle \sigma \rangle = \int_0^\infty \sigma(E)\chi(E)dE \qquad (11)$$

where $\sigma(E)$ is the reaction cross-section and $\chi(E)$ is the normalized neutron spectrum $\left(\int_0^\infty \sigma(E)\chi(E)dE\right)$.

A few analytical expression have been recently used to represent the neutron spectrum of U-235 thermal fission [18], where E is the neutron spectrum energy in Mev.

$\chi_1(E) = 0.48395 \cdot \exp(-E) \cdot \mathrm{SINH}\sqrt{2E}$ (12) Watt' formula

$\chi_2(E) = 0.45274 \cdot \exp(-E/0.965) \cdot \mathrm{SINH}\sqrt{2.29E}$ (13) Kranberg formula

$\chi_3(E) = 0.76985 \cdot \exp(-0.775E)\sqrt{E}$ (14) Leachman formula

$\chi_4(E) = 0.5827 \cdot \exp(-0.992E) \cdot \mathrm{SINH}(1.27\sqrt{E})$ (15) Wood formula

Magurno and Ozer [19] also adopted the Maxwellian form of spectrum to verify the dosimetry file ENDF/B-IV when calculating fission - spectrum - average cross - sections:

$\chi_5(E) = 0.770 \cdot \sqrt{E} \cdot \exp(-E/T)$

with the values T = 1.29 Mev and T = 1.32 Mev.

Later on Grundl and Eisenhauer performed a new evaluation of neutron spectra of U-235 thermal fission and Cf-252 spontaneous fission. The results are given in the form of a Maxwellian spectrum with corrections in five energy ranges.

For U-235 : $\chi_8(E) = M(E) \cdot \chi_6(E)$; $\chi_6(E) = 0.7501\sqrt{E} \cdot \exp(-1.50 \cdot E/1.97)$;

For Cf-252: $\chi_9(E) = M(E) \cdot \chi_7(E)$; $\chi_7(E) = 0.6672\sqrt{E} \cdot \exp(-1.50 \cdot E/2.13)$;

Below 6 Mev the correction functions for two spectra are given in Table 5.1.

Table 5.1

Correction functions for two spectra.

Energy range Mev	(E) for U-235	(E) for Cf-252
0 - 0.25	I + 0.800 E - 0.153	I + I.200E - 0.237
0.25- 0.8	I - 0.140 E + 0.082	I - 0.140E + 0.098
0.8 - 1.5	I + 0.040 E - 0.062	I + 0.024E - 0.0332
1.5 - 6.0	1 + 0.010 E - 0.017	I + 0.0006E- 0.0037
6.0 - ∞	1.043 exp{-0.06(E-6.0)/I.043}	I.0exp{-0.03(E-0.60)/I.0}

Selection of representation for the fission spectrum is of insignificant for activation cross-section with low reaction thresholds, but for the reactions with a high threshold (say, about 10 Mev) it is of great importance. The uncertainty in neutron spectrum description reflects the status of experimental data. The greatest error occurs in the region of very soft and hard segments of the spectrum. In the energy range above 8 Mev the fission neutron spectrum is known with

an accuracy about 25%. For neutron field investigation using activation detectors with high - threshold reaction cross-sections and for calculations of helium yield from the (n,α) reaction, the accurace of fission neutron spectra knowledge should be higher.

5.2. Comparison with Integral Data.

When comparing the recommended values of integral cross-sec - tions in the U-235 fission neutron spectrum we basically rely on Refs. [21, 22] and the most recent issue by these authors [23]. In addition to this the results of integral cross-sections evaluation published in Refs. [24 - 26] were used.

Ref. [21] deals with the evaluation of integral microscopic cross-sections measured at the neutron spectrum of U-235 thermal neutrons fission for 29 threshold reactions most essential in reactor dosi - metry and fast reactor engineering.

Most of the integral measurements were performed by the relative method that is why their results were renormalized in Ref. [21].

The recommended values of spectrum-average cross-sections in [21] were obtained through the least-square method averaging by the renormalized authors of the experimental data available, taken "with the weight" equal to the mentioned experimental error.

The recommended data in Ref. [24] include the results of evaluation [21] being unaffected except the cross-section error, which now takes into account an uncertainty of the standard. Besides, all the available measurements of integral cross-sections at the spectrum of U-235 fission neutrons published up to 1974 are analyzed in Ref. [24], and these cross-sections were evaluated by the method similar to that accepted in Ref. [21], the same values of standards having been used at cross-section renormalization.

Recently published Ref. [23] gives the results of new measurements of U-235 spectrum-averaged cross-sections for 17 threshold reactions. Upon the introduction of appropriate corrections for multiple scattering, sample thickness, the measurement results appeared to be in a good agreement with the results of the earlier integral cross-section evaluation by these authors for most of the elements.

The results of calculated and experimental data comparison for the integral cross-sections are shown in Table 5.2. In the whole, a good agreement of recommended cross-section averaged over- the neutron spectrum of U-235 thermal neutron fission with the integral experiment results is observed.

Table 5.2. Comparison of recommended excitation functions of threshold reactions with the emission of charged particles, averaged over U-235 fission neutron spectrum with experimental data.

Reaction	Averaged cross-section, mb						
	Evaluated	BOSPOR-80			Cross-section's post-correction and post-approximation results.		
	Experiment	$X_1(E)$	$X_2(E)$	$X_3(E)$	$X_1(E)$	$X_2(E)$	$X_3(E)$
$^{24}Mg(np)^{24}Na$	1.50 ± 0.06	1.52	1.40	1.56	1.51^+	1.39^+	1.55^+
$^{27}Al(n\alpha)^{24}Na$	$0.706\pm0,028$	0.698	0.638	0.724	0.738	0.677	0.762
$^{27}Al(np)^{27}Mg$	3.95 ± 0.20	3.99	3.82	3.83	4.06	3.89	3.90
$^{31}P\ (np)^{31}Si$	35.5 ± 2.7	32.5	32.0	30.6	32.34^+	31.84^+	30.53^+
$^{32}S\ (np)^{32}P$	66.8 ± 3.7	65.62	64.47	61.94	65.54^+	64.38^+	61.85^+
$^{46}Ti(np)^{46}Sc$	11.6 ± 0.4	12.81	12.28	12.25			
		(11.15)	(10.67)	(10.69)	11.23	10.74	10.77
$^{47}Ti(np)^{47}Sc$	17.7 ± 0.6	22.2	21.8	21.0			
		(17.35)	(17.06)	(16.48)	17.36	17.12	16.57
$^{48}Ti(np)^{48}Sc$	0.302 ± 0.010	0.262	0.241	0.269			
		(0.282)	(0.260)	(0.289)	0.285	0.263	0.292
$^{54}Fe(np)^{54}Mn$	80.5 ± 2.3	82.2	80.4	77.7	82.7	80.94	78.2
$^{56}Fe(np)^{56}Mn$	1.09 ± 0.04	1.078	1.004	1.078	1.076^+	1.002^+	1.076^+
$^{59}Co(n\alpha)^{56}Mn$	0.161 ± 0.007	0.147	0.135	0.151	0.158	0.146	0.161
$^{58}Ni(np)^{58}Co$	105.1 ± 1.1	103.0	101.0	97.9	103.52	101.46	97.97
$^{60}Ni(np)^{60}Co$	2.3 ± 0.4	2.57	2.42	2.53	2.59	2.43	2.54
$^{63}Cu(n\alpha)^{60}Co$	0.500 ± 0.056	0.482	0.452	0.478	0.506	0.475	0.500
$^{64}Zn(np)^{64}Cu$	30.2 ± 0.5	36.8	36.0	34.8			
		(32.02)	(31.25)	(30.25)	32.24	31.46	30.48
$^{90}Zr(np)^{90}Y$	0.38 ± 0.02	0.33	0.31	0.33			
		(0.36)	(0.33)	(0.35)	0.36	0.33	0.35

Note: 1. The post-correction results for the cross-sections on integral data are given in parenthesis.

2. The sign "plus" denotes the cross-section values, which are less than the coresponding averaged cross-sections BOSPOR-80. The deviations are within the limits of approximation accuracy.

REFERENCES

1. Nikolaev M.N. Demand in nuclear data for reactor engineering. In book: Neutron Physics (Proceedings of the 3rd All-Union Conference on Neutron Physics, Kiev, 9 - 13 June, 1975), Moscow, 1976, v. 1, p.5.
2. Manokhin V.N., Usachev L.N. Demands in Nuclear Data for fast neutron reactors. In book: Neutron physics (Proceedings of the 6th All-Union Conference on Neutron Physics, Kiev, October 2-6, 1983), Moscow, 1984, v. 1, p.18.
3. Nuclear Data Standards for Nuclear Measurements. Technical Report Series No 227, IAEA, Vienna, 1983.
   Nuclear Standard Reference Data, Report IAEA-TECDOC-335, Vienna, 1985.
4. Vlasov M.F., Fabry A., McElroy W.W., Khalil N.A. Status of neutron cross-section for reactor dosimetry. Report INDC(NDS)-84/L+M, 1977.
5. Nuclear Data for Radiation Damaga Estimates for Reactor Structural Materials; Report INDC(NDS)-179/G, 1986.
6. Report INDC(SEC)-54/L + DOS, July 1976.
7. Neutron cross sections for reactor dosimetry, vol. 1,2. Report IAEA-208, Vienna, 1978.
8. Cullen D.E., Kocherov N. and McLaughlin P.K. The International Reactor Dosimetry File (IRDF-82). Report IAEA-NDS-41, IAEA,1982.
9. Bychkov V.M. et al. Cross-section of neutron-induced threshold reactions. Moscow, Energoizdat, 1982.
10. Bychkov V.M. et al. Cross-sections of (n,p), (n,α), (n,2n) threshold reactions. Problems of Atomic Science and Engineering. Ser.: Nuclear Constants, 1979, No: I(32), p.27; Report INDC(USSR)--146/LJ, Vienna, IAEA, 1980.
11. Levkovskiy V.N., JETF, 1963, v. 45, p. 305.
12. Lu W., Ranakumar N., Fink R.W. Phys.Rev.,1970, v. c1, p.350.
13. Molla N.I., Qaim S.M. Nucl. Phys., 1977, v. A.283, p. 269.
14. Badikov S.A. et al. The PADE-Approximation of the evaluated data on the cross-section of neutron induced threshold reactions. Problems of Atomic Science and Engineering. Ser.: Nuclear Constants, 1982, No 3(47), p. 66.
15. Badikov S.A., Pashchenko A.B. Approximation of Reaction Cross-Sections with Charged Particle Emission near Threshold. Problems of Atomic Science and Engineering. Ser. Nucl. Const., 1987, No 3.
16. Baz A.I., Zeldovich Ja.B., Prelomov A.M. Scattering,reactions and decays in nonrelativistic quantum mechanics. M., Nauka, 1971, p. 389; Davydov A.S. Theory of atomic nucleus, M.,GIFML, 1958, p. 254.
17. Badikov S.A. et al. Programme of rational approximation PADE-2, Preprint FEI-1686, 1985.
18. Zijp W.L., Baard J.H. Nuclear Data Guide for reactor neutron metrology. Report EUR 7164, 1981.
19. Magurno B.A., Ozer O. "ENDF/B-4 file for dosimetry application" Nuclear Technology, 1975, v. 25, p. 376.
20. Grundl J.A., Eisenhauer C.M. Proc. 1ST ASTM-EURATOM symposium on reactor dosimetry, Petten, 1975, Report EUR 5667 E/F, Part 1, 1977, p. 425.
21. Fabry A. Report BLG-465, 1972.
22. Fabry A., McElroy W.N., Kellogg L.S. et al. Review of micro - scopic integral cross sections data in fundamental reactor dosimetry benchmark neutron fields. Report IAEA-208 (Procee - dings of a consultanta meeting on integral cross-section me - surement in standard neutron fields for reactor dosimetry, Vienna, 15-19 November 1976), Vienna, 1978, v. 1, p. 233-263.
23. Mannhart. Proc. 5th ASTM-EURATOM Symp. Reactor Dosimetry, Geesthacht, FRG, 1984.
24. Calamand A. Cross-sections for fission neutron spectrum induced reactors, report INDC(NDS)-55L, Vienna, IAEA, 1973.
25. Bondars H.Ja,, Lapenas A.A. Recommended cross-sections of activation defectors. Preprint LAFI-054,057, Salaspils, 1983.
26. Bondars H.Ja., Vainberg Ja.K., Lapenas A.A. Activation cross-sections of some threshold reactions. Problems of Atomic Science and Engineering. Ser.: Nuclear constants. 1974, No.15,p.63.

DEVELOPMENT OF THE TIME CORRELATED ASSOCIATED PARTICLE METHOD FOR ABSOLUTE MEASUREMENTS OF REACTION CROSS-SECTIONS

V.I. SHPAKOV, V.N. KUZMIN
Khlopin Radium Institute,
Leningrad, Union of Soviet Socialist Republics

Abstract

A new modification of the TCAP method which enables to avoid some drawbacks of the former techniques has been developed at the Khlopin Radium Institute. The magnetic analysis of the accompanying particles was first introduced. The magnetic separation excluded completely background components due to pretons and tritons from the $D(d,p)^3H$ associated reaction and reduced the background of scattered beam deuterons by a factor of 2-3 orders of magnitude. The modified technique was used to perform neutron induced fission cross section measurements.

Introduction

Following effects are to be determined with absolute measurements of any neutron induced reaction cross section:

- Neutron flux through the sample under investigation,
- Number of reaction events in the sample,
- Mass of investigated nuclide in the sample.

If one omits the question of sample mass determination the main problems which arise in this case can be summarized as follows:

i. Determination of solid angles subtended by both the sample and the neutron flux monitor as well as other geometrical factors.

ii. Account of both angular and spatial distribution of the neutron flux as well as its scattering and attenuation.

iii. Determination of the flux monitor total counting rate, the background contribution and the counting loss due to the amplitude discrimination being carefully determined and taken into account.

iv. Either experimental determination or calculation of the flux monitor efficiency as well as its energy dependence.

v. Determination of the reaction events counting rate in the presence of background induced by both scattered neutrons and those from side reactions.

An absolute method of cross section measurements has been developed at the V.G. Khlopin Radium Institute, USSR, and independently at the Research Center Bruyeres-le-Chatel, France, which is called the Time Correlated Associated Particle method (TCAPM) [1,2] The TCAPM allows to carry out cross-section measurements only at some fixed spot points of neutron energy but enables to exclude a majority of problems mentioned.

The TCAP method.

The basic idea of the TCAP method is illustrated in Fig. 1. An accelerator using the $T(d,n)^4He$ or $D(d,n)^3He$ reaction is a

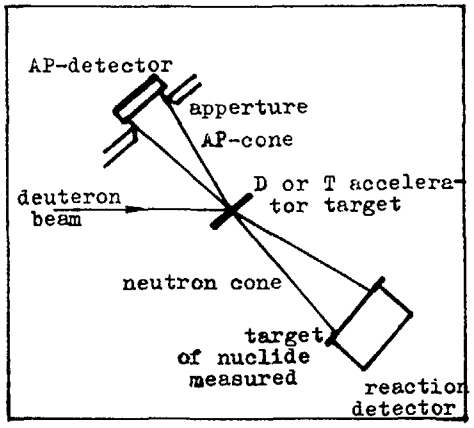

Fig. 1. Main principle of the TCAP method

sourse of neutrons. The ^3He- or ^4He-particles associated with neutrons (AP) are detected by an associated particle detector within a cone, fixed by the detector entrance apperture. The neutrons corresponding to these helions, which also fly inside some cone, hit the sample of investigated nuclide. The reaction events are registered in coincidence with the associated particles (AP).

Provided the neutron cone is insured to be entirely situated within the sample the reaction cross section is determined by the expression

$$\sigma_f = \frac{N_c}{N_{ap} \cdot n}$$

where N_c is the number of recorded coincidences
N_{ap} is the number of recorded associated particles
n is the sample areal density (number of nuclei per cm^2)

is the efficiency of the reaction events registration.

On the basis of this expression the main advantages of the TCAP method can be summarized as follows:

i. There is no need to determine any solid angles and other geometrical factors as well as to take into account angular and spatial distribution of the neutron flux. Only small correction for neutron flux attenuation on the target backings and chamber windows is to be introduced. By a proper choice of material thickness this correction can be reduced to a value of about 1 %.

ii. There is no need to determine either the AP-detector efficiency or the entire number of the AP-counts as the AP counting losses lead to the similar coincidence losses and are equivalent to the neutron flux reduction. Therefore, only a part of the AP pulse-height spectrum can be choosen which includes a minimal background contribution.

iii. All the background components at the reaction events registraration are practically completely suppressed.

To provide the main geometrical constrains: the neutron cone should be entirely situated within the target under investigation both neutron cone profile and its spatial position are to be accurately determined and continuously checked during the measurements by means of either position sensitive detector or a detector of small dimension in coincidence with the AP-detector. Besides, it is necessary to use in measurements samples of high thickness uniformity as the expression mentioned above includes the areal density value. Correction for layer nonuniformity can be calculated by forming a convolution of cone and sample layer profiles, but it results in some additional error.

There is a general belief now that the TCAP method is the most accurate one for absolute measurements. In fact, at present there are no evident origins of systematic errors limiting its accesible accuracy in principle. Moreover, results of five independent measurements of the ^{235}U fission cross section performed by the TCAP technique at the neutron energy of about 14 MeV agree within the range of 1 % [1 - 5].

On the basis of these circumstances the IAEA Consultants' Meeting, held at Smolenice, CzSSR, in 1983 has recommended performance of absolute measurements by the TCAP method at as many neutron energy spot points, as possible [6]. However, further at the Advisory Group Meeting on Standard Reference Data, Geel, 1984, the question of conclusive confirmation of the TCAPM reliability in connection with possible unknown origins of systematical errors has been discussed [7]. As a way of such confirmation it was proposed to perform comparisons of calculated efficiency values for neutron monitors based on the (n-p)-scattering with those obtained by the TCAPM-calibration. High precision of the $_{np}$ value was supposed to provide high accurate efficiecy calculations. Such comparison has been performed in the National Bureau of Standards, USA [8] and the agreement within of 0.2 % was found.

In spite of simplicity in principle of the TCAP method its practical relization in most cases is connected with significant difficulties because of high background in the AP-channel due to scattered primary beam and charged particles emitted in the primary beam interactions with the target materials. To eliminate this background specific AP-channels are to be constructed for measurements at each neutron energy spot point. The description of a number of such channels is presented below.

Measurements at 14 MeV and 2.6 MeV Neutron Energy

Measurements at 14 MeV neutron energy are the simpliest realization of the TCAP method. The $T(d,n)^4He$ reaction and the 150 - 300 keV deuteron beams are used to produce neutrons. The investigated samples are situated in the front hemisphere relative to the beam direction. The AP are registered in the rear semisphere. Due to the high Q-value of the $T(d,n)^4He$ reaction associated alpnas have energies of about 4 MeV. Therefore, the AP-detector can be easily protected from the scattered primary beam by means of a rather thick (up to 1 mg/cm^2) foil, the foil thickness being not crucial.

Either a thin plastic scintillator or a silicon SB-detector can be used to register the AP. The ^1H-, ^2H-, ^3H-particles which are produced by the $D(d,p)^3H$ and $D(d,n)^3He$ background reactions can be the background origin. However, the yield of these particles is small and their background components can be easily eliminated by a pulse-height spectrum discrimination. By means of properly chosen amplitude window background contribution can be reduced to a value of 0.1 %. At present time due to the simplicity there are a number of measurements at the neutron energy of 14 - 15 MeV using the TCAPM. (for example [1 - 5]).

It is rather more difficult to realize the TCAPM at the neutron energy of 2.6 MeV. The $D(d,n)^3He$ reaction low energy deuteron beams are used in this case. As in the previous case, neutrons and helions are utilized, flying forward and backward correspondingly. However, the AP energy amounts in this case to about 700 - 800 keV because ofessentially less the reaction Q-value. Though the AP-detector can also be protected from the scattered beam by means of a foil, the foil thickness as well as its quality become crucial.

In practice 250 mg/cm^2 thick foils with the 5 mg/cm^2 spread were used to provide both efficient separation of scattered deuterons and sufficient spectrometric quality of AP pulse-height spectra. The foil quality is to be carefully checked as a presence of some microscopic holes can result in a large and uncertain background of scattered beam deuterons. Silicon SB detectors can be used to detect the AP. The background protons and tritons from the $D(d,p)^3H$ associated reaction can be separated by an amplitude window. Sufficiently high spetrometric quality of the electronic cirquits is required to minimize the ^1H and ^3H background components while the time resolution must be at the level of 100 nsec to allow high AP counting rate.

Two difficulties are to be mentioned connected with these measurements. The first one is a possibility of "parasitic" targets in the vicinity of the conventional deuteron target due to absorption of deuterons on structural materials. Therefore the primary beam must be carefully collimated by means of distant collimator to a 2 - 3 mm diameter. The second one is connected with the neutron cone broadening because the AP low energy causes an an increase of the Coulomb scattering effect. In spite of the difficulties mentioned this TCAPM modification has been successfully used at absolute measurements performed in the Khlopin Radium Institute [9], in the Technical University of Dresden, GDR [10] and the National Bureau of Standard, USA [8].

Measurements at 4.5, 8.5 and 19 MeV Neutron Energy

The AP-channel realization and measurement performance have some peculiarities which are common for all the three cases. The $D(d,n)^3He$ (for 4.5 and 8.5 MeV) and $T(d,n)^4He$ (for 19 MeV) reactions are used to produce neutrons. The deuteron beam energy amounts to 6 - 9 MeV in this case. Because of rather momentum brought in by neutrons both reaction products - neutrons and helions fly forward. Therefore thin selfsupporting deuterium and tritium targets are to be used to provide the possibility of the AP detection. Thin films of deuterated polyethilene and selfsupporting titan-tritium targets were used in the absolute fission cross section measurements performed in collaboration of the Khlopin Radium Institute and the Technical University of Dresden (for example [3,11]). It is impossible in this case to protect the AP- detector by any foil. Deuterons of the scattered primary beam cause the background in the AP-channel which is 2 - 3 orders higher than the AP-counting rate. Besides, another background origin arises in this case which is alphas produced by (d,α)-reactions in the target materials (titan, carbon, etc.), having energy approximately the same as the AP.

The background of scattered deuterons can be suppressed by means of application of thin silicon SB detectors using the difference of helion and deuteron ranges but to separate the AP helions from the background alphas it is necessary to apply the ΔE-E_r telescope comprising the 8-12 mm and 30-70 mm thick completely depleted detectors. The detector parameters are to be carefully chosen for each neutron energy spot point to get the best AP separation. An example of twodimensional spectrum in the $\Delta E, E_r$ coordinates is presented in Fig. 2.

Separation of the AP on the basis of this spectrum is an essential problem as conventional methods (computer processing or application of electronic cirquits forming the $\Delta E \times E_r$ products) are inapplicable because of the 100 nsec time resolution is necessary. Therefore a new method was developed for the fast analysis of twodimensional spectra based on linear approximation in a narrow energy range. Linear combinations $U_i = a_i \Delta E + b_i E_r$ are formed by means of proper electronic cirquits. The a_i and b_i coefficients are obtained by attenuation of the ΔE and E_r signal amplitudes. Two parallel spectrometric channels are used to form simultaneously two such combinations with different values of the coefficients. Coincidences of the signals from both channels within the pulse-height windows ΔU_1 and ΔU_2 correspond to a separation of some region in the twodimensional spectrum. Proper choise of

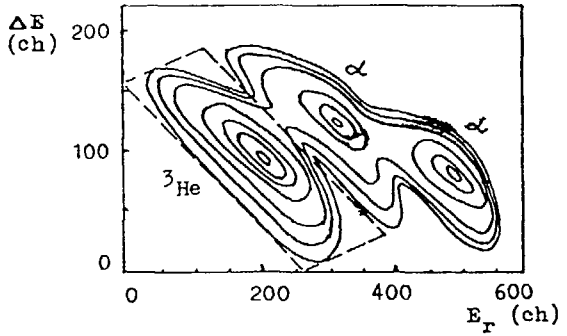

Fig. 2. Twodimensional spectrum in the ΔE-channel at measurements for 8.5 MeV-neutrons

both the coefficients and the window width permits to set the optimal shape and size of such region including a minimal background contribution. This region is represented in Fig. 2 by the dashed lines. Fig. 3 shows an example of the pulse-height spectrum obtained in one channel in coincidence with the amplitude window in the other channel. This method enables to reduce the background contribution to a 1 - 3 % level. The background value can be accurately determined by means of replasement of deuterated polyethilene with conventional one. An accesible value of the proper uncertainty component does not exceed a value of 0.1 - 0.3 %.

Measurements by the TCAP technique at the listed neutron energies werw performed only in the collaboration of the Khlopin Radium Institute and the Technical University of Dresden [3,11].

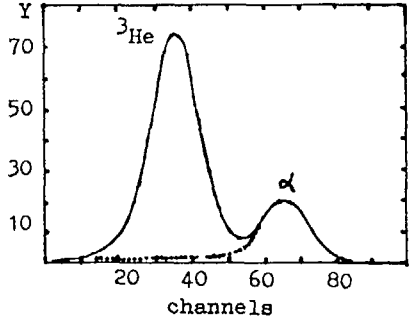

Fig. 3. Pulse-height spectrum in the U_1 amplitude window in coincidence with the U_2 amplitude window

Measurements at 1.9 - 2.4 MeV Neutron Energy

A new modification of the TCAP-method has been developed in the Khlopin Radium Institute which enables to avoid some drawbacks in the former modification, to rise the measurements reliability and to check possible unknown origins of systematic errors.

The $D(d,n)^3He$ reaction and the deuteron beam with energy of 3 - 3.5 MeV were used to produce neutrons. Thin foils of deuterated polyethilene were applied as accelerator targets. Associated helions were registered at small angles with respect to the beam direction. Corresponding neutrons flew backward. Such configuration has the following advantages:

1. Associated helions have rather high energy (about 4 MeV) what fasilitates their registration and separation.

2. As it can be seen in Fig. 4 the neutron energy weakly depends on the deuteron energy and consequently is weakly influenced by the deuteron energy losses in the target. This fact permits to improve the neutron energy fixation as well as to minimize the energy spread.

However the background of scattered beam deuterons is extremely high at this configuration due to the fast increase of the Coulomb scattering cross section at low angles with respect to the beam axis. Therefore the former modifications of the TCAPM are inapplicable. To suppress the deuteron background a separation of charged particle trajectories in an uniform magnetic field was applied.

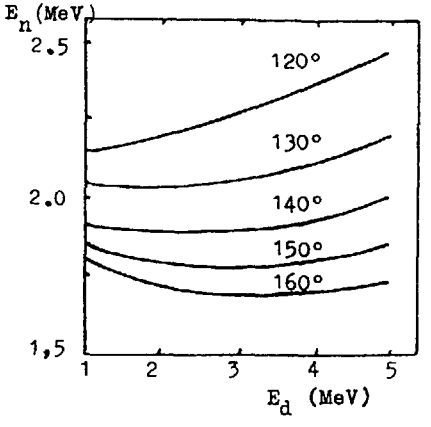

Fig. 4. Dependence of neutron energy on deuteron energy for various neutron flight angles

The schematic drawing of the experimental arrangement is presented in Fig. 5. The target chamber was situated outside the magnetic field. The AP-cone was formed by a collimator and got into the magnetic analyser which was a 4 mm depth flat chamber with covers of magnetic iron, situated between magnetic poles. The trajectory lengths were about 40 - 60 cm. The magnetic field induction was about 0.5 T. As the AP-cone collimator was situated outside the magnetic field any magnetic field variations did not changed the neutron cone position but resulted only in variation of the neutron intensity. The magnetic field induction was nevertheless stabilized (by means of winding current stabilization) within 0.1 %.

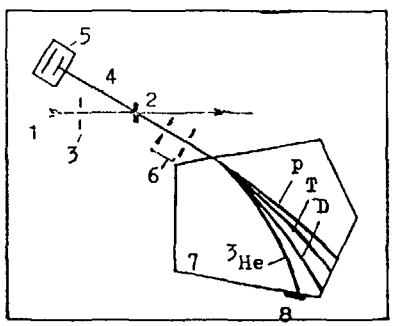

Fig. 5. Schematic drawing of the experimental set-up with magnetic analysis.
1. deuteron beam; 2. accelerator target; 3. beam collimator; 4. neutron cone; 5. investigated sample; 6. AP-cone apperture; 7. magnetic analyser; 8. AP-detector.

The magnetic separation excluded completely background components due to the protons and tritons from the $D(d,p)^3H$ associated reaction and reduced the background of scattered beam deuterons by a factor of 2 - 3 orders. However, a low energy part of scattered deuterons could reach the AP-detector as well as protons of residual hydrogen in the target knocked out by the beam and those from the $^{12}C(d,p)$-reaction. Therefore, an additional separation based on difference of the helion and other particle ranges was used together with the magnetic one by means of a silicon SB-detector with small depth of depleted zone.

The AP-channel pulse-height spectrum thus obtained is shown in Fig. 6. Excelent separation of the peak can be seen. A small background contribution determined by the replasement of deuterated polyethilene with conventional one did not exceed the value of 0.1-0.3 %. In general, in the case of magnetic analysis an essential problem is to embrace the whole neutron cone by the AP-detector, as the cone cross section at the magnetic field output becomes large because of the long flight path inside the analyser chamber. However, at the experimental conditions chosen the AP-cone was compressed in the horizontal plane relative to the neutron cone due to the reaction cinematics. It permitted to decrease horizontal size of the AP-detector. To compress the AP-cone in the vertical plane a vertical focusing was introduced. It was provided by the effect of the AP olique flight angles relative to the magnetic field border. As a result the 2 x 4.5 cm^2 large AP-detector was sufficient to provide complete covering of the investigated sample by the neutron cone, the neutron cone cross section being round. The background suppression by means of simultaneous application of the magnetic separation and the SB detector with low depth of depleted zone was efficient enough and did not put any requirements to spectrometric quality of the electronic circuits.

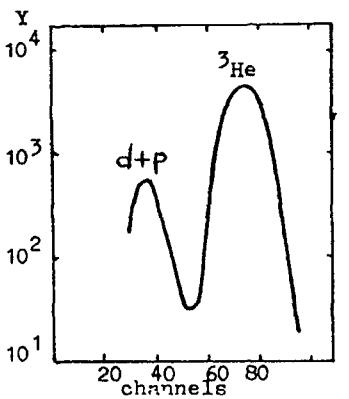

Fig. 6. Pulse-height spectrum in the AP-channel

A fast current amplifier was used in the AP channel, amplitude discrimination in the fast channel being sufficient. Some problem was to detect current pulses from the detector which had rather intrinsic capacity (about 10 nF). A current preamplifier with 4 parallel input channels was used to meet the goal.

The TCAPM modification described was used in the Khlopin Radium Institute to perform neutron induced fission cross section measurements for a number of heavy nuclides. The results obtained are in excellent agreement with those, obtained in measurements performed before by means of former modification of the TCAPM. This agreement seems to confirm both the TCAPM reliability and absence of some unknown origins of systematic errors.

The last modification employing the magnetic separation seems to be the most promising one and though being used at the 2 MeV neutron energy, can be applied for set of neutron energies in a large energy region.

The TCAP technique was used in all the works cited for fission cross section measurements. However it is obviously that this technique can be successfully applied for precise absolute measurements of other reaction cross sections in all cases when the reaction product can be directly registered.

REFERENCES

1. Alkhazov I. D. et al. Proc. of 2-nd Conferece on Neutron Phys., Kiev, USSR, 1974, vol. 4, p. 13.
2. Cance M., Grenier G. Nucl. Sci. and Eng., 68, 197 (1978)
3. Arlt R. et al. Proc. of Internat. Conf. on Nucl. Cross Sect. for Technology, Knoxwille, USA, 1979. NBS spec. Publ. 594, Washington, USA, 1980, p. 990
4. Wasson O. A., Carlson A. D., Duvall K. C. Nucl. Sci. and Eng. 80, 282 (1982)
5. Li Jingwen et al. Proc. of Internat. Conf. on Nucl. Data for Science and technology. Antwerp, Belgium, 1982, p. 55
6. Conclusions and Recommendations. Proc. of the IAEA Consultants' meeting on the U-235 Fast Neutr. Fiss. Cross Sect. Smolenice, CzSSR, 1983, INDC(NDS)-146, p. 20
7. Sowerby M. G., Patrick B. H. Proc. of an Advisory Group Meeting IAEA-TECDOC-335, 1985, p. 151
8. Carlson A. D. et al. Ibid. p. 332
9. Alkhazov I. D. et al. Proc. of the X-th Internat Symp. on Selected Topics of the Interaction of Fast Neutrons and Heavy Ions with Nuclei. Gaussig, GDR, 1980, ZfK-459, Dresden, 1981, p. 40
10. Arlt R. et al. Ibid. p. 44
11. Arlt R. et al. Ref. as in 7, p. 174

NEUTRON YIELD FROM REACTIONS PRODUCED BY ALPHA PARTICLES WITH ENERGIES UP TO 10 MeV

V.A. VUKOLOV, F.E. CHUKREEV
I.V. Kurchatov Institute of Atomic Energy,
Moscow, Union of Soviet Socialist Republics

Abstract

Basing on the estimated values of the cross sections of the (a,n) reactions for lithium, beryllium, boron, carbon, fluorine and oxygen the neutron yields have been calculated for targets prepared of these materials. The yields for chemical compounds of actinides with light nuclei have been also calculated. The general approach in performing such calculations with charged particles and the evalution method are discussed.

INTRODUCTION

Wide application of charged-particle beams in various fields of science and technology has made to create the data library in the exchange format (EXFOR) for charged-particle reactions. The library contains mainly experimental values of cross sections and yields. Its volume is continuously increasing but at the same time the range of requests is also expanding. Typical examples of arising situations are:

- the library contains experimental cross sections and yields are required;
- yields are available and yields of the same reactions but for different target compositions are required;
- experimental cross sections are contained and more reliable data are necessary, etc.

Use of the calculation methods enables, to a great extent, solution of these problems.

The present lecture describes the calculation method for nuclear reaction yields. Its algorithm has been partly realized in the Center for Nuclear and Atomic Data of the Kurchatov Institute. (CAJaD). As an example the data on neutron yields from the (α, n) reactions for energies of α-particles up to 10 MeV are presented.

Structural scheme of the calculation complex

To solve the problem to have been set the calculation complex must have a sofware package which permits to carry out the following basic operations:

1. Formation of the experimental data file including:
   - retrieval of information relevant to the demand on the EXFOR library;
   - translation of the graphical information into numeral type and its entering into the file or entering of the tabular information from the literature sources lacking in the library.
2. Analysis of experimental data including possibilities of:
   - correction of the data for refined values of physical or normalization constants used in the experiment;
   - data approximation by polynom class functions for smooth dependences, splain polynomials for piecewise smooth dependences and rational fraction expressions for resonance dependences;
   - integration of the function over specified ranges.
3. Formation of the output data file including:

- calculation of the evaluated values and their uncertainties;

- calculation of the stopping-powers;

- calculation of the reaction yields or, on the contrary. determination of the cross sections by estimated yields;

- description of the evaluated values in terms of a supposed theoretical model for the purpose not only to compare bu also to calculate the reaction characteristices other than the initial ones.

Calculation of the neutron yields in the (α, n) reactions

Here we shall consider application of the scheme proposed for evaluation of the (α, n) reaction cross sections on lithium, beryllium, boron, carbon, fluorine and oxygen targets and calculation of yields from these targets as well as from targets of chemical compounds of light elements with actinides. Similar calculations were carried out earlier /1-5/ but mainly using cross section measurement results obtained in individual works. The analysis of experimental data on reaction cross sections reveals that the discrepancy between the results of individual measurements exceeds the accuracy reported by the authors and reaches (30 - 60)% . From the analysis /6/ it also follows that because of difficulties preparing isotopically pure targets with a known number of nuclei investigated, attainment of an accuracy better than 10% in measurements with thin targets remains problematic. A progress in reducing the calculation data uncertainty could be reached on the basis of joint analysis and estimation of both the (α, n) reaction cross sections and the neutron yield measurements.

Peculiarity of the cross-section evaluation for (α, n) - reaction consists in that for all elements considered the excitation function has the resonance character, is usually presented in the picture form and, with the rare exception /12,13/ its values were lacking in the EXFOR library. That is why the experimental data file is mainly constructed by means translation of the picture information to numeral type using the computer-aided system SKOLKA; the translation accuracy is 3%.

The evaluation method has been described in more detail in Ref. /7/. The present paper gives a brief list of the main stages.

1. The experimental data were reduced to comparable energy ranges by matching an approximating curve in the form of a polynomial and its integrating within the range from 250 to 500 MeV.

2. Within each energy range the weight-average value of the cross section was determined:

$$\bar{\sigma} = \sum_{i=1}^{n} \omega_i \sigma_i / \sum_{i}^{n} \omega_i$$

and errors:

inner - $\Delta\sigma = 1/\sqrt{\sum \omega_i}$,

outer - $\Delta\sigma^* = \sqrt{\frac{1}{(n-1)} \frac{\sum \omega_i (\sigma_i - \bar{\sigma})^2}{\sum \omega_i}}$,

$\omega_i = 1/(\Delta\sigma_i)^2$ - is the weight of the experimental value.

3. The Berdge criterion was calculated:

$$K = \frac{/(\Delta\sigma)^2 - (\Delta\sigma^*)^2/ (n-1)}{(\Delta\sigma)^2 \sqrt{2}} .$$

If $k < 2$ then as the estimated value is taken $\bar{\sigma}$ with an error equal to the larger of $\Delta\sigma$ and $\Delta\sigma^*$ values. If $K > 2$ and there are no justified reasons for its reducing then as the esti-

mated value is taken the arithmetic average one from the set of experimental data (n) with an error:

$$\Delta\sigma = \tau_p(n) \cdot \sqrt{\frac{1}{n(n-1)} \sum_i (\sigma_i - \bar{\sigma})^2},$$

where $\tau_p(n)$ is the student's coefficient for (n-1) degrees of freedom and probability of finding the true value beyond the error range P. P was normally taken as 0.3.

On the basis of the analysis of the whole set of experimental data the estimated values of cross sections were obtained in the region of α - particle energies from the reaction threshold to 10 MeV and their uncertainties for Li - 5%, ^{9}Be - 5%, ^{13}C - - 7%, ^{19}F - 10%, ^{17}O and ^{18}O - 10%.

The neutron yield was calculated using the common formula:

$$Y(E_\alpha) = C \int_{E_\alpha}^{0} \sigma(E) / (dE/dx)\, dE,$$

where C is the number of isotope nuclei in one gram of the target material on which the (α, n) reaction proceeds; σ(E) is the estimated value of the reaction cross section at the α - particle energy E; (dE/dx) is the stopping-power of the target material. The stopping-power values for the compound targets were calculated in accordance with the Bragg rule:

$$(dE/dx) = \frac{\sum_j a_j A_j (dE/dx)_j}{\sum_j a_j A_j},$$

where A_j is the isotope mass number, a_j is the number of this isotope nuclei in the substance molecule.

In the algorithm of the yield calculation $(dE/dx)_j$ are represented as:

$$\ln (dE/dx)_j = \sum_{i=0}^{4} C_i (\ln(E))^i,$$

C_i - coefficients are tabulated in Ref. /11/.

In the calculations for the actinides heavier than uranium the stopping-power were taken the same as for uranium.

The yield calculation data are presented in Fig.1 in comparison with the recommended values /14/. A significant discrepancy is observed between them, particularly, in the reactions with carbon and oxygen. This discrepancy is mainly due to use of the recent results /8-10/ in our estimate. Table I shows an example of calculation of neutron yield from the beryllium target.

Table 2 lists the calculated neutron yields for some compounds being used in nuclear technology. Also in this table are presented the published measured yield values. A reasonable agreement between the experiment and calculation is observed practically for all materials. Exceptions for this are ^{241}Am-F and ^{238}Pu-^{13}C compounds. Such a large discrepancy between the experiment and calculation data for these compounds cannot be explained by inaccurately known (α, n) reaction cross sections or stopping-power. The difference seems to be connected with the circumstance that the homogeneous targets used in the experiment /3/ differ from the chemical compounds AmF and PuC and, as shown by the calculation, are closer to the compounds AmF_3 and PuC_3 in their composition.

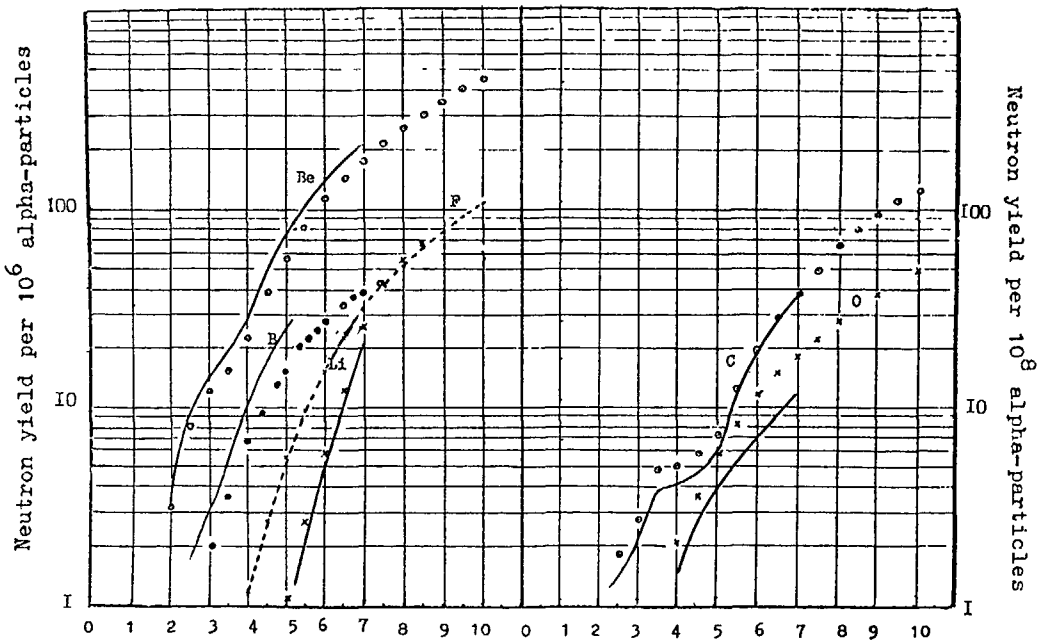

Fig.1. Neutron yields on the thick targets:lithium -x,beryllium -0,boron -●,fluorine - ----,carbon -O,oxygen -x; solid lines indicate the data /14/.

TABLE 1. EVALUATED (α,n) CROSS-SECTIONS AND NEUTRON YIELD FOR Be-9 TARGET

NEUTRONS FROM (ALPHA,N) REACTION

E MEV	SIG MB	DSIG MB	STOP EV/F+15AT/CM**2	E MeV	Y N/A
1.550	+0.969E+01	+0.499E+00	+0.2112E+02	1.500	+0.5799E-08
1.650	+0.200E+02	+0.100E+01	+0.2058E+02	1.600	+0.5231E-07
1.750	+0.920E+02	+0.500E+01	+0.2006E+02	1.700	+0.1507E-06
1.850	+0.260E+03	+0.130E+02	+0.1956E+02	1.800	+0.6150E-06
1.950	+0.243E+03	+0.120E+02	+0.1909E+02	1.900	+0.1959E-05
2.050	+0.186E+03	+0.900E+01	+0.1864E+02	2.000	+0.3247E-05
2.150	+0.172E+03	+0.900E+01	+0.1821E+02	2.100	+0.4206E-05
2.250	+0.162E+03	+0.800E+01	+0.1779E+02	2.200	+0.5201E-05
2.350	+0.148E+03	+0.700E+01	+0.1740E+02	2.300	+0.6122E-05
2.450	+0.140E+03	+0.700E+01	+0.1702E+02	2.400	+0.6982E-05
2.550	+0.148E+03	+0.700E+01	+0.1666E+02	2.500	+0.7836E-05
2.650	+0.132E+03	+0.700E+01	+0.1631E+02	2.600	+0.8734E-05
2.750	+0.112E+03	+0.600E+01	+0.1598E+02	2.700	+0.9551E-05
2.850	+0.960E+02	+0.500E+01	+0.1566E+02	2.800	+0.1025E-04
2.950	+0.900E+02	+0.500E+01	+0.1536E+02	2.900	+0.1087E-04
3.050	+0.900E+02	+0.500E+01	+0.1506E+02	3.000	+0.1146E-04
3.150	+0.940E+02	+0.500E+01	+0.1478E+02	3.100	+0.1207E-04
3.250	+0.100E+03	+0.500E+01	+0.1451E+02	3.200	+0.1271E-04
3.350	+0.104E+03	+0.500E+01	+0.1425E+02	3.300	+0.1340E-04
3.450	+0.114E+03	+0.600E+01	+0.1400E+02	3.400	+0.1414E-04
3.550	+0.128E+03	+0.600E+01	+0.1376E+02	3.500	+0.1496E-04
3.650	+0.146E+03	+0.700E+01	+0.1353E+02	3.600	+0.1590E-04
3.750	+0.168E+03	+0.800E+01	+0.1330E+02	3.700	+0.1699E-04
3.850	+0.200E+03	+0.100E+02	+0.1309E+02	3.800	+0.1826E-04
3.950	+0.316E+03	+0.160E+02	+0.1287E+02	3.900	+0.1980E-04
4.050	+0.344E+03	+0.170E+02	+0.1267E+02	4.000	+0.2227E-04
4.150	+0.330E+03	+0.160E+02	+0.1248E+02	4.100	+0.2501E-04
4.250	+0.352E+03	+0.180E+02	+0.1229E+02	4.200	+0.2767E-04
4.350	+0.376E+03	+0.190E+02	+0.1210E+02	4.300	+0.3056E-04
4.450	+0.392E+03	+0.200E+02	+0.1193E+02	4.400	+0.3369E-04
4.550	+0.390E+03	+0.200E+02	+0.1175E+02	4.500	+0.3699E-04
4.650	+0.386E+03	+0.190E+02	+0.1159E+02	4.600	+0.4033E-04
4.750	+0.401E+03	+0.200E+02	+0.1143E+02	4.700	+0.4369E-04
4.850	+0.433E+03	+0.220E+02	+0.1127E+02	4.800	+0.4722E-04
4.950	+0.468E+03	+0.230E+02	+0.1112E+02	4.900	+0.5109E-04
5.050	+0.488E+03	+0.240E+02	+0.1097E+02	5.000	+0.5532E-04
5.150	+0.494E+03	+0.250E+02	+0.1083E+02	5.100	+0.5980E-04
5.250	+0.521E+03	+0.260E+02	+0.1069E+02	5.200	+0.6439E-04
5.350	+0.552E+03	+0.280E+02	+0.1055E+02	5.300	+0.6929E-04
5.450	+0.573E+03	+0.290E+02	+0.1042E+02	5.400	+0.7456E-04
5.550	+0.584E+03	+0.290E+02	+0.1029E+02	5.500	+0.8009E-04
5.650	+0.610E+03	+0.300E+02	+0.1016E+02	5.600	+0.8579E-04
5.750	+0.618E+03	+0.310E+02	+0.1004E+02	5.700	+0.9183E-04
5.850	+0.596E+03	+0.300E+02	+0.9928E+01	5.800	+0.9802E-04
5.950	+0.576E+03	+0.290E+02	+0.9813E+01	5.900	+0.1040E-03
6.250	+0.560E+03	+0.280E+02	+0.9700E+01	6.000	+0.1099E-03
6.750	+0.574E+03	+0.290E+02	+0.9175E+01	6.500	+0.1396E-03
7.250	+0.576E+03	+0.290E+02	+0.8708E+01	7.000	+0.1717E-03
7.750	+0.649E+03	+0.320E+02	+0.8291E+01	7.500	+0.2056E-03
8.250	+0.653E+03	+0.330E+02	+0.7914E+01	8.000	+0.2456E-03
8.750	+0.716E+03	+0.360E+02	+0.7573E+01	8.500	+0.2827E-03
9.250	+0.747E+03	+0.370E+02	+0.7263E+01	9.000	+0.3360E-03
9.750	+0.708E+03	+0.350E+02	+0.6979E+01	9.500	+0.3885E-03

TABLE 2. THE NEUTRON YIELD IN SEC PER GRAM ALPHA-EMITTER OF VARIOUS COMPOUNDS

Compound	Intensity of α - particles	Average energy (MeV)	Calculated yield $Y_{calc.}$	Experimental yield Y_{exp}	References	$(1-\frac{Y_{exp}}{Y_{calc}})*100$
1	2	3	4	5	6	7
$^{234}UF_6$	2.299×10^{8}	4.761	508 ± 51	576 ± 20	17	-12
$^{235}UF_6$	7.98×10^{4}	4.393	$(9.0\pm0.9)\times10^{-2}$	$(12.2\pm0.9)\times10^{-2}$*	17	-25
$^{236}UF_6$	2.388×10^{6}	4.484	3.2 ± 0.3	(3.95 ± 0.29)*	17	-19
$^{238}UF_6$	1.241×10^{4}	4.185	$(10\pm1)\times10^{-3}$	$(12.9\pm0.9)\times10^{-3}$	17	-22
$^{238}PuO_2$	6.321×10^{11}	5.487	$(1.52\pm0.15)\times10^{4}$	$(1.435\pm0.21)\times10^{4}$	19	+6
$^{238}Pu^{13}C$	6.321×10^{11}	5.487	$(9.61\pm0.67)\times10^{5}$	$(4.61\pm0.19)\times10^{6}$	3	-379
$^{239}PuBe_{13}$	2.291×10^{9}	5.148	$(9.33\pm0.46)\times10^{4}$	$(8.43\pm0.44)\times10^{4}$	15	+11
$^{239}PuF_3$	2.291×10^{9}	5.148	$(6.1\pm0.6)\times10^{3}$	$(5.3\pm0.4)\times10^{3}$	16	+15
$^{239}PuF_4$	2.291×10^{9}	5.148	$(7.2\pm0.7)\times10^{3}$	$(6.1\pm0.5)\times10^{3}$	16	+18
				$(7.1\pm0.7)\times10^{3}$	20	+2
$^{241}AmBe_{13}$	1.267×10^{11}	5.479	$(65.2\pm3.2)\times10^{5}$	$(70.1\pm1.9)\times10^{5}$	3	-7
$^{241}AmO_2$	1.267×10^{11}	5.479	$(3.0\pm0.3)\times10^{3}$	$(2.78\pm0.41)\times10^{3}$	18	+8
				$(3.17\pm0.18)\times10^{3}$	3	-5
$^{241}Am-F$	1.267×10^{11}	5.479	$(2.2\pm0.2)\times10^{5}$	$(4.36\pm0.16)\times10^{5}$	3	-50
$^{242}CmO_2$	1.222×10^{14}	6.102	$(4.2\pm0.4)\times10^{6}$	-		
$^{244}CmO_2$	2.987×10^{12}	5.795	$(8.7\pm0.9)\times10^{4}$	-		

* - recommended values from work /17/.

REFERENCES

1. Boneh Y., Goshen S., Karpas Z., Shahal O., Wolf A., - NSE 86, 106, 1984.
2. Walton R.B., Reilly T.D., Parker J.L., Menzel J.H., Marshal E.D., Fields L.W., - Nucl.Techn., v.21, p. 133, 1974.
3. Capgras A., "Examples of Theoretical and Experimental determination of neutron yield from (a,n) reactions in the light elements", Paper to Meeting on "Neutron Sources Properties", Debrecen, Hungary, p. 310, 1980.
4. Kumar A., Nagarajon P.S. - Atomkernenergie, v.37, p. 219, 1981.
5. Bulanenko N.I., Frolov V.V., Tsenter E.M. - Atomnaya energiya, t. 53, N 3, s. 160, 1982.
6. Vukolov V.A., Chukreev F.E., Materials of conf. on nuclear and physical investigations, Khar'kov, 4-6 Oct., 1982 "Physics of atomic nucleus and elementary particles", part 2, p. 218, Moscow, 1983.
7. Vukolov V.A., Chukreev F.E., Atomnaya energiya, t. 62, 1987.
8. West D., Sherwood A.C., - Ann.Nucl.Energy, v.9, p. 551, 1982.
9. Jacobs G., Liskien H., - Ann.nucl.Energy, v.10, p. 541, 1983.
10. Bair J.K., Gomes del Campo J., - NSE, 71, 18, 1979.
11. Anderson H.H., Siegler J.F., - Stopping and ranges of ions in matter, v.4, Pergamon Press, 1977.
12. Gibbons J.H., Maclin R.L., - Phys.Rev., 114, 571, 1959.
13. Sekharan K.K., Divatia A.S., Menta M.K., Kerekatte S.S., Nambiar K.B., - Phys.Rev., 156, 1187, 1967.
14. Liskien H., Paulsen A., - Neutron yields of light elements under alpha-bombardment, - Atomkernenergie, v.30, p.59, 1977.
15. Michaud G., Boucher R., - Can. J. Phys., v. 38, p. 555, 1960.
16. Ovechkin V.V., Atomnaya energiya, t. 48, N 1, s. 48, 1980.
17. Sampson T.E. - Nucl.Sci.Eng., v.54, p. 470, 1974.
18. Lees E.W., Lindley D., - Ann.nucl.energy, v.5, p. 133, 1978.
19. Bair J.K., Butler H.M., - Nucl.Techn., 19, 202, 1973.
20. Tsenter E.M. e.a. , In "Proceedings of III-rd CMEA Symp. "Investigations on reprocessing of irradiated fuel", t. 3, Prague, CsSSR, p. 202, 1974.

MEASUREMENT OF ACTIVATION INTEGRALS IN NEUTRON FIELDS

V.S. TROSHIN
Institute of Physics and Engineering,
Moscow, Union of Soviet Socialist Republics

Abstract

The most widespread methods of activation integral measurements by β and γ counting conversion electron detection, $\beta-\gamma$ coincidences are discussed in detail. Possible sources of errors are underlined and the necessary correction factors are calculated.

In experiments in neutron fields with high flux density the most suitable and often the single method of field characteristic definition is the method of activated detectors, based on radioactive measurement which appeared as a result of neutron and neutron sensitive nuclide interaction.

Radioactivity (or activity) of activated detectors depends on neutron spectrum and reaction cross sections. The rate of radioactive nuclei formation of i-type is defined as the following ratio:

$$q_i^* = n_0 G \int_0^{\infty} T_F(E)\,\sigma_i(E)\,\varphi(E)\,dE \qquad (1)$$

where $\varphi(E)$ is differential energy density of neutron flux (neutron spectrum), $\sigma_i(E)$ - is reaction cross section, n_0 - the number of nuclei of neutron sensitive nuclide, $T_F(E)$ is the function of neutron pass by filter, which is used in detector irradiation, G - is coefficient taking account of neutron spectra distortion inside and outside of a sample because of interaction with detector material. The quantity $q_i = \int_0^{\infty} T_F(E)\ \sigma_i(E)\ \varphi(E)\,dE$ is called activated integral.

The purpose of activated measurements is getting q_i by experimental way and the following information obtaining about neutron spectrum in known reaction cross section (or vice versa).

Consider the process of detector activation. In common case the active nuclei can be formed by both direct activation and through the intermediate neuclei state. The most widespread case of intermediate state is the formation of isomers. Neutrons interact with the nuclei formed and this reduces the directed activity. Taking into account the decay the formed activity A is connected with neutron spectrum by the following equations:

$$\frac{dA_g}{dt} = -\lambda_g A_g + n_0 G \lambda_g \int_0^{\infty} T_F(E)\,\sigma_g(E)\,\varphi(E)\,dE - A_g \int_0^{\infty} T_F(E)\,\sigma_g^*(E)\,\varphi(E)\,dE + \lambda_g p_m A_m$$

$$\frac{dA_m}{dt} = -\lambda_m A_m + n_0 G \lambda_m \int_0^{\infty} T_F(E)\,\sigma_m(E)\,\varphi(E)\,dE - A_m \int_0^{\infty} T_F(E)\,\sigma_m^*(E)\,\varphi(E)\,dE \qquad (2)$$

where Ag and Am are activities of the basic and intermediate states, $\sigma_g(E)$, $\sigma_m(E)$ are reaction cross-sections of corresponding processes of activation, λ_g, λ_m are decay constants, $\sigma_g^*(E)$, $\sigma_m^*(E)$ are reaction cross-sections bringing to "burning down" of nuclei being formed, p_m is a part of conversion of intermidiate state into basic one.

After stopping the irradiation by neutrons:

$$\frac{dA_g}{dt} = -\lambda_g A_g + \lambda_g p_m A_m \qquad \frac{dA_m}{dt} = -\lambda_m A_m \qquad (3)$$

For time independent neutrons fields at the exposition τ and at time t after irradiation, the activities are equal to:

$$A_g(\tau,t) = n_0 G \frac{\lambda_g}{\Lambda_g}\left(1-e^{-\Lambda_g\tau}\right)e^{-\lambda_g t}\cdot\left[q_g + \frac{\lambda_m}{\Lambda_m}\frac{\Lambda_m}{\Lambda_m-\Lambda_g}p_m q_m\right] +$$
$$+ n_0 G \frac{\lambda_m}{\Lambda_m}\left(1-e^{-\Lambda_m\tau}\right)e^{-\lambda_g t} p_m q_m \left[\frac{\lambda_g}{\Lambda_g-\Lambda_m} - \frac{\lambda_g}{\lambda_g-\lambda_m}\right] -$$
$$- n_0 G \frac{\lambda_g}{\lambda_m-\lambda_g}\left(1-e^{-\Lambda_m\tau}\right)e^{-\lambda_m t} p_m q_m \qquad (4)$$

$$A_m(\tau,t) = n_0 G \frac{\lambda_m}{\Lambda_m}\left(1-e^{-\Lambda_m\tau}\right)e^{-\lambda_m t}\cdot q_m$$

$$q_g = \int_0^\infty \tilde{T}_F(E)\sigma_g(E)\varphi(E)dE \qquad q_m = \int_0^\infty \tilde{T}_F(E)\sigma_m(E)\varphi(E)dE$$

$$\Lambda_g = \lambda_g + \int_0^\infty \tilde{T}_F(E)\sigma_g^*(E)\varphi(E)dE \qquad \Lambda_m = \lambda_m + \int_0^\infty \tilde{T}_F(E)\sigma_m^*(E)\varphi(E)dE$$

In a case of absence of essential neutrons interactions with the nuclei formed and intermediate states the formula (4) is considerably simplified

$$A_g(\tau,t) = n_0 G\left(1-e^{-\lambda_g\tau}\right)e^{-\lambda_g t}\cdot q_g \qquad (5)$$

The radioactive nuclides formed as a result of activation, including the isomers, can emit γ-photons, X-rays, β-particles, positrons and conversion electrons. Activity is defined by photon registration or by charged particles registration. Various methods of tool activity definition, lots of which are of high accuracy, have been developed. However, not all of them can be applied in neutron activated measurements because of specific pecularities of activated method:

- presence of "background" reactions;
- time-limit of activity measurements in a reaction for products with relatively small period of life-time;
- considerable number of reactions being used;
- insufficient activity for applying destriction detectors methods and so on.

In view of it the most widespread methods of activity definition are methods β-particles count and conversion electrons, γ-spectrometry and β-γ-coincidences.

The simpliest settings for measuring the activity are β-counters. In applying 4π-counters the least error is acheived. In defining the activity by β-particles count it is necessary to measure the count rate/exposure time dependence. The analysis of this dependence allows to take into account the influence of "Background" reactions or reveal possible pollution of detector.

The quantity of counter rate is defined at the moment of irradiation stop for the reaction being considered

$$n_\beta(t)\cdot\left[1-\tau_M n_\beta(t)\right]^{-1} = \sum_{K=1}^{m} n_{\beta,K}(t=0)\exp\left(-\lambda_K t\right) \qquad (6)$$

where n_β -is the count rate of β-counter, τ_M is "dead" time of setting.

If the nuclide being of interest has decay time much more than other nuclides, the dependence of count rate is measured for times of after irradiation at which the influence of other nuclides is unessential. In any case the method of the least squares can be applied for analysing this dependence. To achieve high accuracy in this case it's necessary to have dependence plot where the contribution of reaction being considered is significant.

The activity is connected with count rate of 4π-counter by following equation:

$$A_K(\tau, t=0) = k_{cn}\cdot k\cdot k_\varepsilon\cdot n_{\beta,K}(t=0) \qquad (7)$$

where k_{cn}, k and k_ε - are corrections to selfabsorption, absorption in a film, holder of a detector, and the effectiveness of registration of β-particles correspondingly.

The absorption of β-particles can be described approximately by exponential law. This law is for nuclides, having simple decay scheme (one β-junction) and thin absorbers. For nuclides, having compound decay scheme, it is necessary to take into account the relaxation for each β-junction.

The quantities of mass absorption coefficient of β-particles can be defined out of empiric expressions, obtained in analysing absorption and selfabsorption. A number of such dependences which often differ are given in literature

$$\bar{\mu} \approx 15.5E_{\beta}^{-1.41} \approx 17E_{\beta}^{-1.43} \approx 15.2E_{\beta}^{-1.51} \qquad (8)$$

where $\bar{\mu}$ is average mass absorption coefficient in cm^2/g
E_β is max energy of spectrum in MeV.

Author suggests the dependence of absorption coefficient on mean energy of β-junction $(\bar{E}_i)$

$$\bar{\mu}_i \simeq (8.6 \pm 0.6)\ \frac{Z}{A} \cdot \bar{E}_i^{-1.25} \qquad (8a)$$

where $\frac{Z}{A}$ is effective ratio charge to atomic mass.

In such approximations the corresponding corrections can be defined as

$$k = 2 \cdot \left[1 + \frac{\sum_{i=1}^{n} p_{\beta i} \exp\left[-\bar{\mu}_i(\bar{E}_i) d_n\right]}{\sum_{i=1}^{n} p_{\beta i}}\right]^{-1}$$

$$k_{cn} = \left[\sum_{i=1}^{n} p_{\beta i} \left(1 - \exp\left[-\bar{\mu}_i(\bar{E}_i) d\right] / \bar{\mu}_i(\bar{E}_i) d\right]^{-1} \qquad (9)$$

where $\bar{\mu}_i(\bar{E}_i)$ is absorption coefficient of β-radiation for i-junction, $p_{\beta i}$ is a part of decay realizing i-junction, d_n, d are film thickness of holder and detector.

The absorption of β-particles in a film holder doesn't exceed 3% for spectra with the highest energy $0,4 \div 0,7$ MeV and 1% at $E_\beta \geq 0,8$ MeV for metallized organic films with thickness $0,5 \div 1$ mg/cm^2. If necessary the correction can be defined experimentally out of count rates of β-particles of nuclide being measured for a single (N_1) and double film of holder (N_2) ratio.

$$k = 2 - \frac{N_2}{N_1}$$

The correction to selfabsorption can be defined out of analysis of count rate and detector thickness dependence at constant specific activity.

The correction to effectiveness of registration takes into account the difference of counter effectiveness from factor of one and registration -photons nuclide (in most cases with the error of 1% it can be adopted as factor of one).
In using the experimental corrections to selfabsorption the error of activity definition by 4π -count method is $2 \div 7\%$.

In defining activity according to photon radiation a single-crystal scintillation or semiconducting spectrometer is often used. For increasing the electorality the peak of complete absorption (photopeak) is usually regiatrated. The detector activity is defined by the number of pulses, registered in photopeak.

Two methods of activity defining can be used - relative (substitution method) and absolute.

The substitution method is based on comparison the count rates from a detector being measured and reference photon source which is closed by form to a detector and has the same photon energy. In applying it, one can use both multychannal and monochannal amplitude analyser. The advantage of substitution method is the absence of necessity to define the effectiveness of photon registration. The method is applied in measurements with detectors of the same type, one of which is measured by absolute method.
The possibility of using the method in other cases is limited by presence of continuous distribution in apparatus spectra and choice of suitable reference photon source.

In view of it the absolute method of activity definition with the use of multichannel analyser is more universal. In order to define the number of pulses in photopeak a part of

apparatus spectrum, containing the photopeak being considered, is presented as a sum of continuous distribution, being made by compton interaction and background and by full absorption peak. A computer is usually used for processing apparatus spectra.

The continuous part of apparatus spectra is presented by following descriptions: linear, parabolic, cubic, spline or polynomial of higher-degree. Photopeak is presented by either gauss distribution (scintillation spectrometer), or gauss distribution with addition of photopeaks being considered the asymmetry (semiconducting spectrometers).

For example, in program AUTOS, the chosen part of apparatus spectrum, containing photopeaks is described as follows

$$N(x) = \sum_{m=1}^{m_0} \frac{S_m \exp\left[-(c_m - x)^2 / 2 \cdot (\sigma_m + K_m (c_m - x))^2\right]}{\sqrt{2\pi}\,(\sigma_m + K_m (c_m - x))} + ax^3 + bx^2 + cx + d$$

where $S_m, C_m, \sigma_m, K_m, a, b, c, d$ are parameters being defined.

The activity of detector is connected with the number of pulses in photopeaks from -photons with energy E by the following ratio:

$$A(\tau, t) = \frac{k_{cn}\, k_{\Delta t}\, k_c\, k_d\, S_\gamma(t)}{(\Delta t - t_\mu)\, p_\gamma(E)\, \varepsilon(E)} \qquad (10)$$

where k_{cn}, $k_{\Delta t}$, k_c, are the corrections to selfabsorption -photons, the decay in time of measurement and summing up -photons cascades; k_d is the correction, taking into account the difference of detectors dimensions from reference sources dimensions; Δt, t_μ are time of measurement and dead-time of analyser; $p_\gamma(E)$ is the output of -photons with energy E to a decay; $\varepsilon(E)$ is the effectiveness of -photons registration with energy E.

The effectiveness of registration

The effectiveness of registration is the ratio of the number of pulses registered in photopeaks to the number of -photons emitted by a source (detector). As the experiments and calculations show, in energy range 0,3-3,0 MeV the effectiveness is well described by a following energy function of incident quanta

$$\varepsilon(E) = a E^{-b} = \varepsilon_\phi(E)\,\Omega$$

where a and b are coefficients, depending on material and sizes of spectrometer crystal and mutual disposition source-crystal, $\varepsilon_\phi(E)$ is photoeffectiveness, Ω is relative solid angle. The dependence of effectiveness on energy is defined experimentally with the help of reference isotropic sources. In the USSR a set of sources of ОСГИ being registered according to activity and output of γ-radiation with error of 2,5% in being produced. The set involves the sources with radionuclides ^{241}Am, ^{57}Co, ^{139}Ce, ^{203}Hg, ^{113}Sn, ^{22}Na, ^{137}Cs, ^{54}Mn, ^{65}Zn, ^{88}Y, ^{60}Co. It is useful to add isotopes ^{198}Au, ^{95}Nb, ^{24}Na, the activity of which can be defined with high accuracy on installation $\beta-\gamma$ - coincidences and ^{51}Cr to the set . In applying the sources (detectors), the diameter of which is much less than the diameter (D) of a crystal, coefficient b doesn't depend on the distance crystal source-surface of spectrometer (h). The dependence of coefficient a on this distance is usually as follows

$$a(h) = a_0 / H_{эф}^2 \qquad H_{эф} = h_0 + h \qquad (11)$$

where h_0 -is the distance from spectrometer surface to effective centre of registration.

The position of effective registration centre is defined by measurement of count rate in photopeak from reference sources at different distances and plotting the dependence

$$Y(h) = \left[\frac{S_\gamma(h)}{\Delta t - t_M} \right]^{-1/2} \qquad (12)$$

The dependence (12) is linearized according to h under the condition (11). The cross point of straight line with absciss axis defines quantity h_0. If the dependences made for sources the -photons energies of which include the whole range, cross in the same point it confirms the independence of coefficient b on - photon energy and the possibility of definition a for distances analyzed by formula (11).

Correction to selfabsorption

The strict registration of γ-rays seifabsorption on a source by calculation is rather difficult. However, when the selfabsorption quantities are not large (20-25%) one can use the method described below, which gives a small error in defining a part of absorbed quanta ($k_{cn} - 1$) approximately 5-10%. The approximation is based on a suggestion that the radiation of each elementary layer of detector material can attenuate as point source radiation, having the same activity and being on an axis of crystal. The integration over detector thickness gives the expression

$$k_{cn} = \frac{\mu_m d (1 - \cos\alpha_0)}{0.5 \cdot (1 - \cos^2\alpha_0) - E_3(\mu_m d) + \cos^2\alpha_0 \, E_3(\mu_m d / \cos\alpha_0)} \qquad (13)$$

where μ_m is mass attenuation coefficient of γ-radiation (all types of interactions are taken into account except coherent scattering). When quantity $\mu_m d$ is small (less 0,1) the suitable approximation for (13) is expression

$$k_{cn} = \frac{\mu^*_m d}{1 - \exp(-\mu^*_m d)} \qquad (14)$$

$$\mu^*_m = \mu_m \frac{\ln\cos\alpha_0}{\cos\alpha_0 - 1} \quad ; \quad \cos\alpha_0 = \left(\sqrt{1 + \left(\frac{D}{2H_{sp}} \right)^2} \right)^{-1}$$

where D is crystal diameter.

Correction to summing up. If γ-quanta are emitted in cascades, there is a possibility to registrate them as sums of amplitudes being created by each quantum. It results in loss of pulses out of photopeaks.

In registrating -photon with energy E_I, being emitted in cascad with -photon energy E_2, the correction to summing up is

$$k_c = \left[1 - p_\gamma(E_2) \bar{W} \varepsilon(E_2) / \mathcal{P}(E_2) \right]^{-1} \qquad (15)$$

where $p_\gamma(E_2)$ is a part of -photon with energy E_2 for a decay; $\mathcal{P}(E_2)$ is the ratio of the number of pulses in full absorption peak to all registered pulses of a spectra; $\bar{W}$ is a factor taking into account angle correlation of -photons as the effectiveness reduces with the distance it is necessary to increase the source-crystal distance of spectrometer ($W/\mathcal{P}(E_2)$ depends slightly on this distance) for reducing of corrections to summing up effect. Experimentally the correction to summing up effect can be defined by comparison the registered count rate with count rate of the same source at such distances when correction to summing up is practically equal to factor of one or by the number of pulses in the peak of sum.

$$k_c = 1 + S_\Sigma / S_\gamma \cdot \mathcal{P}(E_2) \qquad (16)$$

where S_Σ is the number of pulses is the peak of sum.

Corrections $k_{\Delta t}$ and k_d. In case of absence of "background" reactions corrections to isotop decay during measuremen and dead time are introduced simultaneously:

$$k_{\Delta t} = \frac{\lambda (\Delta t - t_M)}{1 - \exp[-\lambda (\Delta t - t_M)]} \cdot \frac{\exp(\lambda t_M) - 1}{\lambda t_M} \qquad (17)$$

Generally the second comultiplier of formula (17) differs from unit for isotopes with time-decay 2-5 min and having great activity. Correction to decay is defined by "living" time. Modern analyser are equipped with "living" time counters. Correction k_d takes into account the changes of registration effectiveness for final thickness detectors as the effectiveness is defined by thin sources. It is sufficient at great gradients of effectiveness:

$$k_d = 1 + \frac{d}{\mathcal{H}_{эф}} \qquad (18)$$

In registrating annihilation radiation with high energy of positrons correction is introduced even for such then detectors as a part of positrons annihilates far from spectrometer crystal. Taking into account the systematical error of correction introduced for majority of detectors the error of activity definition is not more than 5%.

Coincidence method is applied for measuring the isotops activity, γ-radiation of which is accompanied by irradiation of one or some quanta (β-γ-coincidence method). Coincidence methods do not demand the effectiveness definition and corrections to selfabsorption in a source thanks to which high accuracy of measurement can be achieved.

The principle of β-γ - coincidence method consists in measurement of output β and γ-radiations of counters, sensible to β and γ- radiations correspondingly and in measurement of the number of coincidences of registration acts. The rate of γ-counter pulses registration (n_γ), β-counter (n_β) and the rate of coincidences registration ($n_{\beta\gamma}$) are connected with ratio activity

$$A(T,t) = \frac{(n_\gamma - n_\gamma^\phi)(n_\beta - n_\beta^\phi)}{n_{\beta\gamma}} k_e\, k_{c1}\, k_\beta\, k_{\Delta t} \qquad (19)$$

where n_γ^ϕ, n_β^ϕ are count rate of and -counters background correspondingly; k_e, k_{c1}, k_β, and $k_{\Delta t}$ are corrections to conversion electrons registration, accidental coincidences, -photons β-counter$ and decay in time of measurements. The corrections introduced here are basic. Lots of corrections depend on a scheme of installation being applied.

In applying detectors by absorbing the neutrons which can not be ignored their activity will be less than with "ideal" thin detector. It is taken into account by correction coefficients the basic of which are corrections to selfscreening and neutron field depression. Correstion to depression is introduced by neutron field measurements in a medium; it is not sufficient in air space of enough dimension. Let's consider corrections to shielding.

For monoenergetic neutrons the ratio of rates activation $\frac{q}{q_0}$ -detectors with d thickness and ideal detector is equal to

$$\frac{q}{q_0} = \frac{1 - \exp(-\tau)}{\tau} \qquad \tau = \Sigma_a d \qquad \text{(for a beam)} \quad (20)$$

$$\frac{q}{q_0} = \frac{1 - 2E_3(\tau)}{2\tau}\left[1 + \mathcal{E}(\tau)\right] \qquad \text{(for isotopic field of neutron)}$$

where Σ_a is macroabsorption cross-section of neutrons in a detector; $E_3(\tau)$ is exponential integral of third order; $\mathcal{E}$ is correction to edge effect in applying final dimension detectors.

With sufficient accuracy for disk detector with diameter D one can use the following ratio:

$$\mathcal{E}(\tau) = \frac{2\tau}{1 - 2E_3(\tau)} \frac{d}{\pi D}\left[1 - \frac{\pi}{6}\tau\right] \qquad (21)$$

Corrections to neutrons selfshielding in spectrum $\varphi(E)$:

$$G = \frac{q}{q_0} = \int_0^\infty \frac{1-\exp[-\tau(E)]}{\tau(E)} \sigma(E)\varphi(E)dE \Big/ \int_0^\infty \sigma(E)\varphi(E)dE \quad \text{(for a beam)} \quad (22)$$

$$G = \frac{q}{q_0} = \int_0^\infty \frac{1-2E_3[\tau(E)]}{2\tau(E)} [1+\varepsilon[\tau(E)]]\sigma(E)\varphi(E) \Big/ \int_0^\infty \sigma(E)\varphi(E)dE$$

(for isotopic field of neutrons).
This point is given in detail in the book by K.H.Beckurts, R.Wirtz "Neutron Physics" /I/.

For increasing of deposit in neutrons activation of different energy groups to be increased strong absorbing filters are used.
The filters from cadmium and ^{10}B are more frequently used. Cadmium, having main resonance at 0,178± 0,002 eV energy, absorbs thermal and slow neutrons. The function of cadmium filter penetration can be presented by the following stepped function

$$T_{cd}(E) = \begin{cases} 0 & E < E_{cd} \\ 1 & E \geq E_{cd} \end{cases} \quad (23)$$

The value of cut off energy absorption by cadmium filter E_{cd} is defined by ratio:

$$q_{cd} = \int_0^\infty T_{cd}(E, d_{cd})\sigma(E)\varphi(E)dE = \int_{E_{cd}}^\infty \sigma(E)\varphi(E)dE \quad (24)$$

where d_{cd} is cadmium filter thikness. The cut off energy absorption is determined for reaction cross-section of $1/\sqrt{E}$ type. In common case E_{cd} depends not only on thickness and form of a filter being applied, but on neutrons spectrum and their angle distribution.

The value of flat filter E_{cd} for isotropic distribution and monodirected neutrons beam with I/E spectrum is given in table I. V.P.Yarjina suggested the analytic approximation of cut off energy as a function of cadmium thickness for cylindrical screens at isotropic radiation /2/:

$$E_{cd}\,[eV] = 0.520 + 0.162 \ln \delta \quad (25)$$

$$\delta = \xi_{cd} d_{cd} \qquad d_{cd} = 0.5 \div 1.5\,mm$$

Table I. Cut off energy absorption for flat cadmium filter E_{cd}, eV.

d_{cd}, mm	isotropic field	beam	d_{cd}, mm	isotropic field	beam
0,508	0,553	0,425	1,524	0,768	0,576
0,635	0,590	0,451	1,905	0,822	0,614
0,762	0,622	0,473	2,032	0,839	0,627
1,016	0,678	0,512			

For cylindrical screen with hight to diameter ratio χ

$$\xi_{cd} = \begin{cases} 1 + 1{,}5 \exp(-3{,}5\chi) & \chi = 0 + 0{,}5 \\ 1{,}58 - 0{,}82\chi + 0{,}38\chi^2 & \chi = 0{,}5 + 1{,}3 \\ 1{,}035 + 0{,}11\chi - 0{,}011\chi^2 & \chi = 1{,}3 + 5{,}0 \end{cases}$$

It is recommended to use cadmium filters with thickness not less than 1 mm as otherwise the neutrons spectrum influence on quantity E_{cd} is appreciable.

Filters with boron are used for deposit increasing to fast neutrons activation. The thickness of filter equals 0,5 - 2 g/sm^2 to ^{10}B . The function of passing is usually calculated by

Monte-Carlo method as it is necessary to take into account not only absorption but material and binding substance.So it is necessary to make calculations for filter being applied.

Summarizing it can be said that taking into account the basic corrections activated integrals can be measured with error 2÷10% .

REFERENCES

1.K.H.Beckurts, K.Wirtz. Neutron Physics,Berlin,1964

2.Б.А.Брикcман, В.В.Генералова, Е.А.Крамер-Агеев, В.С.Трошин. Внутриреакторная дозиметрия М.,Энергоатомиздат,1985.

DEFINITION OF THE PROBLEM OF NEUTRON SPECTRA UNFOLDING BY MEASURED REACTION RATES

H.Ya. BONDARS
Latvian State University,
Riga, Union of Soviet Socialist Republics

Abstract

The paper describes the main mathematical and physical features of the problem, determines the role of the initial approximations, classifies the methods of unfolding and errors and lastly defines the task of neutron spectra unfolding by measured reaction rates.

(A31.00; E41.20) INIS DESCRIPTORS:

neutron spectra: M1; spectra unfolding: Q1; nuclear reaction kinetics; integral equations; computer codes.

Purpose of the work: to determine the initial premises for devising a methodology for neutron spectra unfolding as a function of a priori information, the use of the results of unfolding, a set of measured reaction rates, the errors thereof, the availability of information and calculation resources, etc. The paper describes the main mathematical and physical features of the problem, determines the role of the initial approximations, classifies the methods of unfolding and the errors and, lastly, defines the task of neutron spectra unfolding by measured reaction rates.

As a rule, the unfolding of neutron spectra $\phi(E)$ by measured reaction rates A_i is defined as the solution of a system of activation equations.

$$A_i = \int_{E_L}^{E_U} \sigma_i(E)\,\varphi(E)\,\mathrm{d}E + \varepsilon_i\,, \qquad i = 1, \ldots, N\,.$$

in relation to $\phi(E)$, where the subscript i defines the reaction (detector), $\sigma_i(E)$ is the energy dependence of the cross-section and N is the number of reactions used. The upper and lower boundaries of integration are E_U and E_L, and depend on the specific task. A_i and $\sigma_i(E)$ are given with a measurement error which is reflected in the presence of the term ϵ_i.

The definition of $\phi(E)$ in this formulation is incorrectly stated - it is an unsolved problem. In actual fact, it is necessary, making use of a small number of integrals - A_i, to define a continuous integrand - $\phi(E)$. For this problem to be solvable, its definition has to be supplemented, i.e. the solution sought must be subject to additional conditions [1].

Generally speaking, the solution obtained will depend on the additional conditions. For this reason, these conditions may not be arbitrary ones but must have a physical foundation. It must also be noted that just any mathematical method of solution (even though physically grounded) may not be suitable, since for problems of this kind a consistent method of solution must be sought [1]. The selection and imposition of additional conditions, the evaluation of their influence on the solutions and analysis of the consistency of the method of solution are essential tasks in the solution of equations of this kind.

The choice and use of additional a priori information from incorrect problems will depend on the specific physical application and even on the type of solution. The distinctive features of this physical application may include the following:

1. The number of isotopes used as detectors is limited;
2. Between 20 and 30 detectors are used in individual measurements;
3. The energy dependence of the cross-section is of threshold or resonance shape;
4. The solution in a wide energy range is generally of interest;
5. A different number of detectors "operates" in various energy ranges, and some ranges are not covered at all by the measured reaction rates;
6. Qualitative and quantitative information is available concerning the solution sought.

Qualitative information consists in general concepts relating to the spectrum being sought, e.g. the presence of resonances and troughs in the spectrum and other of its smoothness characteristics. The quantitative information comprises the spectrum given, approximately as obtained from independent sources, e.g. calculations, measurements, the choice from library of spectra of the spectrum closest to the one being sought, and others.

At present, a large number of neutron spectra unfolding programs have been developed and are in use. In these programs, additional information about the desired solution is used in the form of an initial approximation in the construction of a mathematical method for solving the equation and in the analysis of the solutions obtained. As a rule, the unfolding programs are applied formally - without taking into account the special role of using additional information in the solution of incorrect problems. This not only reduces the value of the results obtained but they are without meaning. The effect of various factors on the solution is shown, for example, in Refs.[2-7], where the results for neutrons forming in thermal reactors and from 14 MeV neutron sources is shown in the form of tables and diagrams.

A special place in neutron spectra unfolding is taken by the initial approximation. In some unfolding programs, the initial approximation is given implicitly - in rigorously defined form - or is determined by some means. This is sometimes treated as "the unfolding method's independence of the initial approximation". Practical experience of the use of unfolding methods shows that by varying the initial approximation we can obtain different results at random. This remains valid, although to a lesser degree, even if, from all the initial approximations and solutions obtained, we chose only those that are physically admissible. On the other hand, however, even this actually "saves" the method: in the case of physically sound although considerably differing initial approximations, as a rule we observe limited convergence with the unique solution. The limited convergence means that the result of the unfolding differs considerably less from the solution than does the initial approximation. The correlation between the solution and the initial approximation leads to the conclusion that neutron spectra unfolding has meaning only if the initial approximation, too, can be referred to the initial data. For this reason, the quality of the solution obtained must be evaluated in relation to the initial approximation. And this is usually the case in actual practice: there is some neutron spectrum which is known with some degree of accuracy. It can be obtained from calculations, independent measurements, it can be chosen as the most suitable one from a library of spectra or it can be obtained by some other means, e.g. chosen on the basis of physical premises. The reaction rates calculated according to this spectrum differ from the measured ones by much greater measurement errors. For example, the analysis of basic experiments made in Ref.[8] shows: the difference between the calculated and the experimental data was 30-70% for the integral characteristics of the neutron field and a factor of 3-5 in the case of the differential characteristics. At the same time, the reaction rates can be measured to within 2-10%. The desire to "correct" the available neutron spectrum by means of the measured reaction rates is natural. This correction is effected by mathematical methods of neutron spectra unfolding. Generally speaking, various methods of correcting the initial neutron spectrum can be devised, the results of which differ arbitrarily. Thus, a mathematical method using physical premises should be devised. It should also ensure a consistent and unique solution [1].

Unfortunately, there does not exist at the present time a sufficiently complete, detailed and satisfactory survey of mathematical unfolding methods. Some of these mathematical methods which are now widely used can be found in Ref.[9], where the following unfolding programs and modifications thereof are considered: PM [9], MNP [10], SAND II [11], WINDOWS [12], RFSPJÜL [13] and SPECTRA [14]. Such programs as STAYSL [15], NEUPAC [16], LOUHI [17] and others, which are extensively used at present, were not taken into consideration.

Present-day unfolding programs can be classified in three groups. The first uses direct iterations. In each energy range the initial approximation is corrected in accordance with the degree of difference between the reaction rates calculated for the initial spectrum and the measured ones. The cross-sections of the corresponding detectors are used as a correction weighting. This group includes the SAND II and MHP programs and some of their modifications.

The second group of programs is based on the use of the least-squares method. For this, the functional:

$$\varepsilon_k^2 = \sum_{i=1}^{N} \left(\frac{(A_i - A_i^k)^2}{N} \right) p_i ,$$

is formed, in which P_i is the weight of the i-th measurement. A_i^k is calculated by means of a function with "k" unknown parameters. The unknown parameters are determined from the condition of the minimum of the functional. This group includes the PM program, in which the unknown function is present in the form of the initial approximation and the deformation function, and the deformation function is a polynomial with "k" unknown coefficients. The least-squares method is also used in the STAYSL program, which is widely accepted at present.

The third group of programs uses the regularization method. What is sought is the minimum of the functional:

$$\sum_{i=1}^{N} (A_i - A_i^k)^2 p_i + \alpha f(E) ,$$

where α is the regularization coefficient, f(E) is an additional condition imposed on the solution desired. The NEUPAC, SPECTRA, RFSPJÜL, WINDOWS and other programs come within this group. These programs differ from one another by the form in which the solution is sought, by the additional conditions to which the desired solution is subject, by the choice of the coefficient α, by the method of minimizing the functional, etc.

In the programs of the first group, the mathematical method is constructed on the basis of "reasonable" correction concepts. Those of the second group are based on a "natural" method of processing experimental data - the method of least squares. It is common knowledge that the use of this method gives rise to difficulties in calculation [19], so that the possibilities of the method are limited. For example, in the PM program, acceptable results can be obtained only for small degrees of a polynomial, which often proves to be inadequate. In the description of the STAYSL there is an indication of a similar type of difficulty. The situation can be altered by the addition of a regularization term, which is the imposition of additional limitations on the solution sought for. However, here, too, complications arise in connection with the choice of the regularization coefficients α. This question is resolved in various ways in different programs, but there is no unambiguous and physically grounded choice of α.

In the process of arriving at a solution, the question arises as to the choice of a criterion for discontinuing iteration (in the case of PM, the choice of degree of the polynomial). Ordinarily, the formal criterion for discontinuing iteration is some integral criterion which characterizes reaction-rate and cross-section errors. In some cases, satisfying this integral criterion leads to oscillations in the solution for which there is no physical justification. These are due to the effect of calculation errors, to the fact that the input data are given with errors and that the mathematical unfolding procedures are some approximation or other, and to other factors. For this reason, the solutions obtained must be considered in their entirety and the one that best satisfies the integral criterion chosen and for which there is a physical justification should be selected as the solution.

We designate the difference between the initial approximation and the neutron spectrum of interest as the first-type error. The initial approximation can be determined with some degree of error. We also know, within error, some other initial data as well - measured reaction rates, neutron cross-sections and others. We call the error in initial data second-type error. Error originating with calculation errors and also with the approximate nature of mathematical methods is defined as third-type error.

In neutron spectra unfolding, for the case of a specific unfolding model, it is not appropriate to raise the question of the influence of a first-type error on the unfolding of neutron spectra, since the original approximation is a result of the analysis of a specific physical situation and, of the various alternatives, we shall of course choose the one of highest quality. Such an operation should be carried out only in the case of methodological studies. In some programs based on the transfer of statistical errors (see, e.g. in Ref.[20]) an attempt is made to determine second-type error. It must be borne in mind, however, that in incorrectly formulated problems, third-type errors have a substantial effect. The situation is complicated by the fact that the consistency of the solution depends on concrete values. For this reason, it may be the case that a consistent unfolding procedure can be inconsistent when it comes to determining errors. For determining unfolding errors due to second-type erros, it is more suitable to determine the errors by the simulation of errors in the initial data. In so doing, it must be borne in mind that, in all the unfolding methods, the cross-sections enter as integrand functions. For this reason, in a first approximation, the error due to cross-section error may be considered systematic and be added to the error of the measured reaction rate. The magnitude of this cross-section error can be estimated from the results of reference field measurements [21]. The data presented in Ref.[18] show that the solution in reasonable time limits of a calculation of several tens of varients is possible even on low-power computers (~100 000 operation/s). Inconsistency of the solution is determined directly during the calculation of a specific variant. An error in the unfolding methods can be determined by testing the method in known neutron spectra. An estimate of errors in unfolding methods can also be obtained by using two or more unfolding programs with substantially differing mathemtatical methods of unfolding.

Taking into account the mathematical features of the solved equation of unfolding programs, we may give the following definition: neutron spectra unfolding is the use of a physically grounded and a mathematically consistent correction of an initial approximation, based on the use of measured reaction rates.

In each specific case, the unfolding method used depends on a number of factors, such as the requirements in repsect of the unfolded neutron spectrum, the set of measured reaction rates, the accuracy of the measured reaction rates, the availability of a priori information, etc. A high-quality methodology for neutron spectra unfolding must cover such aspects as planning the measurements and the unfolding, the selection and analysis of the a priori

information, the unfolding of the neutron spectra, the use of two or more unfolding programs, analysis of the effects of errors in the initial data, analysis of the results of unfolding obtained in the individual iteration steps. A superior methodology of neutron spectra unfolding is associated with voluminous routine work. The SAIPS information and computer system [22, 18] represents the automation of this work and also the data and software for it.

REFERENCES

[1] TIKHONOV, A.N., ARSENIN, V.N., Methods of solving incorrect problems, Moscow (1974) (in Russian).

[2] AVAEV, V.N., BAZYKOV, A.I., BONDARS, Kh.Ya. et al., Study of the formation of a reactor neutron spectrum in water, Kernenergie 25 (1982) 105 (in Russian).

[3] BONDARS, Kh.Ya., Analysis of the sensitivity of reactor neutron unfolding in water, Kernenergie 26 (1983) 408 (in Russian).

[4] BONDARS, Kh.Ya., KAMNEV, V.A., TORSHIN, V.S., Use of the SAND II and MMII methods for unfolding fast neutron spectra, Izv. AN Latv. SSR, ser. fiz. tekhn. nauk. 4 (1980) 3 (in Russian).

[5] BONDARS, Kh.Ya., KAMNEV, V.A., TORSHIN, V.S., Use of the MCP, MMII and SAND II methods for unfolding fast neutron spectra, in the book: Questions of dosimetry and radiation shielding, Moscow, 20 (1981) 67 (in Russian).

[6] BERZONIS, M.A., BONDARS, Kh.Ya., Unfolding of neutron spectra in Li and Be assemblies, in the collection: Problems of neutron spectra in the first wall of a thermonuclear reactor and neutron-physics research at Sukhum, 26-29 April 1983, Moscow (1984) 347 (in Russian).

[7] BONDARS, H., Unfolding of neutron spectrum forming in water of light-water reactors, in Proceedings of the Sixth International Conference on Radiation Shielding, Tokyo, Japan (1983) 403.

[8] BOLYATKO, V.V., VYRSKIJ, M.Yu., ILYUSHKIN, A.I. et al., Errors in the calculation of radiation shielding, Moscow (1983) (in Russian).

[9] BONDARS, Kh.Ya., LAPENAS, A.A., Methods of calculating neutron spectra by measured reaction rates in SAIPS, Part 1: Survey of mathematical methods, Izv. AN Latv. SSR, ser. fiz. tekh. nauk. 2 (1980) 3 (in Russian).

[10] BRISKMAN, B.A., GENERALOVA, A.A., KRAMER-AGEEV, E.A., TORSHIN, V.S., Inner reactor dosimetry: practical manual, Moscow (1985) (in Russian).

[11] McELROY, W.N., BERG, S., CROCKETT, T., HAWKINS, R.G., SAND II - A computer-automated iterative method for neutron flux determination by foil activation, AFWI TR 67, 41, 1967, Vol. I-IV.

[12] STALLMANN, F.W., EASTHAM, J.F., KAM, F.B.K., WINDOWS - A program for the analysis of spectral data foil activation measurement, ORNL/TM-6650 (1979), p. 1-104.

[13] FISCHER, A., RFSP-JUL, A program for unfolding neutron spectra from activation data, JUL-1475 (1977).

[14] GREER, C.R., WALKER, J., A procedure for the computation of neutron flux from foil activation data. SPECTRA Code, Radiation Measurements in Nuclear Power (1966).

[15] PEREY, F.G., Least-Squares Dosimetry Unfolding, the Program STAY'SL, ORNL/TM-6062, ENDF-254 (1977).

[16] SASAKI MAKATO, NAKAZAWA MASAHARU, Users' Manual of Neutron Unfolding Code Package "Neupac", PNC No. 941, 80-192 Tr. (1981) 134.

[17] ROUTTI, J.T., SANDBERG, J.V., General Purpsoe Unfolding Program LOUH178 with Linear and Non-Linear Regularizations, Computer Phys. Commun. 21 (1980) 119.

[18] BERZONIS, M.A., BONDARS, H.Ya., Description of SAIPS - Users and Programmers' Manual, Oak Ridge National Laboratory, OLS-84-90, RSIC Computer Code Collection, PSR-203, p.35.

[19] FORSYTHE, J., MALCOLM, M., MOULER, K., Machine methods of mathematical calculations, Moscow (1980) (in Russia).

[20] HUDSON, D., Statistics for physicists, Moscow (1967) (in Russian).

[21] BONDARS, Kh.Ya., LAPENAS, A.A., Recommended cross-sections of activation detectors (RDNL82), Kernenergie 27 (1984) 304 (in Russian).

[22] BERZONIS, M.A., BONDARS, Kh.Ya., Data and software for calculation of neutron spectra by measured reaction rates, Kernenergie 24 (1981) 105.

THERMOLUMINESCENT NEUTRON DOSIMETRY

V.I. GOTLIB
Riga Medical Institute,
Riga, Union of Soviet Socialist Republics

Abstract

The application of TL dosimeters for personal dosimetry in broad energy range neutron fields is discussed. The principles of neutron registration and different configurations of albedo neutron dosimeters using LiF as a registration medium are given in detail.

The operating personnel of nuclear reactors and radiation-chemical industries are most vulnerable to radiation. Therefore, personnel dosimetry represents one of the most important tasks of ionizing radiation dosimetry. Personnel dosimeters should meet certain concrete requirements: they must be compact and convenient in wearing, provide for the long-term storage of the information accumulated and assessment of the contribution of various types of ionizing radiation.

Among currently available individual dosimetry means thermoluminescent dosimeters are thought to be most promising. They are beginning to supplant such traditional dosimeters as small-size ionization chambers and photographic films.

Thermoluminescence presents glowing appearing at heating of previously irradiated solid substances. This principle lies at the basis of the rapidly developing method of solid dosimetry - thermoluminescent dosimetry.

A thermoluminescent detector presents a pellet measuring some millimeters. After the detector has been irradiated thermoluminescence is registered in a special unit in which the detector is heated and the light emitted is registered using photoelectronic multiplier. Virtually all irradiated dielectrics display thermoluminescence, however, due to specific requirements concerning the nature and parameters of luminescence, glow dependence on radiation dose, information retention etc. only a few substances meeting the above requirements could be selected out of many thousands. Only four of them have practical application - LiF, CaF_2, $CaSO_4$, $Li_2B_4O_7$.

Today the TL detector based on LiF is the most widely used. TL detectors have certain advantages over other detectors used in individual dosimetry. These are mainly high sensitivity, wide range of doses registered, possibility of repeated application, registration of various types of radiation.

However, the application of these detectors does not solve the problem of individual neutron dosimetry which we shall discuss in greater detail.

Why does the problem of individual neutron dosimetry remain unresolved today? This is mainly due to the mechanisms of neutron interaction with the substance and strong interaction efficiency dependence on energy which differ in principle from other types of radiation.

The basic parameter to determine the effect of radiation interaction with the substance is the dose absorbed $D = dE/dm$. For instance, when the substance interacts with gamma-radiation, other things being equal, the dose absorbed is the function of only one parameter of effective atomic number Z, and various substances being used as detectors, energy dependence becomes manifest solely in the region of photoeffect predominance, that is, at energies of scores and hundreds kev , since in this region $D \sim Z^5$. Having selected a detector close to tissue Z - in individual dosimetry we are always interested

in D in tissue - we can practically ignore energy dependence. For instance, LiF TL detector has Z_{eff} = 8.2 (tissue Z_{eff} = 7.4) and its energy dependence is ignored.

In neutron dosimetry the matter is altogether different. First of all the dose absorbed is affected by the atomic composition of the substance. Tissue neutron dose is formed by all types of secondary radiation of recoil protons (D_p), recoil nuclei (D_n), ionizing particles formed in nuclear reactions ($D_{fr.}$) and gamma-quanta emerging at neutron trapping (D_γ).

$$D_T = D_p + D_n + D_{fr.} + D_\gamma$$

There is one more circumstance to complicate the determination of the tissue neutron dose. This is various biological effectiveness of different types of radiation. This variable effectivity is characterized by the relative biological effectiveness factor (RBE). It is determined as the ratio of the doses of "reference" radiation and the given radiation producing the same biological effect. ^{60}Co radiation is usually taken as reference radiation. ICRP designated RBE factor as quality factor. The quality factor is determined by the single value of secondary charged particle LET.

Various types of secondary radiation have different quality factors, therefore, the equivalent dose is:

$$H = D_p K_p + D_n K_n + D_{fr.} K_{fr.} + D_\gamma$$

In practice it is necessary to register the equivalent dose. Fig.1 shows the dependence of the specific equivalent dose in $\frac{rem.cm^{-2}}{neutr.}$ on neutron energy. In principle, an ideal neutron dosimeter should have the same sensitivity to neutrons in a broad energy spectrum. None of the currently used individual neutron dosimeter types possesses this feature. Thermoluminescent neutron dosimeters

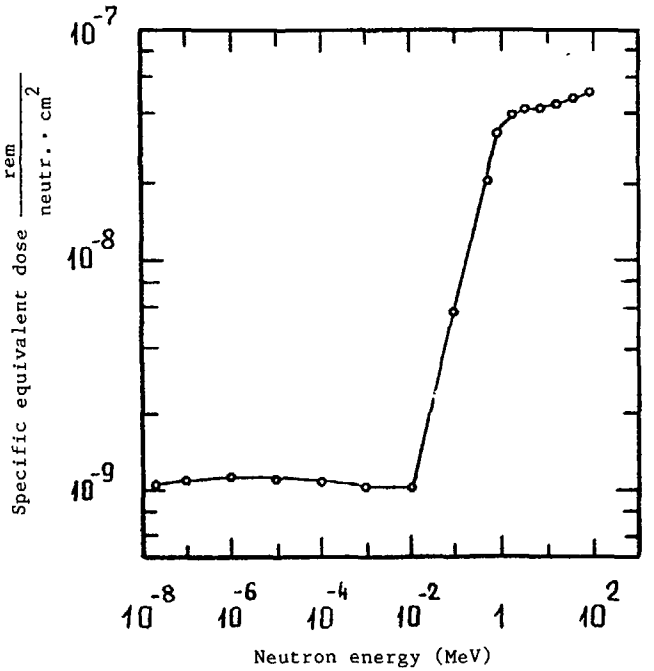

FIG. 1. The dependence of the specific equivalent dose in rem·cm^{-2}/neutron on neutron energy [1].

usually are subdivided into two types. These are thermal-neutron dosimeters and fast-neutron dosimeters.

The possibility of registering thermal neutrons with thermoluminescence detectors is due to some extent to accidental circumstances. The principle of TL dosimeter operation is based on ionization effect in a solid. Such ionization is possible only with secondary radiation resulting from neutron interaction with the substance. The greatest ionization effect is observed in the case of splitting reactions with charged particle emission. Such process is mostly likely for fast neutrons and light nuclei. For slow neutrons only four reactions are known where this process is sufficiently intensive

$^{6}Li(n,\alpha)^{3}H$; $^{10}B(n,\alpha)^{7}Li$; $^{3}He(n,p)^{3}H$; $^{14}N(n,p)^{24}C$

As it has been already noted, the range of thermoluminescence detectors having practical application is very limited, and the favourable concurrence of circumstances consists in that two TL detectors comprise Li and B elements.

The detector based on ^{6}LiF is the most widely used in thermal neutron registration. There is one essential circumstance to complicate thermal neutron registration with TL detectors. It can be formulated as follows: there are no neutrons without gamma-radiation. Any TL detector is sensitive to gamma-radiation and, therefore, it is necessary to distinguish the contribution of neutrons into TL signal from that of gamma-component. This can be achieved by using two TL detectors one of which contains mainly ^{6}Li isotope, and the other -^{7}Li. Thermal neutron cross section for $^{6}Li \simeq$ 942 barn, for ^{7}Li = 0.037 barn. This means that ^{6}LiF detector (as a rule, separation makes up 95.6% ^{6}Li) will register slow neutrons + gamma-radiation, while ^{7}LiF detector (0.007% ^{6}Li) will register actually only gamma-radiation. When the reading of one detector is subtracted from that of the other, one can obtain either the value of neutron flux or the value of the neutron dose in gamma-equivalent depending on calibration. It should be pointed out that ^{6}LiF detector registers not only neutrons; however, effectiveness of their registration decreases as 1/v where v - neutron speed. (Fig.2). ^{6}LiF TL detectors are extremely sensitive to slow neutrons due to the big cross section. ^{6}LiF layer 0.1 mm thick traps about 50% neutrons incident onto it. A flux of 10^{10} cm^{-2} produces the same effect in a ^{6}LiF detector as if it were irradiated with gamma-radiation of ^{60}Co at a dose of $\simeq$ 2000 rad. Taking into account that according to the ICRP recommendations the flux of thermal neutrons of 10^{9} n · cm^{-2} creates the maximum equivalent dose of 1 rem, tenth fractions of rem can be registered even against ten times more intensive gamma-radiation. Practical registration of thermal neutrons presents certain problems of technical nature, however, they are not a matter of principle.

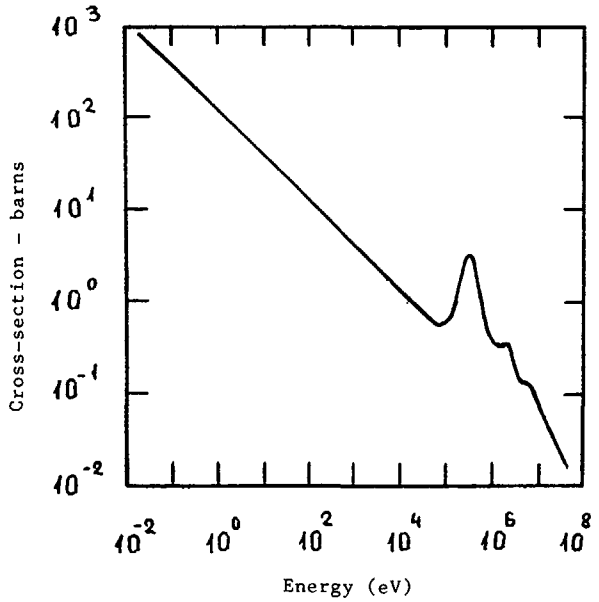

FIG.2. Neutron cross-section for ^{6}Li.

The sensitivity of thermoluminescence detectors to fast neutrons is low. LiF TL detector sensitivity to neutrons calculated by Rinard and Simons is shown in Fig.3[2]The experimental data obtained by different authors are cited here. The sensitivity to neutrons grows together with an increase in their energy. At neutron energy of 15 Mev the sensitivity is 4.07 · 10^{-10} rad/ $n.cm^{-2}$. It means that a ^{7}LiF detector irradiated with a flux of

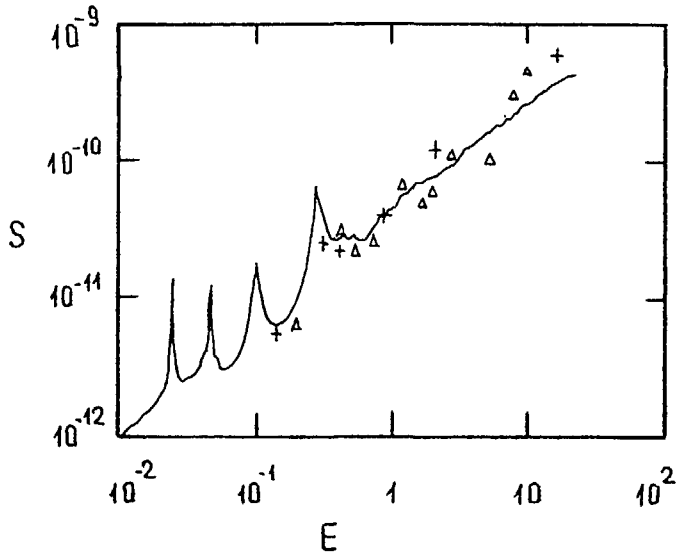

FIG. 3. The calculated and measured sensitivity of ^{7}LiF to neutrons. Neutron energy E (MeV), sensitivity S in (^{60}Co equivalent ^{7}LiF rad/(n·cm^{-2}) [2].

fast neutrons equal to $2.5 \cdot 10^{9}$ n/cm^{2} with energy of 15 Mev will read 1 rad in gamma-equivalent, taking into account, that the lower limit of gamma-radiation registration with LiF TL detectors lies at a level of 10^{-2} rad. The flux of neutrons that can be registered amounts to $2.5 \cdot 10^{7}$ n/cm^{2}. At such neutron energy the maximum equivalent dose is produced by neutron flux of $2 \cdot 10^{7}$ n/cm^{2}, that is, we cannot register an equivalent neutron dose below 1 rem, whereas it is necessary to register at least a hundred times less. Thus, we see that fast neutron registration with TL detectors, especially against gamma-radiation, is practically impossible. It should be pointed out that many researchers tried to increase TL detector sensitivity to fast neutrons, for instance, surrounding detectors with a layer of hydrogen-containing material, sometimes the TL detector registered additionally recoil protons. Some researchers tried to introduce hydrogen directly into LiF detector, various mixtures of thermoluminophor with hydrogen-containing material have been suggested.

Various attempts in this direction have not been successful so far. However, a way out has been found. As far back as in the sixties **Keirim-Markus** suggested the use of thermal albedo-neutrons formed in the human body for fast neutron registration in individual dosimetry. The human body contains 10 weight % of hydrogen which dissipates and slows down neutrons. Thermal albedo-neutrons make up only an insignificant fraction of the total neutron flux (up to 1%), however, the high sensitivity of ^{6}LiF TL detector enables to register this fraction with confidence. The schematic diagram of the simplest personal dosimeter is shown in Fig.4. It is based on two detector pairs ^{6}LiF - ^{7}LiF. To register thermal albedo-neutrons its necessary to eliminate or, at least, to reduce considerably the effect of the direct flux of thermal neutrons. That is why the albedo-dosimeter comprises a partition from materials with the big cross-section of thermal neutron trapping. In practice either cadmium or boron-containing plastic **are used.Thus** a ^{6}LiF detector under a cadmium disc registers albedo-neutrons while **a similar** detector over the cadmium disc registers **incident** thermal neutrons. To exclude **incident** thermal neutrons completely,

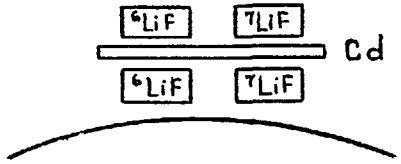

FIG. 4. The basic diagram of albedo-dosimeter.

the absorbing partition diameter must be very large, over 1 cm. Naturally, this is not convenient, such a cassette would be too big and inconvenient in carrying. When using a smaller diameter it has to be taken into account that part of the directly incident neutrons will get into the screened detector, and it must be subtracted from the readings of the bottom detector. The magnitude of this part is determined experimentally for the albedo-dosimeter of a given design by irradiation in the flux of thermal neutrons.

So, having taken the readings of all four detectors and having taken into account the contribution of gamma-radiation and directly incident thermal neutrons, we obtain TL-response proportional to the flux of fast neutrons and the corresponding equivalent dose. However, there is one complication presenting the main drawback of the albedo-dosimeter. The quality of albedo-neutrons leaving the human body depends on the energy of incident fast neutrons at one and the same flux. Typical energy dependence of the albedo-dosimeter is presented in Fig.5. [3]

The response magnitude changes by more than an order decreasing as neutron energy increases. It means that when rgistering the equivalent neutron dose with an albedo-dosimeter we shall have an error of the same magnitude if we know the energy spectrum of incident radiation. Besides, such a pattern of energy dependence is contrary to the pattern of the equivalent dose change. In practice it means that the albedo-dosimeter must be calibrated in the same place, that is, in the neutron spectrum where registration is to be performed. In this case to determine the calibration factor it is common to use two neutron detectors with different energy dependence. Hankins [4], for instance, used a 9-inch polyethylene

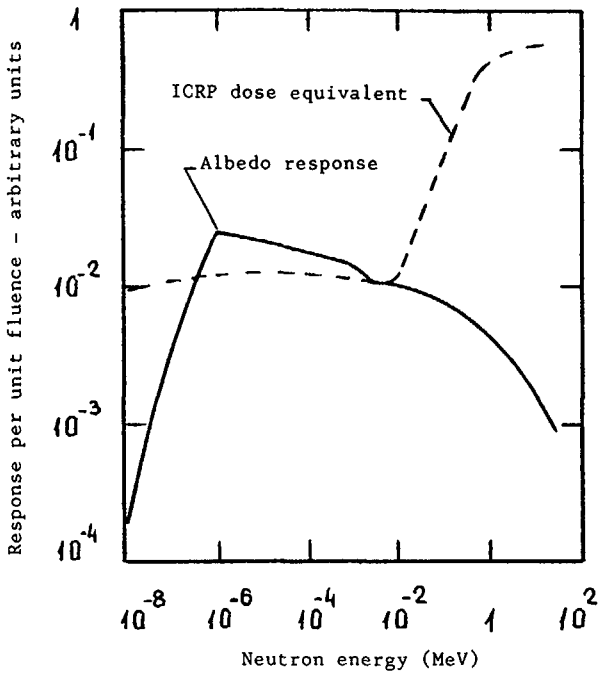

FIG. 5. Typical energy dependence of albedo-dosimeter [3].

ballon around the detector serving as rem-meter and a 3-inch baloon coated with cadmium with predominant sensitivity to low energy neutrons. The calibration factor in different spectra is determined as the ratio of the 9-inch sphere readings to those of the 3-inch one. The calibration factors for Hankins' albedo-dosimeter are shown in Fig.6. It can be seen that the dependence of the calibration factor on the ratio of the readings of the neutron detectors surrounded with different media represents a straight line. It has been found that in many practical cases in the workroom the calibration factor varies within 20-30%, this being the error of the TL albedo-dosimeter. If the variations of the calibration factor are greater additional information is needed to improve the accuracy of its value.

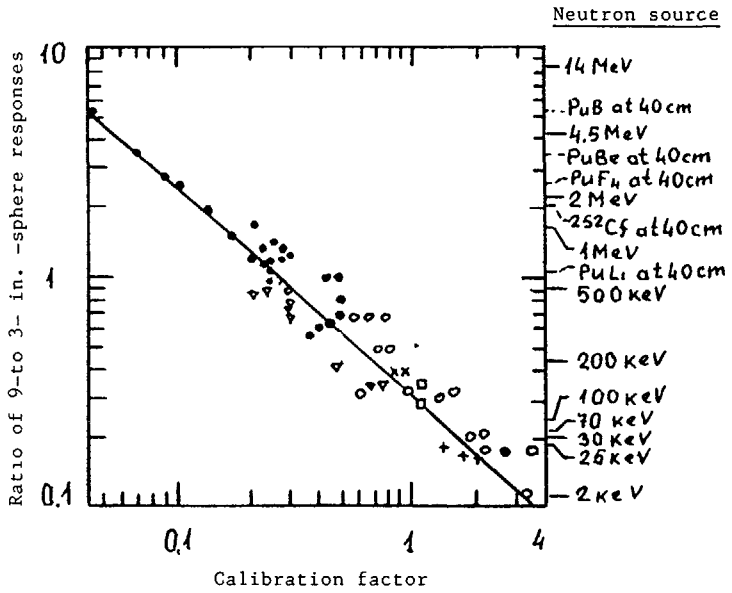

FIG. 6. The calibration factor of Hankins albedo-dosimeter [4].

Modern albedo-dosimeters vary according to the design. TL detectors are frequently surrounded with polyethylene which increases the dosimeter sensitivity, two TL detectors are used instead of four or, vice versa, the number of TL detector pairs is increased which enables to specify some nuances in the readings. Dosimeters are also of different dimensions: from 2 to 6 cm in diameter and are worn on the chest or at the waist, respectively. As it has already been mentioned, the practical application of albedo dosimeters is limited by the necessity of preliminary calibration in the neutron field where measurements are to be made. In many cases when working in certain rooms it is really possible. However, one naturally wants to have a dosimeter that does not depend on the spectral composition of radiation or takes it into account. The latter can be realized in combined dosimeters

where energy dependence of each detector differs essentially. This idea has been realized by the research workers of the IPHE (USSR) in the combined dosimeter consisting of two albedo-detectors and a track one. The track one was a photographic detector based on nuclear photoemulsion K-20. It is common to use mean energies of neutron spectra ($\bar{E}$) to determine energy dependence. The rightfullness of this approach, that is, the statistic dependence of the series of functionals (flux, absorbed and equivalent doses) on $\bar{E}$ in a broad class of the neutron spectra in operating nuclear-physical units has been demonstrated recently by Britvich, Belogorlov et al.[5] Fig.7 shows the theoretical and experimental dependence of the ratio of track detector readings to the albedo-dosi-

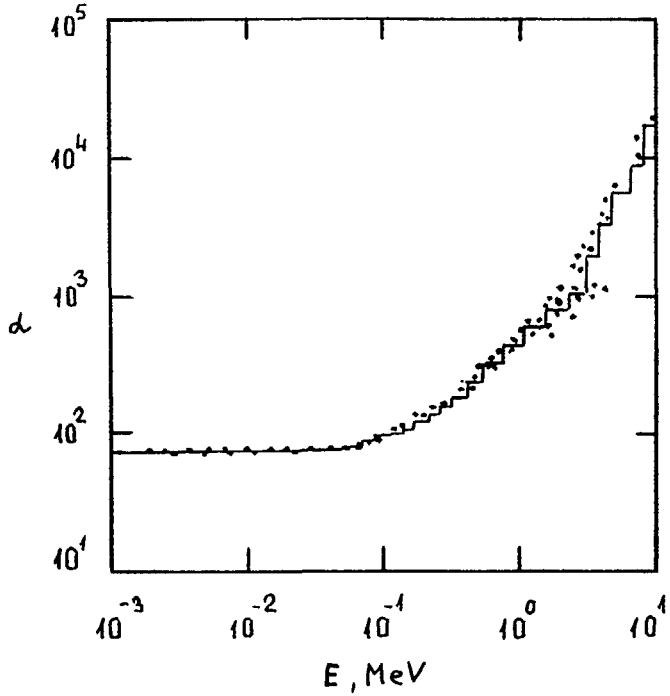

FIG. 7. The ratio of track detector readings to the albedo detector (α) according to energy $\bar{E}$ of neutron spectra [5].

meter (α) according to E of different neutron spectra. Determining this value in practice and knowing the pattern of the energy dependence of the albedo-dosimeter we can determine the value of the maximum equivalent dose with sufficient accuracy.

Thus, in principle the application of combined dosimeters enables to solve the problem of individual dosimetry of broad energy spectrum neutrons. There are some obstacles on the way to the extensive practical use of such dosimeters, of technical nature. These difficulties are connected with the selection of the optimum design of cassettes for albedo-dosimeters, with uneven distribution of the dose absorbed in the material of ^{6}LiF TL detector due to the strong absorption of slow neutrons and its effect on TL-response magnitude and some other reasons. At present a number of laboratories in different countries work on the problems of the application of TL detectors in neutron dosimetry and there is hope that in the nearest future TL dosimetry of neutrons will become a widely used routine method.

REFERENCES

[1] INTERNATIONAL COMMISSION ON RADIOLOGICAL PROTECTION, Supplement to ICRP Publication 15 (1971).

[2] P. RINARD, G. SIMONS, Nucl. Instr. and Meth. **158** (1979), p. 545.

[3] R. GRIFFITH, et al., Health Phys. **36** (1979), p. 235.

[4] D. HANKINS, in Proc. 9th Midyear Topical Symposium, Health Physics Society, Denver, p.861.

[5] BRITVICH, et al., to be published.

DOSIMETRY OF IONIZING RADIATION ON THE BASIS OF NATURAL MATERIALS: A REVIEW

I.A. TALE
Solid State Physics Institute,
Latvian State University,
Riga, Union of Soviet Socialist Republics

Abstract

Physical effects which are used in solid state dosimetry, such as radiophotoluminescence, exoelectron emission, scintillation and ESR are briefly described. The practical problems encountered in such dose measurements and calibrations are described.

1. Introduction

As early as 1895, Widemann and Schmidt irradiated a great number of minerals and inorganic compounds with cathode rays and found, among other phenomena, that fluorite and manganese-activated calcium fluorite exhibits bright luminescence, when heated in the dark [1]. No decay of the accumulated light-sum was observed after holding the samples in darkness for several weeks. So far one of the most widely used phenomena in determining the cumulative doses of ionizing radiation is thermostimulated luminescence (TL).

Further on, the idea of using TL in assessing cumulative doses of radiation was developed in two directions as follows.

First, for purpose of individual dosimetry highly sensitive to small doses TL-materials have been synthezed, which meet the requirements of dosimetric problems. Already in the 1950-s the basic compositions for dosimeters were discovered and proposed

for dosimetric purposes e.g. detectors on the basis of LiF, $CaSO_4$, CaF_2.

Second, for solving geological and archeo-chronological problems applications of the TL of natural materials as well as remnants of artifacts were developed [2]. The fact was made use of that a certain light-sum is accumulated in minerals due to natural ionizing radiation, since rock always contains small concentrations of radioactive nuclei. Measurements of the natural radioactivity level along with the TL of minerals provide information on their thermal history and permits dating of geological formations as well as archeological artifacts - ceramics, glasses, etc. Therefore minerals of natural origin are used as dosimeters of cumulative doses caused by natural radioactivity.

Since individual dosimetry requires high sensitivity, a wide range of doses to be measured, and selectivity to various kinds of ionizing radiation, attention in developing solid-state dosimeters was focused on finding suitable compositions. However, it appears, that the possibilities of using natural minerals in dosimetry are far from being exhausted. For one thing, natural substances permit to solve dosimetric problems, which are outside the reach of current individual dosimetry techniques available. Most important is the problem of restoring the cumulative doses when there is no dosimetric monitoring. Moreover, in emergencies in the absence of personal dosimeters, comprehensive dosimetry can be realized only by using natural materials or some synthetic article of personal everyday usage.

In recent years various additional techniques of solid-state dosimetry have been developed. Progress in natural-material solid-state dosimetry will be considered in more detail below.

2.Techniques of solid-state dosimetry.

The techniques of solid-state dosimetry are based on the fact that radiation causes direct or indirect reactions in electronic and, in certain cases, also in ionic subsystems of solid state. Charged high energy particles, such as electrons, protons, positrons, alpha-particles are known to directly ionize atoms (ions) of solid state, whereas neutral particles such as neutrons, gamma-quanta, give rise to primary charged particles (electrons, ions) due to non-elastic collisions or nuclear reactions. There are a great variety of effects due to the products of atom ionization. Table 1 shows the most important effects used at present in solid-state dosimetry. They are caused by secondary reactions ivolving electrons, holes, intrinsic and extrinsic defects. The main secondary reactions, represented shematically in fig.1, are as follows:

1) Immediate radiational recombination of free electrons and holes via exciton states. This is just one kind of reactions, which give rise to scintillations.

2) Migration and capture of charge-carriers in defect-caused local energy states leading to formation of electron and hole

Table 1. The most important effects used in solid-state dosimetry

Effect	Measured quantity	Dosimeter material	Radiation types	Use for natur. mat.dosim.
Radiophoto-luminescence	Luminescence	Glass	γ	+
Coloration	Optical density	Crystal glass	γ, n	-
Photograhic effect	Optical density	Film	γ, n	-
Exoelectron emission	Number of electrons	Crystal, ceramics	γ, n, β, α	+
Track detection	Number of tracks	Organic film	n	+
Neutron-induced defects	Change of resistance	Semicond. (Si)	n	-
Scintillation	Luminescence	Crystal	γ	-
Paramagnetic resonance	ESR-spectrum	Crystal glass	γ	+

colour centres. Absorbtion of light quanta by these centres causes colouring of crystals and glasses. This efect has been used in dosimetry: the optical density at certain photon energy has been measured and corresponding radiation dose estimated.

Color centres, which are characterized by spin-non-coupled electrons can be detected by the electron spin resonanse (ESR) spectroscopy. The ESR-spectroscopy, as is known, represents resonance absorption of the magnetic component of electrons between the spin-lewels. To observe the ESR-signal, the

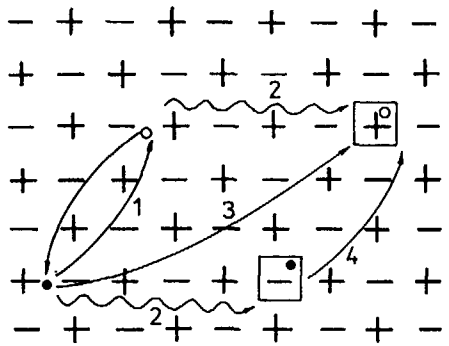

Fig.1 1 - radiative recombination of free electron and hole;
2 - formation of color centre by capture of free electron or hole;
3 - radiative recombination of free electron with trapped hole;
4 - photo- or thermostimulated radiative recombination of released electron with trapped hole

substance should contain paramagnetic colour centres, i.e centres having a non-zero magnetic momentum and, in particular, an odd number of electrons. Paramagnetic colour centres may emerge when a charge-carrier is captured during irradiation. Such colour centres can be utilized in ESR-dosimetry, provided that narrow lines are produced in the ESR-spectrum.

3) Recombination of free charge-carriers with the ones of opposite sign, captured on defects. This reaction like to the first one causes the material to scintilate.

4) Photo- or thermostimulated release of charge-carriers from colour centres (which acts as electron or hole traps) followed by their radiational recombination with opposite-sign ones captured on the colour centres. This reaction is utilised in techniques of radiophotoluminescent and thermoluminescent

dosimetry respectively. In particular, according to the radiophotoluminescence technique the light-sum is measured, which is released in the course of stimulating irradiation by light having a certain photon energy. Similarly, the TL-technique is based on the measurement of the light-sum, released in the course of heating of the material.

The electrons released from the surface layer under thermal stimulation are counted by the exo-electron emission technique.

Part of the effects, used in solid-state dosimetry are not encountered in natural materials at all. From variety of other phenomena only those are used in natural-material based dosimetry, which admit of samples in the form of polycrystals or powders. As a result, natural-material based dosimetry can practically be realized only on such effects as radiophotoluminescence, TL, exo-electron emission and the ESR.

At present the ESR-spectroscopy is the most widely examined technique for natural-material-based dosimetry. An analogous use of the TL technique is also beginning to be developed. The techniques and equipment used for dating of geological and archeological events, are successfully extended to natural-material-based dosimetry. Although the other effects enumerated above seem to be rather promising, they have not been dealt with as yet.

We are now going to consider the progress made in using natural materials in TL- and ESR- techniques.

3. Natural materials.

Dating geological or archeological events by both TL- and ESR techniques are based on practically the same natural materials.Table 2 presents the main minerals, currently used in dating. It is seen that the paramagnetic centres are produced and light sum created, under effect of ionizing radiation, in minerals often found in nature. They are encountered both in rock of volcanic origin (quartz, field spar), as well as sediments (quartz, carbonates). This is why ESR- as well as TL-dating are becoming the basic techniques used in geochronology.

Table 2 Most important natural materials for solid-state dosimetry

Mineral	Geological formation	Composition	ESR-centre	Ref.
Calcite	Shells coralls stalagmite	$CaCO_3$	$C\theta_3^{3-}$	2,3
Aragonite	Shells coralls	$CaCO_3$	CO_3^{3-}	4
Zirkon	Igneous rocks			5
Quartz	Volcanic rocks plagioclase sediments	SiO_2	Al-centres Ti-centres	6,7
Feld spare	Laterite basalts		Al-O -Al	8

A great variety of articles of every day use contain carbonates and silicates. Such are, e.g., buttons, watches, spectacles etc. Therefore the experience gained in solving

geochronological problems can be used in developing the ESR- and TL-dosimetry techniques.

It can be assumed that in certain cases things which contain silicates or carbonates are useful as dosimeters in restoring the cumulative doses absorbed by man. Still the doses absorbed in a life time of man can apparently be adequately assessed by using some human substance as dosimeter material. Such human substance has to be used as is never renewed during the life time. According to data available, the most promising natural human material, permitting the ESR-dosimetry is tooth enamel, 90% of it being of hydroxyapatite [9-11]. Let it be noted, that attempts have been made to use also hair and skin as dosimetric material, since they contain radiation-sensitive proteins.

4. TL-dosimetry

The equipment for determining the "natural" TL-lightsum, in principle, may be identical to that used for traditional TL-dosimetry. Use of natural minerals and other materials as TL-detectors involves additional requirements. The minerals have a rather low TL-sensitivity, therefore the apparatus should have an extremally high light-sensitivity, e.g. the photon counting system and the solitd angle of litght collection approaching 4π steradians. It is important to have a fast heating rate supplemented by discrimination against thermal radiation. Any non-radiation-induced TL should be suppressed by making the measurements in an atmosphere of dry oxygen-free nitrogen.

The procedure of determining cumulative doses compared to the traditional TL-dosimetry involves additional operations. The major ones are:

1) Extracting the mineral from rock and purifying it. Each kind of rock and mineral used requires its own individual treatment.

2) Determining the stimulation temperature interval, in which the emitted light sum adequately characterizes the dose absorbed.

3) Calibrating the TL sensitivity of the sample.

4) Determining the cumulative dose from the results of the measurement of the accumulated light sums.

Operations 2,3,4 involve measuring the light sums.

Calibration. Unlike manufactured TL-dosimeters, the TL-sensitivity of each sample of natural material should be estimated and therefore corresponding sample calibration made. The latter is based on the measurements of the additional TL-light sum accumulated due to the exposure of the sample to a known dose of nuclear radiation from an artificial radio-isotope source.

The typical resulting glow curve - the "artificial" TL as well as the "natural" TL is shown in fig.2. It is known that for a single colour centres (single traps) the glow curve would be a single peak. In the case of natural minerals (quartz, calcites) the glow curve is composed of a number of overlapping peaks because there are several types of electron traps

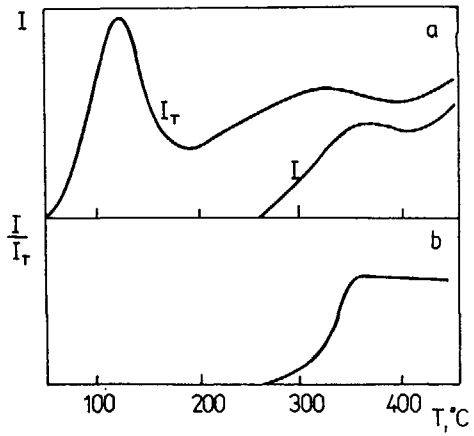

Fig.2 The plateau test. The upper fig. shows the glow curves corresponding to the "natural" (I) and to the "artifical" TL (I_T) following 1000 rad of betta irradiation. The lower fig) shows the equivalent dose, equal to the ratio I /I_T as function of stimulation temperature /11/.

present. Due to fading the "artifical" TL involves some additional peaks as compared to the "natural" TL. Therefore the presence of severa' types of trap has the advantage that it permits the e.g. "plateau-test" to be used to check if the traps are deep enough for stable retention of electrons during the dose-accumulation-times. The "plateau-test" (fig.2,B) involves calculation of ratio

$$\frac{I}{I_T}$$

as function of temperature, I, I_T being intensity of the "natural" and "artifical" TL correspondingly [13]. The onset of the plateau indicates that a sufficiently high stimulation temperature has been reached for the TL to be associated with traps that retain their electrons with negligible leakage during dose-accumulation times. The stimulation temperature region corresponding to the plateau of the ratio calculated could be used for estimation of "natural", S, and "artificial", S_T , TL light sums. The accumulated dose in the simplest case is equal to

$$D = \frac{S}{S_o}$$

S_o being the light sum accumulated per unit dose.

Estimation of TL sensitivity (S_o). The TL sensitivity depends on the gamma-photon energy. The energy response of material is a measure of the energy absorbed by the TL material used in comparision to the energy absorbed by a material taken as reference, when irradiated at the same exposure. Normal reference materials in dosimetry are air and tissue. The energy responses of various materials are represented in fig.3.

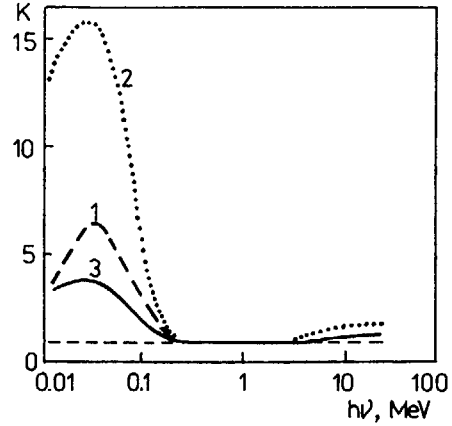

Fig.3 ESR energy response of hydroxyapatyte (1), /11/, and TL response of CaF_2 - (2), /12/; Al_2O_3 (3), /12/.

Natural minerals such as quartz show a considerable increase of energy response for gamma-photon energies below 0.1 MeV.

An accurate estimation of the dose requires to know the energy spectrum of radiation. Fig.4 presents the energy spectrum of Hiroshima A-bomb at a ground range of 1.45 km [14].

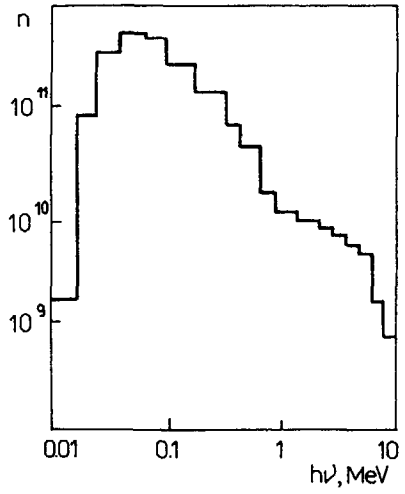

Fig.4 Energy spectrum of Hiroshima A - bomb at a ground range of 1.45 km /10/.

The main part of photons have the energies equal to or greater than 0.1 MeV, i.e. it corresponds to the region having constant energy response. As a consequence, the Co-gamma-ray source could be directly used for estimation of TL sensitivity of natural minerals.

Similarly, the effective gamma-photon energy of radioactive nuclei emitted during the Chernobyl disaster is approximately 0.4 MeV [15], i.e. the above considered Co-gamma source is available for estimation of the energy response.

Unfortunately in practice at high doses the TL dosimetry is more complex than the above considered simple principle might suggest. The major problems caused by the TL phenomenon are non-linear growth of TL with increasing dose (superlinearity, saturation) as well as change of TL sensitivity by heating (the pre-dose effect). The first effect itself can be circumvented by using the additive method of equivalent dose evalution (fig.5). Three (or more) equivalent samples are prepared. The

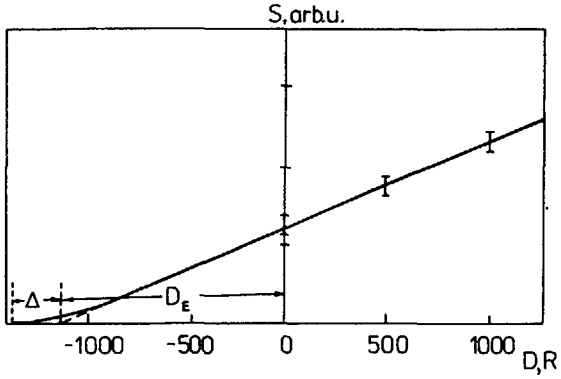

Fig.5 Additive method of evaluting gquivalent dose (D?). Several samples are used to measure N, the "natural" TL, to measure (N+a), (N+2a),...., the "natural" plus "artifical" TL after dose of a, 2a, ... rad. The superlinearity correction is determined by means of a TL growth curve in dependence from irradiation dose using samples from which "natural" TL light sum has been removed. The sum of D_E and Δ equals to the D, the accumulated dose /12/.

first is used to measure S, the "natural" TL light sum, the second one to measure (S+a), the "natural" plus the artificial TL light sum after a dose of a rad, and the third (S+2a), after a dose of 2a rad. The equivalent dose is evaluated in the general case by non-linear interpolation (see fig.5 for a particular case of linear interpolation). An empirical way of

correcting the superlinearity is to use already heated samples to determine the dependence of second-light sum on low-value doses. It is assumed that heating does not affect the TL sensitivity at low doses. These data are subsequently used to evaluate the correction term Δ. It seems that when low cumulative doses are to be determined (tens, hundreds of rad) the superlinearity can be directly evaluated by experiment following the above-described additive method of equivalent dose evaluation.

5. ESR dosimetry

Unlike the TL-dosimetry the ESR-spectroscopy allows directly to measure the ESR spectrum at room temperature without any heating the sample. However, for ESR-spectroscopy there exist the same problems, caused by variation of ESR sensitivity of samples as well as by overlapping of ESR signals of various centres involving those induced by mechanical treatment.

Let us consider the procedure of the measurements developed for the ESR dosimetry using human tooth enamel [10].

PROCEDURE OF THE MEASUREMENT

TOOTH
↓
SEPERATION OF ENAMEL
↓
CRUSHING INTO GRAINS OF 1 mm DIAMETER
↓
WAITING FOR THE DECAY OF THE SIGNAL DUE TO MECHANICAL EFFECT
↓
MEASUREMENT OF THE INITIAL ESR SIGNAL
↓
IRRADIATION OF STANDARD DOSE OF Co-GAMMA RAY (100-200 rad)
↓
WAITING FOR THE DECAY OF THE UNSTABLE RADICALS
↓
MEASUREMENT OF ESR SPECTRUM
↓
REPETITION OF CYCLE IRRADIATION=MEASUREMENT

Fig.6,A presents an ESR spectrum of non-irradiated tooth enamel measured after grinding, fig.6,B - a ESR spectrum of the same sample measured after irradiation with gamma ray. Although the signals produced by radiation were found at g=2.002 and g=1.977 of CO_3^{3-} radicals, a signal produced by mechanical stimulation was found at a different position g=2.006. The latter signal, due to radicals produced by mechanical effects, decayed rapidly, whereas the intensity decay of the CO_3^{3-} ESR spectrum after irradiation is of the order of 20% and should be taken into account in assessing of the ESR sensitivity.

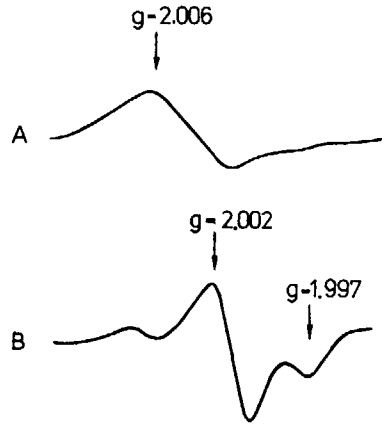

Fig.6 The ESR spectra for nonirradiated tooth enamel when mechanical stimulation was applied (A) and for irradiated by gamma rays tooth enamel after grinding /10/.

A good linearity is obtained between the dose of Co-gamma ray and the radiation induced ESR signal intensity of tooth enamel. Fig.7 shows an example of personal dosimetry [10]. Three samples were supplied from a radiologic technologist. The estimated doses of the three sample coincided. The cumulative

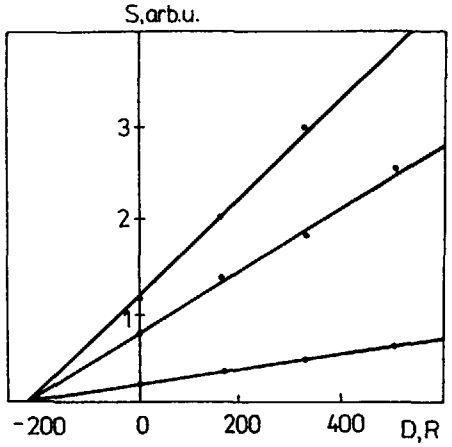

Fig.7 An example of personal dosimetry carried out by ESR - spectroscopy of tooth enamel for three samples. Additive doses are made by Co - gamma rays /10/.

dose is shown by the value of the horizontal axis when the signal intensity is zero. The cumulative dose of A-bomb radiation from survivors at Nagasaki (N) and Hiroshima (H) [10] see Table 3.

Table 3 Cumulative dose (Co-gamma equivalent) of A-bomb radiation using ESR signals of tooth enamel from survivors at Nagasaki (N) and Hiroshima (H)

Id.No	Place	Ground distance (m)	Tissue dose with ESR (Gy)	Reference
A-1	N	691	2.2	16
A-2	N	1200	0.9	10
A-3	N	1300	3.4	16
A-4	N	1400	1.7	16
A-5	N	1500	1.2	10
A-6	N	1800	0.5	10
A-7	H	770-1000	2.1	16
A-8	H	930	5.4	10

For tooth enamel the ESR-spectroscopy had a good property as a dosimetric technique - a good linearity was obtained between the exposure dose and the signal intensity of the CO_3^{3-} radicals. However, in evaluating the cumulative dose similar to the TL dosimetry the energy of the exposed photons must be taken into account (see fig.3).

For carbonates such as bone fossils, shells, etc. some additional difficulties are encountered due to overlapping of various radiation-sensitive ESR signals. A plateau-test should be made to check the region of ESR spectrum available for dosimetry [17]. Unlike the tooth enamel for natural carbonates such as calcites, shells, the ESR signal exhibits saturation behaviour [4,17]. The non-linear fitting function should be used in evaluting the cumulative dose.

Complications. In many situations it is necessary to measure gamma-ray doses in the presence of neutrons, and it may be necessary to correct the results for the sensitivity of the detector to neutrons. In the case of individual TL-dosimetry evalution of cumulative dose of mixed gamma-neutron irradiation is based on use of such dosimetric material~s (f.e. LiF), in which irradiation gives rise to several TL-peaks having different sensitivity to gamma rays and slow neutrons. As rule this is not the case for natural minerals. Moreover unlike to synthetic dosimeters the composition as well as content of different impurities in minerals and therefore the sensitivity

to neutrons change from sample to sample. As consequence the biggest errors in gamma dose assessment should come from the presence of thermal neutrons. However, evolution of an experimental procedure in order to assess the sensitivity of different samples to neutrons at present remains an unsolved problem.

6.Final remarks

Both the TL and the ESR dosimetry are convenient in assessing the cumulative doses absorbed by humans as well as other objects.

The sensitivity threshold for natural materials is considerably lower than that for industrially produced dosimeters and will, obviously, be tens of rad. Nonethless, such a threshold permits assessment of the cumulative dose in many cases of irradiation being higher than that caused by the natural background.

Use of natural materials seems to be promising in solving certain probems in inside-reactor dosimetry too.

Further development of dosimetry techniques is required to achieve highest sensitivity and precision.

REFERENCES

1. Wiedemann E. and Schmidt G. C.- Ann.Phys.Chem., 1895, v.54, p.604

2. Ikeya M.- Dating a stalactite by electron paramagnetic resonance., Nature, 1975, v.253, p,48-50.

3. Rossi A.,Poupeau G. and Danon J.- On some paramagnetic species in natural calcites by - and -rays irradiation., ESR dating and dosimetry ed. M.Ikeya, Ionics, Tokyo, 1985, p.77-85.

4. Ninagawa K.,Yamomoto I.,Yamashita Y.,Wada T.,Sakai H. and Fuji S.- Comparison of ESR with TL for fossil calcite shells., ESR dating and dosimetry, ed. M.Ikeya, Ionics, Tokyo, 1985, p.105-114.

5. Zeller E.S.- Use of electron spin resonanse for measurement of natural radiation damage., Thermoluminescence of geological materials, ed.MacDougall D.J.,Acad.Press, London, 1968, p.271-279.

6. Yokoyama Y.,Falgueres C.and Quageber J.P.- ESR dating of sediment baked by lava flows: comparison of paleo-doses for Al and Ti centers., ESR dating and dosimetry ed. M. Ikeya, Ionics, Tokyo, 1985, p.197-204.

7. Griscom D.L.- The physics of SiO and its interfaces., Pergamon Press, New-York, 1978.

8. Nambi K.S.V. and Sankran A.V.- ESR dating of laterite of basaltic origin., ESR dating and dosimetry ed. M. Ikeya, Ionics, Tokyo, 1985, p.175-180.

9. Rodas Duran J.E. ,Panceri H. and Mascarenhas S.- ESR dosimetry of irradiated human teeth., ESR dating and dosimetry ed. M. Ikeya, Ionics, Tokyo, 1985, p.391-396.

10. Tatsumi-Miyajima J. and Okajima S.- ESR dosimetry using human teeth enamel., ESR dating and dosimetry ed. M. Ikeya, Ionics, Tokyo, 1985, p.397-405.

11. Hoshi M.,Sawada S.,Ikeya M. and Miki T.- ESR dosimetry for Hiroshima A-bomb survivors., ESR dating and dosimetry ed. M. Ikeya, Ionics, Tokyo, 1985, p.407-414.

12. Wagner G.A.- Application of TLD for dating., Applied thermoluminescence dosimetry, ed. M. O. Berhofer and A. Sharmann, Adam Hilger, Bristol, 1979, p.347-359.

13. Aitken M.J.- Physics and archaelogy, Oxford, Clarendon Press, 1974.

14. Loewe W.E.- Initial radiations from tactical nuclear weapons., Nucl. Tech., 1984, v.70, 274-284.

15. Итоговый доклад МКГЯБ о совещании по рассмотрению причин и последствий аварии в Чернобыле, Вена, 30 авг. - 5.сент. 1986г.- Международное Агентство по Атомной Энергии. Генеральная конференция, GC(SPL.1)/3,24 sept.1986.

16. Ikeya M., Miyajima J. and Okajima S.- ESR dosimetry atomic bomb survivors using shell butons and tool enamel., Jap. J. Appl. Phys., 1984, v.23, L697-L699.

17. Molodkov A. and Huett G.,- ESR dating of subfossil shells: some refinements., ESR dating and dosimetry ed. M. Ikeya, Ionics, Tokyo, 1985, p.145-155.

APPLICATION OF COVARIANCES IN THE EVALUATION OF DOSIMETRY REACTION EXCITATION FUNCTIONS

S. TAGESEN
Institut für Radiumforschung und Kernphysik,
University of Vienna,
Vienna, Austria

Abstract

Application of the least squares method to the evaluations of excitation functions is considered for the cases of absolute, ratio and shape measurements. Updating of existing evaluations because of new measurement results is also described. A practical example for demonstration is given.

1. Introduction

Gathering the data for an evaluation of a dosimetry reaction excitation function is already a quite troublesome procedure. The "additional" effort of thoroughly extracting covariance information is often considered unnecessary. It is not yet commonly realized that neglecting correlations will certainly produce unreliable uncertainty estimates if evaluated data enter into subsequent calculations. As we shall see later on, even the result of an evaluation itself may be different for the "normal" weighted average and a procedure including covariances.

To underline the importance of including correlations and to provide some introductory information on the procedure, let us consider a standard experiment and perform a simplified evaluation:

Supposed 3 foils of different elements i, containing N_i nuclei each, were irradiated together in a common neutron field Φ. The induced activity has subsequently been measured with a detector with efficiency ε_i for the respective characteristic radiation.

The number of counts detected, C_i, is

$$C_i = N_i . \sigma_i . \Phi . \varepsilon_i . f_i \qquad (1)$$

where f_i represents a normalization factor, containing all other corrections except the ones given explicitly. Inverting this formula gives the relation for the desired cross section σ_i

$$\sigma_i = C_i \; / \; (N_i . \Phi . \varepsilon_i . f_i) \qquad (2)$$

For simplicity we shall assume no uncertainty in N_i and f_i and then set up a table of uncertainty contributions

foil #	1	2	3
uncertainty component			
C	0.5 %	1.0 %	0.3 %
ε	1.6 %	2.2 %	1.3 %
Φ	2.0 %	2.0 %	2.0 %

(3)

where the counting uncertainty is purely statistical, the efficiency uncertainty is partially correlated (e.g., due to a common calibration source, Eu) and the neutron flux uncertainty is completely correlated. For the moment without any explanation, I state correlations of

$$\text{corr}\,(\varepsilon_1,\varepsilon_2) = 80\ \% \ , \ \text{corr}\,(\varepsilon_1,\varepsilon_3) = 50\ \% \ , \ \text{corr}\,(\varepsilon_2,\varepsilon_3) = 60\ \% \qquad (4)$$

Our relative covariance matrix $\bar{V}$ is then composed in the following way

$$\begin{matrix} & \sigma_1 & \sigma_2 & \sigma_3 \end{matrix}$$

$$\begin{matrix} \sigma_1 & \left[(0.5)^2+(1.6)^2+(2.0)^2\right] & & \\ \sigma_2 & \left[1.6*2.2*0.8+2.0*2.0\right] & \left[(1.0)^2+(2.2)^2+(2.0)^2\right] & \\ \sigma_3 & \left[1.6*1.3*0.5+2.0*2.0\right] & \left[2.2*1.3*0.6+2.0*2.0\right] & \left[(0.3)^2+(1.3)^2+(2.0)^2\right] \end{matrix} \qquad (5)$$

which leads to

$$V = \begin{pmatrix} 6.81 & & \\ 6.82 & 9.84 & \\ 5.04 & 5.72 & 5.78 \end{pmatrix} \qquad (6)$$

since the relative uncertainty is

$$\frac{\Delta\sigma_i}{\sigma_i} = \sqrt{v_{ii}} \qquad (7)$$

and the correlation is

$$c_{ik} = \frac{v_{ik}}{\sqrt{v_{ii} . v_{kk}}} \qquad (8)$$

we get as final result a correlation matrix of

$$\begin{array}{lll} \sigma_1 \;+\!-\; 2.61\,\% & \left(\begin{array}{lll} 1.00 & & \\ 0.83 & 1.00 & \\ 0.80 & 0.76 & 1.00 \end{array}\right. & \left.\begin{array}{l} \\ \\ \end{array}\right) \\ \sigma_2 \;+\!-\; 3.14\,\% & & \\ \sigma_3 \;+\!-\; 2.40\,\% & & \end{array} \qquad (9)$$

Up to now there seems to be no difference between our results and simply summing the squared uncertainty contributions as usual. The correlation matrix looks impressive, but what is its value?

Supposed, you or somebody else have to decide, whether a certain project poses an acceptable or unacceptable risk. To point out the difference, let us assume, that the cross-sections enter into the risk calculation in two different functional relationships:

a. as a product
b. as a quotient

Following common practices, uncertainty propagation is the same in both cases, namely

$$\Delta \text{ product} = \Delta \text{ quotient} = \sqrt{\left(\frac{\Delta\sigma_1}{\sigma_1}\right)^2 + \left(\frac{\Delta\sigma_2}{\sigma_2}\right)^2}$$

$$= \sqrt{V_{11} + V_{22}} = 4.08\,\% \qquad (10)$$

Taking into account the existing correlations leads, however, to a different result

$$\frac{\Delta f}{f} = \sqrt{v_{11} + v_{22} \pm 2 * v_{12}} \qquad (11)$$

where the + sign applies for the product and the - sign for the quotient. Hence the correct uncertainty estimate is

product: 5.5 % quotient: 1.74 % (12)

which might very well change an unacceptable risk to an acceptable one or vice versa.

Since results of evaluations may enter into much more complicated calculations, it is impossible to generally predict the influence of neglecting correlations. The preceding realistic example should, however, provide sufficient evidence to justify the additional effort.

2. The evaluation procedure

The following block diagram (fig. 1) outlines the general steps of an evaluation. Central part is box 3, which merges the original measured

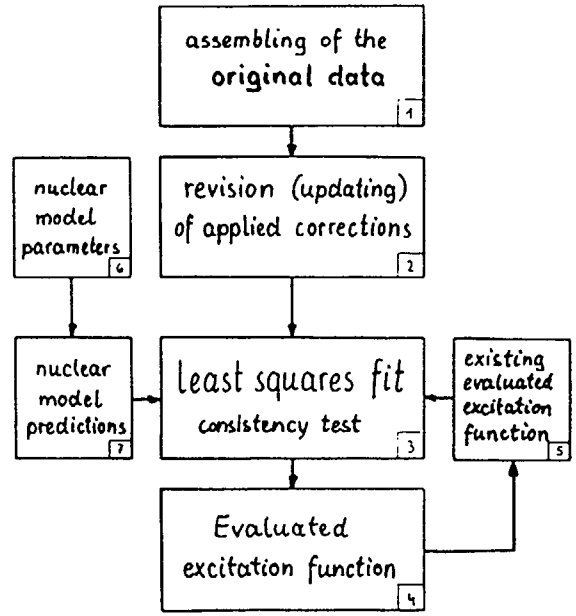

Fig.1
The evaluation procedure

data into an evaluated excitation function (box 4), providing at the same time information on consistency of the input data set(s). Casually, it might be necessary to "bridge" energy regions where no measurements exist, by including nuclear model predictions. In such cases, the calculated cross sections (box 6) have to be subject to the same preparatory procedure as the measured data to provide a means of uncertainty and correlation predictions for the result of the nuclear model calculations.

Equally well, an existing earlier evaluation result could be "updated" by new measurements. This would, however, only be efficient if the existing evaluation contained predominantly carefully prepeared and correctly treated data and provided the necessary uncertainty and correlation information. For all of these possibilities there exist adequate procedures, which will be presented in the following sections.

3. Preparing the input to an evaluation

The general way of calculating a reaction cross section from measured count rates C of some induced radiation with some added background b can be expressed by the following formula

$$\sigma_x(E) = \frac{C_x(E) - b_x - \sum_i b_{xi}(E)}{C_n(E) - b_n - \sum_i b_{ni}(E)} \cdot \prod_k a_k \cdot \prod_j f_j(E) \qquad (13)$$

The factors a_k denote energy independent corrections (e.g. branching ratios), while the $f_j(E)$ represent the energy dependent corrections (e.g. absorption corrections). The subscript n in the denominator applies to "absolute" measurements with some kind of neutron monitor. It has to be replaced by y for any reference ("standard") reaction in case of "ratio" measurements.

$$n \to y, \sigma_x(E) \to R_{xy}(E) = \frac{\sigma_x(E)}{\sigma_y(E)} \qquad (14)$$

The third type, "shape" measurements, are characterized by an undetermined energy independent faktor K

$$S(E) = K \cdot \sigma(E), \quad K = \prod_k a_k \qquad (15)$$

The task of preparing data for an evaluation could then roughly be described by the following "flowchart":

- whenever possible, try to get the actually measured quantities (original publication)
- extract all relevant factors (corrections) according to formula (13) and their uncertainties. An uncertainty contribution should be considered "important", if it adds more then a few percent to the total uncertainty.
- verify the reported uncertainty definitions and change the reported uncertainty to one standard deviation, if necessary
- review the corrections for recently published updates and include such improvements, if any.
- set up a table (fig. 2) of data and all individual uncertainty contributions.

Energy	En.-Unc.	En.-Res.	Data	Unc. stat.	correlated uncertainty components 2	3	...	l	...	L	total uncertainty
E_1	ΔE_1	$E_R(E_1)$	σ_1	u_{11}	u_{12}	u_{13}	..	u_{1l}	...	u_{1L}	$\Delta\sigma_1$
E_2	ΔE_2	$E_R(E_2)$	σ_2	u_{21}	u_{22}	u_{23}		u_{2l}	.	u_{2L}	$\Delta\sigma_2$
	.		.					.		.	
E_i	ΔE_i	$E_R(E_i)$	σ_i	u_{i1}	u_{i2}	u_{i3}		u_{il}	..	u_{iL}	$\Delta\sigma_i$
		.		.	.						.
E_n	ΔE_n	$E_R(E_n)$	σ_n	u_{n1}	u_{n2}	u_{n3}	.	u_{nl}	....	u_{nL}	$\Delta\sigma_n$

Fig. 2: Presentation of measured quantities and associated uncertainty contributions

The following proposal of a "questionnaire for data uncertainty analysis" may serve as a helpful guideline.

QUESTIONNAIRE FOR DATA UNCERTAINTY ANALYSIS

Please specify uncertainties at one standard deviation confidence limits in absolute units or as a percentage of the data value.

☐ Absolute units ☐ Percentage

Uncertainty origin — Uncertainty value — Correlation

1. Uncorrelated
   Statistical counting uncertainty plus other contributions specific to each measured point

2. Correlated uncertainties

   a) Sample related uncertainties

      Sample thickness (weight)
      Geometric effects
      Multiple scattering
      Self absorption
      Isotopic abundance (chemical purity)

   b) Detected radiation/particle uncertainties

      Half-life (measurement timing)
      Intensity (branching ratios)
      Background

   c) Detector related uncertainties

      Efficiency
      Calibration

   d) Normalisation uncertainties

      Monitor cross section
      Neutron flux determinations (including corrections for variations during time of irradiation)

   e) Others

   Total correlated uncertainty

   (quadratic sum of 2a —— 2e)

A special kind of uncertainty is the cross section uncertainty caused by energy uncertainty, due to

- the energy dependence of the cross section
- the energy dependence of corrections $f_i(E)$

It can be expressed as

$$\Delta\sigma_E^2 = \left(\frac{\partial\sigma}{\partial\varepsilon}\right)^2 \Delta\varepsilon^2 + \sum_i \left(\frac{\partial\sigma}{\partial f_i}\right)^2 \left(\frac{\partial f_i}{\partial\varepsilon}\right)^2 \Delta\varepsilon^2 + 2\sum_{i,k} \frac{\partial\sigma}{\partial f_i}\frac{\partial f_i}{\partial\varepsilon}\frac{\partial\sigma}{\partial f_k}\frac{\partial f_k}{\partial\varepsilon}\Delta\varepsilon^2 \qquad (16)$$

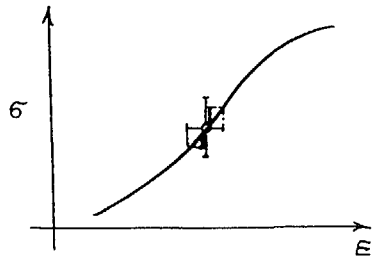

At least the first term, which is of first order, should always be taken into account. The other terms are of second order and are likely to be of negligible influence, compared to the rest of the uncertainty contributions.

Once this table of uncertainty components has been properly compiled, most of the work is done. The construction of the covariance matrix $\overline{\overline{V}}$ is now an almost straightforward task. Its elements are given by

$$v_{ij} = \sum_{\ell=1}^{L} s_{ij\ell} \cdot u_{i\ell} \cdot u_{j\ell} \qquad (i,j = 1..n) \qquad (17)$$

The $s_{ij\ell}$ are parameters characterizing the degree of correlation. The diagonal elements are of course

$$s_{ii\ell} = 1 \qquad (i = 1..n,\ \ell = 1..L)\ , \qquad (18)$$

the off diagonal elements could be within the range

$$-1 =< s_{ij\ell} <= +1 \qquad (19)$$

This would, however, pose the problem of being obliged to report an enormous number of such coefficients. Is there really a necessity for coefficients $s_{ij\ell} \neq \pm 1$? To answer this question, let us reconsider expressions (3) and (4) from our introductory excample.

Partial correlations arise if the uncertainty of a single contribution is composed as

$$u_{i,total} = \sqrt{(u_{i,statistical})^2 + (u_{i,correlated})^2} \qquad (20)$$

because the correlation between any two (u_i, u_j) in a set is given by

$$corr_{ij} = \frac{(u_{i,corr}) * (u_{j,corr})}{(u_{i,total}) * (u_{j,total})} \qquad (21)$$

Making use of these relations (20), (21) we can decompose $u_{i,total}$ into its constituents and sum up all the statistical parts into column 5 of the uncertainty table. So, there are only completely correlated contributions left for u_{i2} to u_{iL}, which leads to $s_{ij\ell} = \pm 1$ for all contributions.

To re-execute our example (3) we would start from

	1	2	3	
ε				stat.
	x	y	z	corr.

corr (1,2) = 80 %
corr (1,3) = 50 %
corr (2,3) = 60 %

Due to (21), we have

x*y /(1.6*2.2) = 0.8 , x*z /(1.6*1.3) = 0.5 , y*z /(2.2*1.3) = 0.6

Solving these equations and applying (20) to the result leads to

ε	0.85	0.19	1.06	stat.
	1.31	2.15	0.80	corr.

which would have been the proper way of reporting the uncertainty contributions.

In view of this situation, I recommend authors the following:

1. Try to keep correlated and uncorrelated uncertainty contributions strictly separated. This will make the life of evaluators much easier.

2. Do not report a covariance matrix only, without giving the complete "uncertainty table". This would definitely prohibit any future improvements, when updates on decay data, say, became available.

4. The least squares method

The following chapter recalls the principles of the least squares method in matrix formalism. The formulae are given without proof. For more details the reader is referred to the preceding lecture on "Basic concepts of measurement uncertainties" and "Basic principles of covariances", given by Dr. W. Zijp, or to the texts from the literature list.

The least squares method constitutes a procedure of determining a "best value" of a solution vector

$$\vec{X} (x_1, x_2, \ldots , x_I) \qquad (22)$$

from a set of available quantities (measured values)

$$\vec{Y} (y_1, y_2, \ldots , y_M) \qquad M > I \qquad (23)$$

which are related by a system of approximate equations

$$\begin{aligned} y_1 &\cong a_{11}x_1 + a_{12}x_2 + \ldots\ldots + a_{1I}x_I \\ &\vdots \\ y_k &\cong a_{k1}x_1 + a_{k2}x_2 + \ldots\ldots + a_{kI}x_I \\ &\vdots \\ y_M &\cong a_{M1}x_1 + a_{M2}x_2 + \ldots\ldots + a_{MI}x_I \end{aligned} \qquad (24)$$

An alternative common representation would be

$$y_k \cong \sum_{i=1}^{I} a_{ki}x_i \qquad (k = 1 \ldots M) \qquad (24a)$$

In matrix notation this appears as

$$\vec{Y} \cong \bar{A} \cdot \vec{X} \qquad (25)$$

Uncertainties for $\vec{Y}$ and their correlations are given in a square covariance matrix $\bar{V}$, which is of dimension M. The diagonal elements are the squared uncertainties (1 standard deviation) of the measurements.

The best solution vector $\vec{X}$ is the one which minimizes χ^2, given by

$$\chi^2 = (\vec{Y} - \bar{A} \cdot \vec{X})^T \cdot \bar{V}^{-1} \cdot (\vec{Y} - \bar{A} \cdot \vec{X}) \qquad (26)$$

Superscript T denotes "transpose", $\bar{V}^{-1}$ is the inverse of the covariance matrix. If there were no correlations, this would be exactly the weighted sum of squared deviations from the best solution.

The least squares solution minimizing χ^2 is given by

$$\vec{X} = (\bar{A}^T \cdot \bar{V}^{-1} \cdot \bar{A})^{-1} \cdot \bar{A}^T \cdot \bar{V}^{-1} \cdot \vec{Y} \qquad (27)$$

where the first part of the expression

$$(\bar{A}^T \ \bar{V}^{-1} \ \bar{A})^{-1} \ =: \ \bar{C} \qquad (28)$$

constitutes the covariance matrix for the solution $\vec{X}$.

To see more clearly how this looks in practice, we shall calculate a simple example in detail:

Given two measurements of a single cross section σ with an estimated correlation of 50 %

$$\sigma_1 = 1.85 \text{ b} \pm 6 \%$$
$$\sigma_2 = 1.94 \text{ b} \pm 8 \%$$

The measurement vector (23) is therefore

$$\vec{Y} (\sigma_1, \sigma_2)$$

the solution vector (22) contains of course just 1 element

$$\vec{X} (\sigma)$$

The system of approximate equations (24) then reads

$$\sigma_1 \cong 1 * \sigma$$
$$\sigma_2 \cong 1 * \sigma$$

with a coefficient matrix

$$\bar{A} = \begin{pmatrix} 1 \\ 1 \end{pmatrix}$$

The covariance matrix is calculated as

$$\bar{V} = \begin{pmatrix} (1.85*0.06)^2 & (1.85*0.06*1.94*0.08*0.5) \\ (1.85*0.06*1.94*0.08*0.5) & (1.94*0.08)^2 \end{pmatrix}$$

To proceed with the formalism, we have

$$\bar{V} = \begin{pmatrix} .01232 & .008614 \\ .008614 & .02409 \end{pmatrix} \qquad \text{and} \qquad \bar{V}^{-1} = \begin{pmatrix} 108.2 & -38.7 \\ -38.7 & 55.35 \end{pmatrix}$$

and $(\bar{A}^T \cdot \bar{V}^{-1} \cdot \bar{A}) = (1 , 1) \begin{pmatrix} 108.2 & -38.7 \\ -38.7 & 55.35 \end{pmatrix} \begin{pmatrix} 1 \\ 1 \end{pmatrix}$

$$= (69.5 \quad 16.65) \begin{pmatrix} 1 \\ 1 \end{pmatrix} = 86.15 = \bar{C}^{-1}$$

The "covariance matrix" of the solution, which in this case contains a single element only, is therefore

$$\bar{C} = 0.01161 = (\Delta\sigma)^2$$

and the solution is

$$\sigma = \bar{C} \cdot \bar{A}^T \cdot \bar{V}^{-1} \cdot \vec{Y} = 0.01161 \cdot (69.5 , 16.65) \begin{pmatrix} 1.85 \\ 1.94 \end{pmatrix}$$

$$= \underline{1.868 \pm 0.1077 \text{ b}} \quad (= \pm 5.8 \%)$$

The "normal" weighted average, instead, would have been

$$\bar{\sigma} = \frac{\frac{\sigma_1}{(\Delta\sigma_1)^2} + \frac{\sigma_2}{(\Delta\sigma_2)^2}}{\frac{1}{(\Delta\sigma_1)^2} + \frac{1}{(\Delta\sigma_2)^2}} = \underline{1.880 \pm 4.8\ \%}$$

which differs in the solution as well as in the uncertainty.

5. Application of the least squares method to the evaluation of an excitation function

In the following three subsections I shall gradually step through evaluation problems of increasing complexity, to illustrate the application and the principal simplicity of this very general method.

5.1. Evaluation of several sets of measured absolute cross sections.

The following fig.3 may serve as a realistic example to specify the problem.

Given a number M of cross section measurements $s_j(E)$, originating from K different experiments (resp. authors). I shall assume that we have already done all the preparatory work discussed in chapter 3. Thus there is a table of uncertainty components according to fig.2 available.

The solution we are looking for, is a representation of the excitation function by a series of I "evaluated group cross sections" σ_i, representing average cross section values within certain energy limits. The decision on number and size of these energy groups is

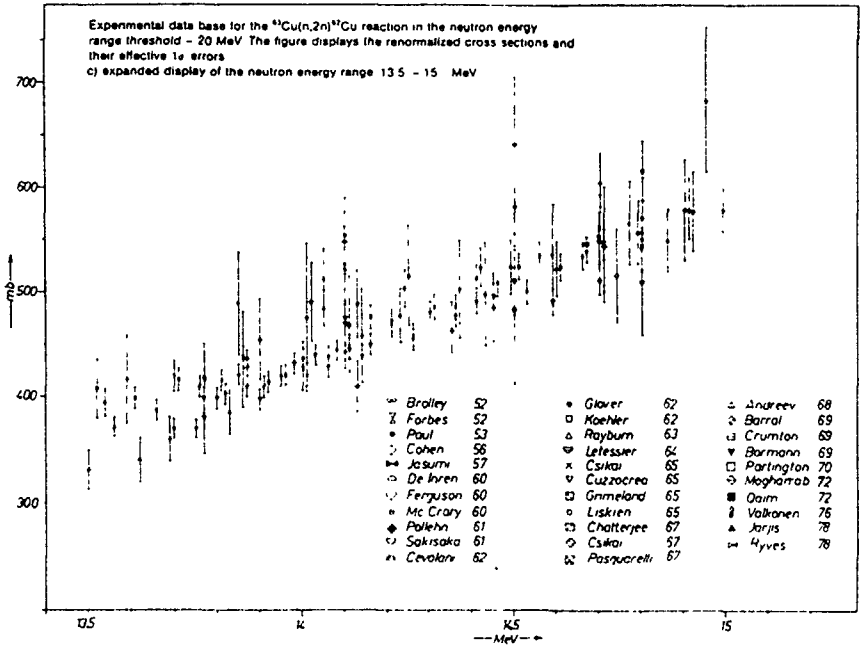

Fig.3 Example of a data base for an evaluation

always a compromise between various desirable features. Two of the most important would be

- for each group several data points, preferably originating from different experiments, should be available
- the cross section within the group limits should be approximately constant, i.e., possibly not change more then 20 %.

Further criteria might be the experimental neutron energy resolution or aspects like the "feasibility" of the computing problem.

Formally we therefore represent our problem as indicated by fig.4.

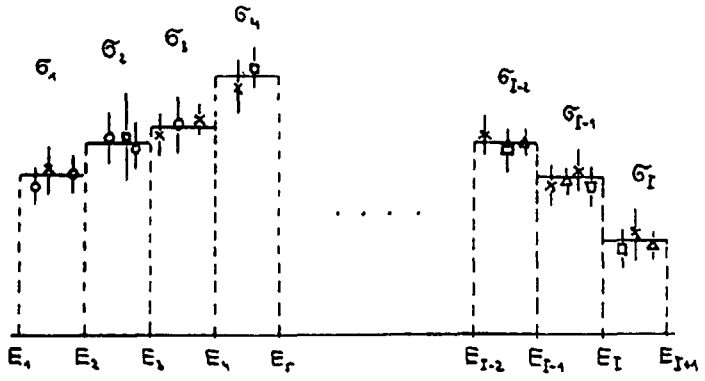

Fig.4 Grouping of data into energy intervals

Since we had to admit a certain cross section change inside any group, we have to take into account the slope of the excitation function by renormalizing the experimental data to group center energies previous to evaluation (fig.5).

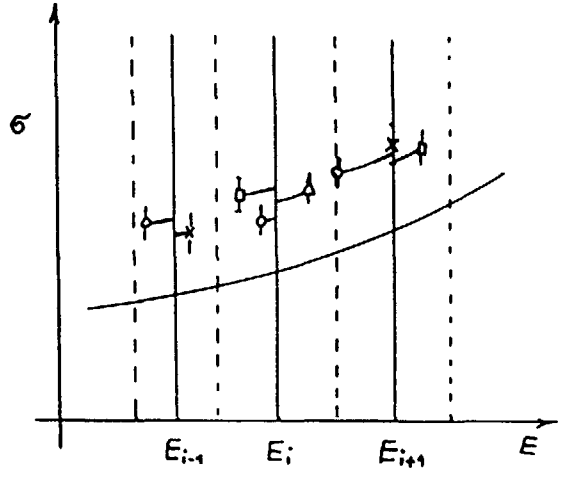

Fig. 5 A priori or 'preliminary' excitation function.

We may then write down the following system of approximate linear equations

$$
\begin{aligned}
s_1 &\cong a_{11}\sigma_1 + a_{12}\sigma_2 + \ldots\ldots\ldots\ldots + a_{1I}\sigma_I \\
&\vdots \\
s_k &\cong a_{k1}\sigma_1 + \ldots\ldots + a_{kj}\sigma_j + \ldots\ldots + a_{kI}\sigma_I \qquad (29) \\
&\vdots \\
s_M &\cong a_{M1}\sigma_1 + \ldots\ldots\ldots\ldots\ldots\ldots + a_{MI}\sigma_I
\end{aligned}
$$

Note that each of the equations contains only one coefficient $a_{kj} = 1$, all the rest are zeros ! This is due to the fact that each measured cross section belongs to exactly one energy group. Some important precautions may further help to keep the necessary amount of calculations within manageable limits:

- average all data from a given experiment which fall into the same energy group to a single value
  consequently each experiment will contribute a number of data points $\leq I$
  consequently the dimension of the associated covariance matrix will be $\leq I$.

- data originating from different experiments will quite often have no or negligible correlations
  grouping of the data into K mutually uncorrelated sets will facilitate the necessary calculations.

$$\vec{S} = (S_1(s_{11},..,s_{1M_1}), \ldots, S_K(s_{K1},..,s_{KM_K}))$$

$$\sum_{\ell=1}^{K} M_\ell = M \qquad M_\ell \leq I \quad (\ell = 1 \ldots K)$$

The dimension of the result covariance matrix will be the number of chosen energy groups I. The dimension of the data covariance matrix

equals in principle the number of available data points M. With properly grouped data sets it appears, however, as ensemble of much smaller submatrices, which may be inverted separately.

$$\bar{V} = \begin{pmatrix} [\bar{V}_1] & & & 0 \\ & [\bar{V}_2] & & \\ & & [\bar{V}_3] & \\ & & & \ddots \\ 0 & & & [\bar{V}_K] \end{pmatrix}$$

The calculations would then be carried out according to the following scheme:

$$\bar{V}^{-1} = \begin{pmatrix} \bar{V}_1^{-1} & & & \\ & \bar{V}_2^{-1} & & \\ & & \ddots & \\ & & & \bar{V}_K^{-1} \end{pmatrix}, \quad \bar{A} = \begin{pmatrix} \bar{A}_1 \\ \bar{A}_2 \\ \vdots \\ \bar{A}_K \end{pmatrix}$$

$$\vec{\sigma} = \bar{C} \cdot \bar{A}^T \cdot \bar{V}^{-1} \cdot \vec{S}$$

$$= \bar{C} \cdot \left(\bar{A}_1^T \cdot \bar{V}_1^{-1} \cdot \vec{S}_1 + \cdots + \bar{A}_K^T \cdot \bar{V}_K^{-1} \cdot \vec{S}_K \right)$$

$$\bar{C}^{-1} = \bar{A}^T \cdot \bar{V}^{-1} \cdot \bar{A}$$

$$= \bar{A}_1^T \cdot \bar{V}_1^{-1} \cdot \bar{A}_1 + \cdots + \bar{A}_K^T \cdot \bar{V}_K^{-1} \cdot \bar{A}_K$$

5.2. Generalization for absolute, ratio and shape measurements

Up to now we have only discussed situations where the measured quantities were connected to the sought evaluated data by a linear relationship. There are, however, numerous cases where not actually the desired cross section but the ratio of two cross sections has been measured, one of which frequently is a so called "standard" or "reference cross section". In principle there is no justification for a distinction of different "classes" of cross sections. It is just common to point out certain excitation functions which appear to be known with less uncertainty. As we shall see, a correct evaluation procedure will automatically pay regard to this fact.

Instead of measured absolute cross sections, our input data now are M measured quantities m_j which are some functions $f(\vec{\sigma})$ of the sought cross section set $\vec{\sigma}(\sigma_1,\ldots,\sigma_I)$. To match this problem to our proven least squares formalism we expand the given function into a truncated Taylor's series

$$f(\vec{\sigma}) \approx f(\vec{\sigma}_0) + \sum_{i=1}^{I} \left(\frac{\partial f}{\partial \sigma_i} \right)_{\sigma_{0i}} \cdot (\sigma_i - \sigma_{0i}) \qquad (30)$$

which is justified in the vicinity of a reasonable estimate $\vec{\sigma}_0$. After performing the following substitutions

$$\sigma_i - \sigma_{0i} = x_i \quad , \qquad f_j(\vec{\sigma}) - f_j(\vec{\sigma}_0) = y_j$$

$$\frac{\partial f_j}{\partial \sigma_i} = a_{ij} \qquad (31)$$

we recognize our well known system of approximate equations (24) or (29) resp.

$$y_j \approx \sum_{i=1}^{I} a_{ij} x_i \qquad (j = 1 \ldots M) \tag{32}$$

The only difference is that x_i now represents a "correction" to the estimate $\vec{\sigma}_0$, y_j the deviation of our measured quantities from a "prediction" given by applying the function f to the cross section estimate, and the coefficients a_{ij} are the partial derivatives with respect to the sought cross sections. Notice again, that there are now usually one or two, at most three nonzero coefficients in any of the equations.

If the measured quantity would be an absolute cross section, the coefficient would be 1 as before. In case of a ratio σ_1/σ_2 there would be two coefficients, namely $1/\sigma_2$ and $-\sigma_1/\sigma_2^2$. In case of a shape measurement there would be an additional unknown energy independent factor. $f_j = a\sigma_i$, hence there are two coefficients σ_i and a.

A practical example covering both chapters 5.2. and 5.3. will be given in chapter 6.

5.3. Updating of an existing evaluation with new measurements

As we have seen in the previous subchapter 5.2. in the general case there is a need for an a priori estimate which will be "corrected" in the course of the evaluation. In fact, this is exactly what we would like to do in the case where additional measurements became available for an already existing evaluation. The difference is that possibly the number of new measurements M_n would be less then the number of existing energy groups I. This would lead to an underdetermined system of approximate linear equations. This apparent handicap can, however, be overcome by taking the existing data including their covariance matrix $\bar{C}_0$ plus the new data with their covariance matrix $\bar{V}_m$ as input to the evaluation.

The system of approximate equations appears as

$$\begin{aligned}
\sigma_{01}-\sigma_{01} &= 1*(\sigma_{11}-\sigma_{01}) + 0 \ldots\ldots\ldots\ldots\ldots 0 \\
\sigma_{02}-\sigma_{02} &= 0 + 1*(\sigma_{12}-\sigma_{02}) + 0 \ldots\ldots\ldots 0 \\
&\vdots \\
\sigma_{0I}-\sigma_{0I} &= 0 \ldots\ldots\ldots\ldots 0 + 1*(\sigma_{1I}-\sigma_{0I})
\end{aligned} \tag{33}$$

$$f_{I+1}(\vec{\sigma}) - f_{I+1}(\vec{\sigma}_0) = a_{I+1,1}(\sigma_{11}-\sigma_{01}) + \ldots\ldots\ldots + a_{I+1,I}(\sigma_{1I}-\sigma_{0I})$$

$$\vdots$$

$$f_{I+M_n}(\vec{\sigma}) - f_{I+M_n}(\vec{\sigma}_0) = a_{I+M_n,1}(\sigma_{11}-\sigma_{01}) + \ldots\ldots + a_{I+M_n,I}(\sigma_{1I}-\sigma_{0I})$$

The procedure leading to the sought updating corrections is then as usual with some advantageous details:

$$\bar{A} = \begin{bmatrix} 1 & & 0 \\ & \ddots & \\ 0 & & 1 \\ & \bar{A}_m & \end{bmatrix} \qquad \vec{Y} = \begin{bmatrix} 0 \\ \vdots \\ 0 \\ \vec{Y}_m \end{bmatrix}$$

$$\vec{X} = \bar{C}_1 \cdot \begin{bmatrix} \bar{A}_0 \\ \bar{A}_m \end{bmatrix}^T \cdot \begin{bmatrix} \bar{C}_0^{-1} & 0 \\ 0 & \bar{V}_m^{-1} \end{bmatrix} \cdot \begin{bmatrix} \vec{0} \\ \vec{Y}_m \end{bmatrix} = \bar{C}_1 \cdot \bar{A}_m^T \cdot \bar{V}_m^{-1} \cdot \vec{Y}_m$$

$$\bar{C}_1^{-1} = \begin{bmatrix} \bar{A}_0 \\ \bar{A}_m \end{bmatrix}^T \cdot \begin{bmatrix} \bar{C}_0^{-1} & 0 \\ 0 & \bar{V}_m^{-1} \end{bmatrix} \cdot \begin{bmatrix} \bar{A}_0 \\ \bar{A}_m \end{bmatrix} = \bar{C}_0^{-1} + \bar{A}_m^T \cdot \bar{V}_m^{-1} \cdot \bar{A}_m$$

$$\underline{\sigma_{1i} = \sigma_{0i}(1 + x_i)}$$

6. A practical example to demonstrate the outlined procedures

To demonstrate some of the essential points we have been talking about in a practical example I assume that there were two sets of data with their covariance matrices already available:

a. ^{27}Al (n,α)

E_n (MeV)	σ (mb)	std.dev. (%)	
13.6	123.3	4.2	$\overline{V}_{Al}$
14.0	120.6	5.0	
14.6	114.0	4.8	

b. ^{65}Cu (n,2n)

13.6	832.0	5.5	$\overline{V}_{Cu}$
14.0	891.9	6.3	
14.6	959.6	5.8	

A new set of ratio measurements $R = \sigma_{Cu}/\sigma_{Al}$ were to be combined with these two in an evaluation. Since the incident neutron energies in the ratio measurement do not correspond to the ones in the existing sets we have to decide on some "grouping" at new energies E_n', which consequently requires also renormalization of the ratios to the new energies according to the "slope" in the actually measured set, leading to new ratios R'. Both of these corrections are already entered in the following table of the new measurements:

E_n	R	E_n'	R'	std.dev. (%)	
13.55	6.62		6.70	2.3	
13.62	6.68	13.6	6.65	2.9	
13.69	6.98		6.83	2.5	
13.92	7.18		7.31	2.4	
14.05	7.58	14.0	7.50	2.2	V_R
14.53	8.12		8.24	2.8	
14.61	8.44	14.6	8.42	2.5	
14.68	8.67		8.53	2.0	

According to (33) our coefficient matrix appears as

$$
\begin{array}{c}
\begin{array}{cccccc} \sigma_1(Al) & \sigma_2(Al) & \sigma_3(Al) & \sigma_1(Cu) & \sigma_2(Cu) & \sigma_3(Cu) \end{array} \\
\left(\begin{array}{cccccc}
\left(\begin{array}{ccc} 1 & 0 & 0 \\ 0 & 1 & 0 \\ 0 & 0 & 1 \end{array}\right) & & & \left(\begin{array}{ccc} 1 & 0 & 0 \\ 0 & 1 & 0 \\ 0 & 0 & 1 \end{array}\right) & & \\
-\sigma_1 C/(\sigma_1 A)^2 & 0 & 0 & 1/\sigma_1 A & 0 & 0 \\
\text{-"-} & 0 & 0 & \text{-"-} & 0 & 0 \\
\text{-"-} & 0 & 0 & \text{-"-} & 0 & 0 \\
0 & -\sigma_2 C/(\sigma_2 A)^2 & 0 & 0 & 1/\sigma_2 A & 0 \\
0 & \text{-"-} & 0 & 0 & \text{-"-} & 0 \\
0 & 0 & -\sigma_3 C/(\sigma_3 A)^2 & 0 & 0 & 1/\sigma_3 A \\
0 & 0 & \text{-"-} & 0 & 0 & \text{-"-} \\
0 & 0 & \text{-"-} & 0 & 0 & \text{-"-}
\end{array}\right)
\end{array}
$$

and the covariance matrix is composed of three submatrices of dimension 3, 3 and 8

$$
\left(\begin{array}{ccc}
\left(V_{Al}\right) & & 0 \\
& \left(V_{Cu}\right) & \\
0 & & \left(V_R\right)
\end{array}\right)
$$

Since $\vec{Y}_{Al} = (\vec{0})$ and $\vec{Y}_{Cu} = (\vec{0})$ the solution is

$$\vec{X} = \bar{C}_1 \; \bar{A}_R^T \; \bar{V}_R^{-1} \; \vec{Y}_R$$

and the result covariance matrix is derived as

$$\bar{C}_1^{-1} = \begin{pmatrix} \left(\bar{V}_{Al}^{-1}\right) & \\ & \left(\bar{V}_{Cu}^{-1}\right) \end{pmatrix} + \bar{A}_R^T \, \bar{V}_R^{-1} \, \bar{A}_R$$

The second term in the sum now adds nonzero off diagonal elements, expressing correlations between the excitation functions of Al and Cu.

The final result is

E_n (MeV)	σ_{Al} (mb)	std.dev.(%)	σ_{Cu} (mb)	std.dev.(%)
13.6	123.2	3.4	832.3	3.5
14.0	120.5	3.9	894.4	4.0
14.6	113.9	3.7	961.6	3.8

with correlation matrix given in %

13.6	100						↑
14.0	82	100					^{27}Al
14.6	89	79	100				↓
13.6	87	72	80	100			↑
14.0	76	90	75	76	100		^{65}Cu
14.6	83	76	90	86	82	100	↓
E_n	13.6	14.0	14.6	13.6	14.0	14.6	
	←	^{27}Al	→	←	^{65}Cu	→	

The whole formalism may, of course, equally well be formulated in a relative notation. Compare for example the publication by Poenitz (lit.4). In this case the covariance matrix would be replaced by the correlation matrix which is much easier to interpret, since its elements are all in the range -1 to +1 and therefore give an immediate reference to the degree of existing correlations.

Such a representation would also be the suitable way for immediate processing of the uncertainty information contained in the ENDF-B files 33 (lit.11)

SOME BOOKS AND PUBLICATIONS RELATED TO ERROR ANALYSIS AND NUCLEAR DATA EVALUATION

1. S. L. MEYER, "Data Analysis for Scientists and Engineers", John Wiley and Sons, Inc., (1975)
2. S. BRANDT, "Statistical and Computational Methods in Data Analysis", North Holland Publ. Comp., (1970)
3. P. R. BEVINGTON, "Data Reduction and Error Analysis for the Physical Sciences", McGraw-Hill Book Company, (1969)
4. W. P. POENITZ, "Data Interpretation, Objective Evaluation Procedures and Mathematical Techniques for the Evaluation of Energy-Dependent Ratio, Shape and Cross Section Data", Proceedings of the Conference on Nuclear Data Evaluation Methods and Procedures, September 22-25, 1980 at Brookhaven National Laboratory, Report Nos. BNL-NCS-51363 or NEANDC (US)-209, Vol.I., p. 249, (1981)
5. W. MANNHART, "A Small Guide to Generating Covariances of Experimental Data", Report No. PTB-FMRB-84, Physikalisch Technische Bundesanstalt, Braunschweig, (1981)
6. IAEA Specialists' Meeting on Covariance Methods and Practices in the Field of Nuclear Data, Rome, Italy, November 17-19, 1986.
7. F. H. FROEHNER, "Principles and Techniques of Data Evaluation", KFK 4099, Kernforschungszentrum Karlsruhe, F.R. Germany, (1986)
8. D. L. SMITH, "Covariance Matrices and Applications to the Field of Nuclear Data", ANL-NDM-62, Argonne National Laboratory, (1981)

9. H.VONACH and S. TAGESEN, "Evaluation Methods and Procedures with Emphasis on Handling Experimental Data" and references given there, Proceedings of the Brookhaven Conference Sept. 1980 (see ref. 4 above)

10. R. W. PEELE, "Requirements on Experiment Reporting to meet Evaluation Needs", Proceedings of the NEANDC/NEACRP Specialists Meeting on Fast Neutron Fission Cross Sections, June 28-30, 1976, at Argonne National Laboratory, Report Nos. ANL-76-90 or NEANDC (US)-199/L (1976)

11. "Data Formats and Procedures for the Evaluated Nuclear Data File" ENDF/B-V, ENDF-102, edited by R. Kinsey (1979) and revised by B. A. Magurno (1983), Brookhaven National Laboratory

12. D. M. HETRICK and C. Y. FU, "GLUCS: A Generalized Least-Squares Program for Updating Cross-Section Evaluations with Correlated Data Sets", ORNL/TM-7341 (ENDF-303), Oak Ridge Nat.Lab., (1982)

PRINCIPLES, TECHNIQUES AND APPLICATIONS OF SOLID STATE NUCLEAR TRACK DETECTORS

Shi-Lun GUO
Institute of Atomic Energy,
Beijing, China

Abstract

This lecture describes the basic principles, the commonly used techniques and the successful and novel applications of solid state nuclear track detectors as if the listeners are those who are looking for new trends in rapid developing fields and anxious to acquire the necessary information to step into modern research fronts.

1. Introduction

Radiation damage tracks created by fission fragments in mica was first observed by E. C. H. Silk and R. S. Barnes [1] and the etching technique was first described by D. A. Young[2]. But their papers remained comparatively unnoticed. It was the remarkable work of P. B. Price, R. L. Fleischer and R. M. Walker in 1962 [3-7] that put forward a new type of nuclear track detector named solid state nuclear track detector (SSNTD). In their creative work they showed that radiation damage tracks created by heavily ionizing particles in solids could be etched by certain reagents and enlarged to much bigger sizes to become visible under optical microscopes; they discovered that all insulating solids including crystalls, glasses and organic polymers could retain radiation damage tracks; they discovered the capability of solid state nuclear track detectors to identify particle charges [8] and they initiated the research work with these detectors in a variety of fields which include nuclear physics, radiation dosimetry, cosmic ray physics, geology, archaeology and many technical applications [7,9,10]. Their work was followed by many laboratories all over the world and

hundreds of research groups are involved in nuclear track studies and applications. About 4000 papers have been published.

In this course we shall discuss the basic principles, the commonly used techniques and the successful and novel applications of SSNTDS as if the listeners are those who are looking for new trends in rapid developing fields and anxious to acquire the necessary information to step into modern research fronts.

2. Basic Principles of Solid State Nuclear Track Detectors

2.1. Materials of Solid State Nucler Track Detectors

All insulating solids including crystalls, glasses and organic polymers can record radiation damage tracks. Metals and semiconductors with electrical resistivities lower than about 2,000 ohm-cm can not store radiation damage tracks [11]. Table 1 is the list to show the relations of track recording behaviors of some typical materials to their electrical resistivities [11]

TABLE 1. RELATION OF TRACK REGISTRATION TO ELECTRICAL RESISTIVITY

Materials	Resistivity range (Ohm-cm)	Track registration
Insulators:		
Silicate minerals, Alkali halides, insulating glasses, Polymers	10^{20}-10^{6}	Yes
MoS_2	25,000-3,000	Yes
V_2O_5 glass	20,000-2,000	Yes
Germanium, Silicon	2,000-10	No
Metals:		
Aluminum, Copper, Gold, Platinum, Tungsten, Zinc	10^{-4}-10^{-6}	No

TABLE 1 (cont.)

All track recording materials are usually called solid state nuclear track detectors. They can also be divided into natural and man-made solids. More than 150 kinds of minerals, natural and man-made glasses and plastics have been used as nuclear track detectors. They exist in the whole nature: in our living articles, in stones and soils, in the moon and meteorites and so on. Their application fields are as wide as their existences.

2.2 Formation of Radiation Damage Tracks in solids

When a heavily ionizing particle, such as proton, α-particle, heavy ion and fission fragment, enters an insulating solid, the particle loses its energy and creates a long damaged region along its trajectory in the solid. The diameter of the damaged region is about 50 to 100 Å [10]. It can be seen under electron microscopes as shown in Fig. 1. The damaged region is called radiation damage track or latent track, which is composed of interstitial atoms and vacancies in inorganic solids and molecular fragments, free radicals and isolated atoms in organic polymers.

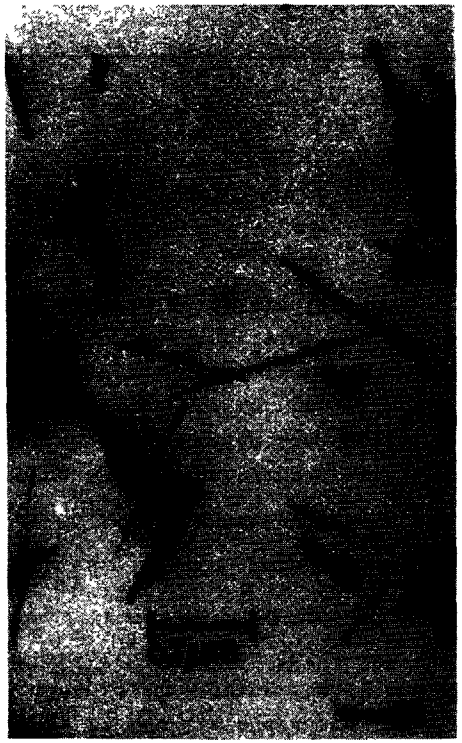

Fig.1. Transmission electron micrograph of fission fragments in mica. These tracks have not been etched and show the diameters of primary radiation damage tracks [10].

2.3. Chemical Etching of Radiation Damage Tracks

When a solid object containing radiation damage tracks is immersed into certain chemical solution (etchant), the damaged materials interact preferentially with the etchant because of their high reactivities and the resultants are dissolved into the solution. The radiation damage regions gradually become hollows along the trajectories of the particles. At the same time the solid matrix material from all surfaces interacts with the etchant(bulk etching) at a speed slower than the damaged materials. These two types of interactions result in the formation of etched tracks in the solid. Because of the bulk etching from the surfaces in the track hollows the diameters of the the tracks become bigger and bigger. When the diameters of the tracks increase to the sizes comparable with the wavelength of light (about 0.5 μm for visible light) the tracks strongly scatter the light , forming dark images in transmitted light or bright images in reflected light, which can be easily seen with optical microscopes as shown in Fig. 2.

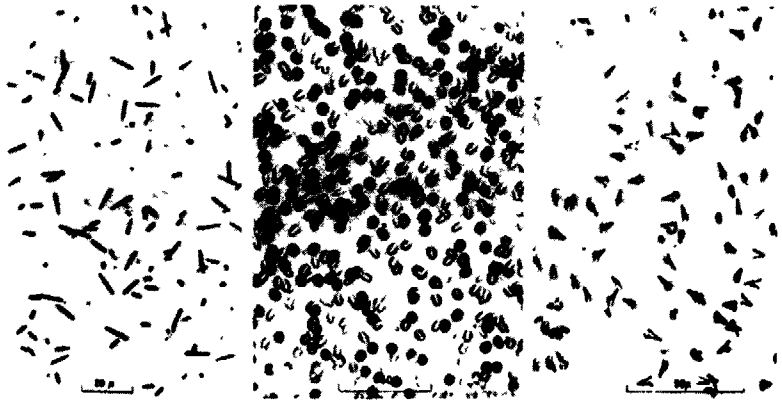

Fig.2. Etched tracks of fission in Polycarbonate foil (left), soda lime glass (middle) and feldspar (right) [10].

A specific solid requires certain etchants to develop particle tracks. For convenience the etching conditions of some commonly used detectors for fission fragments are listed in Table 2.

TABLE 2. ETCHING CONDITIONS OF FISSION FRAGMENTS FOR COMMONLY USED DETECTORS [10, 12]

Material	Etching Conditions
Mica (biotite, $K(Mg, Fe)_3AlSi_3O_{10}(OH)_2$)	20% HF, 1-2 min, 23°C
Mica (Muscovite, $KAl_3Si_3O_{10}(OH)_2$)	48% HF, 10-240 min, 23°C; or 15 N NaOH, 135°C, 5-600 h.
Mica (Phlogopite, Lepidomelane, $KMg_2Al_2Si_3O_{10}(OH)_2$)	48% HF, 1-5 min, 23°C
Olivine ($(Mg, Fe)_2SiO_4$)	1ml H_3PO_4 : 1g oxalic acid: 40g EDTA: 100ml H_2O: 4.5g NaOH (to adjust pH to 8.0), 2-3h, 125°C (or 6h, 95°C)
Orthopyroxene ($(Mg, Fe)SiO_3$)	3g NaOH: 2g H_2O, 35-70 min, boiling.
Quartz (SiO_2)	KOH(aq.), 3 h, 150°C; or 48% HF, 24 h, 23°C.
Sphene ($CaTiSiO_5$)	Conc. HCl, 0.5-1.5 h, 90°C; or 6N NaOH, 20-30 min, 130°C
Zircon ($ZrSiO_4$)	H_3PO_4, few sec, 375-500°C; or NaOH(aq.), 0.25 h, 220°C; or 2ml 48% HF: 1ml 80% H_2SO_4 at 180°C in a pressure bomb
Obsidian	48% HF, 30 Sec.
Phosphate glass	48% HF, 5-20 min

TABLE 2 (cont.)

Material	Etching Conditions
Soda lime glass (Microscope slide, cover glass, window glass)	48% HF, 5 sec (better: 5% HF, 2 min); or 24% HBF_4: 5% HNO_3: 0.5% acetic acid, 1 h
Tektite	48% HF, 30 sec. or 24% HBF_4: 5% HNO_3: 0.5% acetic acid, 1 h
Cellulose nitrate (Kodacel; Triafol T; Cellit)	1ml 15% NaClO: 2ml 6.25N NaOH, 1 h, 40°C; or 25g NaOH: 20g KOH: 4.5g $KMnO_4$ 90g H_2O, 2-30 min, 50°C
Cellulose nitrate (Diacell, Nixon -Baldwin)	6.25N NaOH, 2-4h, 23 °C.
Cellulose triacetate (Kodacel TA 401, unplasticized; Bayar TN)	1ml 15% NaClO: 2ml6.25N NaOH, 1 h, 40°C
HBpalT (Polyester, $C_{17}H_9O_7$)	6.25 N NaOH, 8 min, 70°C
Polycarbonate (Lexan; Makrofol; Merlon; Kimfol; Tuffak)	6.25 N NaOH + 0.4%Benax, 20 min, 70°C
Polyethylene terephthalate (Mylar; Chronar; Melinex; Terphane)	6.25 N NaOH, 20 min, 50 C. $KMnO_4$ (25% aq.), 1h, 55°C; or 6.25 N NaOH, 10 min, 70 C.
Polystyrene	sat. $KMnO_4$, 2.5h, 85°C; or 10g $K_2Cr_2O_7$: 35ml 30% H_2SO_4 3h, 85°C
CR-39 ($H_{18}C_{12}O_7$)	6.25N NaOH, 30min, 40 C

A more complete list of etching conditions of track detectors can be found in Ref. 10 with exception of being discovered after 1975.

To find a successful etchant for a new insulating solid some guidelines can be followed: The etchant must be able to dissolve slowly the matrix material because the enlargement by bulk etching is necessary; For polymers, degrading agents are desired for being able to break polymer chains at random along their lengths. Oxidizing agents can provide needed degradation and hence are suitable etchants. But solvents disperse the long chain molecules into solution thus producing gummy mess. Thus etchant must not be a good solvent for the polymer.

2.4. Threshold of Solid State Nuclear Track Detector

Every material of solid state nuclear track detector has its own sensitivity to recording particle tracks. For example, meteorite minerals have low sensitivities, they can not record Ar and lighter particles; Mica can not record tracks of particles lighter than Ne; The most sensitive materials cellulose nitrate foil and CR-39 can record low energy protons and heavier particles. β-and γ-rays and neutrons can not be recorded with all materials of solid state nuclear track detectors. Generally speaking, mineral crystalls are less sensitive than organic polymers.

Every insulating solid has a threshold of damage density, below which particle tracks can not be etched. Only when the radiation damage density exceeds the threshold of the detector, the particle tracks can be etched. Fig. 3 shows the radiation damage densities in various solids as a function of the velocities of nuclei. The horizontal lines represent the thresholds of different detectors.[10]

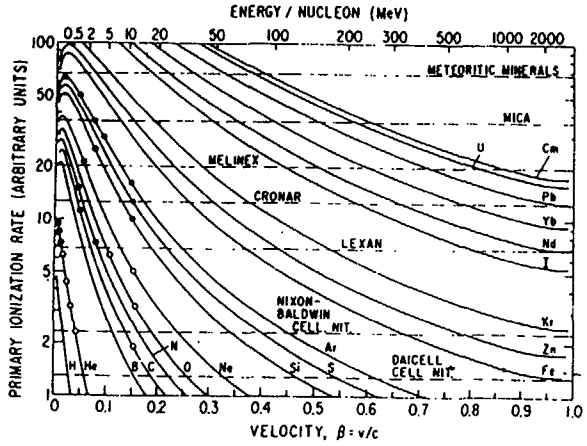

Fig. 3. Damage density vs. Velocity for different charged particles in various solids. Horizontal lines represent thresholds of different detectors.[10]

The threshold properties of solid state nuclear track detectors are very useful to scientists. One can use these properties to discriminate lighter particle backgrounds and only record desired particle tracks. For example, one can use mica to record fission fragments and against α-particles from the fission sourses. All solid state nuclear track detectors can be used in strong fields of β - and γ-rays and neutrons to record beavy charged particles. The threshold properties can also be used to roughly identify particle charges. For example, a track in mica must be produced by a particle heavier than Ne.

2.5. Charge Identification of Solid State Nuclear Track Detectors

Etching threshold of a special detector can give a charge limit for an incident particle forming the track. But this method is too rough to tell the charge and energy of the particle.

In 1967 P. B. Price and R. L. Fleischer discovered that the etching rate (V_T) along a track is a function of radiation damage density (J):

$$V_T = f(J) \qquad (1)$$

Measuring V_T carefully can give the value of J. J is a function of the charge Z and velocity v of track forming particle:

$$J = g(Z, v) \qquad (2)$$

as shown in Fig. 3. Therefore V_T is a function of Z and v:

$$V_T = \Psi(Z, v) \qquad (3)$$

Equation (3) has two independent variables. Thus one must at least measure V_T at two points along a track to get Z and V values. One point can be the stopping point of the incident particle. This method of charge identification is called track length method. Fig. 4 shows the response curve of laxan for incident particles from Ne to U, where R is the residual range of the particles, which is a measure of the velocities of particles. The residual ranges of heavily ionizing particles with the same charge and velocity are propertional to their masses. Therefore, measuring V_T and R, one can principlely identify isotopes of an element.

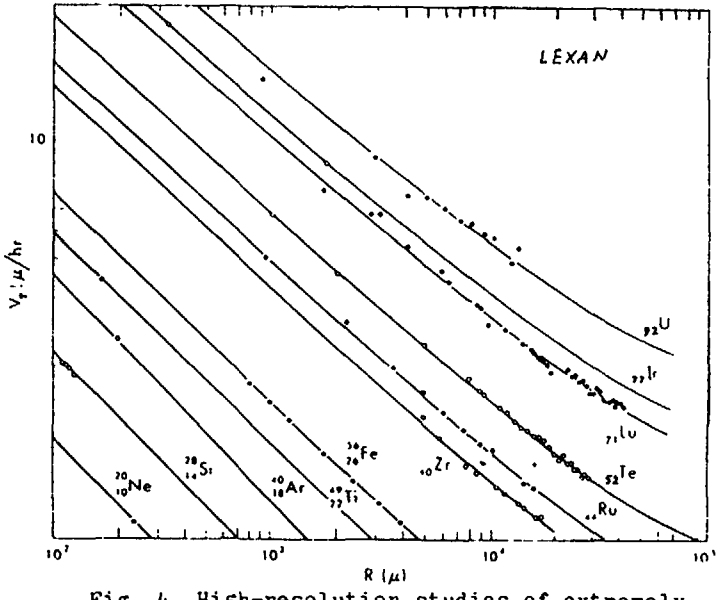

Fig. 4. High-resolution studies of extremely heavy cosmic rays in lexan stack by track length method.[10]

Track diameters on the surface of a detector is a measure of the charges of the normal incident particles. This is straightforward especially for relativistic nuclei, such as cosmic rays. Identification of charges by track diameters is called track diameter method. Fig. 5 is an example of charge identification by track diameter method with CR-39[13].

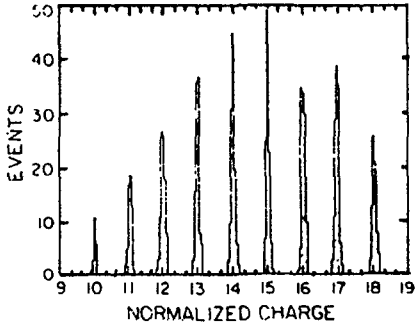

Fig. 5. Charge distribution of nuclear interaction fragments from a 1.85 GeV/N ^{40}Ar beam in CR-39(DOP), after averaging over 16 sheet surfaces.[13]

The individual CR-39 sheet resolution was found to be 0.25e at $10 \leq Z \leq 36$[14]. By the same method the charge resolution of Tuffak is 0.9e for relativistic uranium . The combination of CR-39 and Tuffak has the exclusive charge resolution in the entire region of the Periodic Table over any other kinds of radiation detectors.

From Fig. 3 one can see that only a part of the range where radiation damage density exceeds the threshold can be etched. The length of this part of the track is a monotonic function of particle charge for a given material. Measuring the maximum etchable track length one can identify particle charges. This method is called maximum etchable track length method. Fig.6 is an example to show this ability of olivine.[9] This is one of the method to search for superheavy elements with meteorite minerals. Because the threshold of solid state nuclear track detectors are not very sharp[16], the precise length of the etchable part is related to the etching time. Thus, the charge resolution of this method is poor for heavy nuclei.

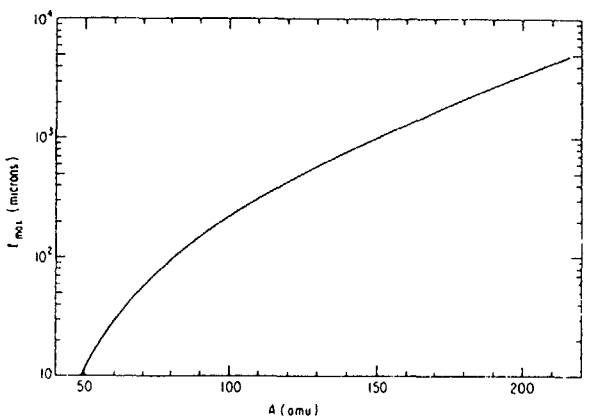

Fig. 6. Maximum etchable track lengths vs atomic numbers of heavily ionizing particles in olivine[9].

Several other methods to identify particle charges have been suggested but they are not used very often. One can refer to the original papers[9,10,17] of the methods.

2.6. Critical angle of Solid State Nuclear Track Detectors

Critical angle is another specific property and limiting factor to reveal tracks. It has been clarified that the tracks with radiation damage densities exceeding the threshold can be etched to become visible. But one exception is that if the angle θ between the track and the surface of the detector is less than a certain angle θ_c, the track can not yet be etched to become visible. The reason for this is that only when the component normal to the detector surface of etching rate V_T is greater than bulk etching rate V_G, the track can be etched to form an etch-pit on the etched surface as shown in Fig. 7A. If the component $V_T \sin\theta$ is less than V_G (Fig. 7C), the surface is removed so quickly that the preferential etching fails to keep ahead and no etch-pit is left on the etched surface. The critical condition (Fig. 7B) is

$$V_T \sin\theta = V_G \qquad (5)$$

or

$$\theta = \arcsin \frac{V_G}{V_T} \qquad (6)$$

This angle θ is named as critical angle $\theta_c = \arcsin \frac{V_G}{V_T}$. Because of the existence of critical angle , etching efficiency of nuclear tracks is always less than 1 for an isotropic source[10,12,18].

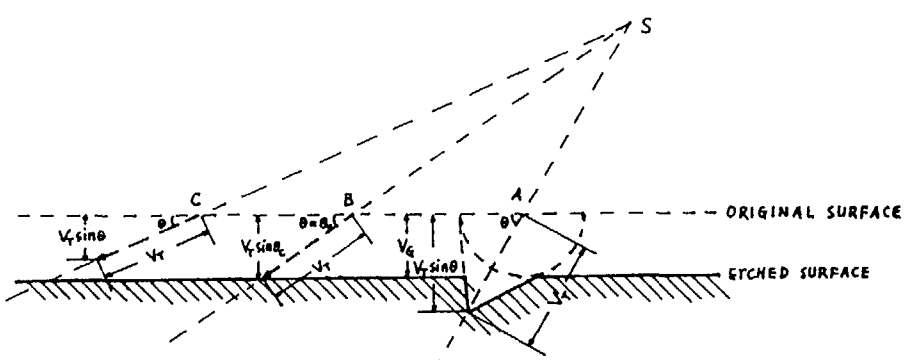

Fig 7. Critical angle of solid state nuclear track detectors.

2.7 Thermal Annealing of Radiation Damage Tracks

Radiation damage tracks can be stored almost permanently in solids at room temperature. For example, fission fragment tracks in muscovite mica can be kept over the entire history of earth below 145°C. However, if the temperature is sufficiently high, the radiation damage tracks will disappear completely very soon. In this respect, 540°C annealing for 1 hour is sufficient to erase the tracks in muscovite mica.

The track fading process can be described by Arrhenius equation

$$t = \text{const} \exp (E_o / kT) \qquad (7)$$

where t is the annealing time, E_o is the avtivation energy for defect restoration, k is Boltzman's constant, T is the temperature in °K.

Typically the observed activation energies have the same magnitude as those for atomic diffusion, which implies that the annealing process in crystalls corresponds to the diffusion of displaced atoms back to proper lattice positions [10].

According to a new model of track formation proposed by Dartyge et al [20] the latent track correspond to a statistical array of extended defects surrounded by a cloud of point defects. The etchability is dominated by the extended defects. During annealing the extended defects are much more stable than the point defects. More detailed studies of track annealing assume that different sizes of defects correspond to different activation energies [21, 22, 23] .

one must prevent track annealing in certain cases. For example, mica detectors must be kept below 200-300°C and polycarbonate detectors must be kept below 70°C [24] when they are used as nuclear track recorders in laboratories. Track annealing can be used to erase lighter particle backgrounds which are easier to erase than heavier particle tracks . Annealing effects

of fission tracks in minerals have been employed to date some geological objects [25], provide the information of geological heat history [26,27] and measure the speed of mountain rising [28, 29].

2. 8. Registration Temperature Effect of Solid State Nuclear Track Detectors

It was reported in 1979 by O'sullivan et al [31] and Thompson et al [30] that the track response of polymers depends on the temperature during registration. They showed that the track response increases with decrease in registration temperature above-137°C. Fig.8 shows the results obtained by Thompson and O' sullivan [30-33] and Doke et al [34]. The slope of the response from ^{56}Fe in the region of temperature 20°C to - 137°C is equivalent to shifts in the charge scale of about 0.02 and 0.04 charge units per °C for Lexan and CR-39 respectively. In the region above 20°C the shifts of charges appear to be considerably greater. The temperature effect seems to be dependent upon ionization [32, 33] . For high ionizing uranium in the temperature region of 18 to - 78 C the fractional change in signal strength per °C is considerably greater than for Fe [33].

Another noteworthy behavior of temperature effects is that below - 137°C the responses change anomalously. It deviates from the pattern of increasing sensitivity with decreasing temperature as in the region of - 137 to 95°C. It may not be caused by oxygen liquification, because in air and in vacuum it has the same behavior [34] . No appropriate explanations has been supposed for the anomalous behavior of temperature effect.

The temperature effect of track response is one of the major problems to be solved in coming years for cosmic-ray abundance studies with nuclear track detectors in earth orbit or on high altitude balloons because of the large temperature differences in space and in laboratories. For charge identifi-

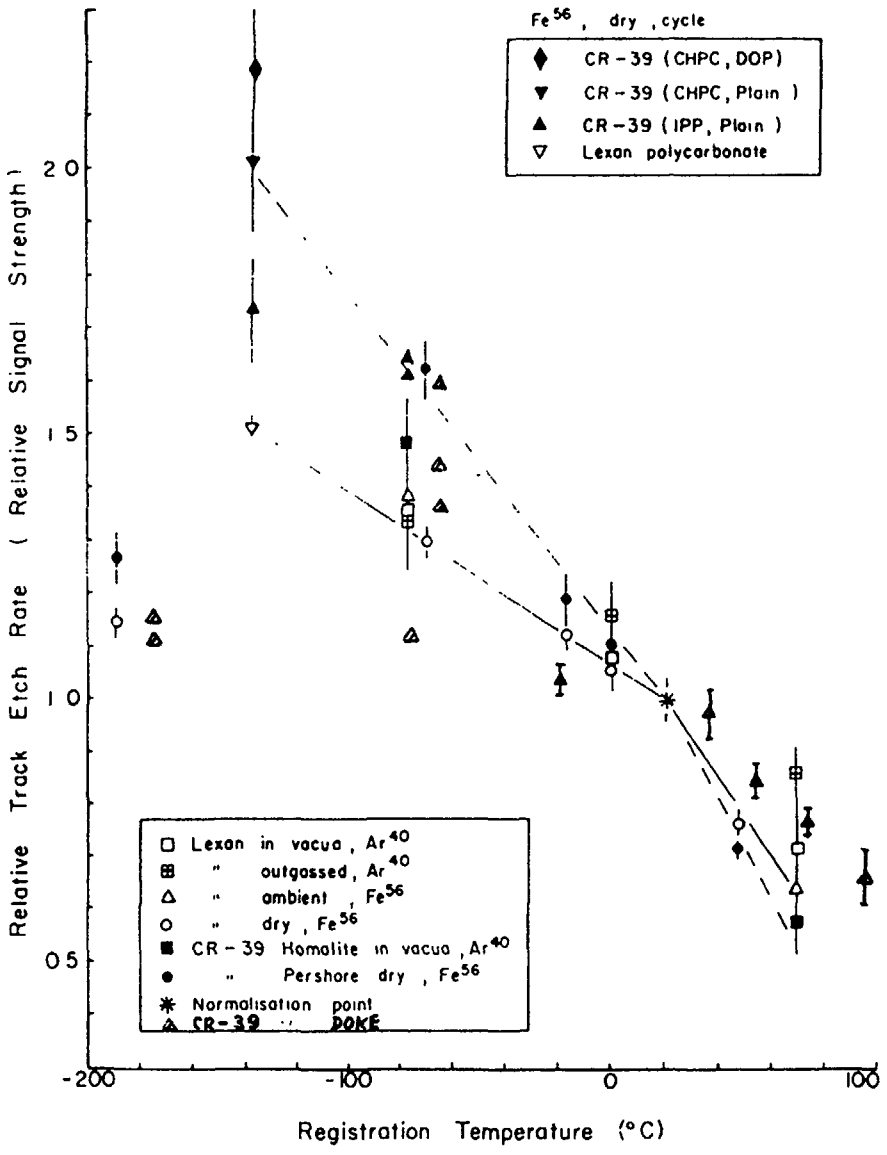

Fig. 8. Registration temperature effect of solid state nuclear track detectors.

cation in laboratories one must also take temperature effect into consideration.

2.9 Models of Track Formation in Solid State Nuclear Track Detectors.

Some models have been proposed to predict for each solid which particles will produce etchable tracks and which one will not. The first model named total energy loss rate model was proposed by Fleischer, price and Walker in 1964 [35]. On the basis of limited, early experiments, they suggested that track formation was governed by the total energy loss rate, (dE/dX), of the track forming particles as that for nuclear emulsion. For each solid there exists a critical energy loss rate $(dE/dX)_c$, if the energy loss rate exceeds the critical value, the solid will record tracks.

More extensive experiments, however, made it clear that this was not a satisfactory description. One glaring violation of the dE/dX criterion was the prediction that relativistic Fe nuclei would leave etchable tracks in cellulose nitrate, in contrast to observation.

In 1967 Fleischer, Price and Walker suggested a new model — primary ionization rate model [36] to overcome the difficulty of dE/dX criterion. They supposed that primary ionization rate J, the number of ions produced by incident particle per unit distance along its path, is a measure of radiation damage density as shown in Fig. 3. For each solid there exists a critical primary ionization rate Jc. If J > Jc, the solid will record tracks.

Primary ionization rate is suggested based on ion explosion spike, which notes that ionization by the track forming particle creates a narrow cylinder of materials with net positive charges as shown in Fig. 9a. The mutual Coulomb repulsion of the ions making

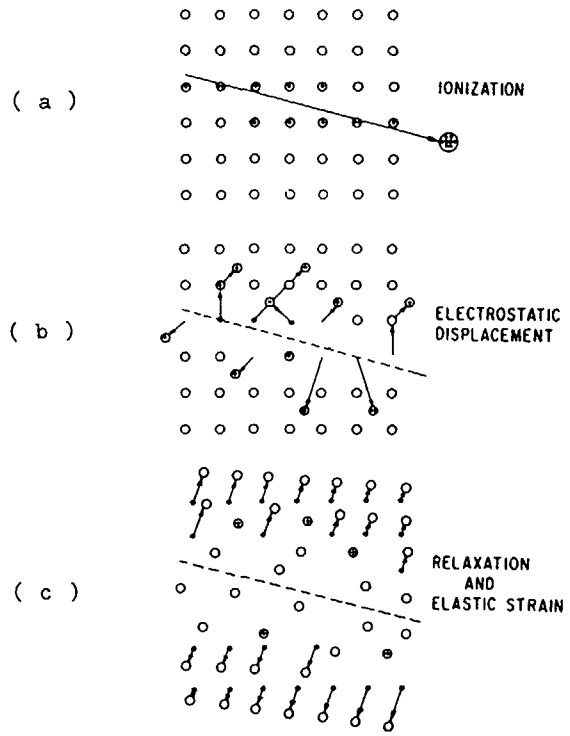

Fig. 9. The ion explosion spike mechanism for track formation in inorganic solids.[10]

up this region subsequently produces catastrophic atomic displacement and leads to a dense array of interstitials and vacant lattice sites (Fig. 9b) and to subsequent relaxation that produce long range strain fields (Fig. 9c). Only when $J > Jc$, ion explosion spike occurs. The strain fields are what are visualized by electron microscope in inorganic solids.

The average energy of secondary electrons increases with increasing energies of incident particles. For the same amount of energy loss, the higher the energy of the incident particle, the less the number of the incident ionization and vice versa.

Therefore The curves of J are lifted up at low energy part and pull downwards at high energy part than the trend of dE/dX curves. J criterion fits data very well as shown in Fig. 3.

The obvious shortcoming of primary ionization rate model is that it does not consider the effect of secondary electrons on track formation. Secondly, the average ionization energy expended on track formation in plastics is only 2 eV which corresponds only to the energy for breaking chemical bond as shown in Fig. 10.

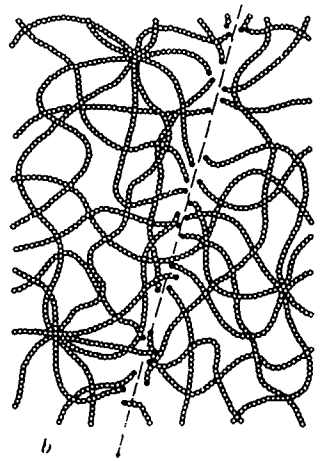

Fig. 10. The atomic character of a particle track in a polymer. New chain ends and other chemically reactive sites are formed [10]

But primary ionization rate model can fit experiments well for both inorganic solids and organic polymers.

In 1967 Benton [37,38] suggested that restricted energy loss rate of charged particles can be used to predict track formation in plastics. Restricted energy loss rate $(dE/dX)_{w < w_0}$

is the portion of the total energy loss that produces delta rays of less than some specific energy w_0. An etchable track is formed when the restricted energy loss rate $(dE/dX)_{w<w_0}$ exceeds a critical value $\left[(dE/dX)_{w<w_0}\right]_c$ for that material.

Benton and Henke recommended that w_0 = 350 eV[37]. The electrons with energy of more than 350 eV would escape into far away distance from the damaged core region and make no contribution to the track formation. Only the secondary electrons with energy less than 350 eV deposit their energy in the core region where the preferential etching occurs.

This criterion has obvious meanings and fit experimental data well in most of the energy region. The calculation of restricted energy loss rate is easy and gives absolute values. But at low energy part the fitting with experiments is not very well.[0 37] Additional data, reviewed by Ahlen[39] are clearly contradictory to the restricted ionization criterion.

In 1968 Fleischer and Hubetich[40] proposed energy deposition model. They assumed that when a critical dosage of ionization energy is deposited at a critical distance from the ion path by secondary electrons etchable tracks is produced in dielectric solids. Within the critical cylinder, molecular fragments more soluble than the parent molecule are formed. The radius of the critical cylinder is taken to be approximately 20 Å, as is appropriate to the passage of the etchant along the track and diffusion of radiation products back to the surface. At the critical radius the dosage approximates doses producing bulk damage under irradiation. This model fits experiments for both inorganic and organic solids in most part of energy region but deviates from experiments in low and high energy region[0]. In conception this model neglects the direct (primary) ionization, the proportion of which is about from 40% to 20% in the energy region from 1 MeV/amu to 1000 MeV/amu. The calculation of this model is more complicated than other model.

Improved calculations which include primary and secondary ionization have been proposed. These calculations would be more complicated than any calculations of other models.

In summary, every track formation model has its own advantages over others to predict the thresholds of detectors, but non of them is perfect. They have shortcomings either in concepts or experiments or both and non of them can be used to derive etching rate behaviors of tracks by certain etchant in specific solids.

3. Techniques of Solid State Nuclear Track Detectors

A vast techniques are generally used to obtain informations with solid state nuclear track detectors. In order to have some ideas about this let us overlook the whole process of the work with nuclear track detectors. It is usually composed of the following stages:

(1) Preparation of nuclear track detectors, which includes manufacture of special detector materials in laboratory or in factory, selection of minerals from geological, archaeological or space objects.

(2) Processing of the detectors, which includes fixing, grinding and finishing of small mineral grains, evaporating target materials onto the surfaces of the detectors and so on.

(3) Irradiation of nuclear track detectors in laboratory, inside or outside nuclear reactors, on balloon or in satellite.

(4) Development of nuclear track detectors with various means which include various chemical etching, grafting, dyeing, decoration and crystallization.

(5) Observation or measurement of nuclear tracks by means of flow of light, electricity, liquid, gas or particle beam.

In every stage there are many particular techniques for nuclear track detectors. One must learn, practise and sometimes develop the techniques and then obtain scientific informations from the detectors. Facing the forest of nuclear track techniques, we shall only describe the most important and commonly used ones.

3.1. Chemical Etching

Among the various methods chemical etching is the most useful and reliable one to develop radiation damage tracks. Based on chemical etching, track counting and identification have been made successful. Over 150 kinds of detector materials have already had their proper etchants. But nobody has found a successful etching method for polytetrafluoroethylene.

The equipments needed to perform the chemical etching can be from extremely primitive to very sophisticated depending on the purpose and requirement of the particular experiment.

(1) Simplest operation of chemical etching

If you want to develop and count the tracks of fission fragments in polycarbonate foil, you can pour some NaOH solution into a glass and put the polycarbonate foil with latent tracks into the solution to start etching. When the time is over (see Table 2), take out the foil from the solution and then dip it into water to wash off the remained NaOH, after drying in air the detector is ready to scan under optical microscope. Of course this simple performance does not always yield very good results for a number of reasons: the temperature of the etching tank (glass) varies with time, there is a temperature gradient within the etching tank, inducing changes in etching speed, the reaction products may concentrate arround the detector, building up some sort of protective sheath arround it, the concentration of the etchant changes because of evaporation etc. In order to overcome these difficulties, special types of etching equipment have been built in different laboratories for special purposes.

(2) High reproducibility etching bath

Fig. 11 shows a special type of etching bath used in most of nuclear track laboratories. The main

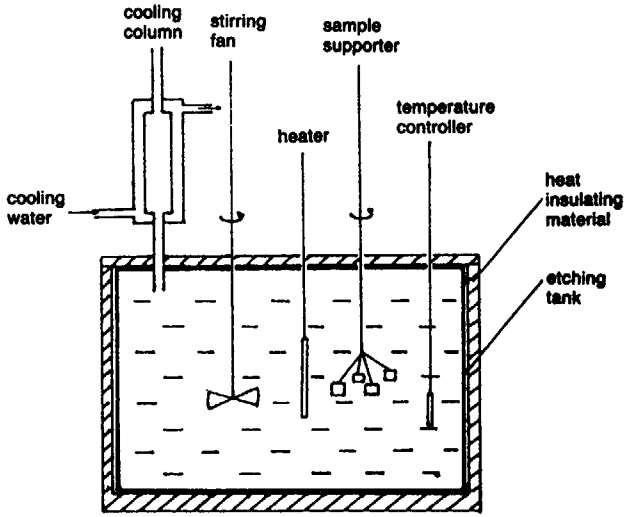

Fig. 11 A sketch showing a complete etching bath

part of etching bath is the container, in which the etchant is contained and controlled to a constant temperature by one or several heaters and a temperature controller. Temperature gradient is avoided and the etching products is removed from detector surface by stirring the etchant with a fan, whose rotating speed is adjustable and kept constant. A lid and cooling column prevent evaperation thus avoiding

concentration changes. Outside the etching bath is a thick layer of heat insulating material (or a water bath with heaters and temperature controller). It is necessary to have a frame supporting (and rotating) the detectors. In this type of etching bath the temperature can be kept constant within 0.03°C for a few liters of reagent and better for bigger volume of reagent (for example, hundreds of liters).

For some purpose the temperature control is very important. For spark counting of fission fragment tracks with accuracy of 2%, it requires the temperature control to be better than 0.4°C. For making nuclear track microfilters it requires temperature control to be better than about 0.2°C to obtain an uniformity 2% in pore diameters. The charge identification of cosmic ray nuclei with $14 \leq Z \leq 36$ by track diameter method requires the temperature control to be better than about 0.05°C to separate the nearby charges. Therefore a bare glass of etchant is not always suitable for some particular work.

(3) Very high temperature etching

Sometimes the etching must be performed with highly concentrated solutions at very high temeperature to speed up the etching process. In this case some special measures must be taken to keep constant temperature and concentration of the etchant. Boiling point is a constant temperature for the liquid. Boiling-point liguid can be used in outer bath to keep etching tank constant in temperature. Boiling-point etchants are often used in high temperature etching. For example, boiling water can keep etching tank at 100°C. 15N NaOH solution has a boiling temperature ~140°C. In order to keep the concentration of the etchant constant a cooling column is often used as in Fig. 11. Some time a sealed bomb made of stainless steel is used as etching tank to keep all etchant inside it.

3.2. Electrochemical Etching

Electrochemical etching was first proposed by Tommasino[41] as a method to enlarge nuclear tracks in plastics up to a size visible by naked eye. This method has been used in radiation dosimetry to measure low dose of neutrons and α-particles.

The principle of electrochemical etching is that an alternating voltage is applied across the detector during ordinary chemical etching. The ac voltage at least has two effects. First, it enhances the penetration of the etching agent both into the latent track and into the bulk of the polymer. Once the etching process has started, track pits are formed. At the tips of the pits, due to needle effect, electrical fields can be much stronger than the average fields applied to the detector. Thus localized electrical breakdowns occur producing the so-called "treeing phenomenon" because the damage has the same shape as that of a tree, the track itself being the trunk with branches radiating from the top at breakdown location as shown in Fig. 12. As a result, large

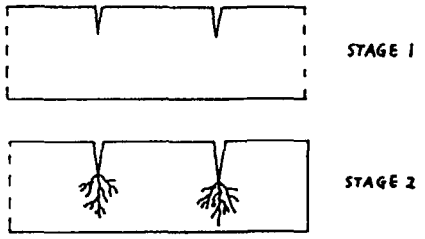

Fig. 12 Treeing discharge phenomenon

tracks are developed in the form of dark spots with diameters over several tens of microns, which are easier to observe with simple methods or even with naked eye.

The equipment for electrochemical etching is composed of two units: etching tank and high voltage supply. Fig. 13 shows the typical set-ups.

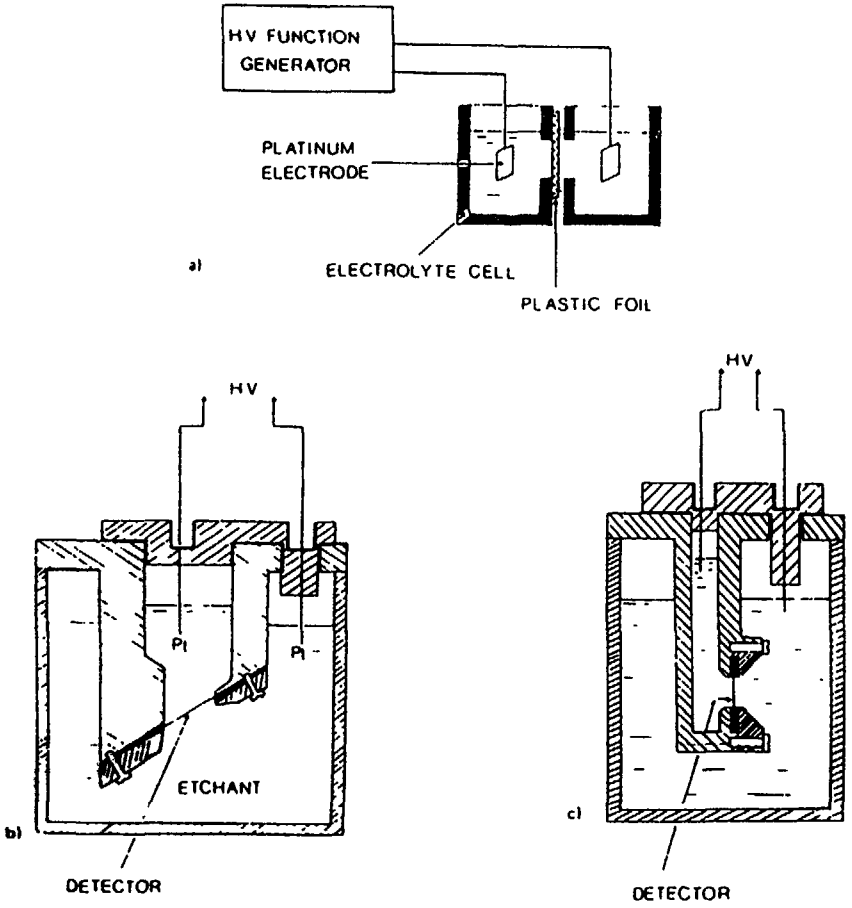

Fig. 13. Electrochemical etching set-ups designed by Tommasino (a) and Somogyi (b and c).[42]

The results of electrochemical etching mainly depend on the field strength, frequency, etchant characteristics and etching time.

Fig. 14 shows the relation of track diameter to field strength. There is a threshold value of the field strength, below which no treeing phenomenon is induced. Then the diameters of the tracks increase with increasing of field strength.

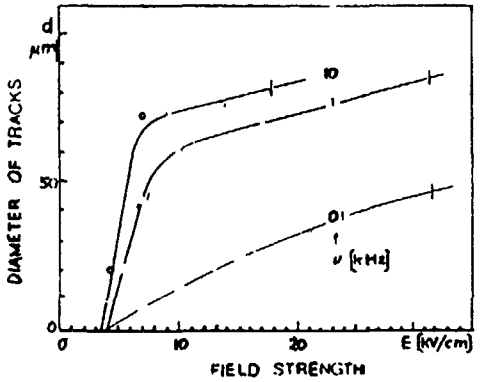

Fig. 14. Relation of track diameter to the field strength applied to the two sides of the detector.[42]

Fig. 15 shows the relation of the track diameter to the frequency of voltage.

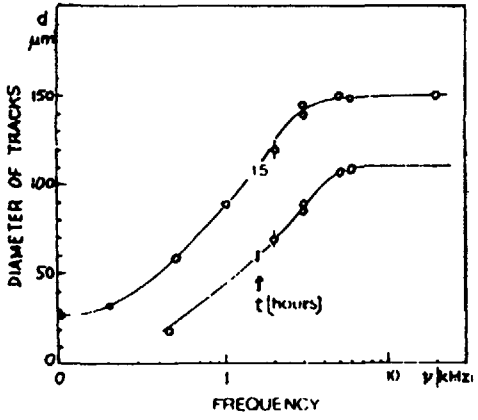

Fig. 15. Relation of track diameter to the frequency of the voltage.[42]

The diameter of electrochemiaal etched tracks is an increasing function of the frequency.

Typical curves of the relation between track diameter and etching time is shown in Fig. 16. The diameter of tracks increases with increasing of etching time.

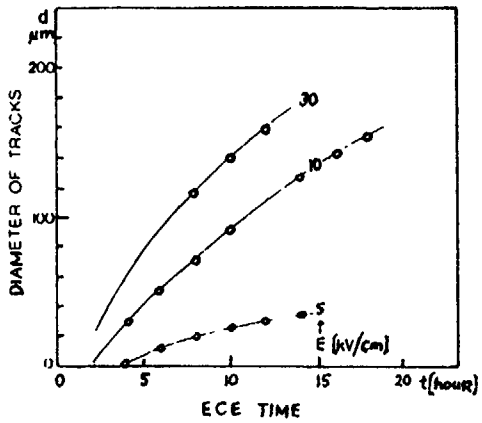

Fig. 16. Relation between track diameter and etching time of electrochemical etching.[42]

A very interesting behavior of electrochemical etching is that the overlapping of tracks never occurs between two tracks, which is very convenient for high track density measurements.

One of the promissing properties of electrochemical etching is that the characteristics of the incident particles have an effect on the etching process: High LET particles develop larger tracks than low LET ones.

Another promissing property of electrochemical etching is that the trees of tracks grow directionally depending on the directions of molecular chains of the polymer. This has become a new approach to study the directional structure in polymerization.

3.3. Optical microscope

Optical microscope is the most useful and main instrument in the study of nuclear track detectors. The resolution of microscope is about 0.5μm determined by the wavelength of visible light. One can measure the number, density, coordinats (x, y and z), and consequently length and zenith angle of a track. Some optical microscope can give azimuth angle. The track density which can be measured by optical microscopes changes from 1 to 10^7 track/cm^2.

The shortcoming of optical microscopes is that one can not see tracks smaller than about 0.5μm. The focus distance is so small that one can not see any images far below the upper surface. Another problem of optical microscope is that the scanning of nuclear track detectors is time consuming and paintaking. That is why many scientists are devoting their efforts to developing new methods to measure nuclear tracks.

The scanning electron microscope provides excellent shape contrast and resolution. Its resolution is about one order of magnitude higher than that of optical microscope. For observing structures deep inside track channels it requires replica technique.

Transmission electron microscope is an dispensable tool for the observation of individual latent tracks. It has several advantages over the scanning electron microscope for observing fine details of etched tracks. But it requires replica techniques for producing thin, electron-transparent samples. The resolution is again an order of magnitude higher (about 10 Å) than that of scanning electron microscope.

3.4. Nuclear Track Spark Counter

Nuclear track spark counter was first designed and described by Cross and Tommasino[43]. It has been widely used in radiation dosimetry, nuclear physics and element mapping.

The principle of nuclear track spark counter is as follows. A thin detector with through-etched tracks is placed

between a flat high voltage electrode and a thin aluminum electrode. This thin Al-electrode is an aluminized polyester film. Through an RC network a high dc voltage is applied and causes a spark to occur through one hole in the film as shown in Fig. 17.

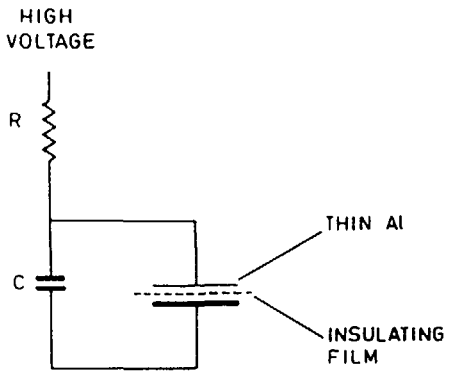

Fig. 17. Basic set-up for nuclear track spark counter.

The energy carried by the spark is sufficient to evaporate a large area (< 0.1 mm in diameter) in the thin Al-electrode. The distance from the high voltage electrode to the Al layer through this hole becomes too far to continue sparking. The spark stops. As soon as the voltage restores to the level at which sparking occurs, the spark through another hole occurs. In this way the sparking jumps from one hole to another until it has passed through all the holes and the discharge finally stops. As a result, the thin Al layer was punched many holes. The number of the holes is equal to the number of tracks through which the spark took place. The Al holes distribute in the same pattern as the tracks on the original detector and can been seen by naked eye. Moreover, the current pulse of the sparks can be counted directly by a scaler and the noise of the sparks can be heard clearly to show the end of sparking. For a few seconds the number of the tracks is provided by the scaler.

The main limit to spark counter is that the density of tracks must be lower than about 5000 tracks/cm^2. For higher density the number of sparks will be less than the number of tracks. The reason for this is that the tracks which are located in the area where Al layer has been punched away by former spark through the nearby track can not induce spark. The higher density, the more tracks will be lost.

The reproducibility of detection efficiency of nuclear track spark counter is relatively poor for 2π geometry exposure. In this case the heavy particles enter the detector isotropically. The depths of the tracks distribute from o to the thickness of the detector (if the thickness of the detector is less than the range of the particles). The variations of the detector thickness, etching condition and sparking voltage will give very big effect on the reproducibility of the detection efficiency. But for normally incident particles with a moderate density and the work in which the requirement for accuracy is not high, nuclear track spark counter is a rapid, efficient, reliable and inexpensive device.

3.5. Automatic Image Analyser

Automatic image analysers are the most powerful, fast and precise instruments for counting, parameter analysis (coordinate x, y and z, diameter, length, zenith and azimuth angle) of nuclear tracks. They have been used in many Laboratories all over the world. Some types of them are commercially available (Quantimet, Classimat, Leitz T. A. S. and Compumetric AMS-100 System)

The automatic image analyser are usually composed of microscope (optical or electron), video camera, TV monitor, video signal analyser and microcomputer. The images of the tracks in the detector are formed and amplified by an optical microscope onto the photosensitive part of a video camera.

The video signals from the camera are then stored and analysed in the video signal analyser and microcomputer. The images from the camera can be displayed on the screen of the monitor. Multiple analysis of the scanned area by the computer allows the measurement of integral or differential track densities, the statistical distribution of the track parameters (diameters) and many other track parameters, depending on the instruments.

With these instruments, the accuracy level (1-2%) for track counting is comparable with human observations. But the speed is much higher than the latter.

The main problem of this type of instruments is very expensive, which hinders the wide-spreading of them.

4. Applications of Solid State Nuclear Track Detectors

Solid state nuclear track detectors can be used in a variety of fields from a small nucleus to big galaxy, from the remote past (a few billion years ago) to right present time, from a devil cancer cell to a big flying bird. The following sections only tell you some successful and novel examples of the fields.

4.1. Nuclear Physics and Elemental Particles

Nuclear Physics is the first and active field of the applications of solid state nuclear track detectors. Recently, Barwick, Price and Stevenson[44] discovered that ^{232}U nucleus can spontaneously emit a ^{24}Ne nucleus.

This discovery demonstrates that nuclei heavier than Pb can decay not only by α- and β - emission (as we knew before 1984), but also by emission of heavy ions with masses over a wide range heavier than ^{14}C. This is a newly discovered decay mode of heavy nuclei. In this work, about 10^{12} α-particles would hit on the plastic detector, while only one ^{24}Ne nucleus was emitted. The huge number of α-particles did not give any effects on the detector because of the threshold property of solid state nuclear track detector (in this work, Cronar), but ^{24}Ne could create damage track in the plastics. The ^{24}Ne tracks were identified from the diameter and length of the etched tracks. A few months earlier, price et al[45] discovered radioactive decay of ^{222}Ra and ^{224}Ra by ^{14}C emission, using plastic track detector Tuffak, which followed Rose and Jone's discovery of ^{14}C emission by ^{223}Ra[46].

Table 3 lists all results of heavy ion emission from nuclei. Up till now, 15 species have been checked. 8 cases have

TABLE 3. HEAVY ION EMISSION FROM NUCLEI

Decay	$\lambda_{HI}/\lambda_{\alpha}$	Detector	year	Reference
$^{222}Ra \rightarrow {}^{14}C + {}^{208}Pb$	$3.7\pm0.6\times10^{-10}$	SSNTD	1985	(45)
$^{223}Ra \rightarrow {}^{14}C + {}^{209}Pb$	$8.5\pm2.5\times10^{-10}$	E- E Telescope	1984	(46)
	$5.5\pm2.0\times10^{-10}$	E- E Telescope	1984	(66)
	$6.1\pm1.0\times10^{-10}$	SSNTD	1984	(45)
$^{224}Ra \rightarrow {}^{14}C + {}^{210}Pb$	$4.3\pm1.2\times10^{-11}$	SSNTD	1985	(45)
$^{226}Ra \rightarrow {}^{14}C + {}^{212}Pb$	3×10^{-11}	E- E Telescope	1985	(67)
	$2.9\pm1.0\times10^{-11}$	SSNTD	1986	(60)
$^{230}Th \rightarrow {}^{24}Ne + {}^{206}Hg$	$5.6\pm1.0\times10^{-13}$	SSNTD	1985	(64)
$^{231}Pa \rightarrow {}^{24}Ne + {}^{208}Pb$	6×10^{-12}	SSNTD	1984	(65)
$^{232}U \rightarrow {}^{24}Ne + {}^{208}Pb$	$2.0\pm0.05\times10^{-12}$	SSNTD	1985	(44)
$^{233}U \rightarrow {}^{24}Ne + {}^{209}Pb$	$7.5\pm2.5\times10^{-13}$	SSNTD	1985	(63)
	$5.3\pm2.3\times10^{-13}$	SSNTD	1986	(59)
$^{221}Fr \rightarrow {}^{14}C + {}^{207}Tl$	$< 5.0\times10^{-14}$	SSNTD	1985	(60)
$^{221}Ra \rightarrow {}^{14}C + {}^{207}Pb$	$< 1.2\times10^{-13}$	SSNTD	1986	(60)
$^{225}Ac \rightarrow {}^{14}C + {}^{211}Bi$	$< 4.0\times10^{-13}$	SSNTD	1986	(60)
$^{232}Th \rightarrow {}^{26}Ne + {}^{206}Hg$	$< 5\times10^{-11}$	SSNTD	1986	(61)
$^{237}Np \rightarrow {}^{30}Mg + {}^{207}Tl$	$< 4\times10^{-14}$	SSNTD	1985	(64)
$^{240}Pu \rightarrow {}^{34}Si + {}^{206}Hg$	$< 1.3\times10^{-13}$	SSNTD	1986	(61)
$^{241}Am \rightarrow {}^{34}Si + {}^{207}Tl$	$< 5\times10^{-13}$	SSNTD	1985	(64)
	$< 1.6\times10^{-14}$	SSNTD	1986	(61)
$^{234}U \rightarrow {}^{28}Mg + {}^{206}Hg$	$< 1.0\times10^{-11}$	SSNTD	1987	(70)

been discovered nudergoing heavy ion emission. 6 cases out of 8 were first discovered by means of solid state nuclear track detectors. The other 7 species have been set stringent upper limit also by solid state nuclear track detectors. It would be extremely difficult to do the same job, if one used other detectors.

In 1960s and 1970s, solid state nuclear track detectors played a major role in the determination of half-lives of spontaneous fission isomers. The first half-life 14 ms of spontaneous fission isomer ^{242m}Am was determined using phosphate glass track detectors. Among more than 30 spontaneous fission isomers discovered up till now, more than two thirds of the half-lives of them were determined with solid state nuclear track detectors. The range of half-lives changes from 5×10^{-11} second to 14 milliseconds.

With solid state nuclear track detectors and various devices, the time range which can be measured for the half-lives of compound nuclei is from 10^{-18} second to 10^{16} years.

By virtue of high capability against background of less ionizing particles, Burnett et al have been able to measure fission cross section down to 10^{-35} cm^2 of $^4He + ^{197}Au \longrightarrow ^{201}Tl \longrightarrow$ fission using mica detectors.[47] The similar work was identification of first synthesized transuranium element z =104. Large number of studies on low energy nuclear interactions have been done with nuclear track detectors.

At high energy, solid state nuclear track detectors have been used to study multiprong sequential fission bombardments of heavy nuclei with heavy nuclei[48]. In the exit channels, two, three, four, five or six heavy particles can be seen with mica, CR-39 or other detectors. By measuring event numbers, track lengths and angles with beam and between tracks, one can determine the total and partial interaction cross sections, mass and energy of each fission fragment, mass transfer in the first step of the interactions, total kinetic energy loss in inelastic collision. From the above data, one can construct the process of the nuclear interactions[49,50]. Nuclear track detectors are best suitable to study the multiprong decay events with multiplicity higher than three, no other detectors can replace them.

In relativistic nuclear interactions, Freidlander et al. in 1980 confirmed in nuclear emulsion that several percent of relativistic projectile fragments have a relatively short mean free path in matter than mormal nuclei. The nuclei with this property are called "anomalons", which had been noticed in 1950s in cosmic ray study. Tincknell et al.[51] have demonstrated that anomalons can be observed in CR-39 for $11 \leq z \leq 17$ in projectile fragmentation of 1.85 GeV/amu ^{40}Ar. Theoretical explanations of anomalons effect are shown in fig. 18.

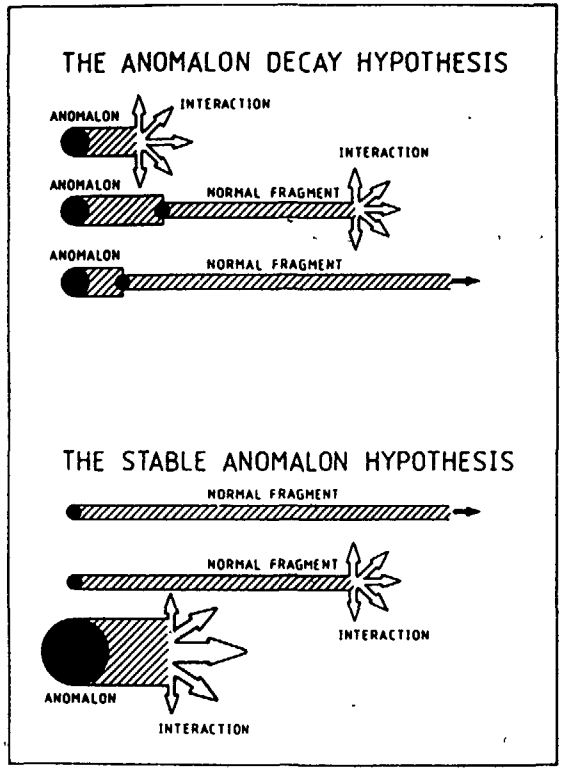

Fig. 18. An artist drawing of the two hypothesis for anomalons production

There are two hypothesis for anomalons production. In the anomalons decay hypothesis it is assumed that a fraction of the fragments are anomalons which decay to normal fragments within a short time. In the stable anomalons hypothesis it is assumed that a fraction of relativistic fragments are anomalons which have very big cross section to interact with the nuclei targets.

In the third workshop on anomalons, held in GSI, Darmstadt, West Germany in October, 1984, about two thirds of about 30 contributions on study of anomalons had positive results confirming anomalons behavior of relativistic fragments. But the other one third had negative results. The experimental data are not yet conclusive enough to finally establish that anomalons exist and if they are exist what is the correct explanation of their behavior.

In recent study with relativistic Au projectiles[52], we showed that fissions of relativistic projectile fragments have the similar properties as fissions at low energy. With CR-39 stack we can measure small zenith angles ($\leq 0.028^{o}$) and azimuth angles ($\leq 2.8^{o}$). These angle resolutions are comparable with that of nuclear emulsion. We suggested to use combinations of CR-39 and nuclear emulsion to study high energy nuclear interaction, because nuclear emulsion has high sensitivity to less ionizing particles and CR-39 has very high charge resolution to heavily ionizing particles and both have very high angular resolution.

According to Dirac expectation and Grand Unified Theories there exist magnetic monopoles in the universe. A recent study with mica track detector placed an upper limit of 10^{-17} to 10^{-16} Cm^{-2} Sr^{-1} S^{-1} on the flux of grand-unified-theory monopoles having velocity 3×10^{-4} C to 1.5×10^{-3} C [53]. After scanning larger area of mica, a new upper limit 10^{-18} $cm^{-2}Sr^{-1}S^{-1}$ has been placed. A monopole should pick up a nucleus with big magnetic momentum, such as ^{27}Al, while passing through the earth, and such a bound system will produce an etchable track due to elastic collisions of the nucleus with atoms in mica, subject only to the requirement that the system remain bound. Fig.19 illustrate the technigue used in these searches. Fig.20 shows the results of mica searches compared with other upper limits. Another work with CR-39 has placed an upper limit $\sim 1 \times 10^{-13}$ Cm^{-2} Sr^{-1} S^{-1} for bare monopoles with $v \sim 10^{-4}$ C for dyons and monopole-proton bound states with $v > 3 \times 10^{-5}$ C, and for supermassive singly

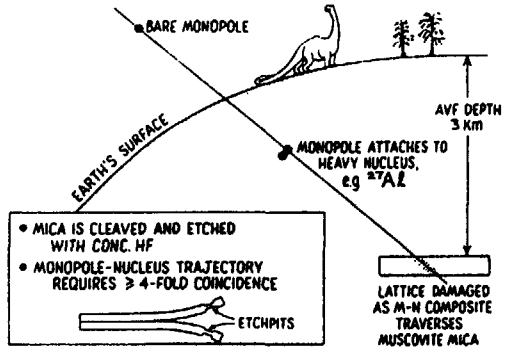

Fig. 19 Mica technique for searching for slowly moving supermassive magnetic monopoles predicted by Grand Unified Theories.

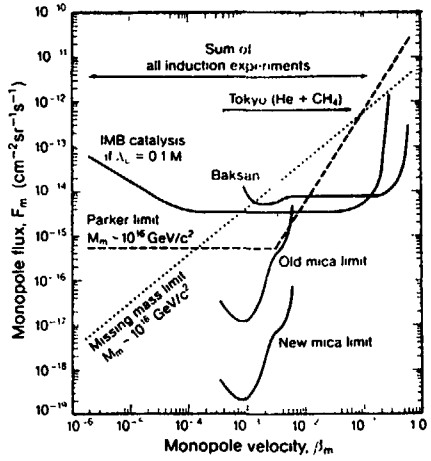

Fig. 20 Negative results of mica searches for monopoles compared with other upper limits.

-charged particles with 3×10^{-5} C < v < 0.05c[54]. Doke et al have placed 1000 M^2 CR-39 in a mine 1000 M depth in the earth to detect magnetic monopoles. They will etch the CR-39 sheets after detecting for three years.[55]

4.2. Astrophysics, Space Science, Meteoritics and Cosmic Ray Study

Cosmic ray, meteorites and solar particles are samples from galaxy and solar system. They provide informations about the stars, the sun and the planets arourd the sun. From the compositions, intensities and energy spectra, scientists can get informations such as: where do the cosmic ray come from? What is going on in the sources? How far are the sources from the earth? What is the age of the cosmic rays? How do the cosmic rays get their energy? How do they propagate from the sources to the earth region? Are there any differences between ancient cosmie rays and present cosmic rays? From solar particles one can get information about the sun, solar flare and solar wind. Solid state nuclear track detectors have played an important role in understanding of solar behaviors. Meteorites have provided plenty informations about the synthesis of elements in the early universe, the time interval from the element synthesis to cooling down, the cooling speed, fission track age of meteorite, exposure age of meteorite, the erasion of meteorite in passing through atmosphere. The new efforts on cosmic ray study are to detect superheavy cosmic rays, by which one can get information about the roles of r —— process and s —process in cosmic ray sources. The flying LDEF I from 1984 and planned LDEF II in 1986-1988 devote to this job. These would be the biggest missions of spacecrafts for cosmic ray study in recent twenty years.

4.3. Geology, Archaeology and Geochronology

All rocks or minerals contain minute amount of uranium. ^{238}U nuclei undergo spontaneous fissions at a constant rate in the geological history. The fission fragments were recorded in the minerals as radiation damage tracks. The number of the tracks is related to the uranium content and the age of the rock or mineral. Determining the uranium content and the number of tracks of ^{238}U spontaneous fissions, one can determine the age of the rock or mineral. If some minerals were formed or heated to a temperature high enough to erase the damaged tracks by an event which is related to mankind, dating the minerals provides the age of ancient man.

The advantage of fission track dating over other radioactive methods is the wide range of time from hundreds of years to a few billion years. Particularly, in the range of about 50,000 years to a few million years, other methods are very difficult to get any results.

Fission track dating provides not only geological age but also thermal history, cooling rate and lifting rate of mountains.

One successful example of fission track dating was the demonstration of ocean bottom spreading from the Median Valley of the Mid-Atlantic Ridge and the continental drift of North and South America apart from Europe and Africa.[10]

After dating of ancient man in East Africa by Fleischer et al[10], we have dated Peking Man by fission track method (0.465 ± 0.045 myr at layer 10 of Peking Man Site).[56] Peking Man Site is very important in the study of human evolution, because in this site archaeologists have found a lot of fossils which belong to 46 human bodies and about 100 kinds of ancient animals. Peking Man Site is the place where stone tools were first discovered and identified in the world. Peking Man Site is also the place where exist a lot of ancient ashes which show the early stage of human history. Fig.21 is a restored photo of Peking Man.

Tibet-Qinghai plateau is an active area where the crust of the earth is composed of two layers of crust, one of which was a part of Indian continent which is flowing northwards crashing underneath Tibet-Qinghai plateau. Because of the crashing of the two continents Tibet-Qinghai plateau is rising up. The lifting rate of the plateau near Lhasa was about 300 meters per million years in the time interval from 27.3 Myr to 25.6 Myr ago by fission track dating[28].

Fig.21 . Restored Photo of Peking Man.

4.4. Geochemistry, Cosmochemistry and Analytic Chemistry

Any element or isotope can be analysed with solid state nuclear track detectors if its nuclei emit heavy charged particles either directly from naturally radioactivity or as a result of nuclear reaction when bombarded with neutrons, protons, heavy ions, α-rays and other particles at an accelerator or nuclear reactor. Recording the emitted heavy charged particles with nuclear track detectors and measuring the beam intensity one can quantitatively analyse the element or isotope. The emitted particles could be protons, α-particles, fission fragments and others. Certain isotopes have very large cross sections for specific reactions. They are more suitable to analysis with these techniques. For example, ^{235}U and ^{10}B have large cross sections for thermal neutrons. They can be analysed very easily.

Nuclear track method of element analysis not only provides information on the quantity of the element, but also illustrate its spatial distribution. Therefore it is also called element mapping.

The sensitivity of nuclear track method for some elements are very high. For example, the sensitivities of determination of uranium in quartz and muscovite mica can be over 10^{-14} g/g. Utanium determination in natural water could have a sensitivity about 10^{-11} g/g. The spatial resolutions for solid substances are about 10 μm or less.

The following elements and isotopes have been analysed by nuclear track method: ^{235}U, ^{238}U, ^{239}Pu, ^{232}Th, Pb, Bi, Hg, Au, Ho, Sm, ^{18}O, ^{17}O, ^{15}N, ^{14}N and D. The application fields include concentration, spatial distribution, migration and differentiation of elements and isotopes in geological and space objects, in ore deposits, transportation and deposition of harmful or medical elements in organ, tissue, bone, teeth, brain and blood cells of human body and in leaves of plants and other biological objects. Boron mapping and analysis have been used to improve the properties of special steels .

4.5. Radiation Dosimetry

Some of the unique properties, such as high capability against radiation background, permanent recording of dosage, cheap and small size, of solid state nuclear track detectors make them extremely attractive for radiation dosimetry. The first work on neutron flux measurement with solid state nuclear track detectors was performed in 1963. Since then, radiation dosimetry with solid state nuclear track detectors has become one of the major fields of the applications of nuclear track detectors, which includes thermal neutron dosimetry, fast neutron dosimetry, α-dosimetry and space radiation dosimetry.

Neutrons can not create tracks by themselves. A converter must be used to convert neutrons into highly ionizing particles. For measuring thermal neutrons the converters are usually made

of ^{235}U, ^{233}U, ^{239}Pu, ^{10}B and ^{7}Li. By using ^{235}U converter and ^{235}U (n, f) reaction a fluence from 10^3 to 10^{22} n/cm^2 can be measured. By using ^{10}B converter and ^{10}B (n, α) ^{7}Li reaction the sensitivity can reach 0.013 track/neutron.

For fast neutrons the converters are usually fissile nuclei with energy threshold, such as ^{234}U (0.26 MeV), ^{237}Np (0.32 MeV), ^{238}U (1.30 MeV) and ^{232}Th (1.50 MeV). Tracks of carbon and oxygen recoils induced by fast neutrons in plastic track detectors can be used to measure fast neutrons. It has a sensitivity of about 10^{-5} - 10^{-6} track/neutron depending on the plastic and the neutron energy.

α-dosimetry with solid state nuclear track detectors has been used to measure radon in uranium ore. Recent years a lot of work has concentrate on measurements of Rn in buildings. It shows that if the buildings are not ventilated well. The hazard of high concentration of Rn will cause more cancers in lungs.

As travel in space and in high altitude increases, the dosimetry for space radiation has become a new field of research.

4.6. Uranium and Water Explorations

Solid state nuclear track detectors has been used in uranium exploration. The principle of locating underground uranium ore is as follows: ^{238}U in uranium ore decay successively through a chain of daughters, one of which is ^{222}Rn. ^{222}Rn is a gas with a half-life 3.8 days, which is long enough for radon to be transported to the earth's surface from the ores. Plastic cups, each containing a piece of plastic track detector, such as CR-39 or cellulose nitrate film, are inverted and buried at shallow depth. The detectors record α-particle tracks of ^{222}Rn and its daughers throughout a buried time of two to four weeks. The area where are much more tracks on the detectors is the position of the ore. Uranium exploration by α track counting is more efficient to detect deep ores underground than other methods. The detecting depth is about 300 meters, which is much deeper than that of ionization chamber ($\sim$ 20 meters) and γ-ray detection (a few meters).

Solid state nuclear track detectors have been used to prospect underground water in dry regions. Underground crevices in new structure usually contain natural water.[57] Broken rocks in the crevices have larger surface to release radon than other place. If one buries detector-cups as used in uranium exploration, one will get peak value of track number at the crevice position. Drilling hole into underground one would find natural water. The technique used in water prospecting is similar to uranium exploration. The difference between them is that water is contained in crevices in new structure.

Nuclear track water prospecting is a new, sensitive, simple and cheap method to find water sources in dry region.

4.7. Nuclear Track Microfilters

The idea to make nuclear track microfilter was suggested by Fleischer et al in 1963. One simply expose a thin detector material to a collimated beam of particles that produce tracks across the entire thickness of the sheet and then one etches to produce holes that perforate the membrane. The diameter of the holes changes from 50 Å to several tens of microns.

The main advantage of nuclear track microfilters over conventional filters is their regular pore shape and well-defined pore size and the retained particles can be observed directly on the filter surface. These properties of nuclear track microfilters make them suitable to filtrate, separate and collect microparticles.

Nuclear track microfilters have been used to filtrate aerosol particles from waste gases and liquids in nuclear plant, to prepare super-pure solutions used in electronics industry, to purify injections, to collect or eliminate cancer cell, special bacteria, mould, eggs of insects, molecules of high polymers, to separate isotopes such as ^{235}U and ^{238}U, ^{222}Rn and ^{220}Rn, to produce fruit juices, soft drinks, wine and beer free from bacteria and yeast, to wake man-made kidney and lung.
Single pore membranes are used to make DeBlois-Bean counter to count and measure the sizes and size distribution of blood cells,

bacteria and virus, to study the rigidity of red blood cells and diagnose heart and circulatory-system diseases.

4.8. Miscellaneous Applications

The holes or etched tracks can be filled with appropriate substances, thus new materials with different properties can be produced. For example, the storage density in magneto-optic films can be increased by minimizing the sizes of magnetic domains on the surface of the transparent plastic films. Before, if the sizes of magnetic domains are small, the magnetic domain collapses. Things became much easier with the application of track etching. The etched tracks nail the small magnetic domains tightly on the surface of the film to prevent them from collapsing This method reduces the sizes of magnetic domains and keeps the domains stable and therefore increase the storage density.

The development of so-called electrically superinsulating films was a result of track etching techniques. The breakdown of insulation after metal deposition by sparking is often a trouble in high voltage technique. If etched tracks with high density ($\sim$ 50% of the original surface) are formed on the surface of an insulating material. The resulting structure behaves like a maze of dead-ends for electric current. Even when the paths of the maze and the top of its walls become conductive, there is no coherent path of conductivity through this maze.

For example, the resistance of such a structured surface covered with 0.7 μm gold was 10 orders of magnitude higher than that of a flat surface.

Track etching technique can be used to imprint complicated structures or images on an insulating solid. This technique is called microlithography. Its principle is shown in Fig. 22.

Heavy-ion lithography has a considerable potential as a tool for observing the inner details of microscopic objects without destroying the sample. A simple ion is capable of measuring density variation in the sample. Relativistic

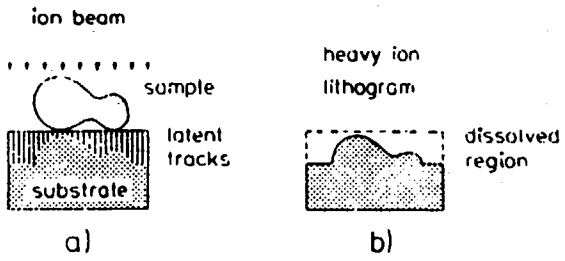

Fig. 22. Principle of heavy ion lithography.[58]
a) Recording the area density distribution of the sample in a track recording substrate.
b) Revealing the resulting range envelope by track etching, resulting in relief pattern as the microscopic objects.

heavy-ion radiography is a kind of lithography, which has been used to diagnose and treat cancers.

The appication of solid state nuclear track detectors has spread into almost every field of science and technology. It is now still mushrooming in the unnoticed new fields.

Referring to the comprehnsive book " Nuclear Tracks in Solids, Principles and Applications " written by R. L. Fleischer, P. B. Price and R. M. Walker (1975)[10] and the new book " Solid State Nuclear Track Detection " written by S. A. Durrani (1986)[67] and the International Journal " Nuclear Track and Radiation Measurements ". One could gain detailed knowledge on solid state nuclear track detectors.

REFERENCES

1. E. C. H. Silk and R. S. Barnes, Examination of fission fragment tracks with an electron microscope, Phil. Mag. 4, (1959) 970

2. D. A. Young, Etching of radiation damage in lithium fluoride, Nature 182, (1958) 375.

3. P. B. Price and R. M. Walker, Electron microscope observation of etched tracks from spallation recoils in mica, Phys. Rev. Letters 8, (1962) 217.

4. P. B. Price and R. M. Walker, Chemical etching of charged particle tracks, J. Appl. Phys. 33, (1962) 3407.

5. R. L. Fleischer and P. B. Price, Tracks of charged particles in high polymers, Science 140, (1963) 1221.

6. R. L. Fleischer and P. B. Price, Charged particle tracks in glass, J. Appl. Phys. 34, (1963) 2903

7. R. L. Fleischer and P. B. Price, and R. M. Walker, Solid-state track detectors: Applications to nuclear science and geophysics, Ann. ReV. Nucl. Sci. 15, (1965) 1

8. P. B. Price, R. L. Fleischer, D. D. Peterson, C. O' Ceallaigh, D. O' Sullivan, and A. Thompson, Identification of isotopes of energetic particles with dielectric track detectors, Phys. ReV. 164, (1967) 1618.

9. P. B. Price and R. L. Fleischer, Identification of energetic nuclei with solid dielectric track detectors: Applications to Astrophysics and planetary studies, Ann. Rev. Nuc. Sci. 21, (1971) 295.

10. R. L. Fleischer, P. B. Price and R. M. Walker, Nuclear tracks in solids: Principles and applications, University of California Press, 1975

11. R. L. Fleischer, Nuclear track production in solids, prog. Mater. Sci. X, (1981) 97.

12. Shi-Lun Guo, Shu-Hua Zhou, Wu Meng, Sheng-Fen Sun, and Ru-Fa Shi, Detection efficiencies of solid state nuclear track detectors for fission fragments, Proceedings of the 11th International Conference on Solid State Nuclear Track Detectors, England, 1981, PP265.

13. M. H. Salamon, J. Drach, Shi-Lun Guo, P. B. Price, G. Tarlé and S. P. Ahlen, Efect of electron capture and loss on the response of polycarbonate track detectors to relativistic uranium ions, Nucl. Instrum. Methods 224, (1984) 217.

14. S. P. Ahlen, T. E. Coan, J. Drach, Shi-Lun Guo, P. B. Price, M. H. Salamon, G. Tarlé and M. L. Tincknell, Identification of relativistic nuclei with $10 \leq z \leq 92$, Nuclear Tracks and Radiation Measurements 8, (1984) 571.

16. Somogyi, K. Grabisch, R. Scherzer and W. Enge, Revision of the concept of registration threshold in plastic track detectors, Nucl. Instrum. Methods 134, (1976) 129.

17. Somogyi, R. Scherzer, K. Grabisch and W. Enge, A spatial track formation model and its use for calculating etch-pit parameters of light nuclei, Nucl. Instrum. Methods. 147 (1977) 11.

18. H. A. Khan and S. A. Durrani, Efficiency calibration of solid state nuclear track detectors, Nucl. Instrum. Methods 98, (1972) 229.

19. R. L. Fleischer, P. B. Price and D. S. Miller, Fission-track ages and track-annealing behavior of some micas, Science 143, (1964) 349.

20. E. Dartyge, J. P. Duraud, Y. Langevin, and M. Maurette, New model of nuclear particle tracks in dielectric minerals, Phys. ReV. B23, (1981) 5213.

21. C. W. Naeser, and H. Faul, Fission track annealing in apatite and sphene, J. Geophys. Res. 74, (1969) 705

22. R. Gold, J. H. Roberts, and F. H. Ruddy, Annealing phenomena in solid state track detectors Nucl. Tracks 5, (1981) 253.

23. E. Märk and T. D. Märk, Fission track temperature age theory, Proceedings of the 11th International Conference on Solid state Nuclear Track Detectors, Bristol, 7-12 Sept., 1981, P389

24. K. Becker, Alpha particle registration in plastics and its applications for radon and neutron personnel dosimetry, Health Physics 16, (1969) 113.

25. D. Storzer, Fission track plateau-ages: A new method for correcting thermally lowerd track ages, Geochronology Conference, "ECOG II", Oxford, 3-8 sept. 1973. P67.

26. G. A. Wagner, Archaeological applications of Fission-track dating, Nuclear Track Detection 2, (1978) 51

27. Shi-Lun Guo, Fission track methods for geological and archaeological dating, Proceedings of the Third . Nationwide Conferende on Quaternary Geology-of China. Beijing, 1979. P.

28. Liu Shunsheng, Application of solid state nuclear track detectors in geology and archaeology, (to be published in Nuclear Technology, 1985)

29. G. A. Wagner and G. M. Reimer, Fission track tectonics: The tectonic interpretation of fission track apatite ages, Earth and Planetary Science Letters 14, (1972) 263.

30. A. Thompson, D. O'sullivan, J. Daly, C. O' Ceallaigh, V. Domingo, A. Smit and K.-P. Wenzel, A high resolution study of ultra heavy cosmic ray nuclei using Long Duration Exposure Facility (LEDF). Proc. 16th Internat. Cosmic Ray Conf., Kyoto, 11, (1979), P103.

31. D. O' Sullivan, A. Thompson, J. Daly, C. O' Ceallaigh, V. Domingo, A. Smit and K.-P. Wenzel, A solid state track detector array for the study of ultra heavy cosmic ray nuclei in earth orbit, Poc. 10th Internat. Conf. on Solid State Nuclear Track Detectors. Lyon, 1979, P1033.

32. D. O' sullivan, A. Thompson, J. A. Adams, and L. P. Beahm, New results on the investigation of the variation of nuclear track detector response with temperature, Nuclear Tracks and Radiation Measurements 8, (1984) 143.

33. Thompson, and D. O' sullivan, Preliminary results on the registration temperature effect for uranium ions in various solid state nuclear track detectors, Nuclear Tracks and Radiation Measurements 8, (1984) 567

34. R. Hamasaki, T. Hayashi and T. Doke, The dependence of track response of CR-39 on registration temperature in vaccum. Nuclear Tracks 9, (1984) 149

35. R. L. Fleischer, P. B. Price, R. M. Walker and E. Hubbard, Track registrition in various solid state nuclear track detectors, Phys. Rev. 133A, (1964) 1443.

36. R. L. Fleischer, P. B. Price, R. M. Walker and E. L. Hubbard, Criterion for registration in dielectric track detectors, Phys. Rev. 156, (1967) 353.

37. E. V. Benton and R. P. Henke, On charged particle tracks in cellulose nitrate and Lexan, Univ. of San Francisco Tech. Report 19 July (1972)

38. E. V. Benton, Charged particle tracks in polymers no. 4: Criterion for track registration, USNRDL-TR-67-80, U. S. Nav. Rad. Def. Lab. Report, San Francisco (1967).

39. S. P. Ahlen, Theoretical and experimental aspects of the energy loss of relativistic heavily ionizing particles, ReV. Mod. Phys. 52, (1980) 121

40. R. Katz and E. J. Kobetich, Formation of etchable tracks in dielectrics, Phys. Rev. 170, (1967) 401.

41. L. Tommasino, Solid dielectric detectors with breakdown phenomena and their application in radiation protection, Nucl. Instrum. Methods 173, (1980) 73.

42. G. Somogyi, A study of the basic properties of electrochemical track etching, Radiation Effects 34, (1977) 51.

43. W. G. Cross and L. Tommasino, Rapid reading technique for nuclear particle damage tracks in thin foils, Radiation Effects 5, (1970) 85.

44. S. W. Barwick, P. B. Price and J. D. Stevenson, Discovery of radioactive decay of ^{232}U by ^{24}Ne emission, Phys. ReV. Rev. C31, (1985), 1984.

45. P. B. Price, J. D. Stevenson and S. W. Barwick, Discovery of radioactive decay of ^{222}Ra and ^{224}Ra by ^{14}C emission, Phys. Rev. Letters. 54, (1985), 297.

46. H. J. Rose and G. A. Jones, A new kind of natural radioactivity, Nature 307, (1984) 245.

47. D. S. Burnet, R. C. Gatti, F. Plasil, P. B. Price, W. J. Swiatecki and S. G. Thompson, Fission barrier of Thallium -201, Phys. Rev. 134 B (1964) 952.

48. R. Brandt, P. A. Gottschalk and P. Vater, An application of SSNTD to nuclear physics: multiprong events in heavy ion reactions due to multiple sequential fission, Nucl. Instrum. Methods 173 (1980) 111.

49. P. A. Gottschalk, G. Grawert, P. Vater and R. Brandt, Two, three, and four-particle exit channels in the reaction (806 MeV) Kr + U, Phys. ReV. 27C (1983) 2703.

50. P. Vater, E. U. Khan, R. Beckmann, P. A. Gottschalk and R. Brandt, Sequential fission studies in the interaction of 9.03 MeV/N ^{238}U with ^{nat}U using mica track detectors, (To be published in Nuclear Tracks and Radiatiion Measurements, 1985)

51. M. L. Tincknell, Study of anomalous nuclear projectile fragments in CR-39 etched track detectors, Ph. D. Thesis, Department of Physics, University of California at Berkeley, October 4, 1984

52. Shi-Lun Guo, M. L. Tincknell and P. B. Price, Fission of relativistic intermediate-mass nuclei, Phys. Rev. C 30 (1984) 1737

53. P. B. Price, Shi-Lun Guo, S. P. Ahlen and R. L. Fleischer, Search for grand- unified-theory magnetic monopoles at a flux level below the Parker Limit, Phys. Rev. Letters 52(1984)1265.

54. P. B. Price, Limit on flux of supermassive monopoles and charged relic particles using plastic track detectors, Physics Letters 140 B (1984) 112.

55. T. Doke, T. Hayashi, I. Matsumi, M. Matsushita, H. Tawara, K. Kawagoe, K. Nagano, S. Nakamura, M. Nozaki, S. Orito and K. Ogura, Search for massive magnetic monopoles using plastic track detectors characteristics of CR-39 plastic for detecting monopoles, Nuclear Tracks and Radiation Measurements. 8 (1984) 609.

56. Guo Shi-Lun, Zhou Shuhua, Meng Wu, Zhang Pengfa, Sun Shenfen, Hao Xiuhong, Liu Shunsheng, Zhang Feng, Hu Ruiying and Liu Jingfa, Fission track dating of peking Man, KEXUE TONGBAO (A Monthly Journal of Science). 25 (1980) 770.

57. Shi Yuchun, Search for crevice water in new stucture using the alpha-track method, Nuclear Techniques 1982, No. 1, P66.

58. B. E. Fischer and R. Spohr, Production and use of nuclear tracks: imprinting structure on solids, Rev. Mod. Phys. 55 (1983) 907.

59. S. W. Barwick, Observation of Novel Radioactive Decay by Spontaneous Emission of Complex Nuclei.Ph. D. Thesis. 1986.

60. S. W. Barwick and P. B. Price, Systematics of Spontaneous Emission of Intermediate Mass Fragments from Heavy Nuclei, phys. Rev. C34, (1986) 362.

61. P. B. Price and S. W. Barwick, Spontaneous, Highly Asymmetric Binary Fragmentation of Heavy Nuclei, Proc. Inter. School-Seminar on Heavy Ion Physics, Dubna, USSR, 1986.

62. P. B. Price and S. W. Barwick, Experimental Studies of Heavy Ion Radioactivities.

63. S. P. Tretyakova, A. Sandulescu, Yu. S. Zamyatnin, Yu. S. Korotkin, and V. L. Mikheev, Ne Imission by Spontaneous Decay of ^{233}U, JINR Rapid Comm. 7, (1985) 23.

64. S. P. Tretyakova, A. Sandulescu, V. L. Mikheev, D. Hasegan, I. A. Lebedev, Yu. S. Zamyatnin, Yu. S. Korotkin, and B. F. Myasoedov, On the Spontaneous Emission of Clusters by the ^{230}Th, ^{237}Np and ^{241}Am Nuclei, JINR Rapid Comm. 13,(1985) 34.

65. A. Sandulescu, Yu. S. Zamyatnin, I. A. Lebedev, B. F. Myasoedov, S. P. Tretyakova, and D. Hasegan, Ne Emission by Spontaneous Decay of ^{231}Pa, JINR Rapid Comm. 5, (1984) 5.

66. S. Gales, E. Hourani, M. Hussonnois, J. P. Schapira, L. Stab, and M. Vergnes, Exotic Nuclear Decay of ^{223}Ra by Emission of ^{14}C Nuclei, Phys. Rev. Lett. 53, (1984) 759.

67. E. Hourani, M. Hussonnois, L. Stab, L. Brillard, S. Gales, and J. P. Schapira, Evidence for the Radioactive Decay of ^{226}Ra by ^{14}C Emission, Phys. Rev. Lett., 160B, (1985) 375.

68. P. B. Price, Advances in Solid Atate Nuclear Track Detectors, Nuclear Tracks and Radiation Measurements. 12, (1986) 5.

69. S. A. Durrani. Solid State Nuclear Track Detection, Pergamon Press, To be published.

70. S. P. Tretyakova, V. I. Furman, V. L. Mikheev, Yu. M. Chuvilisky, S. G. Kadmensky. Cluster Radioactivity--Achievements and Prospects. Proceedings (abstracts) of the 37th Conference on Nuclear Spectroscopy and Nuclear Structure. Yurmala (USSR), 14-17 April, 1987.

SOLID STATE NUCLEAR TRACK DETECTORS FOR REGISTRATION OF NUCLEAR REACTION PRODUCTS

N.P. KOCHEROV, O.E. SHIGAEV
Khlopin Radium Institute,
Leningrad, Union of Soviet Socialist Republics

Abstract

Practical aspects of exposing, etching and scanning of solid state detectors are reviewed. Detector response functions and particle identification methodologies are discussed. Applications for personal neutron dosimetry, fission studies, radon monitoring and behaviour in high background radiation conditions are outlined.

1. Introduction

The registration of charged particle tracks in solids was discovered in 1959 by Silk and Barnes /1/ who were the first to observe the damage created by fission fragments on the surface of the electron microscope samples. Then in a very short period a number of experiments was performed which lead to the discovery of etching technique /2/. Simplicity and availability of materials needed for implementation greatly contributed to quick and successful spread of the technique in many fields of science and technology. The aim of the lecture is to describe the properties of the most widely used solid state nuclear track detectors (SSNTD). For more details please see references /3,4/.

2. Formation of tracks in SSNTD

The process of track formation can be formally considered to take place in several stages. During the first stage (10^{-13} - 10^{-12} sec) the charged particle transfers energy to matter, the energetic δ-electrons formed during this process spend their energy on excitation and ionisation of atoms and molecules of matter in the vicinity of the particle trajectory. The specific energy losses of charged particle are equal to

$$\frac{dE}{dx} = C_1 \frac{Z^2_{eff}}{\beta^2}\left[\ln \frac{W^2_{max}}{I^2} - 2\beta^2 - \delta - U\right]$$

The notion of restricted energy loss (REL) meaning a portion of energy lost by particles in collisions leading to production of δ-electrons with energies less than a certain amount W_{max} is also often used. REL is given by

$$\left(\frac{dE}{dx}\right)_{W<W_0} \equiv REL \equiv C_1 \frac{Z^2_{eff}}{\beta^2}\left[\ln \frac{W_{max} \cdot W_0}{I^2} - \beta^2 - \delta - U\right],$$

where $C_1 = \frac{2\pi n_e e^4}{m_e c^2}$; $W_{max} = 2m_e c^2 \beta^2 \gamma^2$; $\gamma = (1-\beta^2)^{1/2}$

δ-correction for polarization of matter, U -correction for screening, I -ionization potential. The result of the first stage is the formation of radiation damaged zone or the primary latent image.

During the second stage (10^{-12} - 10^{-9} sec) the redistribution of energy takes place and thermal equilibrium is established.

The third stage (10^{-8} - several seconds) includes a number of chemical and physical processes leading to chemical equilibrium in the area of the latent image. The substance of the latent image differs in its structure, density, solubility etc from the properties of the bulk matter. I must be remembered that the latent image substance can react with certain agents from the ambient medium and can alter its properties in the result of this interaction (fading is one of the examples).

3. Sensitivity of SSNTD to charged particles

Depending on particular experimental conditions (type of particles to be registered, background etc) one should choose a suitable detector for a given problem. The SSNTD's differ greatly in their sensitivity: starting with total absence of sensitivity and going up to registration of 18 MeV protons. Particles with less specific losses cannot at present be registered with any known SSNTD.

Thresholds of registration for most widely used detectors are given in Table 1.

4. Visualization of tracks

Chemical etching is the most commonly used method of making tracks visible in an optical microscope. Some other methods are also known but they will not be considered here. When the radiation effect of a charged particle exceeds a certain threshold value the velocity of etching along its trajectory V_T becomes higher than the velocity of bulk etching V_B . The boundary condition for track formation is $V_T/V_B \cdot \sin\Theta = 1$, where Θ is the angle of incidence. Most commonly used etching agents are hydrofluoric acid for glasses and alkali metal hydroxide solutions for polymer detectors. Etching conditions for obtaining medium sensitivity in a number of detectors can be found in Table 1.

TABLE 1.

Detector	Composition	Least ionization registered	Etching procedure	Time etching	Density
Quartz	SiO_2	100 MeV, ^{40}Ar	48 % HF	1 min	2.27-2.65
Muscovit mica	$KAl_3Si_3O_{10}(OH)_2$	2 MeV, ^{20}Ne			
Silicate glass	SiO_2	16 MeV, ^{40}Ar			
Soda Lime glass	$23SiO_2:5Na_2O:5CaO:Al_2O_3$	20 MeV, ^{20}Ne	25%NaOH, 50°C	3 hrs	
Polythylene terephtalate (mylar, Cronar Melinex)	$C_5H_4O_2$	20 MeV, Be, B	25 % NaOH, 70°C	10 min	1.22-1.38
Lavsan	$C_{10}H_8O_4$				
Cellulose nitrates					
LR-115	$C_{12}H_{17}O_{16}N_3$	4 MeV, ^4He	25 % NaOH, 40°C	0,5 hr	
CA-80-15	$C_6H_8O_9N_2$	0,5 MeV, ^1H			1.52
CN-85	$C_6H_8O_9N_2$				1.42-1,45
Daicel	$C_6H_8O_9N_2$				
Polycarbonates					
(Lexan, macrofol)	$C_{16}H_{14}O_3$	Li, Be	25 % NaOH, 60°C	3 hrs	1,2
CR-39	$C_{12}H_{18}O_7$	18 MeV, ^1H	25 % NaOH, 70°c	4 hrs	1.31

Track parameters and sensitivity of detectors can be changed by varying the temperature and concentration of etching solutions, duration of etching, addition of certain compounds etc. Etching is a very simple process but during practical work a number of precautions should be fulfilled in order to get reproducible results.

1. The temperature of solutions should be kept constant within 1°C. Only pure chemicals should be used.
2. One should remember that the etching products are accumulated during the process and give different effects depending on the nature of detector material. For example, accumulation of etching products causes an significant increase of V_B for Lexan and CA-80-15 detectors, and strongly decreases V_B in case of CR-39. Therefore it is always recommended to use fresh solutions, calibration detectors should be etched together with those used in experiments.
3. Effect of fractional (stepwise) etching can be quite pronounced.

When the abovementioned factors are taken into consideration reproducible results can be obtained.

5. Effect of ambient conditions

The registration properties of SSNTD's depend also on ambient conditions during and after exposure such as high temperature and pressure, strong electric fields, high doses of UV or electron radiation, presence of strong oxidants or reducing chemical agents etc.

Let us briefly consider the effects of these factors.

For all SSNTD's increase of temperature causes total or partial loss of sensitivity. In all SSNTD's tracks of low ionizing particles disappear first. For example, in Daicel detectors 50 % of α-particle tracks disappear at 130°C, and 50 % of fission tracks disappear at 140°C /5/. In quartz 100 % fission tracks survive up to 1000°C and in muscovite mica up to 500°C. High pressure leads to similar effects.

The effect of chemical agents present in the ambient atmosphere is more specific. Numerous experiments with plastic detectors have shown that the presence of such oxidants as O_2, O_3, H_2O_2, water vapour during irradiations causes a marked increase of V_T and irradiation in N_2, Ar and in vacuum decreases V_T. A polycarbonate detector irradiated with Ar ions and kept in vacuum for 6 months was found to be insensitive. It should be noted that such effects are not observed in glasses and crystals.

The electric discharges lead to formation of O_3, nitrogen oxides etc. and their effect is similar to the one described above.

The effect of UV radiation was studied, for example, in /6/. It was found that after irradiation of Lexan detectors with 3100 Å light in the presence of oxygen the sensitivity has considerably increased and the detectors which were insensitive to α-particles started to register them up to the energy of 5 MeV. The irradiation of plastic detectors with electrons and other low ionizing particles causes a similar effect: it reduces the bulk etching rate V_B and does not influence V_T. This means that the registration effectiveness increases due to decrease of the critical angle of registration $\theta_{cr} = \arcsin V_B/V_T$.

Glasses show only slight influence of radition and in crystals these effects were not seen at all.

6. Detector response function and particle identification

Response function is most commonly defined as an experimental dependence of $V = V_T/V_B$ on the calculated restricted energy loss REL dE/dX_{W_0} of an ion in the detector material.

There are several ways of experimental determination of V. If an etching cone angle α can be measured then $V = 1/\sin \alpha/2$. When the angle of incidence of a particle is 90° V can be obtained from the measurement of the visible track length according to the expression $V = \frac{L + h}{h}$, where $h = V_B\ t$ - is the thickness of etched layer during t time interval. In the most general case the value of V can be determined from the measurements of D_G and D_L (big and small axes of the track ellipse) with the help of expression

$$V = \frac{\sqrt{(1 - B)^2 + 4A^2}}{1 - B^2}, \quad \text{where} \quad A = \frac{D_G}{2h}, \quad B = \frac{D_L}{2h}$$

The expressions given above hold for V_T = Const approximation and for etching duration $t \leq R/V_T$, R - particle range. Fig. 1 shows a response function of CR-39 detector made at the Radium Institute in Leningrad /7/.

Some of the measured track parameters can be obtained by calculations. Comparison of these calculated data with experimental values permits to identify the nature of the registered particle. For identification of high energy particle $V = f(R)$ calculated

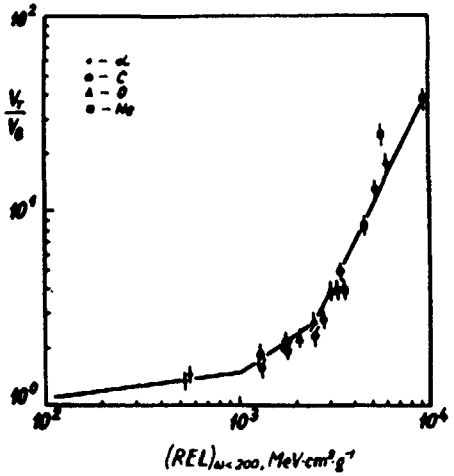

Fig. 1. Detector response function - V_T/V_B versus $REL_{Wo} < 200$

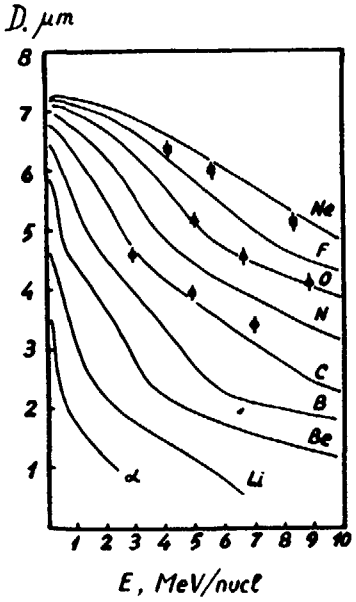

Fig. 2. Calculated relationships of track diameters on kinetic energy of ions. Experimental points are shown for ^{12}C, ^{16}O and ^{22}Ne.

relationships are compared with experimentally measured V and R. The accuracy is about $\Delta Z < 1$, $\Delta A \approx 1$.

There are cases when reaction products to be measured have low kinetic energy (several MeV per nucleon), like in fission. In this case identification is done by measurements of ellipse diameters D_G and D_L on the surface of detector. One should determine at what stage each track is. Usually one distinguishes 3 stages: cone, cone + sphere and sphere. In /5/ you can find analytical formulae for calculations of D_G and D_L for any O. For the cone phase we have expressions

$$D_L = 2h\left[\frac{V\sin\Theta - 1}{V\sin\Theta + 1}\right]^{1/2} \quad ; \quad D_G = 2h\,\frac{(V^2 - 1)}{V\sin\Theta + 1}$$

The expresions hold when $t \leq R/V_T$. Using these formulars and $V = f\,(dE/dX)_{Wo}$ function one can easily get $V = f/E/$ and $D_{L,G} = f\,(E)$ relationships. Comparing the measured track parameters with these calculated valuos one can identify the nature of the registered particles . Fig. 2 illustrates this situation. The method gives charge resolution $\Delta Z \approx 0{,}5$ and mass resolution $\Delta A > 1$.

7. Application of SSNTD's

7.1. Personal neutron dosimetry

Most important parameters of detectors used for neutron dosimetry are the energy response function and sensitivity. The former depends greatly on type of etching and material of the medium which is in contact with detector. CR-39 is the best detector for this application. For neutron enrgies up to 10 MeV recoil protons are the main particles registered by the neutron dosimeter and at higher energies recoil nuclei and α -particles from (n,α) reactions also contribute to the neutron response . An example of the dependence of the response function on neutron energy is given in Fig. 3. Solid line - calculated number of protons produced in CR-39 or a 1 mm polyethylene absorber in contact with detector, dashed curve - the number of tracks registered in CR-39. Changing radiator thickness it is possible to a certain extent to change the response function /8/. This effect is illustrated in Fig. 4.

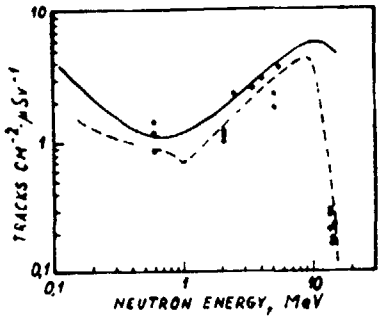

Fig. 3. Effectiveness of registration of recoil protons at different energies with 1 mm thick polyethylene radiator

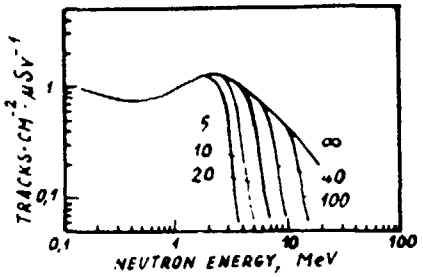

Fig. 4. Effectiveness of registration of recoil protons at different energies with different radiator thicknesses

7.2. Registration of fission fragments in light nuclei fission

CR-39 detectors were used to study the products emitted in irradiation of Al target with 70 MeV protons. A search for a quasi-fission process of compound nuclei ^{28}Si was made. One could expect emission of nuclei from ^{9}Be to ^{16}O /9/.with energies 1,1 - 0,3 MeV/nucl /10/.

Calculated relationships $D_L = f(D_G)$ for such fragments are shown in Fig. 5. The medium curve corresponds to $\theta = 45°$, the left and right curves correspond to 29° and 57°, the limiting angles of incidence in the conditions of experiment. Points are experimental values. As can be seen they are concentrated in the region from Be to Ne. From this experiment it was possible to estimate the cross section of quasifission of excited ^{28}Si nuclei $\sigma_f = (0,13 \pm 0,02)$ 10^{-27} cm^{-2}, which is in reasonable agreement with data /9/.

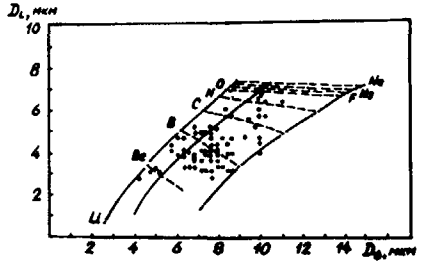

Fig. 5. Products of nuclear reaction Al + p 70 MeV. Curves are calculated dependences

7.3. Particle registration at high background

The ability to registrate particles on a background of accompanying irradiations with lower specific energy losses was always one of the advantages of the SSNTD's which is still very important for experiments. For example, recently a new radioactive decay of ^{223}Ra with emission of ^{14}C was discovered. The first 3 experiments were made with semiconductor technique, but in all the following experiments SSNTD technique was used. We have observed a very remarkable stability of registration to α -particle background even of such a highly sensitive detector as CR-39. Fig. 6 shows photomicrographs of fission fragments and ^{12}C nuclei on the background of 10^{11} α -particles/cm^2 in CR-39. Such a heavy background increases both V_B and V_T. The latter corresponds to the sum of the REL of ions and α -particles. So the whole energy response curve is shifted to higher specific energy losses, but the registration properties remain quite satisfactory.

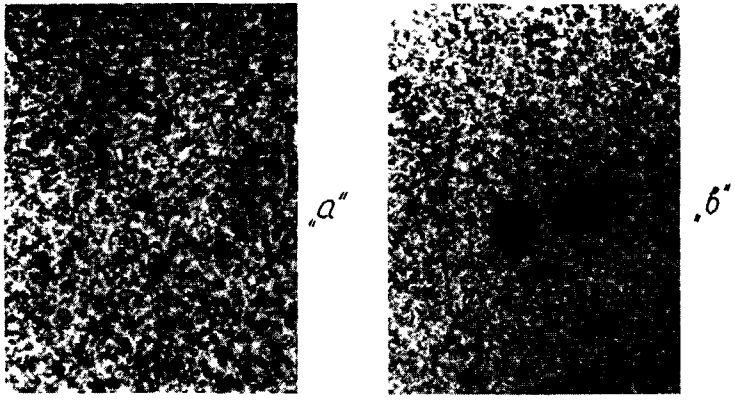

Fig. 6. a) ^{12}C and b) fission fragments registered in CR-39 on the background of 10^{11} α -particles/cm^2

7.4. Radon monitoring

During the last decade radon monitoring with the help of SSNTD's became very widespread. Radon is measured in dwellings, in geological search for U and also for forecasting earthquakes in active seismic regions.

The techniques of radon measurement as follows. The SSNTD with 1 - 5 cm^2 area is put inside a plastic cup with dimensions ϕ 50 x 100 and the opening of the cup is covered with a thin polymer film (tens of mcm). The cup with a detector inside is exposed usually for periods from severel hours to one month. The detectors are then etched and scanned. A thin film over the cup stops aerosoles, and only ^{222}Rn and its daughters will be registered. The SSNTD's used for this purpose are usually cellulose nitrates or polycarbonates. It is also possible to measure radon contents directly in water. To get absolute results one should, however, calibrate the devices in standard radon atmosphere chambers or solutions, containing radon.

REFERENCES

1. E.C.M.Silk, R.S.Barnes, Phil.Mag., 4, 970-971, 1959.
2. P.B.Price, E.M.Walker, J.Appl.Phys., v. 33, N 12, p. 3407-3412, 1963
3. R.L.Fleischer, P.B.Price, R.M.Walker, "Nuclear Tracks in Solids" Univ. of California Press, Berkeley-Los,Angeles-London, 1975
4. A.M.Marenny, Dielectric Track Detectors, Energoatomizdat, Moscow, 1987 (in Russian).
5. G.Somogyi, Rad.Effects 16, p. 245-251, 1972.
6. R.A.Stern, P.B.Price, Nature Phys.Sci., 240, p. 82-83, 1972.
7. A.V.Voronov, N.P.Kocherov, O.E.Shigaev et al. Preprint RI-195 , Leningrad, 1986 (in Russian)
8. W.G.Cross, Nucl. Tracks and Rad.Meas., v. 12, N 1-6, p. 533-542, 1986.
9. V.G.Bogdanov, N.P.Kocherov, F.G.Lepekhin et al., Letters to JETP, 44, N 7, p. 306-308, 1986.
10. V.E.Viola, K.Kwiatkowski, M.Walker, Phys.Rev., C31, N 4, p. 1550-1553, 1985.

HOW TO ORDER IAEA PUBLICATIONS

An exclusive sales agent for IAEA publications, to whom all orders and inquiries should be addressed, has been appointed in the following country:

UNITED STATES OF AMERICA — UNIPUB, 4611-F Assembly Drive, Lanham, MD 20706-4391

In the following countries IAEA publications may be purchased from the sales agents or booksellers listed or through major local booksellers. Payment can be made in local currency or with UNESCO coupons.

ARGENTINA	Comisión Nacional de Energía Atómica, Avenida del Libertador 8250, RA-1429 Buenos Aires
AUSTRALIA	Hunter Publications, 58 A Gipps Street, Collingwood, Victoria 3066
BELGIUM	Service Courrier UNESCO, 202, Avenue du Roi, B-1060 Brussels
CHILE	Comisión Chilena de Energía Nuclear, Venta de Publicaciones, Amunategui 95, Casilla 188-D, Santiago
CHINA	IAEA Publications in Chinese: China Nuclear Energy Industry Corporation, Translation Section, P.O. Box 2103, Beijing IAEA Publications other than in Chinese: China National Publications Import & Export Corporation, Deutsche Abteilung, P.O. Box 88, Beijing
CZECHOSLOVAKIA	S.N.T.L., Mikulandska 4, CS-116 86 Prague 1 Alfa, Publishers, Hurbanovo námestie 3, CS-815 89 Bratislava
FRANCE	Office International de Documentation et Librairie, 48, rue Gay-Lussac, F-75240 Paris Cedex 05
HUNGARY	Kultura, Hungarian Foreign Trading Company, P.O. Box 149, H-1389 Budapest 62
INDIA	Oxford Book and Stationery Co., 17, Park Street, Calcutta-700 016 Oxford Book and Stationery Co., Scindia House, New Delhi-110 001
ISRAEL	Heiliger & Co. Ltd. 23 Keren Hayesod Street, Jerusalem 94188
ITALY	Libreria Scientifica, Dott. Lucio de Biasio "aeiou", Via Meravigli 16, I-20123 Milan
JAPAN	Maruzen Company, Ltd, P.O. Box 5050, 100-31 Tokyo International
PAKISTAN	Mirza Book Agency, 65, Shahrah Quaid-e-Azam, P.O. Box 729, Lahore 3
POLAND	Ars Polona-Ruch, Centrala Handlu Zagranicznego, Krakowskie Przedmiescie 7, PL-00-068 Warsaw
ROMANIA	Ilexim, P O. Box 136-137, Bucharest
SOUTH AFRICA	Van Schaik Bookstore (Pty) Ltd, P.O. Box 724, Pretoria 0001
SPAIN	Díaz de Santos, Lagasca 95, E-28006 Madrid Díaz de Santos, Balmes 417, E-08022 Barcelona
SWEDEN	AB Fritzes Kungl. Hovbokhandel, Fredsgatan 2, P.O. Box 16356, S-103 27 Stockholm
UNITED KINGDOM	Her Majesty's Stationery Office, Publications Centre, Agency Section, 51 Nine Elms Lane, London SW8 5DR
USSR	Mezhdunarodnaya Kniga, Smolenskaya-Sennaya 32-34, Moscow G-200
YUGOSLAVIA	Jugoslovenska Knjiga, Terazije 27, P.O. Box 36, YU-11001 Belgrade

---

Orders from countries where sales agents have not yet been appointed and requests for information should be addressed directly to:

Division of Publications
International Atomic Energy Agency
Wagramerstrasse 5, P.O. Box 100, A-1400 Vienna, Austria